

10-21-2016

Design and Development of Peptidomimetic Ligands for Targeting Radiopharmaceuticals, Imaging Probes, and Immunotherapeutics in Oncologic Disease

Michael Lawrence Doligalski
University of South Florida, mldoligalski@gmail.com

Follow this and additional works at: <http://scholarcommons.usf.edu/etd>

 Part of the [Organic Chemistry Commons](#)

Scholar Commons Citation

Doligalski, Michael Lawrence, "Design and Development of Peptidomimetic Ligands for Targeting Radiopharmaceuticals, Imaging Probes, and Immunotherapeutics in Oncologic Disease" (2016). *Graduate Theses and Dissertations*.
<http://scholarcommons.usf.edu/etd/6492>

This Dissertation is brought to you for free and open access by the Graduate School at Scholar Commons. It has been accepted for inclusion in Graduate Theses and Dissertations by an authorized administrator of Scholar Commons. For more information, please contact scholarcommons@usf.edu.

Design and Development of Peptidomimetic Ligands for Targeting Radiopharmaceuticals,
Imaging Probes, and Immunotherapeutics in Oncologic Disease

by

Michael Lawrence Doligalski

A dissertation submitted in partial fulfillment
of the requirements for the degree of
Doctor of Philosophy
Department of Chemistry
College of Arts and Sciences
University of South Florida

Co-Major Professor: Mark L. McLaughlin, Ph.D.
Co-Major Professor: Jianfeng Cai, Ph.D.
James W. Leahy, Ph.D.
David L. Morse, Ph.D.

Date of Approval:
October 19th, 2016

Keywords: Peptide Ligands, Radiopharmaceuticals, Imaging Probes, Targeted Alpha-particle
Therapy, Immunoconjugates, Checkpoint Inhibitors

Copyright © 2016, Michael Lawrence Doligalski

DEDICATION

To my wife Chrissy and our son William

ACKNOWLEDGMENTS

I am incredibly fortunate to have established many fantastic mentorships and long-lasting friendships throughout my early scientific career. Without the guidance, advice, and support of these wonderful people, I certainly would not be where I am today. At the great risk of failing to recall someone, I would like to acknowledge them here.

First, I am extremely grateful for the mentorship of Dr. Mark McLaughlin. Thank you for welcoming me into your research group. Dr. McLaughlin's seemingly endless knowledgebase and creativity with a knack for elegant simplicity continues to be a model I strive to emulate. I would also like to thank Dr. David Morse for welcoming me into his research group at Moffitt. Our group's collaborations have been invaluable to helping me understand the bigger picture of our scientific endeavors. I wish to also thank the members of my graduate school committee, Drs. Jianfeng Cai and James Leahy, for their guidance and time in my graduate school journey. I am also indebted to Dr. Shrikumar Nair and the other scientists who helped shape my aspirations while working as a research associate at Affinergy in North Carolina.

I must also thank current and past group members from the McLaughlin, Morse, and Cai labs for their friendships and help with the daily grind of lab work. Particular thanks to Dr. Priyesh Jain, Dr. Sridhar Kaulagari, Dr. Hyunjoo Kil, Dr. Allison Cohen, Dr. Narges Tafreshi, Amanda Huynh, Dr. Phil Murray, Dr. David Badger, Dr. Yi Liang, Dr. Fenger Zhou, Tim Odom, and Josanne Woodroffe. I sincerely appreciate the friendship from many others in the USF chemistry

department, including Dr. Ryan Young, Danielle Demers, Dr. Jackie Fries, Dr. Chris Witowski, Andrew Shilling, and Dr. Laurent Calcul, whom helped to make graduate school life more bearable. Dr. Young deserves a particular acknowledgement for his friendship and mentorship which resulted in many great conversations, research ideas, and a newfound appreciation for expensive scotch.

I would also like to express my gratitude to Drs. Edwin Rivera and Mohanraja Kumar for their mentorship during and after my work with them in their core facilities. I am very grateful for the learning experiences I had while working in both of these facilities. Additionally I had the privilege of working with and befriending other teaching assistants in this capacity: Dr. Andrii Monastyrskiy, Arthur Maknenko, Dr. Susana Lopez, Cole Cerrato, and Yassin El Batrawi.

Finally, I must express my deepest thanks to my wife and family. Dr. Christina Doligalski has been through the highs and lows of this journey, and her love and support (and ruthless editing) has been complete and unwavering. Thank you for everything, Chrissy. Thanks are also due to the rest of our family: my parents Dr. Thomas and Sue Doligalski; in-laws Dr. Mary Ella and Brian Teeter; and my brother, sister-in-law and nephew Steven, Meghan, Owen, for their love and support, especially when we moved to Florida and our visits became less frequent. (Thanks to Southwest Airlines for the affordable airfare and maintaining non-stop flights from TPA to RDU). Last but not least, I must thank our now 3 month old son William for sleeping through the night from an early age and his discerning ear while we read through this dissertation together more times than I can count.

TABLE OF CONTENTS

List of Tables	iv
List of Figures	v
List of Schemes	xii
List of Abbreviations	xiii
Abstract.....	xvi
Chapter One: Introduction of Peptide Targeting Ligands	1
1.1 Cancer	1
1.2 Targeting the Tumor Cell Surface	2
1.3 Targeting Molecules.....	7
1.3.1 Antibodies	8
1.3.2 Antibody fragments	9
1.3.3 Peptides	10
1.4 Medicinal Chemistry of Targeting Ligands	12
1.5 Vision for This Dissertation.....	15
1.6 References.....	16
Chapter Two: Melanocortin 1 Receptor Targeting Ligands and the Development of a Targeted Radiopharmaceutical and Companion Diagnostic Imaging Agent.....	19
2.1 Introduction.....	19
2.2 Results and Discussion	23
2.2.1 Peptide Design and Synthesis.....	23
2.2.2 Chelation of Metals	27
2.2.3 Biological Testing of MC1RL Compounds	33
2.2.4 Biodistribution Modulation	36
2.2.5 Constrained MC1RL Variants	40
2.3 Conclusions	46
2.4 Experimental	48
2.4.1 Materials and Instrumentation.....	48
2.4.2 Experimental Procedures.....	49
2.4.2.1 Linear MC1RL Synthesis	49
2.4.2.2 Alloc Deprotection	50
2.4.2.3 Peptide Branching, Linkers, and Payloads	50

2.4.2.4 Peptide Cleavage, Lyophilization, and Purification	51
2.4.2.5 Mass Spectrometry Characterization: MALDI-TOF and QToF	52
2.4.2.6 Metal Chelation.....	54
2.4.2.6.1 Europium Chelation.....	54
2.4.2.6.2 Gallium-67/69 and Lanthanum-139 Chelation	55
2.4.2.6.3 Indium-113 Reference Compounds	55
2.4.2.7 Constrained Peptide Synthesis	55
2.4.2.8 Lipophilicity Measurements.....	56
2.5 References	59
 Chapter Three: Synthesis of a Toll-Like Receptor 2 Fluorescent Antagonist for Use in Intraoperative Guided Surgery	
3.1 Introduction.....	62
3.2 Results and Discussion	65
3.2.1 Fmoc-Cys(POE)-OH Synthesis.....	65
3.2.2 IR-780-COOH Synthesis	69
3.2.3 TLR2L Peptide Synthesis.....	70
3.2.4 TLR2L Characterization	71
3.2.4.1 Product Purity and Identification	71
3.2.4.2 Optical Characterization	73
3.2.4.3 Lipophilicity Measurement	73
3.2.5 Biological Testing.....	73
3.3 Conclusions	76
3.4 Experimental.....	77
3.4.1 Materials and Instrumentation.....	77
3.4.2 Experimental Procedures	78
3.4.2.1 Monomer Synthesis.....	78
3.4.2.2 Ligand Synthesis, Purification, and Characterization	83
3.4.2.3 Mass Spectral Analysis: QToF and MALDI-TOF.....	84
3.4.2.4 Lipophilicity Measurement	85
3.5 References	85
 Chapter Four: Development of Novel Targeted Immunoconjugates for Use as Peptide-Targeted Immune Effectors.....	
4.1 Introduction.....	87
4.2 Results and Discussion	90
4.2.1 Targeting Ligand Design and Synthesis	90
4.2.2 Immunoconjugate Synthesis.....	96
4.2.3 Immunoconjugate Workup and Characterization: Size Exclusion.....	100
4.2.4 Immunoconjugate Characterization: UV/Vis TAR Determination.....	101
4.2.5 Immunoconjugate Characterization: Mass Spec TAR Determination	104
4.2.6 Biological Testing of Immunoconjugates.....	107
4.3 Conclusions	110

4.4 Experimental.....	111
4.4.1 Materials and Instrumentation.....	111
4.4.2 Experimental Procedures	112
4.4.2.1 Targeting Ligand (TL) Synthesis	112
4.4.3.2 General Antibody Conjugation Protocol.....	114
4.4.3.3 General Immunoconjugate Purification Protocol.....	114
4.4.3.4 Immunoconjugate TAR Determination: UV/Vis	115
4.4.3.5 Immunoconjugate TAR Determination: Mass Spectrometry.....	116
4.5 Targeting Ligand Structures	118
4.6 References	123
Appendix A: Selected Mass Spectra and HPLC Chromatograms of Peptide Targeting Ligands.....	125
Appendix B: Selected ¹ H AND ¹³ C NMR Spectra.....	187
Appendix C: Selected Antibody and Immunoconjugate Characterization.....	201
Appendix D: IACUC Approvals	217
About the Author.....	End Page

LIST OF TABLES

Table 1.1:	Summary of common α -emitting radionuclides.....	4
Table 2.1:	Select previously reported SAR work done on melanotropin message sequence.....	22
Table 2.2:	Linear MC1RL analogs that have been synthesized and characterized by mass spectroscopy.....	28
Table 4.1:	Summary of peptide targeting ligands prepared for subsequent immunoconjugation.....	96
Table 4.2:	Targeting Ligand to Antibody Ratio (TAR) observed from various buffers during immunoconjugation.....	98
Table 4.3:	Recovered protein as a result of the varied immunoconjugation conditions	99
Table 4.4:	Summary of prepared immunoconjugates	103
Table 4.5:	Source and TOF parameters used for antibody and immunoconjugate MS analysis	117

LIST OF FIGURES

Figure 1.1:	FITC targeted agent for folate receptor.....	3
Figure 1.2:	Common metal chelators and binders used to attach radionuclides to targeting ligands.....	5
Figure 1.3:	The somatostatin mimetic octreotide and its DOTA- containing analogs	11
Figure 2.1:	Actinium-225 decay pathway	23
Figure 2.2:	Structure of previously reported lead MC1RL targeting ligand	25
Figure 2.3:	Structures of MC1RL-Ahx-DOTA (R ¹) and MC1RL-Ahx-DTPA (R ²)	26
Figure 2.4:	HPLC chromatographic overlay comparing the time course of metal Chelation with MC1RL-Ahx-DOTA.....	30
Figure 2.5:	Whole-cell competition binding affinities of metallated and unmetallated MC1RL-Ahx-DOTA analogs.....	31
Figure 2.6:	Structure of scrambled-MC1RL-Ahx-DOTA.....	32
Figure 2.7:	Biodistribution of MC1RL-Ahx-DOTA:Ac in tumor bearing mice.....	34
Figure 2.8:	Structure of MC1RL-IR800CW	35
Figure 2.9:	MC1RL analogs synthesized to modulate lipophilicity.....	37
Figure 2.10:	Graphical display of experimentally determined LogD _{7.4} for MC1RL analogs.....	38
Figure 2.11:	Biodistribution of indium-111 labeled MC1RL analogs	40
Figure 2.12:	Structure of [half-Cys ⁴ ,half-Cys ¹⁰]α -MSH.....	41
Figure 2.13:	Structure of MT-II (melanotan-II).....	42
Figure 2.14:	Summary of constrained MC1RL compounds	46

Figure 2.15:	QToF analysis of gallium-chelated MC1RL-Ahx-DOTA	53
Figure 2.16:	QToF analysis of lanthanum-chelated MC1RL-Ahx-DOTA	53
Figure 2.17:	MRM transitions developed for MC1R-Ahx-DOTA:La	57
Figure 2.18:	Product ion scan for MC1RL-Ahx-DOTA:La with precursor selected as 537.55 m/z	58
Figure 2.19:	Fragmentor voltage (A) and collision energy (B) optimization experiments for the MRM method	59
Figure 3.1:	Diacyl-TLR2L-IR800CW	63
Figure 3.2:	Structure of major product from the first attempt to synthesize Fmoc-Cys(POE)-OH	67
Figure 3.3:	HPLC chromatogram of purified TLR2L-780	72
Figure 3.4:	Optical characterization of IR780-COOH (3.7) and TLR2Li-780	72
Figure 3.5:	Competition binding assay SU.86.86 pancreatic tumor cells with endogenous TLR2 expression.....	74
Figure 3.6:	Functional bioassay measuring downstream signaling of TLR2 upon treatment with listed compound	74
Figure 3.7:	<i>In vivo</i> and <i>ex vivo</i> near infrared (NIRF) guided imaging using TLR2L-780.....	75
Figure 4.1:	Key cell surface molecular interactions in T cell signaling	88
Figure 4.2:	Structure of Cyanine Dye 5.5, NHS-ester	94
Figure 4.3:	Solution-phase modifications to targeting peptide ligand	95
Figure 4.4:	Bioconjugation reaction for the addition of targeting ligand to immune effector antibody.....	97
Figure 4.5:	Size exclusion experiment demonstrating the separation of conjugated and unconjugated immune effectors	101
Figure 4.6:	Experimental UV/Vis extinction coefficients for TAR calculations.....	102
Figure 4.7:	MS analysis of deglycosylated α PD-1	105

Figure 4.8:	MS analysis of deglycosylated immunoconjugate α PD-1 + 4.5	106
Figure 4.9:	Immunoconjugate competition binding assays for DOR expressing cells	108
Figure 4.10:	Differential uptake of immunoconjugate (D26A TAR 4.2) in DOR(-) and DOR(+) tumors	109
Figure 4.11:	Comparison of immune modulator efficacy with and without TL in a mouse model	110
Figure A2.1:	MC1RL; Mass Spectrum.....	125
Figure A2.2:	MC1RL; HPLC Trace	126
Figure A2.3:	MC1RL-Ahx-FBA; Mass Spectrum	127
Figure A2.4:	MC1RL-Ahx-FBA; HPLC Trace	128
Figure A2.5:	MC1RL-Ahx-DTPA; Mass Spectrum.....	129
Figure A2.6:	MC1RL-Ahx-DTPA:Eu; Mass Spectrum	130
Figure A2.7:	MC1RL-Ahx-DTPA:Eu; HPLC Trace	131
Figure A2.8:	MC1RL-Ahx-DOTA; Mass Spectrum.....	132
Figure A2.9:	MC1RL-Ahx-DOTA; HPLC Trace	133
Figure A2.10:	Scrambled-MC1RL-Ahx-DOTA; Mass Spectrum (prepared by Dr. Hunjoo Kil).....	134
Figure A2.11:	Scrambled-MC1RL-Ahx-DOTA; HPLC Trace (prepared by Dr. Hunjoo Kil)	135
Figure A2.12:	MC1RL(D5)-Ahx-DOTA; Mass Spectrum	136
Figure A2.13:	MC1RL(D5)-Ahx-DOTA; HPLC Trace	137
Figure A2.14:	MC1RL-Ahx-DOTA:La; Mass Spectrum.....	138
Figure A2.15:	MC1RL-Ahx-DOTA:La; HPLC Trace.....	139
Figure A2.16:	MC1RL-Ahx-DOTA:Ga; Mass Spectrum.....	140

Figure A2.17: MC1RL-Ahx-DOTA:Ga; HPLC Trace	141
Figure A2.18: MC1RL-Ahx-DOTA:Eu; Mass Spectrum	142
Figure A2.19: MC1RL-Ahx-DOTA:Eu; HPLC Trace	143
Figure A2.20: MC1RL-Ahx-DOTA:In; Mass Spectrum	144
Figure A2.21: MC1RL-Ahx-DOTA:In; HPLC Trace	145
Figure A2.22: MC1RL-diDGlu-DOTA; Mass Spectrum (prepared by Dr. Hunjoo Kil).....	146
Figure A2.23: MC1RL-diDGlu-DOTA; HPLC Trace (prepared by Dr. Hunjoo Kil)	147
Figure A2.24: MC1RL-diDGlu-DOTA:In; Mass Spectrum (Precursor prepared by Dr. Hunjoo Kil)	148
Figure A2.25: MC1RL-diDGlu-DOTA:In; HPLC Trace (Precursor prepared by Dr. Hunjoo Kil)	149
Figure A2.26: MC1RL-diDLys-DOTA; Mass Spectrum (Precursor prepared by Dr. Hunjoo Kil)	150
Figure A2.27: MC1RL-diDLys-DOTA; HPLC Trace (Precursor prepared by Dr. Hunjoo Kil)	151
Figure A2.28: MC1RL-DOTA; Mass Spectrum	152
Figure A2.29: MC1RL-DOTA; HPLC Trace.....	153
Figure A2.30: MC1RL-DOTA:La; HPLC Trace	154
Figure A2.31: MC1RL-DOTA:La; HPLC Trace	155
Figure A2.32 MC1RL-DOTA:Ga; Mass Spectrum	156
Figure A2.33: MC1RL-DOTA:Ga; HPLC Trace.....	157
Figure A2.34: MC1RL-DOTA:Eu; Mass Spectrum.....	158
Figure A2.35: MC1RL-DOTA:Eu; HPLC Trace.....	159
Figure A2.36: MC1RL-DOTA:In; Mass Spectrum.....	160

Figure A2.37: MC1RL-DOTA:In; HPLC Trace.....	161
Figure A2.38: cMC1RL-B43-cyclic; Mass Spectrum	162
Figure A2.39: cMC1RL-B43-cyclic; HPLC Trace	163
Figure A2.40: cMC1RL-B43-linear; Mass Spectrum	164
Figure A2.41: cMC1RL-B43-linear; HPLC Trace.....	165
Figure A2.42: cMC1RL-B52-cyclic; Mass Spectrum	166
Figure A2.43: cMC1RL-B52-cyclic; HPLC Trace	167
Figure A2.44: cMC1RL-B52-linear; Mass Spectrum	168
Figure A2.45: cMC1RL-B52-linear; HPLC Trace.....	169
Figure A2.46: cMC1RL-B53-cyclic; Mass Spectrum	170
Figure A2.47: cMC1RL-B53-cyclic; HPLC Trace	171
Figure A2.48: cMC1RL-B53-linear; Mass Spectrum	172
Figure A2.49: cMC1RL-B53-linear; HPLC Trace.....	173
Figure A2.50: cMC1RL-B53-cyclic; Mass Spectrum	174
Figure A2.51: cMC1RL-B53-cyclic; HPLC Trace	175
Figure A2.52: cMC1RL-B54-linear; Mass Spectrum	176
Figure A2.53: cMC1RL-B54-linear; HPLC Trace.....	177
Figure A3.1: TLR2L-780; Mass Spectrum.....	178
Figure A4.1: Peptide 4.2; Mass Spectrum.....	179
Figure A4.2: Peptide 4.2; HPLC Trace	180
Figure A4.3: Peptide 4.3; Mass Spectrum.....	181
Figure A4.4: Peptide 4.3; HPLC Trace	182

Figure A4.5:	Peptide 4.4; Mass Spectrum.....	183
Figure A4.6:	Peptide 4.4; HPLC Trace	184
Figure A4.7:	Peptide 4.5; Mass Spectrum.....	185
Figure A4.8:	Peptide 4.5; HPLC Trace	186
Figure B3.1:	^1H NMR (400 MHz, CDCl_3) spectrum of 3.1.....	187
Figure B3.2:	^{13}C $\{^1\text{H}\}$ NMR (400 MHz, CDCl_3) spectrum of 3.1	188
Figure B3.3:	^1H NMR (400 MHz, CDCl_3) spectrum of 3.2.....	189
Figure B3.4:	^{13}C $\{^1\text{H}\}$ NMR (101 MHz, CDCl_3) spectrum of 3.2	190
Figure B3.5:	^1H NMR (400 MHz, CDCl_3) spectrum of 3.3.....	191
Figure B3.6:	^{13}C $\{^1\text{H}\}$ NMR (101 MHz, CDCl_3) spectrum of 3.3	192
Figure B3.7:	^1H NMR (500 MHz, CDCl_3) spectrum of 3.4.....	193
Figure B3.8:	^{13}C $\{^1\text{H}\}$ NMR (151 MHz, CDCl_3) spectrum of 3.4	194
Figure B3.9:	^1H NMR (500 MHz, CDCl_3) spectrum of 3.5.....	195
Figure B3.10:	^{13}C $\{^1\text{H}\}$ NMR (151 MHz, CDCl_3) spectrum of 3.5	196
Figure B3.11:	^1H NMR (500 MHz, CDCl_3) spectrum of 3.6.....	197
Figure B3.12:	^{13}C $\{^1\text{H}\}$ NMR (126 MHz, CDCl_3) spectrum of 3.6	198
Figure B3.13:	^1H NMR (600 MHz, DMSO) spectrum of 3.7.....	199
Figure B3.14:	^{13}C $\{^1\text{H}\}$ NMR (151 MHz, CDCl_3) spectrum of 3.7	200
Figure C4.1:	α -PD-L1 antibody; Mass Spectra	201
Figure C4.2:	α -CD137L antibody; Mass Spectra	202
Figure C4.3:	α -trinitrophenol antibody; Mass Spectra	203
Figure C4.4:	Immunoconjugate α -trinitrophenol + DmtTic (4.2), D41; Mass Spectra	204

Figure C4.5:	Immunoconjugate α -PDL-1 + DmtTic (4.2), D38; Mass Spectra	205
Figure C4.6:	Immunoconjugate α -PD-1 + DmtTic (4.2), D13A; SEC Chromatograph	206
Figure C4.7:	Immunoconjugate α -PD-1 + DmtTic (4.2), D13B; SEC Chromatograph.....	207
Figure C4.8:	Immunoconjugate α -PD-1 + DmtTic (4.2), D26A; SEC Chromatograph	208
Figure C4.9:	Immunoconjugate α -PD-1 + DmtTic (4.2), D26B; SEC Chromatograph.....	209
Figure C4.10:	Immunoconjugate α -PDL-1 + DmtTic (4.2), D38; SEC Chromatograph.....	210
Figure C4.11:	Immunoconjugate α -CD137L + DmtTic (4.2), D39; SEC Chromatograph.....	211
Figure C4.12:	Immunoconjugate α -PD-1 + scrambled-DmtTic (4.5), D40; SEC Chromatograph	212
Figure C4.13:	Immunoconjugate α -trinitrophenol + DmtTic (4.2), D41; SEC Chromatograph	213
Figure C4.14:	Immunoconjugate α -PD-1 + scrambled-DmtTic (4.5), D46; SEC Chromatograph	214
Figure C4.15:	Immunoconjugate α -PD-1 + DmtTic (4.2), D49; SEC Chromatograph.....	215
Figure C4.16:	Immunoconjugate α -PD-1 + DmtTic (4.4), D51; SEC Chromatograph.....	216
Figure D1:	MC1RL IACUC Approval	217-218
Figure D2:	TLR2L IACUC Approval	219-220
Figure D3:	DORL IACUC Approval.....	221-222
Figure D4:	DORL IACUC Approval Renewal.....	223

LIST OF SCHEMES

Scheme 1.1:	Common conjugation chemistries used to functionalize biomolecules.....	6
Scheme 2.1:	Typical solid phase peptide synthesis of linear MC1RL.....	24
Scheme 2.2:	Chelation of metals to Peptide Ligand-DOTA (shown with Ga ⁺³).....	29
Scheme 2.3:	Constraining linear MC1RL around the turn promotion region.....	43
Scheme 2.4:	Constrained MC1RL Synthesis	45
Scheme 3.1:	Retrosynthetic analysis of Fmoc-Cys(POE)-OH	66
Scheme 3.2:	Synthesis of 2-iodoethyl palmitate 3.1	67
Scheme 3.3:	Synthetic route for the preparation of Fmoc-Cys(POE)-OH via hydrogenolysis sensitive PGs.....	68
Scheme 3.4:	Synthetic route for Fmoc-Cys(S-[palmitoyloxyethyl])-OH, 3.6.....	69
Scheme 3.5:	Synthetic route for conjugated IR780 dye.....	70
Scheme 3.6:	SPPS strategy used for TL2RL-780	71
Scheme 4.1:	SPPS strategy used to synthesize the DmtTic targeting ligand.....	92
Scheme 4.2:	Common conjugation chemistries used to functionalize bio molecules.....	93

LIST OF ABBREVIATIONS

AA	amino acid
ACN	acetonitrile
AcOH	acetic acid
ADC	antibody-drug conjugate
Ahx	6-aminohexanoic acid
Alloc	allyloxycarbonyl
α -MSH	alpha-melanocyte-stimulating hormone
BD	biodistribution
Bn	benzyl
Boc	<i>t</i> -butyloxycarbonyl
Cbz	carboxybenzyl
DBU	1,8-diazabicyclo[5.4.0]undec-7-ene
Dbs	diabodies
DCC	N,N- dicyclohexylcarbodiimide
DCM	dichloromethane
DIEA	diisopropylethylamine
DIC	N,N- diisopropylcarbodiimide
DMAP	4-dimethylaminopyridine
DMF	N,N- dimethylformamide
DMSO	dimethylsulfoxide
DNA	deoxyribonucleic acid
DOR	δ -opioid receptor
DOTA	1,4,7,10-tetraazacyclododecane-1,4,7,10-tetraacetic acid
dPEG	discrete polyethylene glycol
DTPA	diethylene triamine pentaacetic acid
EGFR	epidermal growth factor receptor
ESI	electrospray ionization
FA	formic acid
Fab	fragment antigen-binding fragment
FDA	Food and Drug Administration
FITC	fluorescein isothiocyanate
Fmoc	9- fluorenylmethyloxycarbonyl
GPCR	G protein-coupled receptor

HCTU	1H-Benzotriazolium 1-[bis(dimethylamino)methylene]-5chloro-,hexafluorophosphate (1-),3-oxide
HER2	human epidermal growth factor receptor 2
HOBt	hydroxybenzotriazole
HPLC	high performance liquid chromatography
ICG	indocyanine green
IgG	immunoglobulin G
IHC	Immunohistochemistry
IR	infrared
irAE	immune related adverse effects
LCMS	liquid chromatograph mass spectrometry
LG	leaving group
LP	lipopeptide
mAb	monoclonal antibody
MALDI	matrix-assisted laser desorption ionization
Mbs	minibodies
MeOH	methanol
MRD	minimal residual disease
MRM	multiple reaction monitoring
MS	mass spectroscopy /spectrometer
MSKCC	Memorial Sloan Kettering Cancer Center
MWCU	molecular weight cut-off
NHS	N-hydroxysuccinimide
NMM	N-methylmorpholine
NMP	N-methyl-2-pyrrolidone
NMR	nuclear magnetic resonance
NSCLC	non-small cell lung cancer
OC	octreotide
Osu	hydroxysuccinimide
PAMP	pathogen-associated molecular pattern
PEG	polyethylene glycol
RIT	radioimmunotherapy
RNA	ribonucleic acid
RP	reverse phase
RTK	receptor tyrosine kinase
SAR	structure-activity relationship
SEC	size-exclusion chromatography
SPECT	single-photon emission computed tomography
SPPS	solid phase peptide synthesis

PEGO	19-amino-5-oxo-3,10,13,16-tetraoxo-6-azanonadecan-1-oic acid residue
T3P	propylphosphonic anhydride
PRRT	peptide receptor radionuclide therapy
TAR	targeting ligand-antibody ratio
TAT	targeted alpha-particle therapy
TEA	triethylamine
TFA	trifluoroacetic acid
TFE	trifluoroethanol
T_h	T helper cell
THF	tetrahydrofuran
TIC	total ion chromatogram
TIS	triisopropylsilane
TL	targeting ligand
TLC	thin layer chromatography
TLR	toll-like receptor
TOF	time of flight
TRF	time-resolved fluorescence
Trt	trityl
UV/Vis	ultraviolet / visible spectroscopy
VEGFR	vascular endothelial growth factor receptor

ABSTRACT

Cancer is a leading cause of morbidity and mortality in the developed world. While much has been learned about these diseases in the last few decades, one of the main barriers to widespread advancement is the heterogeneity of cancer biology. A growing body of evidence supports the idea that certain protein receptors are overexpressed on the surface of tumor cells as compared to normal tissues. These extracellular biomarkers provide a unique opportunity to selectively target the tumor with both imaging and therapeutic modalities. The research in this dissertation focuses on targeting proteins on the tumor cell surface with peptidomimetic ligands.

Following a description of various extracellular receptors, chapter one discusses targeting ligands designed to specifically and selectively bind these receptors. It reviews recent literature on targeted alpha-particle therapy and ends with an explanation of the advantages of peptide ligands. Three distinct approaches to imaging and therapeutic modalities are then discussed in subsequent chapters. First, a peptide ligand was designed to target radionuclides to malignant melanoma cells in an effort to develop companion radiotherapeutics and diagnostic imaging agents. The second research project describes the synthesis of a novel antagonist peptide ligand with conjugated near infrared dye, and its utility for real-time intraoperative guidance during pancreatic adenocarcinoma resection. Finally, the last chapter describes how the relatively new field of immunomodulatory effectors may be enhanced by their derivatization with peptide targeting ligands.

CHAPTER ONE: INTRODUCTION OF PEPTIDE TARGETING LIGANDS

1.1 Cancer

Advances in modern medicine are improving longevity; between 1990 and 2013, worldwide life expectancy has risen over 6 years, driven largely by advanced therapy for cardiovascular disease.¹ With these longevity increases, chronic diseases have become the leading causes of death, with cancer now the second leading cause of death in the United States.^{1,2} The American Cancer Society projects 1.7 million new cancer diagnoses in 2016.³ Although prevention, early diagnosis, and better treatment options have slowed the rising cancer-related morbidity in recent decades, further research remains critical to the understanding of mechanisms by which tumors proliferate and evade destruction. This research is invaluable to both diagnostics and therapeutics, as the development of better imaging probes can detect aberrant cells earlier and the identification of innovative therapies can provide alternative treatments for patients with few clinical options.

While still an amazingly complex process, the mechanisms by which tumors proliferate are increasingly becoming clearer.⁴ At the cellular level, the many diseases that are encompassed under the broad definition of cancer are quite heterogeneous.⁵ Much of this heterogeneity is understood to result from amplified expression of genes that have lower level expression in other normal

tissues.⁶ Fortunately, the overexpressed protein products of these genes can be leveraged to provide avenues by which cancers can be characterized and targeted for both diagnostics and therapeutics.

Many of these overexpressed genes encode for transmembrane proteins expressed on the tumor cells. Common types of these membrane bound proteins include G-protein coupled receptors (GPCRs) and receptor tyrosine kinases (RTKs). In fact the most abundant five cancers (breast, prostate, lung, colorectal, and cervical) are strongly associated with Erk/Akt activation resulting from RTK signaling at vascular endothelial growth factor (VEGFRs), epidermal growth factor (EGFR), and human epidermal growth factor (HER2) cell surface receptors.⁷ The *HER2/Neu* receptor has been used to both characterize 15-30% of breast cancers, prognosticate, and treat the disease through innovative monoclonal antibody-based therapeutics.⁸ Folate receptor overexpression has been characterized in many malignancies while maintaining low expression in other normal tissues.⁹ Many GPCRs have been implicated in tumor progression through gene expression profiling.¹⁰ Our own collaborators at the Moffitt Cancer Center have described the overexpression of extracellular receptors in malignant melanomas¹¹ and pancreatic adenocarcinomas¹² by way of both tumor micro arrays (RNA expression profiling) and immunohistochemical (IHC) staining.

1.2 Targeting the Tumor Cell Surface

Philosophically, targeting the distinguishing cell surface features of cancer phenotypes is a type of personalized medicine. Because significant heterogeneity exists between different types of cancers as well as between different patients with the same type of cancer, maintaining a large tool box of targeted therapies may provide the most patient-directed therapy for a large number of

patients. Overexpressed extracellular proteins are ideal targets not only because of comparatively lower expression in normal tissues, but because targeting ligands do not have to cross a cell membrane to interact with the protein allowing for selective targeting of imaging probes and therapeutics to cancerous cells.

Classic examples of targeting cell surface receptors exist from the observation of folate receptor overexpression in many malignancies. In 2011, a Dutch group published their development of a real-time intraoperative guided fluorescence imaging agent using folate conjugated FITC dye.¹³ The structure of their molecular probe is shown in Figure 1.1. This probe was used primary for staging and debulking epithelial ovarian cancers, but laid the framework for future near infrared fluorescent probes that could illuminate deeper tumors.

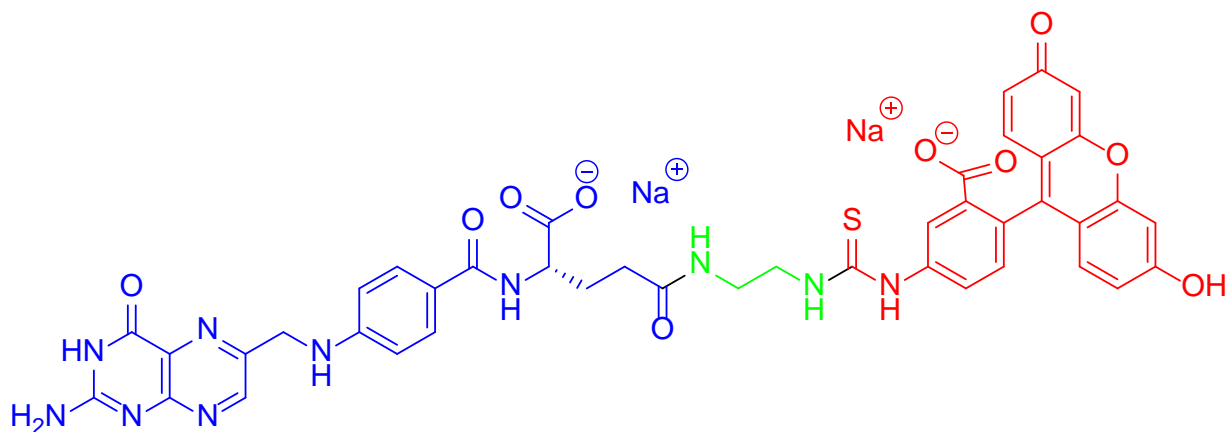


Figure 1.1. FITC targeted agent for folate receptor. Folate is colored blue, an ethylene diamine spacer is shaded green, and the fluorescein isothiocyanate (FITC) is shown in red.

Targeted radiopharmaceuticals provide another avenue by which a targeting ligand can either provide diagnostic/imaging information or act as a therapeutic agent. Typically, targeting ligands are coupled with a chelating molecule that can complex a radionuclide. The type of radioactive disintegration each radionuclide gives off determines how the targeting agent is used.

Emitted radiation may be in the form of high energy photons or positrons when used as imaging agents. Other categories of radionuclides emit β - and/or α - particles. Table 1.1 lists common α -emitting radionuclides. Due to the high energies of these particles, they can be complexed as ligand-targeted payloads. These ‘smart bombs’ may then cause cellular damage to surrounding targeted tissues.¹⁴ As another example of folate receptor targeting, in 2014 a Swiss group complexed the α -emitting radionuclide Tb-149 to a folate analog.¹⁵ They demonstrated efficacy of their targeted therapy in a murine xenograft model by extending overall survival compared with control groups. The targeted delivery of α -emitting radionuclides is termed targeted alpha particle therapy (TAT).

Table 1.1. Summary of common α -emitting radionuclides.

Radionuclide	Emitted Particle(s)	Radioactive Half-Life (min)	α -Particle Energy (meV)
¹⁴⁹ Tb	α (1)	252	4
²¹¹ At	α (1)	432	6
²¹² Bi	α (1), β (1)	60.6	6
²¹² Pb	α (1), β (2)	636	6
²¹³ Bi	α (1), β (2)	46	7.8
²²³ Ra	α (4), β (2)	16,416	6-7
²²⁵ Ac	α (4), β (2)	14,400	6-8

The most commonly utilized chelating molecules for targeted radionuclide therapies in conjunction with biological molecules are 1,4,7,10-tetraazacyclododecane-1,4,7,10-tetraacetic acid (DOTA), diethylene triamine pentaacetic acid (DTPA), and their related analogs (Figure 1.2).

Depending on the how the complexing agent is linked to the targeting ligand, these organic structures feature 3-4 carboxylates that are negatively charged at physiologic pH, and along with the lone pair electrons from each of the 3-4 nitrogens coordinate metal ions like α - and β -emitting radionuclides. Often these chelating molecules are linked to the targeting molecule by forming a new amide bond between an amine on the targeting molecule and a carboxylate on the DOTA/DTPA. This strategy is particularly advantageous in the case of peptide synthesis since the reaction, characterization and purification of the linker addition can be part of the overall synthesis of the targeting ligand.

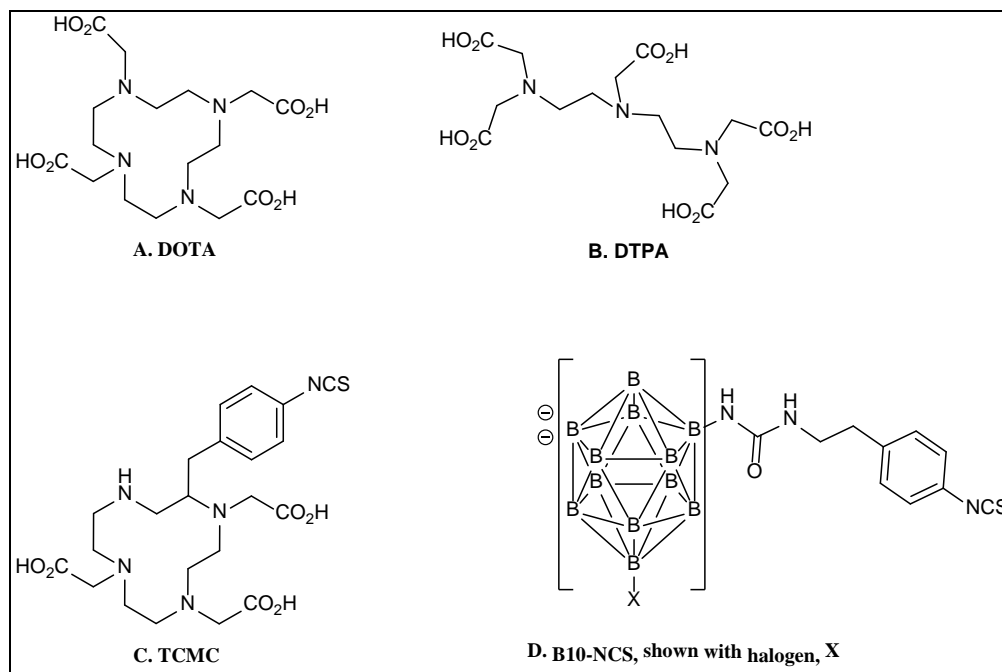
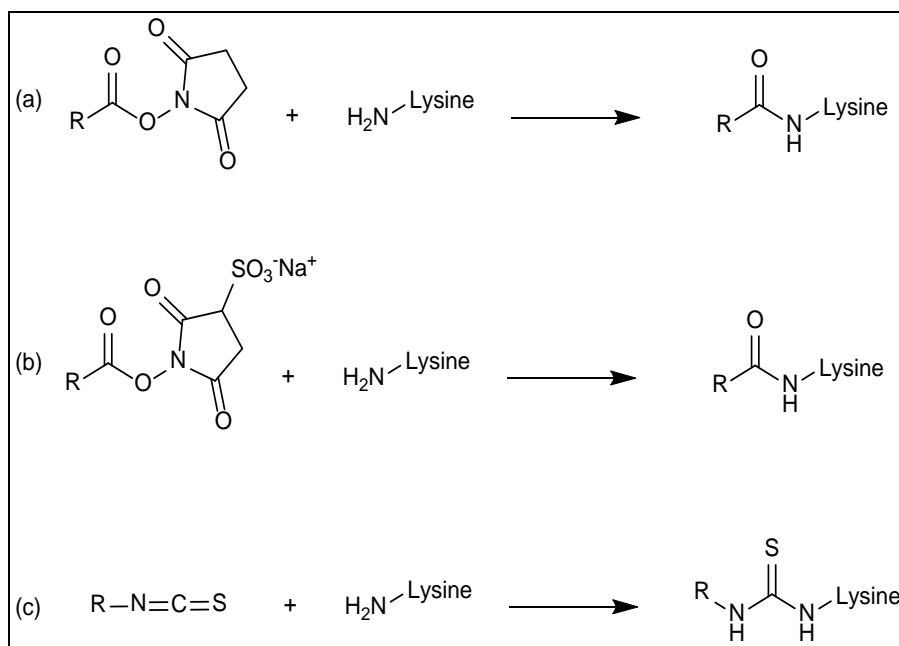


Figure 1.2. Common metal chelators and binders used to attach radionuclides to targeting ligands.

When DOTA/DTPA is linked to proteins like antibodies, amide bonds are often created between a primary amine of surface-exposed lysine residue and an activated carboxylate on the DOTA/DTPA (Scheme 1.1). Another widespread chemistry available to link protein lysines with

DOTA/DTPA is through an isothiocyanate which yields a stable thiourea (Scheme 1.1).^{16,17} While these newly formed amide bonds create the same covalent structure as the synthetic peptide conjugates, there are important distinctions. In the stochastic reaction of any accessible lysine, many different combinations are possible and there is little control over the regioselectivity of the conjugation. It is even possible that targeting ligands could block or hinder the antigen binding sites of the therapeutic antibody. Therefore, site-specific modifications allow for control of the regioselectivity as well as avoidance of targeting ligand interference with antigen-antibody binding.



Scheme 1.1. Common conjugation chemistries used to functionalize biomolecules. Row (a) and (b) show activated NHS and Sulfo-NHS esters reacting to form native amide bonds with lysine side chains from a biomolecule. Row (c) shows isothiocyanate reaction with the same lysine side chain on a biomolecule to form a stable thiourea bond.

The importance of site-specific modifications to biologic targeting motifs has recently been studied. In a 2014 paper from UCLA,¹⁸ diabodies (Dbs) were conjugated site-specifically through reduced cysteines and non-specifically through accessible lysine ϵ -amines to DOTA chelators.

While the tumor-to-blood ratio of the specifically labeled protein was moderately higher than the more heterogeneous product, the more striking result was the renal and hepatic distribution. Kidney uptake levels were almost doubled for the cysteine-labeled Db, and liver uptake levels were reduced for the non-specific amine-labeled Dbs.

1.3 Targeting Molecules

There is no one-size-fits-all answer to the question: what is the best targeting molecule? Rather, the abundance of target molecule classifications allow for a more customized approach to developing targeted agents. Globally, the requirements of a targeting ligand include the ability to concentrate at, and bind to, extracellular targets and the availability of chemical functional groups amenable to the attachment of linkers and chelators. A balance of many other factors such as off-target binding, biodistribution, and pharmacokinetics (particularly with respect to the decaying half-life of the chosen radionuclide) are also critical factors for selection of a proper targeting ligand. Peptides, antibodies, antibody fragments, and even some passive targeting strategies have been investigated to deliver radioisotope payloads.

1.3.1 Antibodies

Full length immunoglobulins (IgGs) are typically in the 150 kDa molecular weight range, and are understood to have high binding affinity and specificity to a broad range of extracellular receptors. Developments in hybridoma cell line technology have opened the door to the

production of monoclonal antibodies (mAbs) which can be labeled with chelating molecules, to which radionuclides can be added. This approach to specifically deliver ionizing radiation payloads is termed radioimmunotherapy (RIT). While many of the examples listed in this section involve radioactive payloads directly conjugated to the protein, antibodies have also been employed to target macromolecular payloads such as nanoparticles and liposomes to cellular targets.¹⁹⁻²¹

A research group based in the Memorial Sloan-Kettering Cancer Center (MSKCC) has reported several accounts of their work labeling trastuzumab with actinium 225. This mAb is the well-known and FDA approved *HER2/ERBB2*-targeting agent. In the beginning, they showed using a spheroid *in vitro* model that their α -RIT scheme could penetrate spheroids, retard growth, and prevent regrowth of colonies in a dose dependent manner.²² While a promising start, this work underscored the importance of target expression and also suggested challenges of RIT due to the slow extravasation of targeting agents in normal tissues and toxicities of released/free decaying daughter products.^{23,24}

Also at MSKCC Scheinberg group's work eventually led to the first clinical trial of an actinium-225 chelated targeted antibody.²⁵ This α -RIT scheme utilized the previously explored humanized anti CD33 antibody, limtuzumab, to target acute myeloid leukemia cells. This work led to the birth of Actinium Pharmaceuticals and a portfolio of targeted ²²⁵Ac conjugated constructs in both preclinical and clinical pipelines.

Other radionuclides in alternative labeling strategies have also been explored. In 2013 Orozco and coworkers coupled a decaborate cage structure (B10, Figure 1.2) with astatine-211 to anti-CD45 antibodies in an attempt to target acute myeloid leukemia.²⁶ More recently Green and

coworkers reported anti-CD20 mAb conjugated with ^{211}At in a similar B10 labeling scheme.²⁷

This study sought to eliminate minimal residual disease (MRD) in a mantle cell lymphoma animal model exploring both disseminated and xenograft models. Interestingly, the disseminated disease model showed remarkable results with 70% disease eradication, while the subcutaneous lymphoma xenograft group had only modest benefit with no cured animals. Therefore while α -RIT is attractive for disseminated disease, benefits appear to be modest at best for bulkier tumors, highlighting the need for adequate tumor perfusion for the targeted alpha therapy to be fully effective.

1.3.2 Antibody Fragments

A limitation of full-size IgGs is their typical 1-3 week serum stability. While this durability may be advantageous for certain therapeutic applications, in RIT it can be serious liability. Excess antibody can continue to circulate, lowering the tumor-to-nontumor (T/NT) ratio particularly with respect to the tumor-to-blood (T/B) ratio. Finally, high levels of continuously circulating alpha-emitters results in hematological toxicities as well as extravasation in normal tissues.

In attempts to shorten the long plasma half-life of full length antibodies, many groups have sought to reduce the size and stability of the mAb while retaining their advantageous binding characteristics. To this end antibodies have been modified through both enzymatic cleavage to smaller antibody fragments as well as *de novo* protein engineering.^{28,29} For comparison, the engineered antibody fragments of diabodies (Db) and minibodies (Mb) have typical circulating half-lives of 2-5 and 5-12 hours respectively, compared to 1-3 weeks for full-length IgG. Monovalent

and bivalent affibodies (7 and 15 kDa respectively) have been developed with targeting specificity to *HER-2* and plasma half-lives of roughly 45 minutes.³⁰ The science of antibodies is ever progressing and new classes are still being observed in nature; nanobodies (13-14 kDa) are heavy chain-only antibodies that have been isolated from *Camelidae* and have lately been conjugated with theranostic radionuclides.³¹ These new categories of targeting constructs are adding to the growing body of evidence that there may be a so-called 'Goldilocks' zone in terms of size of targeting constructs.

1.3.3 Peptides

Peptides are oligomers of amino acids that may exhibit secondary structure, include branched or linear frameworks, and may be composed of varying amounts of non-canonical monomers. The polypeptide chains of peptides can have anywhere from 2 to 70 amino acids but more typical examples of targeting peptides are made of less than 10-15 amino acids (1,000-1,500 MW). Owing to this molecular weight and their capacity to be synthesized and modified with conventional organic synthesis techniques, peptides have long been utilized as targeting agents for radionuclide therapies and diagnostic applications.

Since the 1980s, analogs of the endogenous peptide hormone somatostatin have been developed as therapeutics for neuroendocrine disorders.³² The FDA approved octreotide (OC, Figure 1.3) a cyclic octapeptide upon which much of the early peptide receptor radionuclide therapy (PRRT) was based. Chelating molecules were attached to octreotide and various

radionuclides for β - and α -emission therapies have been reported. Figure 1.3 details the structure of OC and two of its commonly used PRRT ligand analogs, DOTATOC and DOTATATE.

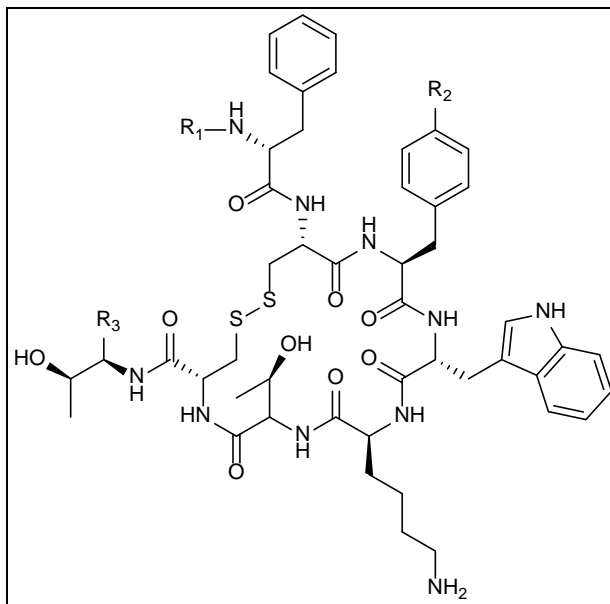


Figure 1.3. The somatostatin mimetic octreotide and its DOTA-containing analogs. octreotide: $R_1 = H$, $R_2 = H$, $R_3 = CH_2OH$; DOTATOC (endotreotide): $R_1 = DOTA$, $R_2 = OH$, $R_3 = CO_2H$; DOTATE (octreotate): $R_1 = DOTA$, $R_2 = OH$, $R_3 = CH_2OH$

Nephrotoxicity is often one of the most pressing theoretical concerns with PRRT due to known reabsorption of the labeled peptide during glomerular filtration.³³ This is especially problematic for beta therapy, more so than with alpha emitting therapies. The first published account of the alpha-emitter ^{213}Bi in an OC analog (DOTATOC, Figure 1.3) was reported in 2006. The radio-peptide ligand was shown to retain its affinity for the somatostatin receptor and inhibited tumor growth in a somatostatin receptor-positive rat pancreatic tumor model (CA20948).³⁴ Importantly the study followed major organ toxicities in rodents. Little to no nephro-, hepatic-, or hematological toxicities were observed in the various doses (13-22.2 Mbcq). The organs with the most toxicity were the adrenals and the pancreas, both of which are known to

express low levels of somatostatin receptors. This favorable toxicity profile may be due, in part, to the limited range of the ejected α -particles and also the short radioactive half-life of ^{213}Bi . Ultimately this study demonstrated that the high energy α -emitting radionuclides do not necessarily have the same toxicities of their β -emitting analogs and represent a more attractive therapy.

In addition to its more favorable toxicity profile, alpha-emitting therapies have been shown to have improved efficacy over their beta-emitting counterparts. In a recent report, tumors that had become radioresistant to β -therapy (^{90}Y and ^{190}Lu - DOTATOC) responded to ^{213}Bi -DOTATOC and cold octreotide therapy in a clinical model of 8 human patients.³⁵ The treatment for each patient was individualized according to their particular disease state and all patients had substantially positive outcomes in terms of tumor regression and survival. Critically, the acute hematological toxicity normally associated with the analogous β -therapies were only moderate with alpha therapies. And where β -therapies are typically limited by their nephrotoxicity, this report suggested only mild reduction in acute renal function. No other major acute toxicities were reported. This first-in-human report of peptide-targeted alpha therapeutic may lay the ground work for future human TAT using peptide-targeted systems.

1.4 Medicinal Chemistry of Targeting Ligands

As previously touched upon, characteristics of various targeting ligands like lipophilicity, molecular weight, and ionization potential are all critical, and modifiable, variables that help modulate targeting ligand properties. For example, small, polar compounds are more likely to

undergo renal excretion and the addition of a PEG linker adds water solubility, bulk, and may help avoid kidney toxicities. Conversely, the removal of an ionizable group (eg. sulfonate or protonated amine at physiologic pH) during medicinal chemistry design may make the targeting ligand more hydrophobic and shift clearance predominantly to the liver. Therefore when working to reduce targeting ligand complexity or increase the ease of synthesis, these physical attributes of the compound must be considered.

An example of the biology mantra, “structure begets function,” is exemplified in the vignette of constrained peptide ligands. Early work from Hruby and collaborators showed how subtle changes to an endogenous peptide hormone like oxytocin could induce conformational restrictions.³⁶⁻³⁸ By limiting available conformational space that the peptide can ‘sample,’ the more correct binding conformation may be found. From an entropic standpoint, enacting these constraints on the binding pharmacophore may yield a tighter binding ligand. Additionally, the change in ligand structure may have the effect of changing the function of the ligand. Whereas the comparatively floppy peptide ligand, oxytocin, was shown to bind to its receptor and elicit downstream signaling, constraining the sequence with a penicillamine point mutation created an antagonist ligand that bound the receptor but inhibited signal transduction. Today synthetic oxytocin is approved clinically to hasten childbirth while constrained antagonist analogs are used to stop preterm labor.³⁹

Antibodies and engineered fragments can also benefit from medicinal chemistry optimization. Many chelators and linkers covalently attached to antibodies and their fragments produce heterogeneous products. In the most typical fashion of linker attachment, surface accessible lysine side chains are utilized to form covalent bonds with radionuclide chelating

molecules (Scheme 1.1). Site specific antibody modifications can yield more homogeneous products. The Rader group at Scripps Florida has made such progress by engineering a selenocysteine residue into targeting antibodies, allowing for complete control of regiochemistry during functionalization due to the increased nucleophilicity of selenium over sulfur.⁴⁰

Another route to increasing T/NT ratios is through pretargeting. These strategies operate under the premise that nonradiolabeled bifunctional targeting agents can be administered to the patient and allowed to sufficiently converge on their target. Once the unbound portion has cleared, a fraction of radiolabeled molecule with a binding affinity for the bifunctional targeting agent is administered. Typically, the radiolabeled agent is designed to clear quickly if unavailable for binding, thus lowering off target radiation. Typical binding partners amenable to pretargeting schemes include avidin/streptavidin – biotin, DNA – DNA, and antibody- hapten interactions.⁴¹ For a more in-depth analysis of pretargeting strategies please see the recent review article from Frampas and colleagues.⁴²

Other important research regarding linkers has uncovered different methods to reduce kidney toxicity due to the renal reabsorption of radiolabeled peptides and antibody fragments as they are filtered by the glomerulus. By taking advantage of renal brush border enzymes, the radionuclide can be cleaved from targeting ligand and excreted. By engineering an antibody fragment with C-terminal lysine, and subsequently modifying the ϵ -amine with DOTA:indium-111, Li and coworkers demonstrated a 50-60% reduction in kidney uptake of the radionuclide.⁴³ More recently the Akizawa group probed the brush border enzymes to understand more about their specificity. They were able to pinpoint a glycine-tyrosine linkage that specifically cleaved a

radio-iodinated benzoate derivative from an antibody Fab fragment.⁴⁴ Presumably a similar approach could be used for the α -emitting halogen, ²¹¹At.

Polyethylene glycol (PEG) linkers are made of repeating $-\text{CH}_2\text{CH}_2\text{O}-$ monomers and are commonly employed by chemists to alter biodistribution and pharmacokinetics. PEGs can be prepared in two categories, polymeric and discrete oligomers. Bifunctionalized versions of these polymers can link targeting molecules with the chelating agent or just add bulk/solubility to smaller molecular weight entities. Researchers wishing to reduce immunologic response to nanoparticles have been known to decorate their macromolecules with PEG¹⁹, as was the case with McLaughlin and coworkers with PEG12 linker used to link 4 nm, ²²⁵Ac containing, nanoparticles to mAb.⁴⁵

1.5 Vision for This Dissertation

Although there are advantages and disadvantages to both antibody- and peptide-based targeting molecules, the theme of this current research utilizes peptides as targeting ligands for many reasons. First, peptides may be synthesized using conventional organic chemistry techniques and through solid phase peptide synthesis. Synthesis may use manual, automated, or a combination of both methods. There is a degree of control in these types of synthesis, which may be monitored, adapted, and optimized to create high purity, discrete ligands. Furthermore, the design of each peptide ligand may be engineered to include non-canonical amino acids and monomers. Structures may be branched and the attachment of various molecular payloads is straightforward. Overall, a chemist has remarkable control over the synthesis of peptide ligands.

Secondly, the physical and biological properties of our peptide ligands match the aims of our research projects. All of our targets are cell surface receptors on vascularized tumor tissues not present in the central nervous system. Peptide ligands are ideal for targeting these receptors since they do not passively cross cell membranes or the blood-brain barrier. Finally, the kinetics and distribution of our ligands are good matches for the various payloads they are capable of carrying, from α -emitting Ac²²⁵ to fluorescent dyes, and immune effectors.

Each of the following three chapters in this dissertation contains a research project regarding a single extracellular receptor that is bonafide biomarker of a particular cancer type. Peptide ligands were designed and synthesized to have various targeting characteristics for each receptor. Furthermore, the peptide ligands were covalently attached to a different payload in each project, each with their own purpose. All of our targeting peptides have at least one imaging modality, and many have a therapeutic aim as well. The overarching theme of this body of work is that peptides are effective targeting ligands for cancer imaging and therapeutic applications.

1.6 References:

- (1) Mortality, G. B. D.; Causes of Death, C. *Lancet* **2015**, *385*, 117.
- (2) Global Burden of Disease Cancer, C. *JAMA Oncology* **2015**, *1*, 505.
- (3) Society, A. C.; Society, A. C., Ed. Atlanta, GA, 2016.
- (4) Green, D. R.; Evan, G. I. *Cancer cell* **2002**, *1*, 19.
- (5) Diaz-Cano, S. J. *International Journal of Molecular Sciences* **2012**, *13*, 1951.
- (6) Lotem, J.; Netanel, D.; Domany, E.; Sachs, L. *Proceedings of the National Academy of Sciences of the United States of America* **2005**, *102*, 18556.
- (7) Kampen, K. R. *The Journal of Membrane Biology* **2011**, *242*, 69.
- (8) Iqbal, N.; Iqbal, N. *Molecular Biology International* **2014**, *2014*, 9.
- (9) Weitman, S. D.; Lark, R. H.; Coney, L. R.; Fort, D. W.; Frasca, V.; Zurawski, V. R.; Kamen, B. A. *Cancer research* **1992**, *52*, 3396.

- (10) Li, S.; Huang, S.; Peng, S. B. *Int J Oncol* **2005**, *27*, 1329.
- (11) Tafreshi, N. K.; Silva, A.; Estrella, V. C.; McCardle, T. W.; Chen, T.; Jeune-Smith, Y.; Lloyd, M. C.; Enkemann, S. A.; Smalley, K. S. M.; Sondak, V. K.; Vagner, J.; Morse, D. L. *Molecular Pharmaceutics* **2013**, *10*, 3175.
- (12) Morse, D. L.; Balagurunathan, Y.; Hostetter, G.; Trissal, M.; Tafreshi, N. K.; Burke, N.; Lloyd, M.; Enkemann, S.; Coppola, D.; Hruby, V. J.; Gillies, R. J.; Han, H. *Biochemical Pharmacology* **2010**, *80*, 748.
- (13) van Dam, G. M.; Themelis, G.; Crane, L. M.; Harlaar, N. J.; Pleijhuis, R. G.; Kelder, W.; Sarantopoulos, A.; de Jong, J. S.; Arts, H. J.; van der Zee, A. G.; Bart, J.; Low, P. S.; Ntziachristos, V. *Nat Med* **2011**, *17*, 1315.
- (14) Sgouros, G.; Roeske, J. C.; McDevitt, M. R.; Palm, S.; Allen, B. J.; Fisher, D. R.; Brill, A. B.; Song, H.; Howell, R. W.; Akabani, G.; In collaboration with the SNM MIRD Committee: Wesley E. Bolch, A. B. B., Darrell R. Fisher, Roger W. Howell, Ruby F. Meredith, George Sgouros, Barry W. Wessels; Zanzonico, P. B. *Journal of Nuclear Medicine* **2010**, *51*, 311.
- (15) Müller, C.; Reber, J.; Haller, S.; Dorrer, H.; Köster, U.; Johnston, K.; Zhernosekov, K.; Türlér, A.; Schibli, R. *Pharmaceutics* **2014**, *7*, 353.
- (16) Baidoo, K. E.; Milenic, D. E.; Brechbiel, M. W. *Nuclear Medicine and Biology* **2013**, *40*, 592.
- (17) Gouard, S.; Pallardy, A.; Gaschet, J.; Faivre-Chauvet, A.; Bruchertseifer, F.; Morgenstern, A.; Maurel, C.; Matous, E.; Kraeber-Bodere, F.; Davodeau, F.; Cherel, M. *Nucl Med Biol* **2014**, *41 Suppl*, e30.
- (18) Tavaré, R.; Wu, W. H.; Zettlitz, K. A.; Salazar, F. B.; McCabe, K. E.; Marks, J. D.; Wu, A. M. *Protein Engineering Design and Selection* **2014**, *27*, 317.
- (19) Chang, M.-Y.; Seideman, J.; Sofou, S. *Bioconjugate Chemistry* **2008**, *19*, 1274.
- (20) Woodward, J.; Kennel, S. J.; Stuckey, A.; Osborne, D.; Wall, J.; Rondinone, A. J.; Standaert, R. F.; Mirzadeh, S. *Bioconjugate Chemistry* **2011**, *22*, 766.
- (21) Zhu, C.; Bandekar, A.; Sempkowski, M.; Banerjee, S. R.; Pomper, M. G.; Bruchertseifer, F.; Morgenstern, A.; Sofou, S. *Molecular Cancer Therapeutics* **2016**, *15*, 106.
- (22) Ballangrud, Å. M.; Yang, W.-H.; Palm, S.; Enmon, R.; Borchardt, P. E.; Pellegrini, V. A.; McDevitt, M. R.; Scheinberg, D. A.; Sgouros, G. *Clinical Cancer Research* **2004**, *10*, 4489.
- (23) Jaggi, J. S.; Seshan, S. V.; McDevitt, M. R.; LaPerle, K.; Sgouros, G.; Scheinberg, D. A. *Journal of the American Society of Nephrology* **2005**, *16*, 2677.
- (24) Singh Jaggi, J.; Kappel, B. J.; McDevitt, M. R.; Sgouros, G.; Flombaum, C. D.; Cabassa, C.; Scheinberg, D. A. *Cancer research* **2005**, *65*, 4888.
- (25) Douer, D.; Center, M. S. K. C., Ed.; National Institute of Mental Health; University of Virginia: 2015.
- (26) Orozco, J. J.; Bäck, T.; Kenoyer, A.; Balkin, E. R.; Hamlin, D. K.; Wilbur, D. S.; Fisher, D. R.; Frayo, S. L.; Hylarides, M. D.; Green, D. J.; Gopal, A. K.; Press, O. W.; Pagel, J. M. *Blood* **2013**, *121*, 3759.
- (27) Green, D. J.; Shadman, M.; Jones, J. C.; Frayo, S. L.; Kenoyer, A. L.; Hylarides, M. D.; Hamlin, D. K.; Wilbur, D. S.; Balkin, E. R.; Lin, Y.; Miller, B. W.; Frost, S. H. L.; Gopal, A. K.; Orozco, J. J.; Gooley, T. A.; Laird, K. L.; Till, B. G.; Bäck, T.; Sandmaier, B. M.; Pagel, J. M.; Press, O. W. *Blood* **2015**, *125*, 2111.
- (28) Yokota, T.; Milenic, D. E.; Whitlow, M.; Schlom, J. *Cancer research* **1992**, *52*, 3402.
- (29) Hudson, P. J.; Souriau, C. *Nat Med* **2003**, *9*, 129.
- (30) Steffen, A. C.; Almqvist, Y.; Chyan, M. K.; Lundqvist, H.; Tolmachev, V.; Wilbur, D. S.; Carlsson, J. *Oncol Rep* **2007**, *17*, 1141.
- (31) D'Huyvetter, M.; Xavier, C.; Caveliers, V.; Lahoutte, T.; Muyltermans, S.; Devoogdt, N. *Expert Opinion on Drug Delivery* **2014**, *11*, 1939.

- (32) Bauer, W.; Briner, U.; Doepfner, W.; Haller, R.; Huguenin, R.; Marbach, P.; Petcher, T. J.; Pless, J. *Life Sciences* **1982**, *31*, 1133.
- (33) Maack, T.; Johnson, V.; Kau, S. T.; Figueiredo, J.; Sigulem, D. *Kidney International* **1979**, *16*, 251.
- (34) Norenberg, J. P.; Krenning, B. J.; Konings, I. R. H. M.; Kusewitt, D. F.; Nayak, T. K.; Anderson, T. L.; de Jong, M.; Garmestani, K.; Brechbiel, M. W.; Kvols, L. K. *Clinical Cancer Research* **2006**, *12*, 897.
- (35) Kratochwil, C.; Giesel, F. L.; Bruchertseifer, F.; Mier, W.; Apostolidis, C.; Boll, R.; Murphy, K.; Haberkorn, U.; Morgenstern, A. *European Journal of Nuclear Medicine and Molecular Imaging* **2014**, *41*, 2106.
- (36) Meraldi, J. P.; Hruby, V. J.; Brewster, A. I. *Proceedings of the National Academy of Sciences* **1977**, *74*, 1373.
- (37) Wood, S. P.; Tickle, I. J.; Treharne, A. M.; Pitts, J. E.; Mascarenhas, Y.; Li, J. Y.; Husain, J.; Cooper, S.; Blundell, T. L.; Hruby, V. J.; al, e. *Science* **1986**, *232*, 633.
- (38) Hruby, V. J. *Trends in Pharmacological Sciences* **1987**, *8*, 336.
- (39) Hruby, V. J.; Chan, W. Y.; Rockway, T. W.; Hlavacek, J.; Ormberg, J. In *Peptides: Design, Synthesis, and Biological Activity*; Basava, C., Anantharamaiah, G. M., Eds.; Birkhäuser Boston: Boston, MA, 1994, p 199.
- (40) Li, X.; Patterson, J. T.; Sarkar, M.; Pedzisa, L.; Kodadek, T.; Roush, W. R.; Rader, C. *Bioconjugate Chemistry* **2015**, *26*, 2243.
- (41) van Rij, C. M.; Frielink, C.; Goldenberg, D. M.; Sharkey, R. M.; Lütje, S.; McBride, W. J.; Oyen, W. J. G.; Boerman, O. C. *Cancer Biotherapy & Radiopharmaceuticals* **2014**, *29*, 323.
- (42) Frampas, E.; Rousseau, C.; Bodet-Milin, C.; Barbet, J.; Chatal, J.-F.; Kraeber-Bodéré, F. *Frontiers in Oncology* **2013**, *3*, 159.
- (43) Li, L.; Olafsen, T.; Anderson, A.-L.; Wu, A.; Raubitschek, A. A.; Shively, J. E. *Bioconjugate Chemistry* **2002**, *13*, 985.
- (44) Akizawa, H.; Imajima, M.; Hanaoka, H.; Uehara, T.; Satake, S.; Arano, Y. *Bioconjugate Chemistry* **2013**, *24*, 291.
- (45) McLaughlin, M. F.; Woodward, J.; Boll, R. A.; Wall, J. S.; Rondinone, A. J.; Kennel, S. J.; Mirzadeh, S.; Robertson, J. D. *PLoS ONE* **2013**, *8*, e54531.

CHAPTER TWO:

**MELANOCORTIN 1 RECEPTOR TARGETING LIGANDS AND THE DEVELOPMENT
OF A TARGETED RADIOPHARMACEUTICAL AND COMPANION DIAGNOSTIC
IMAGING AGENT**

2.1 Introduction

Although it accounts for just over one percent of all skin cancer diagnoses, melanoma is the most deadly type of skin cancer and the incidence continues to rise each year.¹ With approximately 80,000 new diagnoses in 2016, the American Cancer Society estimates that over 10,000 people will succumb to the disease this year.² Cutaneous melanomas account for the majority of cases (91%), while uveal melanomas, for which there is little pharmacotherapy, make up roughly 3% of diagnoses.^{3,4} Melanoma is characterized as a malignancy of the melanocyte, present in the basal layer of the epidermis. In normal tissues, these dendritic-like cells are responsible for skin pigmentation through melanin production. Given their proximity to blood vessels and the lymph system, melanoma often metastasizes quickly, necessitating systemic therapies as compared to localized excision common in other skin cancers.

Clinical staging of melanoma is based on depth of tumor growth, lymph node involvement, and degree of metastases. Conventional therapies for cutaneous melanomas consist of wide surgical excision and external beam radiation which are particularly effective for early stage disease, and yield five and ten year survival rates of 92% and 89% respectively.² However therapy for later

stage diseases is significantly less effective. Five and ten year survival rates of malignant melanomas that have spread past their origin are 63% and 17% respectively.² The poor prognosis, especially with late stage disease, coupled with the growing incidence of melanomas illustrates a definitive need for new treatments and diagnostic tools.

Recent developments have shown differential gene and protein expression levels in subsets of melanomas. For instance, the variable expression of *BRAF* and *NRAS* mutations have been found in 58% of primary melanomas and 63% of metastases,⁵ and have led to new targeted therapies including small molecule inhibitors, dabrafenib⁶ and vemurafenib.⁷ While these and other non-conventional therapies⁸ show tremendous promise, they still leave a large portion of afflicted patients without targeted therapies. The melanocortin-1 receptor (MC1R) has been found in 80% of cutaneous malignant melanomas and 95% of uveal melanomas according to mRNA expression,⁹ and the MC1R is expressed as protein in 97% of melanoma metastases (highly overexpressed in 50%).¹⁰ Furthermore the MC1R is expressed in 42% of metastases that aren't candidates for current melanoma targeted therapy.

The MC1R is one of five isotypes in a family of G-protein coupled receptors present on the surface of melanocytes.¹¹ Isotypes of the receptor have variable expression in normal tissues like kidneys and lungs (MC5R), adrenal glands (MC2R), hypothalamus (MC3R), heart (MC4R), and brain, hair and skin (MC1R). Because most peptides agents do not readily cross a normal blood-brain barrier (BBB), it is easy to discover MC1R peptide ligands that do not concentrate in the brain. Due to the high levels of MC1R cell-surface expression in skin, it serves as good biomarker of malignant, uveal, and metastatic melanomas, making it a potentially valuable target for imaging and targeted radiopharmaceuticals.

Melanotropins are a family of endogenous peptide hormones that are known to interact with melanocortin receptors. Alpha-melanocyte stimulating (α -MSH) hormone is one such peptide that is a non-selective agonist, and is understood to help regulate appetite, metabolism, and sexual function. Based on the primary sequence of α -MSH (Ac-Ser-Tyr-Ser-Met-Glu-His-Phe-Arg-Trp-Gly-Lys-Pro-Val-COOH), a peptidomimetic was developed in the 1980s with high affinity and potency for MC1R ($K_i = 1.8$ nM).¹² This peptide included 2 point mutations at the 4- and 7- positions giving rise to the name 4Nle-7DPhe- α -MSH (NDP- α -MSH). This melanotropin analog lacked selectivity for the MC1R, as it still bound to the MC4R and MC5R isotypes with $K_i = 19$ nM and 9.9 nM, respectively.

Due to the value of MC1R as a biomarker, much SAR research has been done on the pharmacophore of α -MSH to increase its affinity and selectivity for the MC1R.¹³⁻¹⁶ The common pharmacophore in all analogs developed to date have been collectively referred to as the 'message sequence,' a section of four amino acids (His-DPhe-Arg-Trp) attributed to the binding affinity of the ligand.¹⁷ However it was not until the Morse group, in collaboration with BIO5 in Arizona, completed SAR work on both the C- and N- termini of the message sequence that acceptable selectivity was obtained. Table 2.1 lists the most valuable analogs to emerge from this collaboration.¹⁸ The optimized ligand identified was one that capped the N-terminus with a 4-phenylbutyric acid moiety and included a glycine spacer between the C-terminal lysine and the message sequence. This compound (Figure 2.2) exhibits high selectivity for the MC1R over the MC4R and MC5R isotypes.

Some groups have capitalized on the targeting ability of melanotropin analogs by arming the targeting ligands with payloads appropriate for imaging or cytotoxic therapies. Chen and

colleagues made use of the non-selective NDP- α -MSH to image tumors with an attachment of ^{99m}Tc ,¹⁹ while the Morse group and collaborators have examined the imaging capabilities of their lead melanotropin analog by attaching gadolinium-texaphyrin²⁰ polymer micelles to the C-terminal lysine for magnetic resonance imaging.^{18,21} Despite the functionalization with relatively large (~90 nm) micelles, the peptide ligand retained its selective targeting for the MC1R.

Table 2.1. Select previously reported SAR work done on melanotropin message sequence.¹⁸

No	Structure	K _i (nM)				
		MC1 R	MC4 R	MC5 R	1R/4 R	1R/5 R
1	4-phenylbutyryl-His-DPhe-Arg-Trp-NH ₂	0.17	160	27	950	160
2	Ac-homophe-His-DPhe-Arg-Trp-NH ₂	1.8	988	58	560	
3	4-phenylbutyryl-His-DPhe-Arg-Trp-Gly-Lys(hex-5-ynoyl)-NH ₂	0.24	254	46	1058	192
4	NDP- α -MSH	1.8	19	9.9	10	5.5
5	3-targeted polymer	26	~	~	~	~
6	3-targeted micelles	2.9	~	~	~	~

Regarding therapeutics, targeted alpha-particle therapy (TAT) has been utilized with both peptides and antibodies as targeting agents and is an attractive option. The background of TAT is discussed at length in the introduction to this dissertation; in brief, the disintegrations of radioactive ^{225}Ac produce a decay chain of daughter products and four total alpha particles (Figure 2.1). These alpha particles have the mass of helium nuclei and when ejected from the nuclei at great velocities, have tremendous kinetic energy. When targeted to a tumor by peptide targeting of the overexpressed cell-membrane receptors, this cytotoxic alpha-emission can destroy localized tissues.

Analogous to the imaging work completed by Chen and Morse, the purpose of this research was to complex the cytotoxic radionuclide actinium-225 to an optimized version of the

MC1R Ligand (MC1RL). In tandem with this targeted alpha-particle therapy goal, the promise of developing a companion imaging agent was tantalizing. The vision was to create a compound that could be complexed with an imaging radionuclide to assess susceptibility to TAT, a therapeutic radionuclide for TAT, and then repeated imaging to assess efficacy following treatment. Furthermore, by using a peptidomimetic as the targeting ligand, the pharmacokinetics, dynamics, and biodistribution could be optimized with simple modifications to the chemistry.

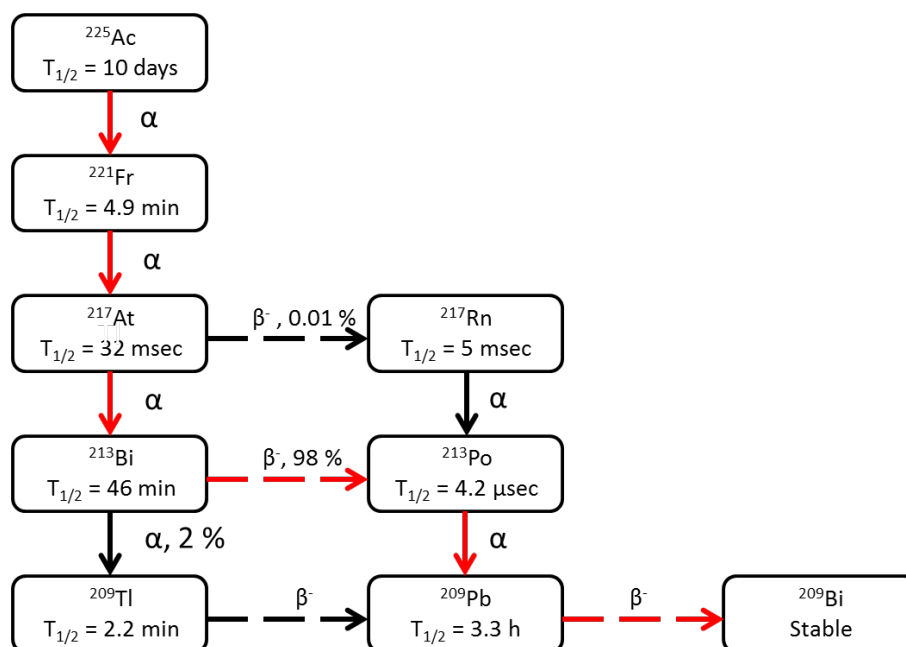


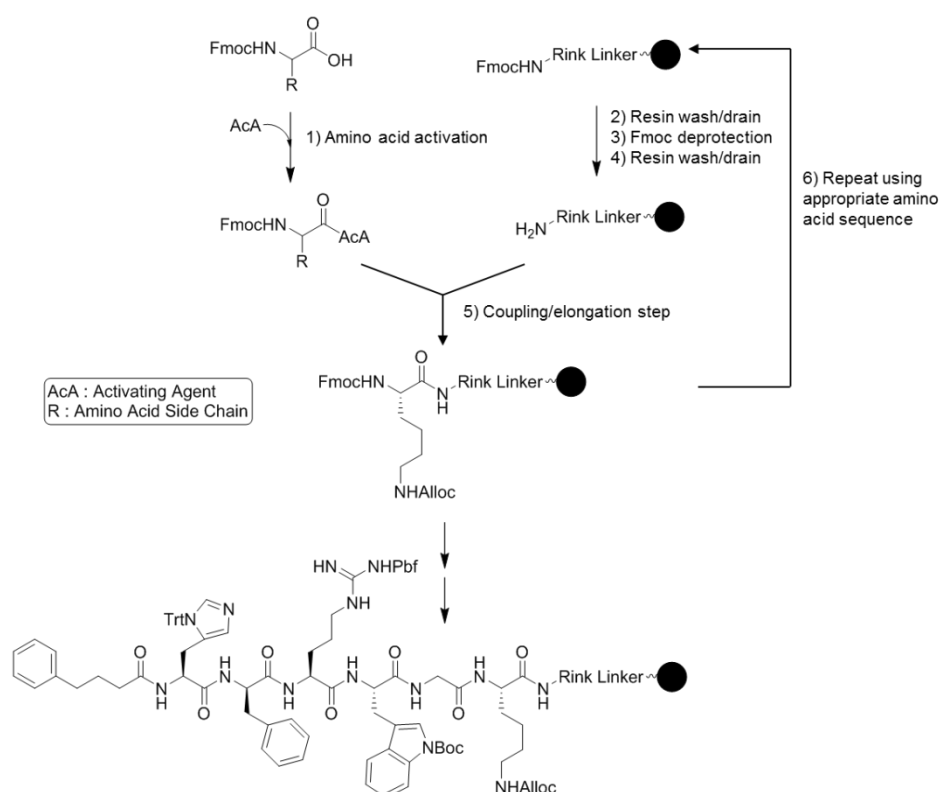
Figure 2.1. Actinium-225 decay pathway.

2.2 Results and Discussion

2.2.1 Peptide Design and Synthesis

The linear MC1RL message sequence has previously been elucidated,¹⁸ with the C-terminal lysine offering a branching point by utilizing an orthogonal allyloxycarbonyl (alloc) protecting group on its ϵ -amine. Not only was this branching critical for the inclusion of a payload

on the targeting ligand, it also helped facilitate efficient synthesis. Using this branching point, the targeting ligand was synthesized in larger batches (typically 0.1-0.5 mmol) up to the point of alloc deprotection. Different linkers and payloads were then appended in split syntheses. Importantly, all of this synthesis was performed on solid support, yielding highly pure product in a manageable fashion. Scheme 2.1 provides an overview of the solid phase peptide synthesis (SPPS) employed for this peptide and its analogs.



Scheme 2.1. Typical solid phase peptide synthesis of linear MC1RL.

Previously, the C-terminal branched lysine of this targeting ligand was coupled to a hexynoic acid monomer (Figure 2.1). This functional group enabled functionalization through so-called ‘Click Chemistry’²² to large (91 nm) polymer micelles with and without texaphyrin-gadolinium.^{21,23} Remarkably, the attachment of macromolecules did not disrupt the binding of the

peptide ligand with the extracellular receptor. The binding affinities of the parent peptide and polymer micelles were reported as 0.24 nM and 2.9 nM, respectively.^{18,21} The ligands also maintained their specificity for the MC1 isoform of the receptor. It was inferred from these studies that the linker tethering the payload to the targeting peptide may have been important to retain high binding affinity for the receptor-target.

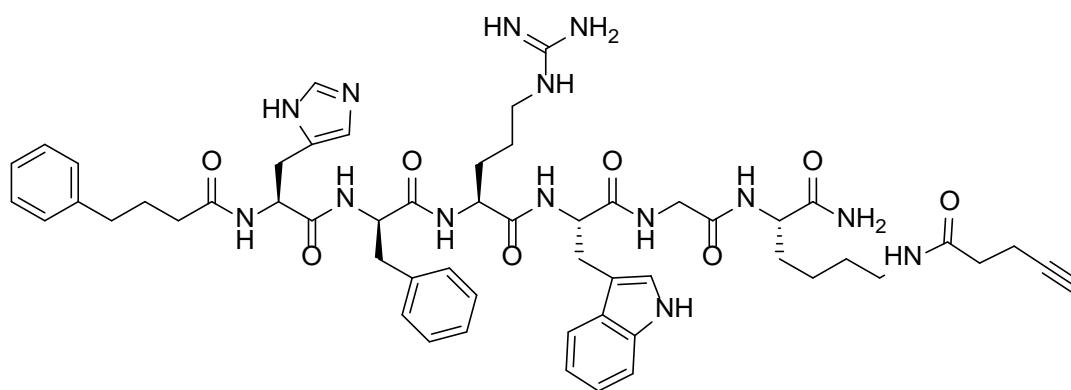


Figure 2.2. Structure of previously reported lead MC1RL targeting ligand.(Barkey, 2011)²³

To mimic the number of spacer atoms in the linker, the first MC1RL compounds for this project included a 6-aminohexanoic acid linker in place of the 5-hexynoic acid linker. The linker was both inexpensive and commercially available as the Fmoc-protected amino acid. It was coupled using the same SPPS strategy with HCTU activation shown in Scheme 2.1. The MC1RL analog was then finished by attaching a DTPA metal-chelating motif to the aminohexanoic acid linker. After an acid cleavage, lyophilization, and subsequent HPLC purifications MC1RL-Ahx-DTPA was isolated as a pure white powder. This compound is shown Figure 2.3, R².

This MC1RL-Ahx-DTPA compound was then complexed with europium and tested for binding affinity for the MC1R. The Morse group ran this assay by testing direct peptide binding on whole-cells expressing the receptor. The detection method for this experiment was release of europium from the complex, and the direct binding of the compound was measured at 1.3 nM (K_d).

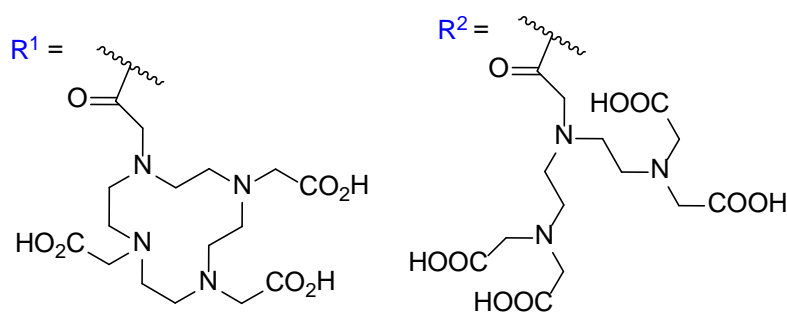
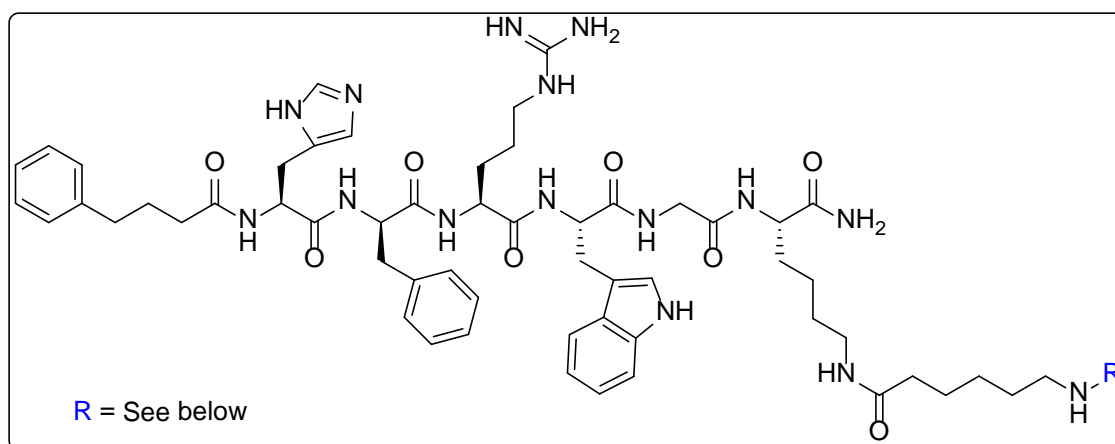


Figure 2.3. Structures of MC1RL-Ahx-DOTA (R^1) and MC1RL-Ahx-DTPA (R^2).

Having proved that a chelating molecule could be functionalized to the C-terminus of MC1RL, complexed with a lanthanide metal and still retain binding affinity, the next compound synthesized contained a DOTA motif. This DOTA molecule would complex positive-three charge metals with tighter binding, and thus be more suitable for *in vivo* experiments. This second

MC1RL analog, MC1R-Ahx-DOTA (Figure 2.3, R¹), was synthesized in an analogous fashion to the point of metal-chelator coupling. At this step, a tri-*t*-butyl-protected DOTA molecule was coupled to the C-terminal branch through an amide bond as shown in Schemes 2.1 and 2.2. Peptide was subsequently cleaved from the resin, and chromatographed to greater than 95% purity by reverse phase HPLC. After lyophilization, the targeting ligand was isolated as a dry white powder in 29% overall yield (93 mg, 0.0631 mmol). MALDI-TOF analysis determined the monoisotopic mass (M+H⁺) to be 1474.9036 (expected: 1474.7954). Table 2.2 lists other linear analogs, including MC1RL-Ahx-DTPA and MC1RL-Ahx-DOTA, which have been synthesized for this project.

2.2.2 Chelation of Metals

Surrogate metal atoms were utilized for method development in place of radioactive radionuclides, our ultimate imaging and therapeutic agents. Due to its oxidation state, size, and periodic table relationship, lanthanum was chosen as a surrogate for the alpha-particle emitting radionuclide, actinium-225. The natural abundance isotopes of gallium (67/69) were an obvious substitute for the positron-emitting radionuclide, gallium-68. Both of these surrogate metals were complexed with the purified MC1RL-Ahx-DOTA (Scheme 2.2).

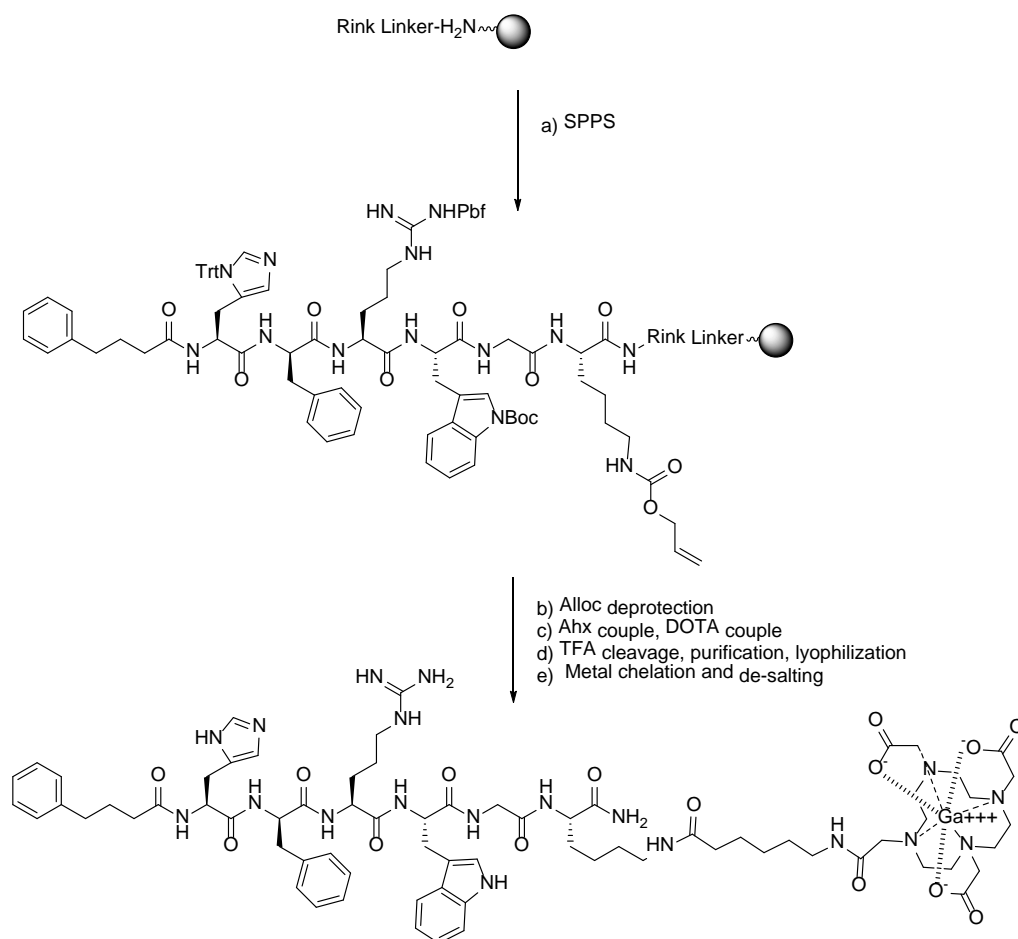
The complexation reaction was affected by stirring the pure DOTA compound with the three charge state chloride salt of each metal in 100 mM ammonium acetate, pH 8. Initial experiments were carried out at room temperature with mechanical stirring. The reaction was

monitored with analytical scale HPLC experiments using pH 6 buffered mobile phase buffer to slow the metal release from complexation.

Table 2.2. Linear MC1RL analogs that have been synthesized and characterized by mass spectroscopy.

Compound	Formula	Expected Mass (M+H ⁺)	Experimental Mass (M+H ⁺)
MC1RL	C ₅₀ H ₆₆ N ₁₄ O ₇	975.5312	975.5312
MC1RL-Ahx-FBA	C ₆₃ H ₈₀ N ₁₅ O ₉ F	1210.6320	1210.6185
MC1RL-Ahx-DTPA	C ₇₀ H ₉₈ N ₁₈ O ₁₇	1463.7430	1463.7946
MC1RL-Ahx-DTPA: Eu	C ₇₀ H ₉₅ N ₁₈ O ₁₇ Eu	1610.6321	1610.6323
MC1RL-Ahx-DOTA	C ₇₂ H ₁₀₃ N ₁₉ O ₁₅	1474.7954	1474.9038
Scram.MC1RL-Ahx-DOTA*	C ₇₂ H ₁₀₃ N ₁₉ O ₁₅	1474.7954	1474.9086
MC1RL(D5)-Ahx-DOTA	C ₇₂ H ₉₈ D ₅ N ₁₉ O ₁₅	1479.8268	1479.9137
MC1RL-Ahx-DOTA: La	C ₇₂ H ₁₀₀ N ₁₉ O ₁₅ La	1610.6783	1610.6553
MC1RL-Ahx-DOTA: Ga	C ₇₂ H ₁₀₀ N ₁₉ O ₁₅ Ga	1540.6975	1540.6762
MC1RL-Ahx-DOTA: Eu	C ₇₂ H ₁₀₀ N ₁₉ O ₁₅ Eu	1624.6931	1624.8046
MC1RL-Ahx-DOTA: In	C ₇₂ H ₁₀₀ N ₁₉ O ₁₅ In	1586.6758	1586.6984
MC1RL-diDGLu-DOTA*	C ₇₆ H ₁₀₆ N ₂₀ O ₂₀	1619.7965	1619.9089
MC1RL-diDGLu-DOTA*: In	C ₇₆ H ₁₀₃ N ₂₀ O ₂₀ In	1731.6769	1731.7107
MC1RL-diDLys-DOTA*	C ₇₈ H ₁₁₆ N ₂₂ O ₁₆	1617.9012	1617.9916
MC1RL-DOTA	C ₆₆ H ₉₂ N ₁₈ O ₁₄	1361.7113	1361.7437
MC1RL-DOTA: La	C ₆₆ H ₈₉ N ₁₈ O ₁₄ La	1497.5942	1497.6658
MC1RL-DOTA: Ga	C ₆₆ H ₈₉ N ₁₈ O ₁₄ Ga	1427.6134	1427.6444
MC1RL-DOTA: Eu	C ₆₆ H ₈₉ N ₁₈ O ₁₄ Eu	1511.6091	1511.7075
MC1RL-DOTA: In	C ₆₆ H ₈₉ N ₁₈ O ₁₄ In	1473.5917	1473.6042

*denotes peptide ligand that was prepared by Dr. Hyunjoo Kill.



Scheme 2.2. Chelation of metals to Peptide Ligand-DOTA (shown with Ga⁺³).

Figure 2.4 depicts the HPLC chromatograms from the reaction monitoring experiments. A time-zero, or pure peptide starting material, is shown for reference in box (a) with retention time of 27 min. After 2.5 h, the gallium reaction was shown to have progressed 80% (b) and was complete by 20 h. The lanthanum chelation was shown to have fully progressed after only 4 h.

A noteworthy observation of the metallated MC1RL peptides is their similar retention times from the HPLC experiments. Both the lanthanum- and gallium-bound compounds had retention times of 25 min using this method. This similarity was a positive indication that the

metal bound peptides had similar physicochemical properties. At this point our suspicion was that these similar properties would likely lead to similarly behaving compounds in terms of pharmacokinetics, pharmacodynamics, and biodistribution.

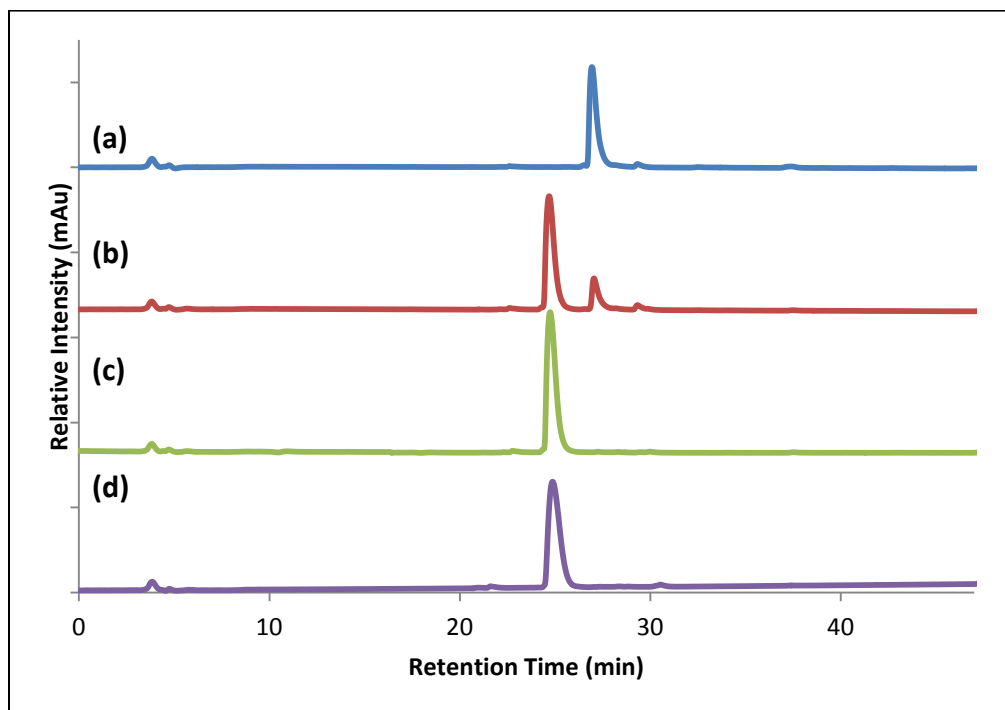


Figure 2.4. HPLC chromatographic overlay comparing the time course of metal chelation with MC1RL-Ahx-DOTA. (a) Time-zero (0 h) run in the absence of metal showing a retention time of 27 min for unchelated peptide. (b) Gallium chelation at 2.5 h showing both the metallated and the nonmetallated version of the peptide. (c) Gallium chelation at 20 h showing complete peptide chelation at ~ 25 min retention time. (d) Complete Lanthanum chelation (4 h) shown at 25 min retention time.

The next test of the surrogate-bound MC1R-Ahx-DOTA compounds was their binding affinity for the MC1R. This assay was performed by the Morse lab in their competition-style time resolved fluorescence binding assay.²⁴ Here a well-known and characterized ligand (NDP- α -MSH) with affinity for the melanocortin receptors was complexed with the lanthanide, europium. A

direct measurement of NDP- α -MSH binding to expressed melanocortin-1 receptors can be made down to the attomole ligand quantity. The test compounds were then allowed to compete with the europium compound to indirectly determine their binding affinity in the cell-based assay. Figure 2.5 shows the binding curves for the unbound ligand and the gallium- and lanthanum- complexes.

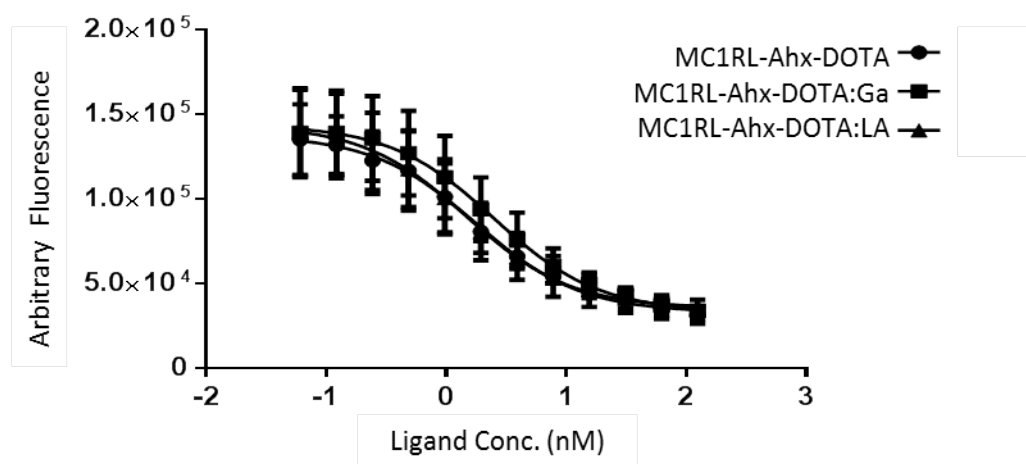


Figure 2.5. Whole-cell competition binding affinities of metallated and unmetallated MC1RL-Ahx-DOTA analogs. Assay performed by Valerie Moberg.

The new MC1RL-Ahx-DOTA compounds were shown to bind with MC1R at similar sub-nanomolar affinities to those previously reported in the literature. The K_i of the tested compounds were recorded as 0.24, 0.23, and 0.34 nM for the ^{139}La -, $^{69/71}\text{Ga}$ -, and the unbound- MC1RL-Ahx-DOTA compounds respectively. Once again, the similar binding affinities of the different surrogate chelates provided evidence that the compounds would behave similarly *in vivo*.

After having successfully labeled the MC1RL-Ahx-DOTA compound with the cold surrogate metals, the empty compound was sent to Wake Forest University for radiolabeling in the

lab of Dr. Thad Wadas. That group has had expertise working with actinium-225 obtained from the Oak Ridge National Laboratory. There, MC1RL-Ahx-DOTA was loaded with ^{225}Ac under similar conditions to our own labeling procedure and then tested for radiochemical purity and plasma stability. The Wadas group labeled the compound in 95% radiolabeling yield and 99.8% radiochemical purity. They also incubated (37 °C) the radiolabeled compound (56 μCi) in human serum and monitored radiochemical purity over the course of 10 days. They reported roughly 90% stability of the actinium-bound targeting ligand at the end of the time course.

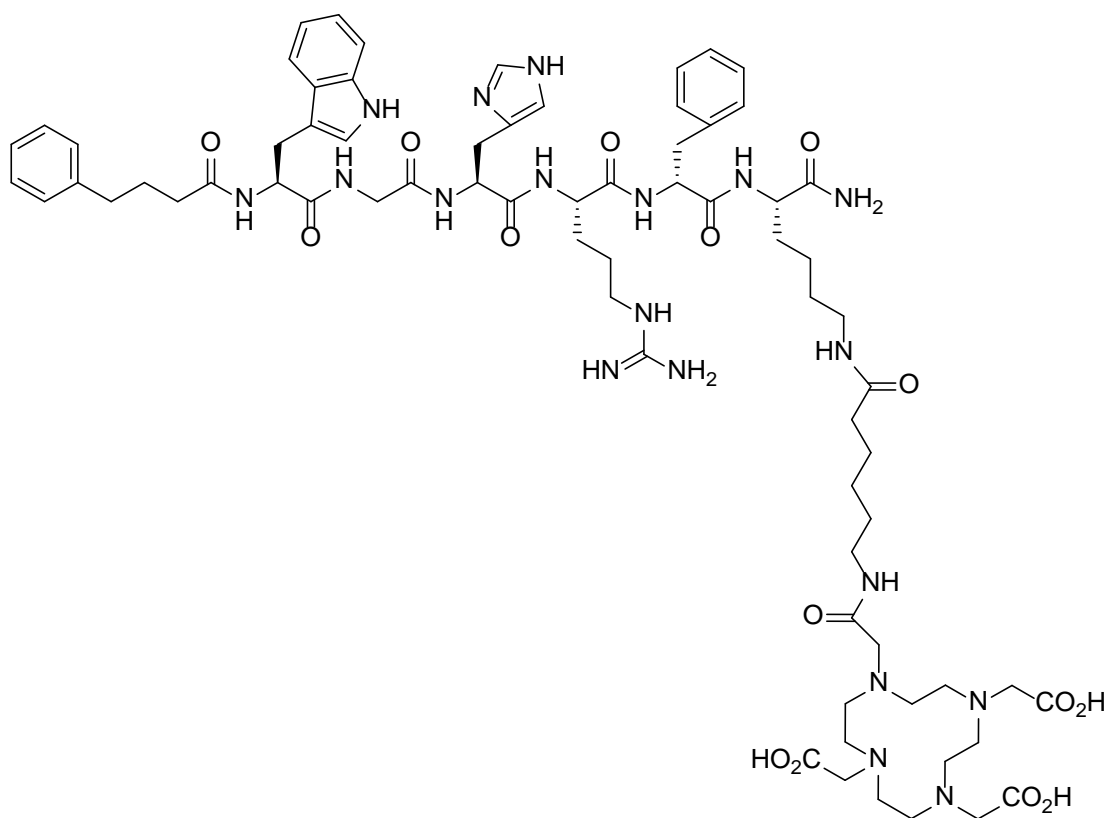


Figure 2.6. Structure of scrambled-MC1RL-Ahx-DOTA.

During this time another version of MC1RL was constructed by Dr. Hyunjoo Kil to be used as a non-binding control for the biological testing. This compound had the primary sequence

of the MC1RL pharmacophore mixed up, or scrambled, to eliminate specific binding to the melanocortin-1 receptor. Instead of the correct binding sequence (His-DPhe-Arg-Trp-Gly) the scrambled sequence was composed of amino acids in the order: Trp-Gly-His-Arg-DPhe. Figure 2.6 shows the structure of the completed scrambled-MC1RL-Ahx-DOTA. Finally both MC1RL-Ahx-DOTA:Ac and its scrambled control were shipped back to the Moffitt Cancer Center the Morse group's testing of the compound in both *in vitro* and *in vivo* studies.

2.2.3 Biological Testing of MC1RL Compounds

The actinium-chelated targeting ligands, MC1RL-Ahx-DOTA:Ac and its scrambled analog, were tested in a barrage of experiments. Dr. Narges Tafreshi led the group's experimentation. The radiolabeled compounds were tested for cytotoxicity by assaying melanocortin-1 receptor positive cells for metabolic activity after dosing with MC1RL-Ahx-DOTA:Ac (MTT assay). A maximum tolerated dose was examined in non-tumor bearing mice. At the time of this writing, efficacy studies had begun to test the MC1RL-Ahx-DOTA:Ac compound against controls of injected saline, the scrambled-MC1RL-Ahx-DOTA:Ac, and the cold lanthanum surrogate, MC1RL-Ahx-DOTA:La.

Another test of the MC1RL-Ahx-DOTA:Ac compound was the determination of biodistribution in tumor bearing mice. Work done by Dr. Tafreshi in the Morse group alongside the medical physicists in the Small Animal Imaging Laboratory (SAIL) at Moffitt produced the biodistribution (BD) graph in Figure 7. This data was gathered by counting gamma ray emission from actinium and radiodecay products in the listed organs and tumors. A valuable output from

this study is the differential uptake in tumors expressing either high or low levels of engineered MC1R. Tumors with higher levels of receptor expression were shown to have substantially more uptake of targeting ligand.

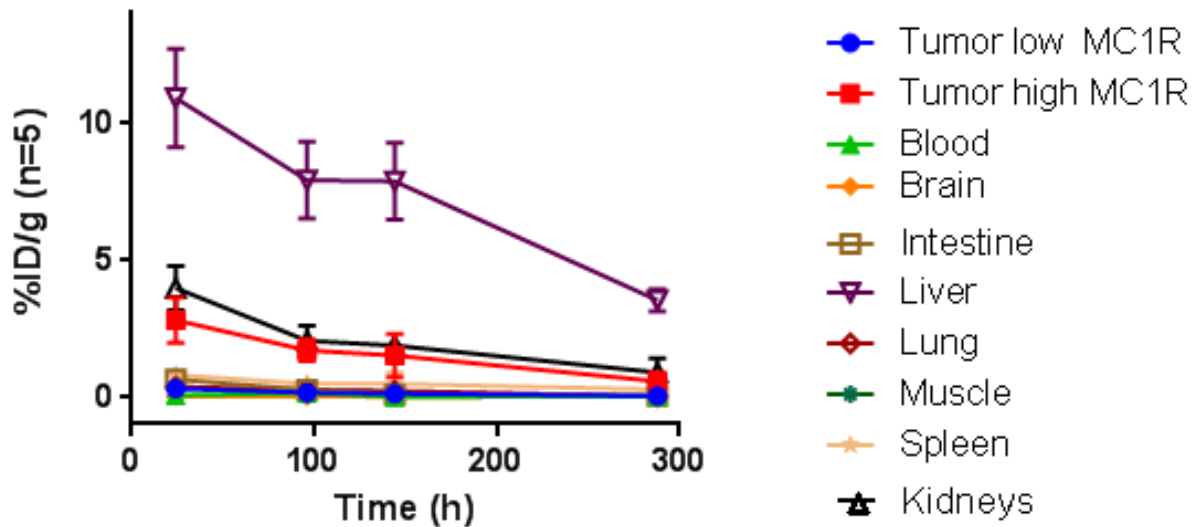


Figure 2.7. Biodistribution of MC1RL-Ahx-DOTA:Ac in tumor bearing mice. BD experiments performed by Drs. Tafreshi and Budzevich.

Another striking feature of this BD study was the amount of actinium uptake in the metabolic organs. Both the liver and kidneys showed increased uptake over the other tissues. Liver uptake was of special concern since it had the highest uptake of any tissue, tumor-bearing or not. Tolerable doses of hepatic and renal radiation, particularly to patients receiving treatment for potentially fatal diseases, is currently unknown. However, a medicinal chemistry solution to this off-target uptake would be particularly helpful.

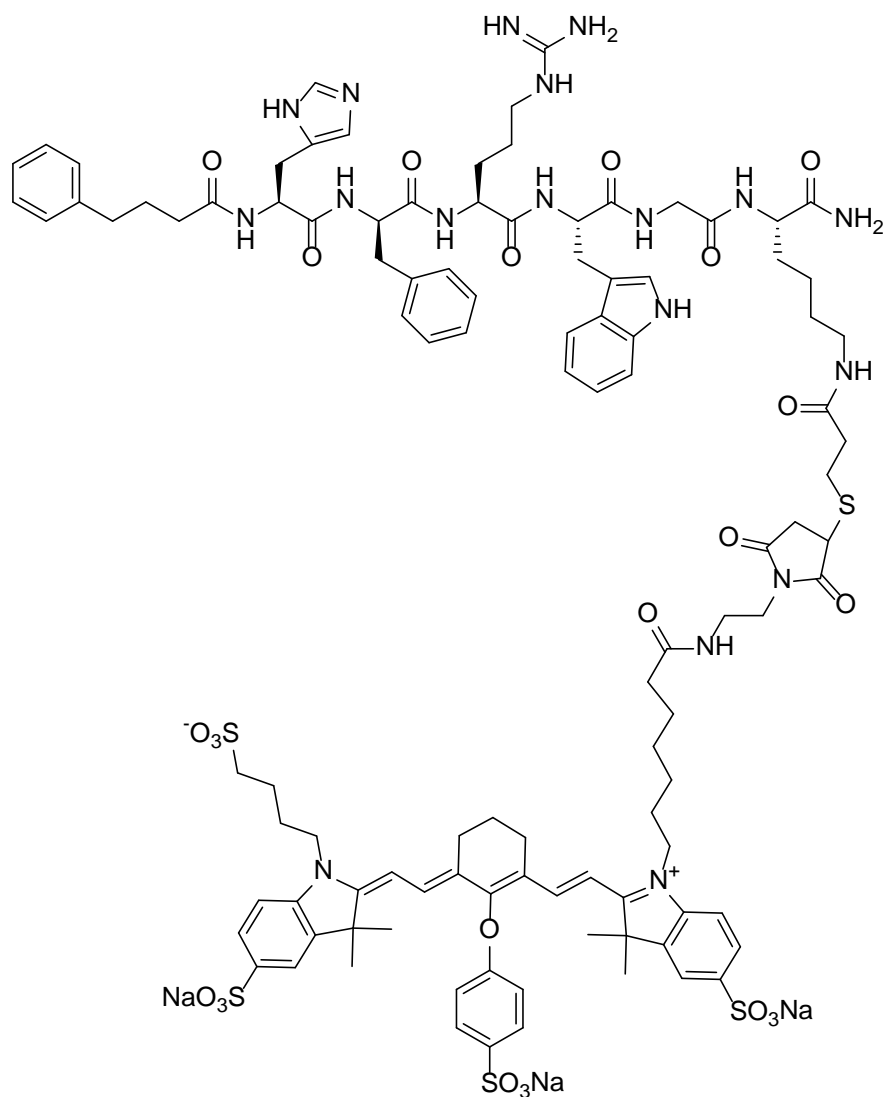


Figure 2.8. Structure of MC1RL-IR800CW.²⁵

A previous version of MC1RL with a fluorescent dye payload was published in 2012 by collaboration of the Morse and Vagner groups at the University of Arizona.²⁵ The compound (shown in Figure 2.8) reported in this publication featured and IR800CW fluorescent dye coupled to the same binding sequence used in our MC1RL. This dye includes 4 sulfonate functional groups appended to its structure to aide in the solubility of the hydrophobic dye. Importantly, this

targeted imaging agent was shown to target MC1R expressing tumors in mice while avoiding hepatic uptake.

2.2.4. Biodistribution Modulation

Surveying the differences in the MC1RL targeting ligands with DOTA and with the IR800CW dye (Figure 2.8), a disparity in lipophilicity is perceived. The fluorescent dye payload should have a negative-three formal charge at physiological pH. In contrast, all of our DOTA compounds with complexed metals should retain neutral payloads at physiologic pH. Therefore a hypothesis was put forward that altering the lipophilicity of the MC1RL payloads could attenuate uptake in off-target organs such as the liver.

To this end, several MC1RL DOTA analogs were synthesized. The plan for this medicinal chemistry project was that hydrophilic linkers could be designed to tether the DOTA payload by either eliminating the 6-aminohexanoic acid linker or by adding ionizable groups, analogous to the sulfonates in the IR800CW compound. Then the lipophilicity of the new constructs could be measured using conventional experimental methods. Finally the MC1RL analogs could be complexed with radionuclides suitable for imaging, and the *in vivo* distribution of these new compounds could be determined.

Three new compounds were prepared for this study with the help of Dr. Hyunjoo Kil and are depicted in Figure 2.9. The first analog was the result of simply omitting the 6-aminohexanoic acid linker. By eliminating this original linker between MC1RL and DOTA, the aim was to increase hydrophilicity by reducing the number of methylene groups. Two other compounds were

designed with either two glutamate residues or two lysine residues in place of the aminohexanoic acid linker. These residues would each impart 2 formal charges to the MC1RL payload at physiologic pH while maintaining a similar linear spacing of atoms between the targeting ligand the DOTA. The inserted amino acids were included as the *D*-configuration to help promote proteolytic stability.

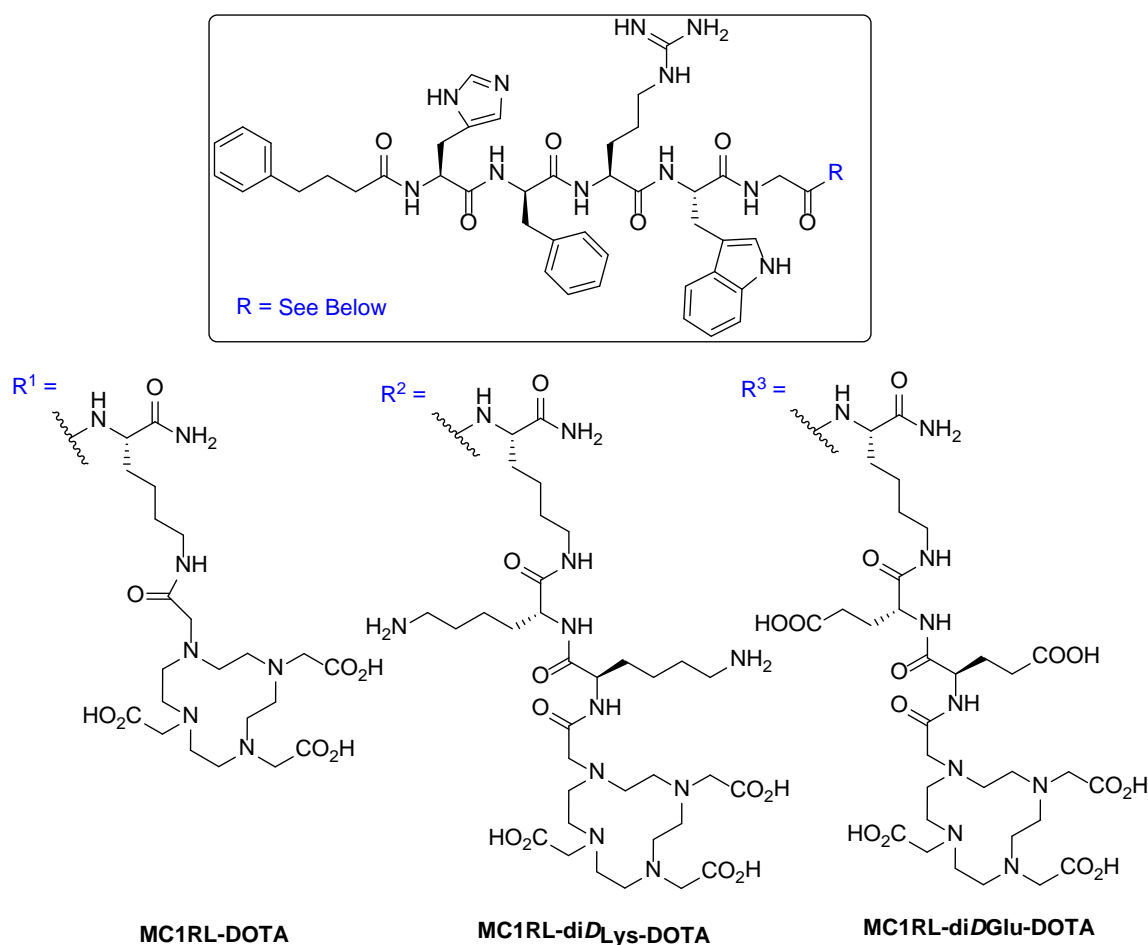


Figure 2.9. MC1RL analogs synthesized to modulate lipophilicity.

With the new MC1RL compounds synthesized, the next step was to test their respective lipophilicities. A simple lipophilicity experiment was conducted by partitioning each individual compound between PBS (pH 7.4) and octanol. Next the concentrations of ligand in each layer

were determined from a LC-MS/MS method and the $\text{LogD}_{7.4}$ of each analog was calculated. A graph of the results of these lipophilicity experiments is included as Figure 2.10.

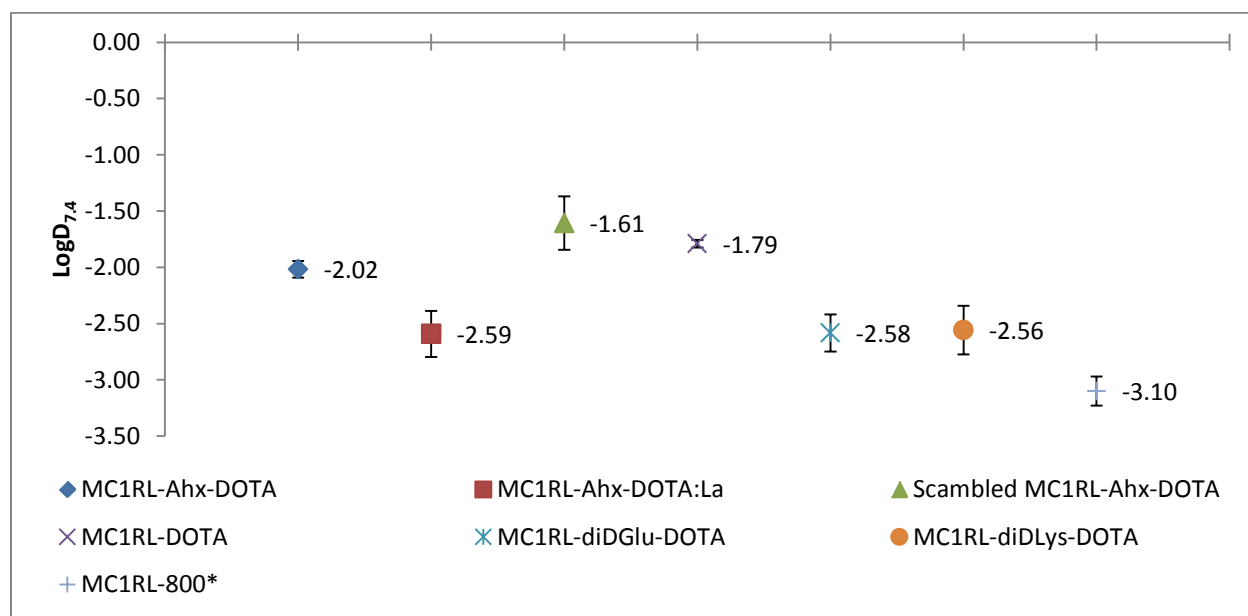


Figure 2.10. Graphical display of experimentally determined $\text{LogD}_{7.4}$ for MC1RL analogs. Compound MC1RL-IR800CW was assayed for $\text{LogD}_{7.4}$ in Tafreshi et al.²⁵

Six MC1RL analogs were assayed for $\text{LogD}_{7.4}$ in this study and plotted in Figure 2.10. The MC1RL-IR800CW compound from Tafreshi et al.²⁵ is also listed with its value of -3.10 ± 0.13 . Briefly, compounds with more negative values are understood to be more hydrophilic. The impetus to create these analogs was to get close to the MC1RL-IR800CW lipophilicity. Our standard compound, Mc1RL-Ahx-DOTA, was measured at 2.02 ± 0.07 . Removing the 6-aminohexanoic acid linker actually increased the lipophilicity to 1.79 ± 0.03 . Adding the di-glutamate or di-lysine linkers resulted in compounds measured at -2.58 ± 0.17 and -2.56 ± 0.22 respectively. Interestingly, complexation of the cold surrogate lanthanum with MC1RL-Ahx-

DOTA dropped the $\text{LogD}_{7.4}$ over half a logarithm to -2.59 ± 0.20 . Extrapolating this change to either the di-glutamate or di-lysine compounds would result in a compound with strikingly similar lipophilicity to the MC1RL-IR800CW compound.

Next, two MC1RL analogs (MC1RL-Ahx-DOTA and MC1RL-diDGlu-DOTA) were complexed with indium-111 in order to determine their biodistribution in mice by SPECT imaging. Reference compounds with natural abundance In-113 were complexed in 100 mM sodium acetate (pH 5.55) with heating to 70 °C. These reference compounds were used by Dr. Haibin Tian's Radiochemistry lab in the complexation of the same precursor MC1RL compounds with 'hot' indium-111. The protocol for the hot synthesis was modified by using 100 mM HEPES buffer (pH 5.5) to reduce the competition of the cadmium daughter product.²⁶ These radiolabeled compounds were again tested by Drs. Tafreshi and Budzevich in the small animal imaging lab at Moffitt.

Figure 2.11 shows the biodistribution in mice of two MC1RL analogs from their SPECT images. The distribution of the peptide with the 6-aminohexanoic acid linker (left) has the highest absorption by the liver, with kidney uptake as the second highest organ. Other organs accounted for very little intensity. By changing the linker from Ahx to the two *D*-glutamate residues, the distribution between the liver and kidneys flip-flopped. The MC1RL-diDGlu-DOTA:In compound (Figure 2.11, right) had the highest uptake in the kidneys and very little uptake in the other organs, including the liver. This remarkable result correlates well with the prediction from the lipophilicity studies. In essence, by including a linker that decreased lipophilicity, the compound behaved like previously published analogs that were initially observed to avoid liver uptake.

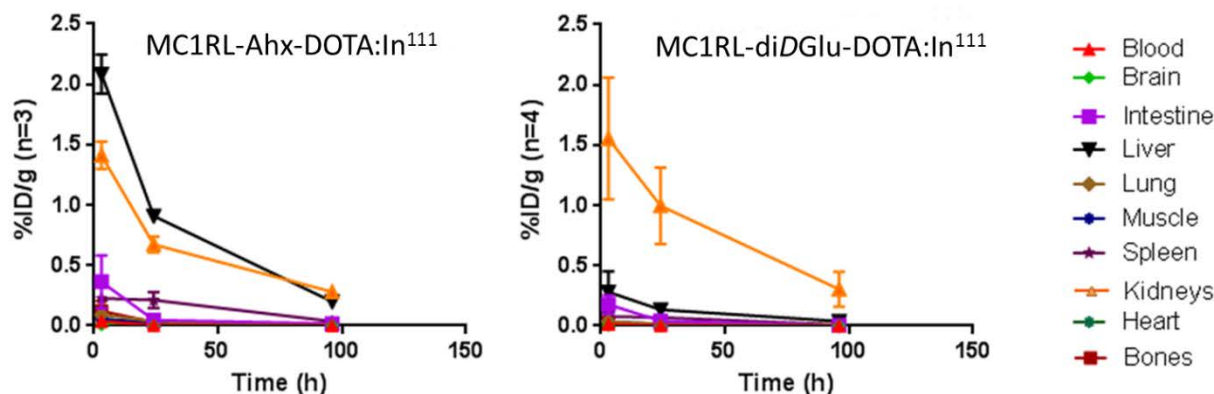


Figure 2.11. Biodistribution of indium-111 labeled MC1RL analogs.

2.2.5 Constrained MC1RL Variants

Constraining peptide ligand conformation is a practice that has long been used to investigate structure-activity relationships, probe the relationship of agonists and antagonists, increase proteolytic stability, and enhance potency. Due to the degree of flexibility and permissible dihedral angles, unrestrained peptide sequences can sample a large amount of chemical space.²⁷ Macrocyclization and the introduction of bulky amino acid monomers may result in rigidifying the peptide ligand backbone.^{28,29} When properly screened, a rigid conformer may be found with increased affinity for its target since it has less chemical space to sample for the most correct conformations.^{30,31} These more rigid structures also typically exhibit qualities of increased proteolytic stability and increased circulatory half-lives due to their ability to appear less peptide-like to proteolytic enzymes.

The evolution of constrained melanotropin analogs dates back to the 1980s when Tomi Sawyer et al. published their work constraining an analog of α -MSH.³² Their new peptide was the

result of two point mutations (p.M4C and p.G10C) in the endogenous tridecapeptide sequence, Ac-Ser-Tyr-Ser-Met-Glu-His-Phe-Arg-Trp-Gly-Lys-Pro-Val-CONH₂. These isosteric substitutions allowed for oxidative macrocyclization through disulfide formation. The resulting constrained peptide was termed [half-Cys⁴,half-Cys¹⁰]α -MSH and is shown in Figure 2.12. The blue section of this peptide is the so-called ‘message sequence,’ responsible for binding to the melanocortin receptor.

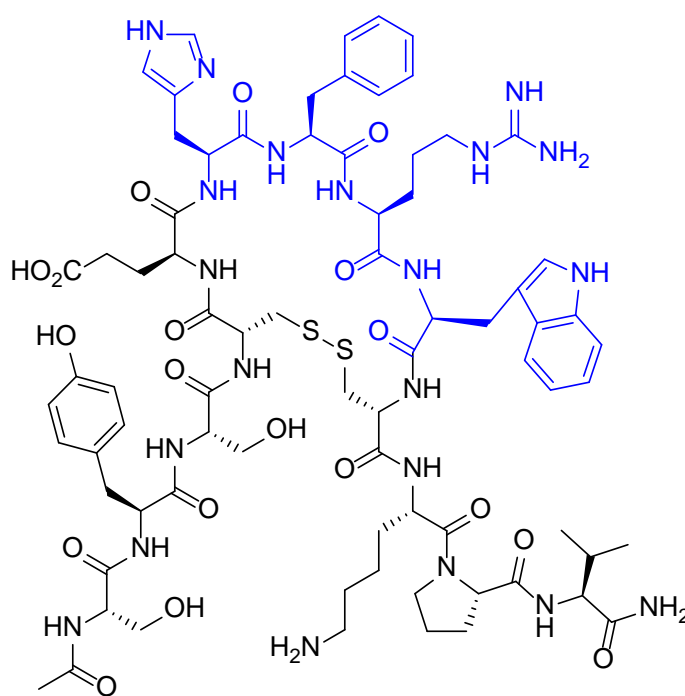


Figure 2.12. Structure of [half-Cys⁴,half-Cys¹⁰]α -MSH.³²

The authors of this paper based their rationale for constraining the linear peptide around their previous discovery of the effect of a *D*-phenylalanine substitution on the native *L*-phenylalanine in position-7. This point mutation was suggested to stabilize a reverse β-turn in the message sequence.³¹ Substituting in the *D*-configured amino acid in the linear message sequence

resulted in 10,000 times more potency in their frog skin activity assay. However this compound lacked the necessary selectivity for the MC1R.

Continued research by the same group, and under the direction of Dr. Victor Hruby, led them to another cyclic peptidomimetic named melanotan-II (MT-II).^{33,34} This melanotropin analog was constrained by a lactam bridge and maintained the critical 'message sequence' pharmacophore from α -MSH (see Figure 2.13). This compound went to phase I clinical trials under the claim that it would darken skin pigmentation in an effort to avoid melanomas. However, due to selectivity issues for other isoforms of melanocortin receptor, it was never approved for human use beyond its clinical trial.

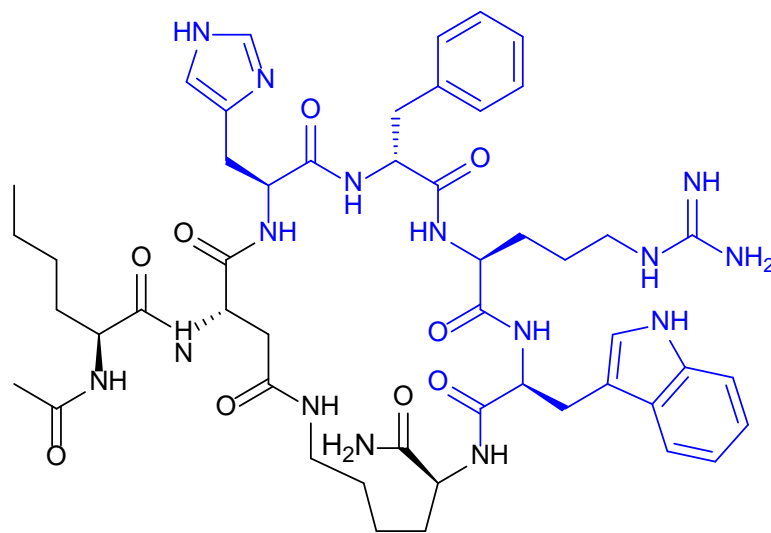
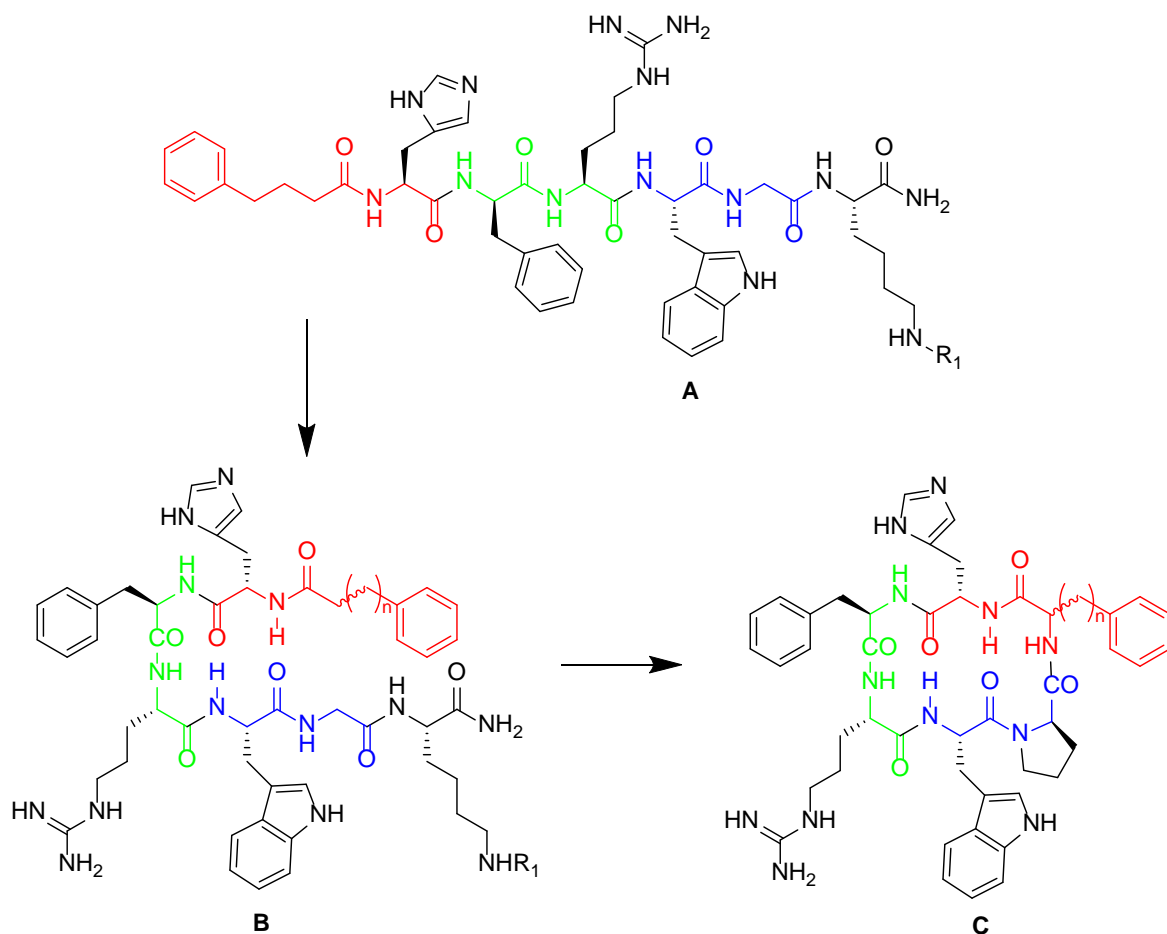


Figure 2.13. Structure of MT-II (melanotan-II).^{33,34}

The current research with constrained melanotropins took these previous macrocyclic peptidomimetics into consideration, and expanded upon previous lab member's work of creating β -hairpin turn peptides. A goal of this work was to develop a more stable ligand, and possibly an antagonist. The conceptualization of our design is shown in Scheme 2.3. The scheme is color

coded to guide the viewer through the thought process of bending the peptidomimetic backbone around the β -turn promoted by the *D*-phenylalanine. The other elements from our MC1RL ‘message sequence’ remain present through the turn, which is held together both through hydrogen bonding of the antiparallel β -sheet-like motif and a *D*-proline inspired turn on the opposite side.



Scheme 2.3. Constraining linear MC1RL around the turn promotion region.

Since the 4-phenylbutyric acid was shown to be important for selectivity,^{14,15} it was envisioned that a phenylalanine homolog could be incorporated to both maintain the phenyl ring and allow for the new amide bond necessary for head-to-tail macrocyclization. However the new

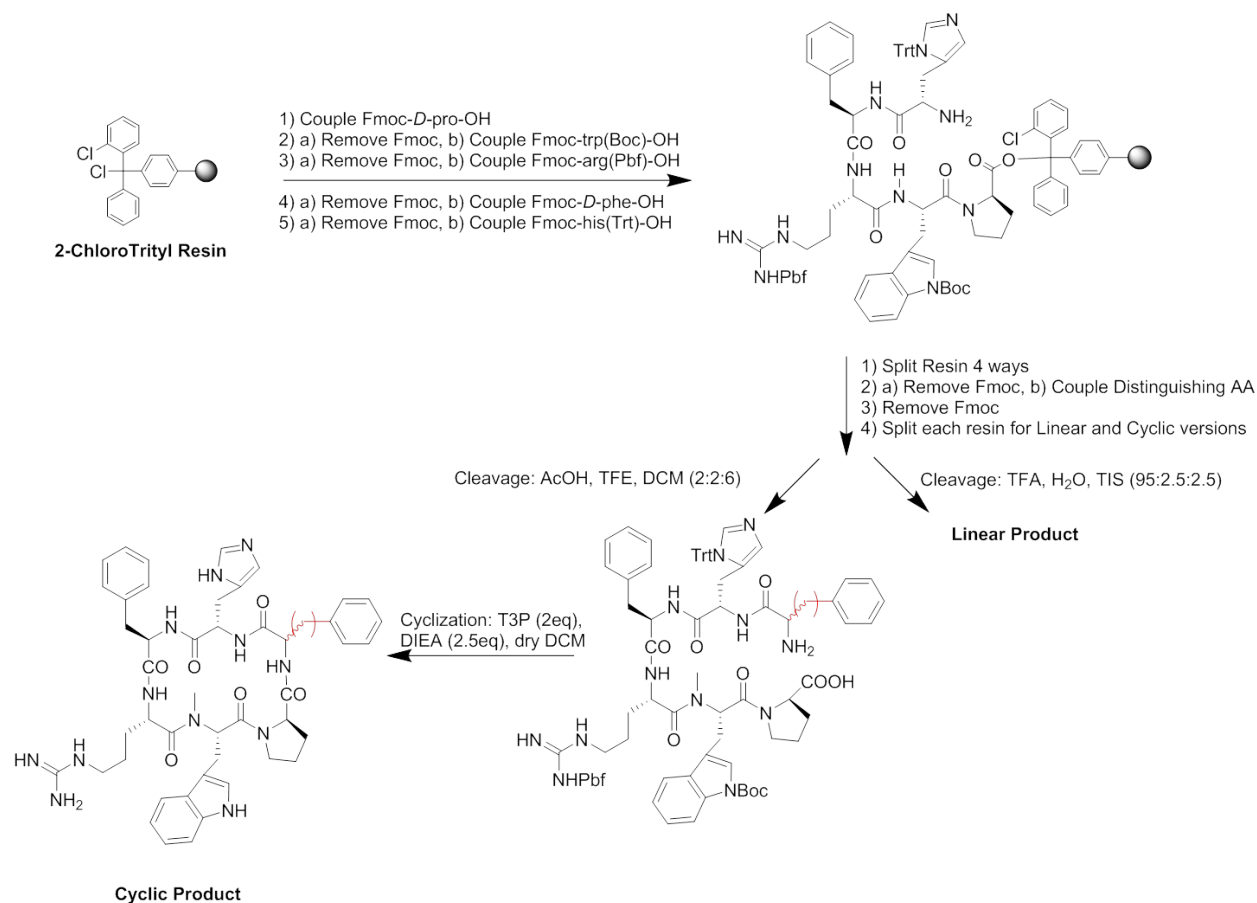
amino acid would set another chiral center and the correct epimer would have to be determined. The phenylalanine homolog would also introduce the opportunity to tune the number of methylene groups between the N-terminus and the phenyl ring. As such, structure-activity relationships were compared from the inclusion of four homologs: *D*- and *L*-homophenylalanine and phenylalanine. The macrocycles were closed through a C-terminal *D*-proline which formed an amide bond with the N-terminal phenylalanine homolog.

Scheme 2.4 lays out the synthesis of each constrained MC1RL analog. Product loss to diketopiperazine formation was observed with proline-loaded Wang resin as solid support. The bulkier chlorotrityl resin was substituted. Conventional N^α-Fmoc strategy SPPS with HCTU activation was employed to couple *D*-Pro, Trp(Boc), Arg(Pbf), *D*-Phe, and His(Trt). At this step in the synthesis the resin was split four ways to allow for the variable position of either *D*- or *L*-homophenylalanine or phenylalanine.

Finally each of the four resin-bound variants were split to accommodate linear and cyclic variations of each ligand. Resin for the linear products was cleaved with a cocktail of TFA, TIS, and H₂O (95:2.5:2.5, v/v). Resin for cyclization was cleaved from solid support with protecting groups intact by AcOH:TFE:DCM (2:2:6 v/v). By maintaining the protecting groups on this subset of analogs, a solution phase cyclization step was done through propylphosphonic anhydride (T3P) condensation. Finally the protecting groups were removed by treatment with TFA cocktail.

The eight MC1RL variants were completed and sent to Dr. Tafreshi in the Morse group to determine binding affinity and functionality. Figure 2.14 lists a table (C) comparing the results from these assays. All compounds were synthesized in acceptable crude yields (32-84%) and the mass spectra confirmed their identities. The compounds with the tightest binding affinity for the

MC1R were the analogs with *L*-homophenylalanine. Both the linear and cyclic analogs with this amino acid achieved single digit binding affinity, K_i of 2.2 nM and 6.5 nM respectively.



Scheme 2.4. Constrained MC1RL Synthesis.

The lead compounds based on binding affinity were then put into a functional assay by Dr. Tafreshi. In the first pass, compound B54 cyclic exhibited antagonistic behavior compared to the controls and compounds B53 linear and cyclic. However, repeating the experiment yielded ambiguous results. The activity directed by receptor binding of the constrained compounds remains unknown.

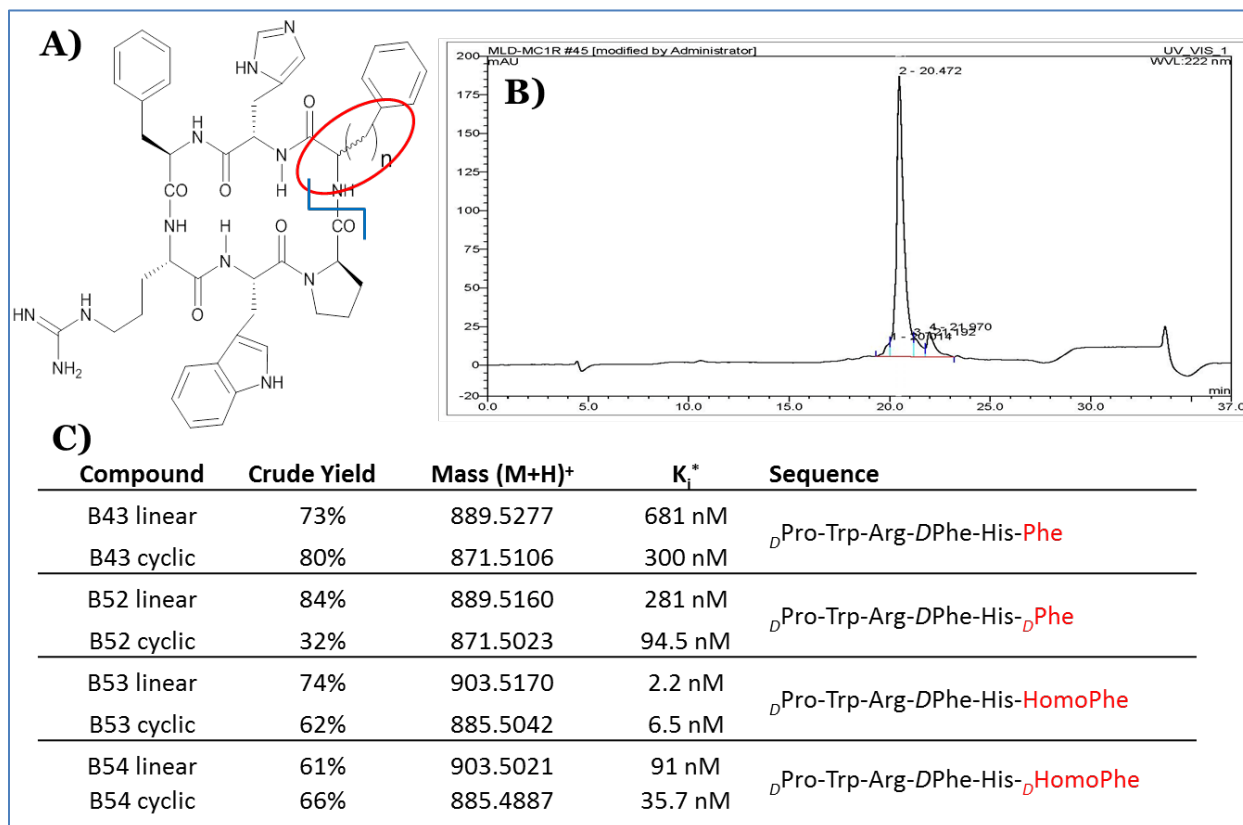


Figure 2.14. Summary of constrained MC1RL compounds. A) Generalized structure of constrained MC1RLs. The blue line denotes the amide bond present in the fully cyclic structure or where the macrocyclic ring would be open for the linear variants. The red circle shows a generic phenylalanine homolog. B) Representative HPLC chromatogram of cyclic MC1RL. C) Table of synthesized compounds listing yields, mass spectral summaries, binding affinities, and sequence information.

2.3 Conclusions

The melanocortin-1 receptor is a valuable cell-surface marker which characterizes a large percentage of uveal and cutaneous melanomas. This protein receptor can be successfully targeted with peptidomimetics derived from the endogenous peptide hormone, α -MSH. Further manipulations of the peptidomimetic have resulted in peptide ligands with high binding affinity

and selectivity, which can be altered to carry payloads of metal chelating molecules. By taking advantage of various radioactive elements in these peptide ligand complexes, companion imaging and therapeutic peptide targeting ligands have been synthesized.

Complexes of targeting ligands with lanthanum-139, gallium-67/69, and indium-113 have been synthesized which can act as surrogates to help inform about physiochemical behavior of their radioactive complements. Radioactive indium-111 has been successfully complexed to track the biodistribution of compounds through SPECT imaging. Further peptidomimetics have been constructed, and also take advantage of SPECT, to explore the connection of linker lipophilicity with biodistribution. These analogs have successfully altered metabolic organ uptake. Finally, actinium-225 complexes of peptide targeting ligands have demonstrated the successes of TAT therapy. Initial efficacy studies showed a complete tumor loss in 22% of treated animals, which resulted in significantly longer survival. When compared with analogous TAT using antibodies, the peptide-based targeting ligands result in a more proper balance of radioactive half-life, pharmacokinetics, and biodistribution of the therapeutic agent.

In addition to the linear MC1RLs, constrained peptidomimetics have also been synthesized. These new constructs retain the high binding affinity for the MC1R and may serve as antagonists. A true antagonistic melanotropin would be the first of its kind. This type of molecule could be used as a dedicated imaging agent or otherwise where receptor activation and internalization could result in deleterious effects. Further work on this class of cyclic melanotropin analogs is necessary to add tethers for payload attachment but the proof of concept for these compounds is promising.

2.4 Experimental

2.4.1 Materials and Instrumentation

All purchased solvents and reagents were obtained at ACS grade or higher purity level and used without further purification unless specified otherwise. Peptide coupling reagents and amino acids were obtained from either Chem-Impex, Novabiochem or Advanced ChemTech. Distilled NMP (99.96%) was purchased from Chem-Impex. Tentagel Resin was obtained from Rapp Polymere. HPLC grade Acetonitrile was purchased from or Fisher was used for HPLC and de-ionized water was processed by Millipore Milli-Q water purifier for HPLC.

Amino acids with the following configurations were purchased from ChemImpex: Fmoc-Lys(Alloc)-OH, Fmoc-Gly-OH, Fmoc-Arg(Pbf)-OH, Fmoc-*D*-Phe-OH, Fmoc-His(Trt)-OH, and Fmoc-6-Aminohexanoic Acid. CDN Isotopes provided the Fmoc-*D*-Phe(*D*5)-OH. Tri-*t*-butyl-protected DOTA (1,4,7,10-Tetraazacyclododecane-1,4,7,10-tetraacetic Acid) was purchased from TCI America (Portland, Oregon). DTPA (diethylenetriaminepentaacetic acid), bought as the dianhydride (DTPAA), and 4-phenylbutyric acid was purchased from Sigma-Aldrich.

A Varian solvent delivery module with Dionex UVD340U diode array detector was used for preparative HPLC chromatography. Analytical scale HPLC was performed using either a Dionex P680 system or an Agilent 1200 system, both with quaternary pumps, autosamplers, and diode array detectors. Mass spectral analysis was performed with either Agilent 6540 QTOF with dual Jet-Stream ESI source coupled to Agilent 1260 Infinity HPLC, Agilent 6460 QQQ with Jet-Stream ESI source coupled to Agilent 1260 Infinity HPLC, Agilent LC/MSD VL single quadrupole with Agilent 1100 series HPLC, or Applied Biosystem 4700 MALDI-TOF-TOF

proteomics analyzer with 355nm Nd:YAG laser. Peptides were lyophilized on a Labconco Freeze Dry/Shell Freeze System.

2.4.2 Experimental Procedures

2.4.2.1 Linear MC1RL Synthesis. MC1RL peptide was synthesized according to conventional N^α-Fmoc peptide synthesis strategy using HCTU/NMM or DCC for monomer activation and coupling (Scheme 1). A glass-fritted peptide reaction vessel was charged with 2 g TentaGel Rink amide resin (0.23 mmol/g, 0.46 mmol) and swollen with DCM (2x 20 mL) followed by NMP (3x 20 mL). The resin was agitated by bubbling with N₂ gas from the bottom glass frit and drained from vacuum filtration on the frit. Next the resin-bound Fmoc was deprotected with a mixture of 20% piperidine, 2% DBU in NMP (15 mL, 15 min, 2x). Following deprotection, the resin wash step was accomplished through resin agitation followed by complete drainage with a sequence of washes: NMP (15 mL, 3x), DCM (15 mL, 3x), and NMP (15 mL, 3x). Next the preactivated amino acid monomer was incorporated as the HCTU ester. The first amino acid, Fmoc-Lys(Alloc)-OH (5 eq) was weighed into a flask with HCTU (5 eq), NMM (15 eq) and dissolved to 0.2 M in NMP. This coupling cocktail was allowed to preactivate at rt for 10 min, and was then added to the resin for coupling with agitation for 1 h. After coupling, the resin was drained, washed as before, and assayed for reaction completeness by Kaiser test. The cycle of Fmoc deprotection, washing and coupling was repeated with Fmoc-Gly-OH, Fmoc-Trp(Boc)-OH, Fmoc-Arg(Pbf)-OH, Fmoc-D-Phe-OH, Fmoc-His(Trt)-OH, and capped with 4-phenylbutyric acid. Qualitative Kaiser assay at the Trp, Arg, and Phe positions revealed incomplete coupling so an additional step of preparing the symmetric anhydride with the amino acid (4 eq) and DCC (2 eq)

was performed by warming (40 °C) the monomer/DCC in DCM for 30 min. The urea byproduct was filtered from the anhydride and filtrate added directly to the already bubbling (10 mL NMP) resin. This coupling reaction was allowed to proceed for an additional hour.

Other linear MC1RL analogs were synthesized by analogous technique, substituting the appropriate amino acid acids in the proper order. For instance, the scrambled sequence (synthesized by Dr. Hyunjoo Kil) incorporated monomers in the following order: Fmoc-Lys(Alloc)-OH, Fmoc-D-Phe-OH, Fmoc-Arg(Pbf)-OH, Fmoc-His(Trt)-OH, Fmoc-Gly-OH, Fmoc-Trp(Boc)-OH, 4-phenylbutyric acid. Another MC1RL analog with 5 deuteriums was synthesized by substituting Fmoc-D-Phe(D5)-OH. This analog was used as in internal standard for the QQQ mass spectroscopy measurements.

2.4.2.2 Alloc Deprotection. After completion of the linear portion of the targeting ligand, the molecule was branched from its C-terminal lysine by deprotection of the orthogonal Alloc group on the ϵ -amine. The resin was bubbled in DCM (15 mL) with catalytic Pd(0)(PPh₃)₄ (5 mol%) and 5 drops of piperidine for 1 hour. Kaiser test and a small test cleavage for MALDI-TOF confirmed the complete deprotection. Resin washes followed in the typical procedure after washes (15 mL, 2x) with 5 mol% sodium diethyldithiocarbamate in NMP and 10% DIEA.

2.4.2.3 Peptide Branching, Linkers, and Payloads. After alloc deprotection, payloads were coupled at the C-terminus through the free ϵ -amine. When linkers such as Fmoc-6-aminohexanoic acid (Ahx), di-Fmoc-D-Lys(Boc)-OH, and di-Fmoc-D-Glu(OtBu)-OH were incorporated, they were

added using typical cycles of washing, Fmoc deprotection, and coupling (5 eq monomer, 5 eq HCTU, 15 eq NMM in NMP).

Payloads such as DOTA and 4-fluorobenzoic acid (FBA, a reference compound prepared for use in the radiochemistry lab) were also coupled with typical preactivation (5 eq monomer, 5 eq HCTU, 15 eq NMM in NMP). Diethylenetriaminepentaacetic dianhydride (DTPAA) was coupled by acyl chloride activation with triphosgene. Triphosgene (bis(trichloromethyl) carbonate (211 mg, 0.712 mmol)) and DTPAA (763 mg, 2.14 mmol) were weighed into a scintillation vial. DIEA (0.75 mL, 4.3 mmol) and 10 mL of NMP were added to the scintillation vial and the preactivation reaction was shaken for 30 minutes before being added to the peptide reaction vessel. The coupling reaction was agitated for 2 hours, drained and washed with the following solvents (15 mL each): NMP, THF, 20% THF (aq.), 10% DIEA/10% H₂O in THF, 20% THF (aq.), THF, DCM.³⁵

2.4.2.4 Peptide Cleavage, Lyophilization, and Purification. Following the completion of peptide synthesis, resin was washed with DCM (15 mL, 2x) and dried under a stream of N₂ gas. The dried resin was agitated with cleavage cocktail (10 mL/g resin) of TFA, diH₂O, TIS (95:2.5:2.5, v/v) for 3 hours at rt. The acid was filtered from the resin, reduced to a thick oil under a stream of N₂, and precipitated with 20 mL ice cold diethyl ether. The precipitate was centrifuged for 5 minutes at 4,000 rpm and the ether was decanted. Ten milliliters of cold ether was added to the crude peptide precipitate and the slurry was again spun and decanted twice more. Finally the crude peptide pellet was reconstituted in H₂O, frozen and lyophilized to yield off-white, crude powder.

Crude peptide was characterized by analytical scale HPLC utilizing an AAPPTEC Spirit Peptide column (C18, 5 μ m, 25x0.46cm). UV detection was monitored at 222 nm and 254 nm. Mobile phase (A: H₂O + 0.1 % TFA, B: ACN + 0.1 % TFA) was pumped 1 mL/min with the following gradient: 2 % B for 3 min to load the samples then 20-40 % B over 20 min, then the column was washed at 95 % and re-equilibrated at 2 % B for the next HPLC experiment.

For purification, crude peptide was chromatographed on an AAPPTEC Spirit Peptide 120 column (C18, 5 μ m 25x2.12 cm). The UV detection was monitored at 222 nm. Mobile phase (A: H₂O + 0.1 % TFA, B: ACN + 0.1 % TFA) was pumped at 15 mL/min with the following gradient: 5 % B for 10 min to load the samples followed by a linear gradient of 20-25 % B over 50 min for separation. Fractions were collected by hand, analyzed by both analytical HPLC and MALDI-TOF. Fractions with purity greater than 95 % were pooled, frozen and lyophilized.

2.4.2.5 Mass Spectrometry Characterization: MALDI-TOF and QToF. MALDI -TOF and -TOF/TOF experiments were used to analyze both crude and pure peptides. Samples were premixed 1:1 (v/v) with a saturated solution of α -cyano-4-hydroxycinnamic acid and then 500 nL was spotted on the MALDI plate. Unless otherwise specified, the instrument was run in positive, reflective mode. For MS/MS experiments Precursor ions were selected after analysis of reflective-mode TOF measurement from 1000-2000 m/z .

For QToF characterization of purified peptides, the samples were introduced to the mass spectrometer as a direct infusion from the HPLC. The instrument was set to high resolution mode in extended dynamic range. Typically, only positive polarity was measured. Real-time reference masses were infused in the second nebulizer during the acquisition.

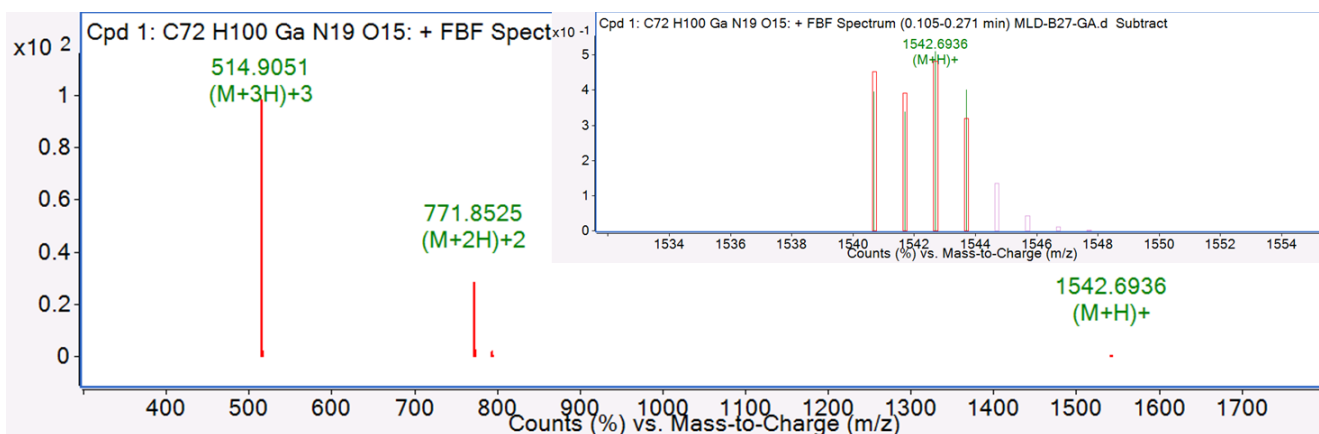


Figure 2.15. QToF analysis of gallium-chelated MC1RL-Ahx-DOTA. The main spectrum shows the m/z range from 300-1800, covering the $M+H^+$, $2H^+$, and $3H^+$ species. The inset spectrum highlights the isotope window around the $M+H^+$ species.

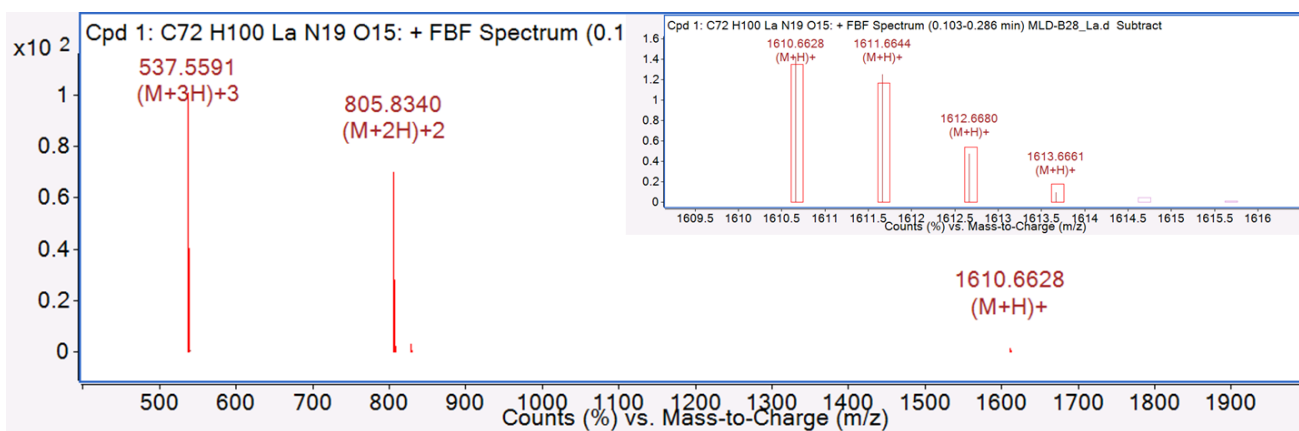


Figure 2.16. QToF analysis of lanthanum-chelated MC1RL-Ahx-DOTA. The main spectrum shows the m/z range from 400-2000, covering the $M+H^+$, $2H^+$, and $3H^+$ species. The inset spectrum highlights the isotope window around the $M+H^+$ species.

For QToF characterization of purified peptides, the samples were introduced to the mass spectrometer as a direct infusion from the HPLC. The instrument was set to high resolution mode in extended dynamic range. Typically, only positive polarity was measured. Real-time reference masses were infused in the second nebulizer during the acquisition.

Figures 2.15 and 2.16 are representative QToF spectra for both the gallium-chelated and lanthanum-chelated MC1RL-Ahx-DOTA peptides, respectively. The red boxes depict a predicted

isotope pattern (showing both predicted intensity and spacing), and the black lines are the actual subtracted, centroid measurements. The $M+H^+$ measurement for Ga-peptide of 1542.6936 m/z is -3.6 ppm (calculated m/z : 1542.6991). The $M+H^+$ measurement for La-peptide of 1610.6628 m/z is -9.6 ppm (calculated m/z : 1610.6783). No un-chelated peptide was detected by QTOF in either Ga- or La- complexed samples. Mass spectral measurements for the other compounds are listed in Table 2.2 and spectra are shown in the appendix.

2.4.2.6 Metal Chelation

2.4.2.6.1 *Europium chelation.* Peptide with DTPA ligand was dissolved in slightly basic ammonium acetate buffer (pH 8) to form the tetra-carboxylate compounds. Three equivalents of europium chloride hexahydrate were added and the resulting clear and colorless solution was stirred at rt. It was anticipated that the degree of chelation could be monitored by analytical HPLC, so aliquots were taken at time zero (before Eu), 16 h, and 40 h and chromatographed on the pH 6 HPLC method (A: H₂O + 0.1 % TEA/AcOH, B: 90 % ACN 10 % phase A adjusted to pH 6 with AcOH). No shift in retention time was noticed but the m/z corresponding to Eu chelated product was shown on QTOF LCMS without any starting peptide. The peptide solution was subsequently frozen and lyophilized. The resulting powder was passed through the preparative HPLC system once more under the pH 6 method and the product peaks were lyophilized to yield the final product.

2.4.2.6.2 *Gallium-67/69 and lanthanum-139 chelation.* MC1RL-Peptide with DOTA was dissolved in 0.1 M ammonium acetate (pH 8) at 5 mg/mL to form the tri-carboxylate compound. Three equivalents of each metal (Gallium (III) Chloride or Lanthanum (III) Chloride) were added and the resulting clear and colorless solution was stirred at room temperature. Reaction monitoring of the chelation progress was done with the pH 6 HPLC method to avoid carboxylate protonation and loss of chelation.

2.4.2.6.3 *Indium-113 reference compounds.* Peptides dissolved in 100 mM sodium acetate, pH 5.55 at 3 mg/mL. Three equivalents of $\text{InCl}_3 \cdot 4\text{H}_2\text{O}$ were added to each reaction and stirred at 70 °C. Reactions were monitored at 20 min by analytical HPLC, and all had complete shifts in retention time by 5 min. Finally 5 mM EDTA was added to each reaction and upon clearing the reaction solutions were chromatographed on the semi-preparative HPLC system. Gradients of acetonitrile and water with 0.1 % TFA were used to isolate the purified products which were subsequently lyophilized to white powder.

2.4.2.7 Constrained Peptide Synthesis. After drying overnight under high vacuum, 1 g of 2-chlorotriyl chloride resin (1.49 mmol) was loaded with Fmoc-D-Pro-OH (1.5 eq) by mixing with dry DCM (20 mL) and DIEA (6 eq). The resin was agitated by nitrogen bubbling at rt for 2 h. Next the resin was washed 3x each with DCM/MeOH/DIEA (17:2:1, v/v), DCM, NMP, DCM and the resin was dried under high vacuum overnight. The Fmoc-loading was measured by

quantitative 290 nm absorbance measurements of dibenzofulvene upon microscale (1 mg resin) deprotection with 20% piperidine in DMF. Loading was calculated to be 0.32 mmol/g.

The following amino acids were coupled with the same SPPS strategy as outlined in the linear MC1RL section: Fmoc-Trp(Boc)-OH, Fmoc-Arg(Pbf)-OH, Fmoc-D-Phe-OH, Fmoc-His(Trt)-OH. At this stage the resin was split to four equal portions. Each portion had a distinguishing phenylalanine homolog coupled. The monomers Fmoc-Phe-OH, Fmoc-D-Phe-OH, Fmoc-HomoPhe-OH, and Fmoc-D-HomoPhe-OH were used as homologs.

Each of the four portions of resin was split once more to produce the linear and cyclic variants. The linear peptides were cleaved in the usual manner with a cocktail of TFA, H₂O, TIS (95:2.5:2.5 v/v), precipitated in cold diethyl ether, and lyophilized. The remaining resin had its peptide cleaved from solid support with AcOH, TFE, DCM (2:2:6) for 2 h at rt. The mixture was filtered and reduced *in vacuo*, yielding thin yellow oil. The compounds were then cyclized by dissolving the oil in dry DCM with DIEA (2.5 eq) and 2 equivalents of propylphosphonic anhydride (50 % in methyl THF). The cyclization reactions were mixed by mechanical stirring overnight under dry N₂ gas. The reactions were quenched with 10 mL H₂O, and the organic layer separated and reduced under vacuum. Finally the cyclized peptides had protecting groups removed by treatment with TFA cocktail and worked up in the usual manner.

2.4.2.8 Lipophilicity Measurements. Prior to performing the lipophilicity experiments, a triple quadrupole MRM method was developed to measure unknown quantities of MC1RL analogs with high specificity and sensitivity. The method used M+3H⁺ charge state precursor ions

for all analogs (examples shown in Figures 2.15 and 2.16). Two transitions for each analog were monitored and optimized in the MRM method. Figure 2.17 depicts the structure of the MC1RL-Ahx-DOTA:La transitions. Since the transitions are characteristic of each peptide structure, each method was specific for the particular analog. The most abundant product ion observed was the result of histidine side cleavage yielding the imidazole immonium ion ($m/z = 110$). A second highly abundant, and very specific, product ion was the two charge state immonium product of a b-type amide bond cleavage.³⁶ An example of a product ion scan for MC1RL-Ahx-DOTA:La is shown in Figure 2.18.

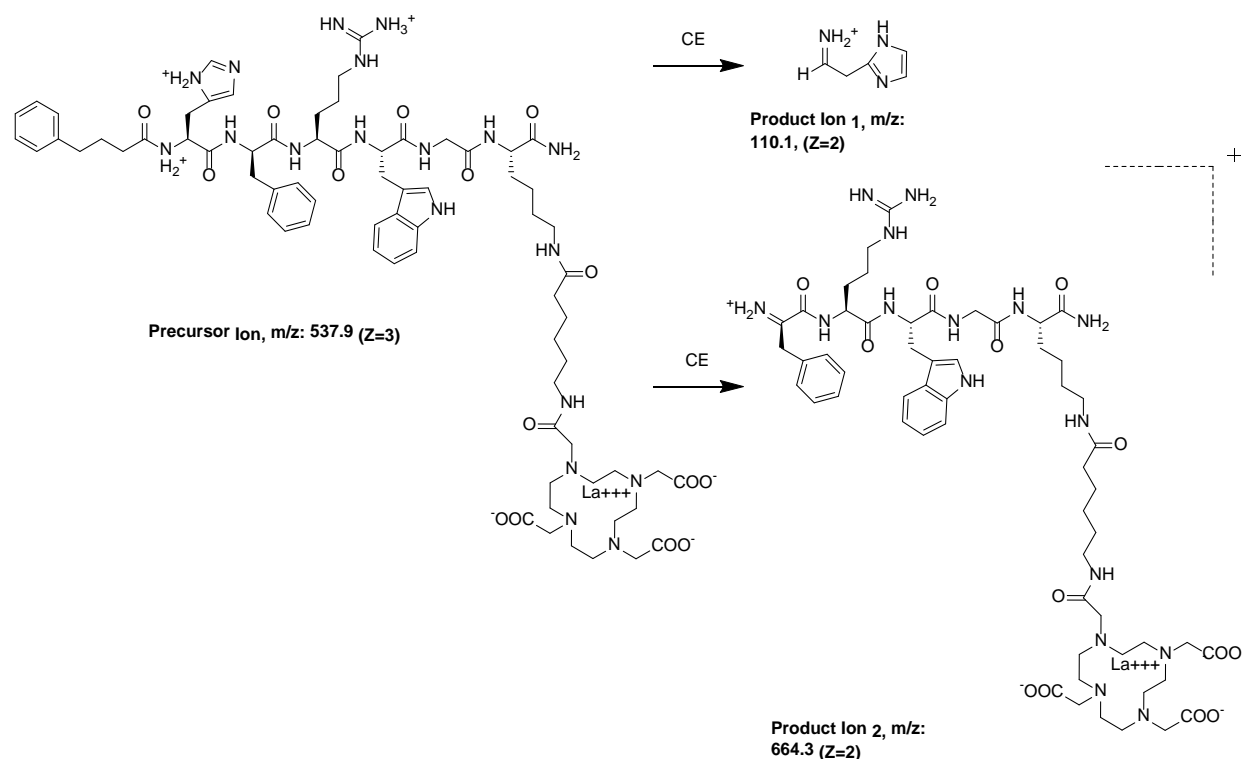


Figure 2.17. MRM transitions developed for MC1R-Ahx-DOTA:La.

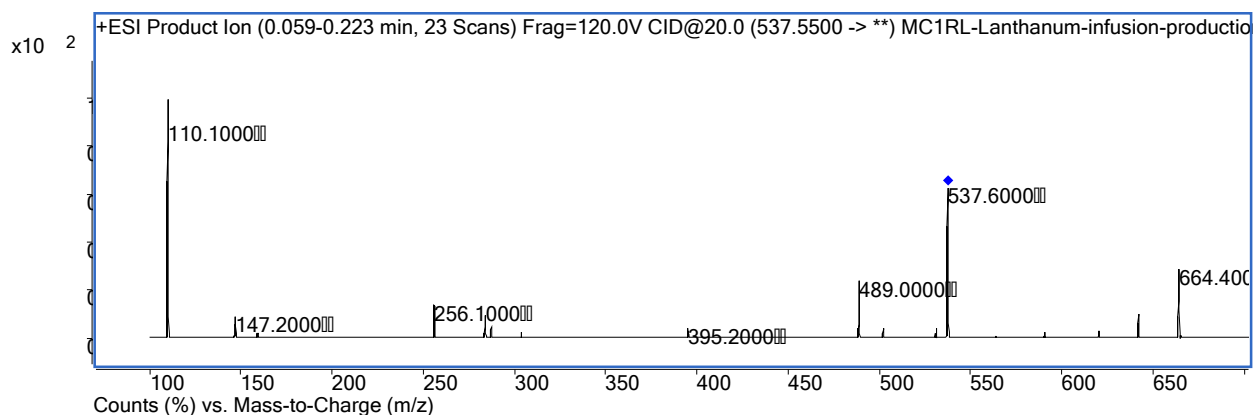


Figure 2.18. Product ion scan for MC1RL-Ahx-DOTA:La with precursor selected as 537.55 m/z.

Once the transitions had been mapped, they were optimized to produce the highest abundances possible. Fragmentor voltages were ramped from 50-225 V while monitoring the relative abundance of precursor ions. Analogously, collision energies were ramped 5-70 eV and the corresponding product ions were recorded. Figure 2.19 shows the results of these optimization experiments.

Next, a standard curve for each peptide was created. Stock solutions were serially diluted from 25 μM to 8 nM and run through the method. Ten microliters of each standard was chromatographed by linear gradient of acetonitrile and water with 0.1 % FA. The eluent was fed to the mass spectrometer where the MRM method summed the specified transitions for each peptide. The transitions for each concentration point were summed, plotted, and a linear regression fit to the data to produce the standard curve for each compound.

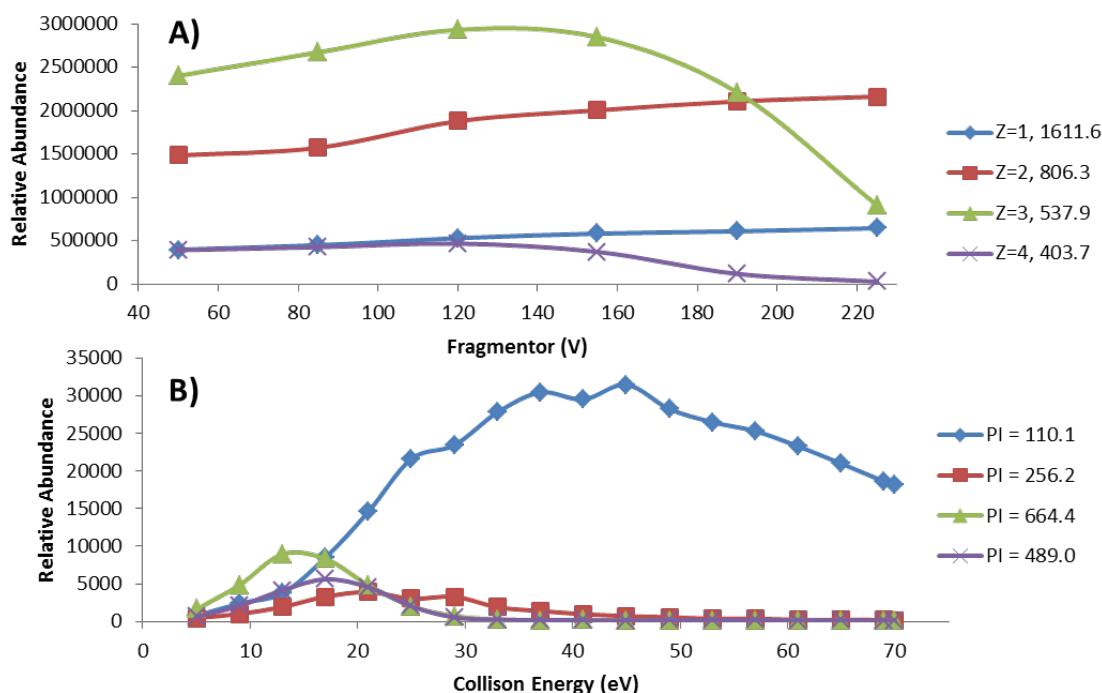


Figure 2.19. Fragmentor voltage (A) and collision energy (B) optimization experiments for the MRM method.

After the standard curves were created, the miniature shake flask method was used to determine the lipophilicity of each compound. Stock solutions of peptide (200 μM) in 25 mM, pH 7.4 phosphate buffer were prepared. Aliquots of the stock solutions were vortexed with three ratios of n-octanol. The resulting emulsions were separated by centrifugation. Triplicate measurements of ligand concentration in each layer were used to calculate a $\text{LogD}_{7.4}$.

2.5 References

- (1) Reed, K. B.; Brewer, J. D.; Lohse, C. M.; Bringe, K. E.; Pruitt, C. N.; Gibson, L. E. *Mayo Clinic Proceedings* 2012, *87*, 328.
- (2) Society, A. C.; Society, A. C., Ed. Atlanta, GA, 2016.
- (3) Chang, A. E.; Karnell, L. H.; Menck, H. R. *Cancer* 1998, *83*, 1664.
- (4) Singh, A. D.; Turell, M. E.; Topham, A. K. *Ophthalmology* 2011, *118*, 1881.

- (5) Colombino, M.; Capone, M.; Lissia, A.; Cossu, A.; Rubino, C.; De Giorgi, V.; Massi, D.; Fonsatti, E.; Staibano, S.; Nappi, O.; Pagani, E.; Casula, M.; Manca, A.; Sini, M.; Franco, R.; Botti, G.; Caracò, C.; Mozzillo, N.; Ascierto, P. A.; Palmieri, G. *Journal of Clinical Oncology* 2012, 30, 2522.
- (6) Hauschild, A.; Grob, J.-J.; Demidov, L. V.; Jouary, T.; Gutzmer, R.; Millward, M.; Rutkowski, P.; Blank, C. U.; Miller Jr, W. H.; Kaempgen, E.; Martín-Algarra, S.; Karaszewska, B.; Mauch, C.; Chiarion-Sileni, V.; Martin, A.-M.; Swann, S.; Haney, P.; Mirakhur, B.; Guckert, M. E.; Goodman, V.; Chapman, P. B. *The Lancet*, 380, 358.
- (7) Chapman, P. B.; Hauschild, A.; Robert, C.; Haanen, J. B.; Ascierto, P.; Larkin, J.; Dummer, R.; Garbe, C.; Testori, A.; Maio, M.; Hogg, D.; Lorigan, P.; Lebbe, C.; Jouary, T.; Schadendorf, D.; Ribas, A.; O'Day, S. J.; Sosman, J. A.; Kirkwood, J. M.; Eggermont, A. M.; Dreno, B.; Nolop, K.; Li, J.; Nelson, B.; Hou, J.; Lee, R. J.; Flaherty, K. T.; McArthur, G. A. *N Engl J Med* 2011, 364, 2507.
- (8) Algazi, A. P.; Tsai, K. K.; Shoushtari, A. N.; Munhoz, R. R.; Eroglu, Z.; Piulats, J. M.; Ott, P. A.; Johnson, D. B.; Hwang, J.; Daud, A. I.; Sosman, J. A.; Carvajal, R. D.; Chmielowski, B.; Postow, M. A.; Weber, J. S.; Sullivan, R. J. *Cancer* 2016, n/a.
- (9) Siegrist, W.; Solca, F.; Stutz, S.; Giuffre, L.; Carrel, S.; Girard, J.; Eberle, A. N. *Cancer research* 1989, 49, 6352.
- (10) Tafreshi, N. K.; Silva, A.; Estrella, V. C.; McCardle, T. W.; Chen, T.; Jeune-Smith, Y.; Lloyd, M. C.; Enkemann, S. A.; Smalley, K. S. M.; Sondak, V. K.; Vagner, J.; Morse, D. L. *Molecular Pharmaceutics* 2013, 10, 3175.
- (11) Yang, Y. *Eur J Pharmacol* 2011, 660, 125.
- (12) Sawyer, T. K.; Sanfilippo, P. J.; Hruby, V. J.; Engel, M. H.; Heward, C. B.; Burnett, J. B.; Hadley, M. E. *Proceedings of the National Academy of Sciences of the United States of America* 1980, 77, 5754.
- (13) Schiöth, H. B.; Mutulis, F.; Muceniece, R.; Prusis, P.; Wikberg, J. E. S. *British Journal of Pharmacology* 1998, 124, 75.
- (14) Koikov, L. N.; Ebetino, F. H.; Solinsky, M. G.; Cross-Doersen, D.; Knittel, J. J. *Bioorganic & Medicinal Chemistry Letters* 2004, 14, 3997.
- (15) Koikov, L. N.; Ebetino, F. H.; Solinsky, M. G.; Cross-Doersen, D.; Knittel, J. J. *Bioorganic & Medicinal Chemistry Letters* 2003, 13, 2647.
- (16) Hruby, V. J.; Cai, M.; Cain, J.; Nyberg, J.; Trivedi, D. *European Journal of Pharmacology* 2011, 660, 88.
- (17) Hruby, V. J.; Wilkes, B. C.; Hadley, M. E.; Al-Obeidi, F.; Sawyer, T. K.; Staples, D. J.; de Vaux, A. E.; Dym, O.; Castrucci, A. M.; Hintz, M. F.; et al. *J Med Chem* 1987, 30, 2126.
- (18) Barkey, N. M.; Tafreshi, N. K.; Josan, J. S.; De Silva, C. R.; Sill, K. N.; Hruby, V. J.; Gillies, R. J.; Morse, D. L.; Vagner, J. *Journal of Medicinal Chemistry* 2011, 54, 8078.
- (19) Chen, J.; Giblin, M. F.; Wang, N.; Jurisson, S. S.; Quinn, T. P. *Nucl Med Biol* 1999, 26, 687.
- (20) Sessler, J. L.; Mody, T. D.; Hemmi, G. W.; Lynch, V.; Young, S. W.; Miller, R. A. *Journal of the American Chemical Society* 1993, 115, 10368.
- (21) Barkey, N. M.; Preihs, C.; Cornnell, H. H.; Martinez, G.; Carie, A.; Vagner, J.; Xu, L.; Lloyd, M. C.; Lynch, V. M.; Hruby, V. J.; Sessler, J. L.; Sill, K. N.; Gillies, R. J.; Morse, D. L. *Journal of Medicinal Chemistry* 2013, 56, 6330.
- (22) Kolb, H. C.; Finn, M. G.; Sharpless, K. B. *Angewandte Chemie International Edition* 2001, 40, 2004.
- (23) Barkey, N. M.; Tafreshi, N. K.; Josan, J. S.; De Silva, C. R.; Sill, K. N.; Hruby, V. J.; Gillies, R. J.; Morse, D. L.; Vagner, J. *J Med Chem* 2011, 54, 8078.
- (24) Handl, H. L.; Vagner, J.; Yamamura, H. I.; Hruby, V. J.; Gillies, R. J. *Analytical Biochemistry* 2004, 330, 242.

- (25) Tafreshi, N. K.; Huang, X.; Moberg, V. E.; Barkey, N. M.; Sondak, V. K.; Tian, H.; Morse, D. L.; Vagner, J. *Bioconjugate Chemistry* 2012, 23, 2451.
- (26) Brom, M.; Joosten, L.; Oyen, W. J. G.; Gotthardt, M.; Boerman, O. C. *EJNMMI Research* 2012, 2, 4.
- (27) Ramachandran, G. N.; Sasisekharan, V. In *Advances in Protein Chemistry*; C.B. Anfinsen, M. L. A. J. T. E., Frederic, M. R., Eds.; Academic Press: 1968; Vol. Volume 23, p 283.
- (28) Ying, J.; Gu, X.; Cai, M.; Dedek, M.; Vagner, J.; Trivedi, D. B.; Hruby, V. J. *J Med Chem* 2006, 49, 6888.
- (29) Haskell-Luevano, C.; Rosenquist, A.; Souers, A.; Khong, K. C.; Ellman, J. A.; Cone, R. D. *J Med Chem* 1999, 42, 4380.
- (30) Mayorov, A. V.; Han, S.-Y.; Cai, M.; Hammer, M. R.; Trivedi, D.; Hruby, V. J. *Chemical biology & drug design* 2006, 67, 329.
- (31) Ying, J.; Kövér, K. E.; Gu, X.; Han, G.; Trivedi, D. B.; Kavarana, M. J.; Hruby, V. J. *Peptide Science* 2003, 71, 696.
- (32) Sawyer, T. K.; Hruby, V. J.; Darman, P. S.; Hadley, M. E. *Proceedings of the National Academy of Sciences of the United States of America* 1982, 79, 1751.
- (33) Al-Obeidi, F.; Hadley, M. E.; Pettitt, B. M.; Hruby, V. J. *Journal of the American Chemical Society* 1989, 111, 3413.
- (34) Al-Obeidi, F.; Castrucci, A. M. d. L.; Hadley, M. E.; Hruby, V. J. *Journal of Medicinal Chemistry* 1989, 32, 2555.
- (35) Josan, J. S.; De Silva, C. R.; Yoo, B.; Lynch, R. M.; Pagel, M. D.; Vagner, J.; Hruby, V. J. *Methods Mol Biol* 2011, 716, 89.
- (36) Wysocki, V. H.; Resing, K. A.; Zhang, Q.; Cheng, G. *Methods* 2005, 35, 211.

CHAPTER THREE:
SYNTHESIS OF A TOLL-LIKE RECEPTOR 2 FLUORESCENT ANTAGONIST FOR USE
IN INTRAOPERATIVE GUIDED SURGERY

3.1 Introduction

While pancreatic cancer is not the most frequently diagnosed cancer (53,000 new cases in 2016, US figure), it is one of the most deadly with 1 and 5 year survival rates of only 29% and 7%.¹ These low survival statistics are due in large part to poor diagnostic tools and a lack of targeted therapies. Surgical resection remains one of the most effective options for early stage treatment, but complete resection is often difficult due to local and distal metastases.² Further, complete resection of the tumors, leaving clean margins have the best prognosis.³

Toll-like receptors are type 1 transmembrane glycoproteins of which there are greater than 10 isotypes known.⁴ Toll-like Receptor 2 (TLR2) is endogenously expressed primarily on the surface of immune cells, and has a role in the recognition of bacterial invaders.⁵ The receptor recognizes pathogen-associated molecular patterns (PAMPs) like those of the lipoprotein components of bacterial cell walls. The molecular recognition of these ligands causes a heterodimerization with either TLR1 or TLR6 which results in an intracellular signaling cascade. An end product of TLR2 receptor activation is the release of proinflammatory cytokines, commencing the host defense of the innate immune system.

At the Moffitt Cancer Center, Dr. David Morse's group has previously confirmed high levels of expression of the receptor on pancreatic adenocarcinomas (70%) through tumor micro arrays and immunohistochemical staining.⁶ The receptor was not found in normal pancreas tissues. It was therefore determined that the receptor could be a valuable extracellular target of the disease. In collaboration with researchers in Arizona, a fluorescently-labeled peptide probe for TLR2 was developed.⁷ This compound is shown in Figure 3.1. The main features include dipalmitoylated cysteine, glycine, and *D*-serine in the pharmacophore, oligomeric PEG linkers flanking the pharmacophore, and a near infrared fluorescent dye (IR 800CW) coupled to the ligand's N-terminus. Unfortunately the bioactivity of this agonist ligand was regarded as a liability for its use as an imaging agent.

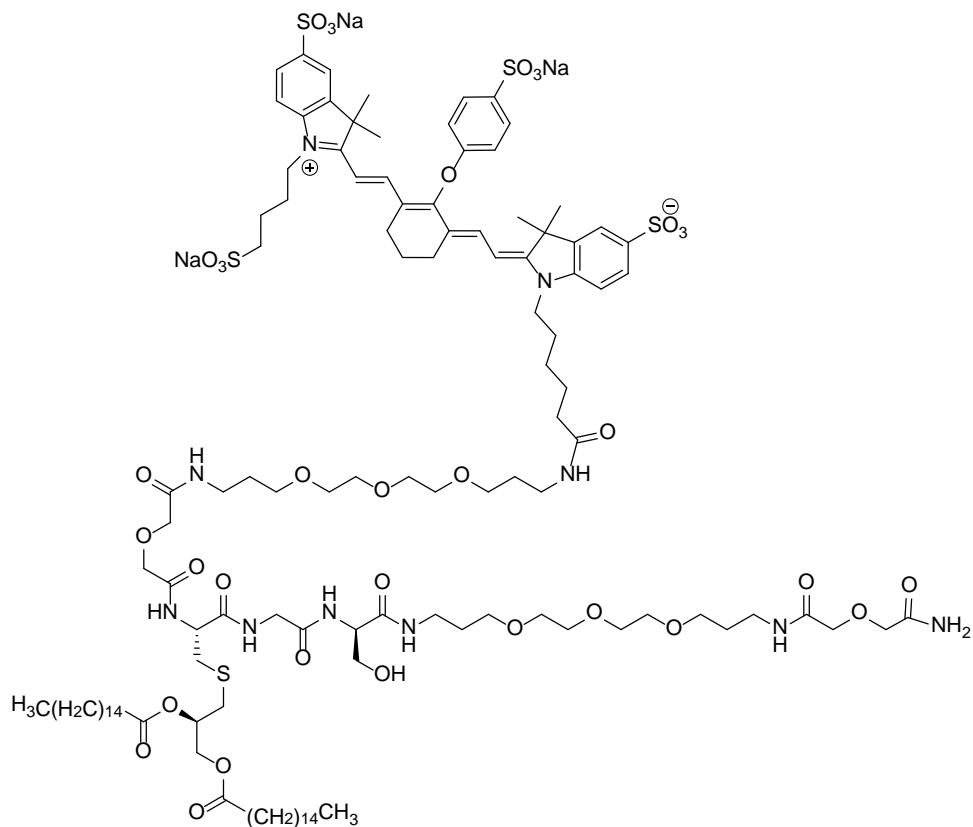


Figure 3.1. Diacyl-TLR2L-IR800CW.⁷

Because of TLR2's role in immune system signaling, it has become a target for immunotherapy and anti-inflammatory therapy. Recently small molecule libraries and natural product libraries have been screened in order to find inhibitors for TLR2.⁸⁻¹¹ Additionally, vaccine adjuvants have been designed as TLR agonists to increase the potency of peptide vaccines.¹² Other studies have designed monoclonal antibodies to blockade TLR2 and have been shown to inhibit several cancers including breast, lung, colorectal, head and neck squamous cell carcinomas.¹³ Finally, peptide-based agonists have been designed to mimic exogenous lipoproteins from microbial cell walls through the inclusion of fatty acids.^{14,15} None of these reported peptide ligands have been potent antagonists or have been conjugated with fluorescent dyes. However, SAR work has been reported in which the simplification of the pharmacophore led to modulation of receptor binding effects.^{16,17} From the review of these studies, a suggestion was made that a monoacylated cysteine in the pharmacophore of the compound in Figure 3.1 might reduce its agonist activity, rendering it more useful as an imaging probe.

An antagonist ligand with specificity for TLR2 and conjugated to fluorescent dye would be a valuable imaging probe for pancreatic adenocarcinoma and could improve the surgical resection of pancreatic tumors. Fitting with the central theme of our research, a peptide-based molecule probe was desired. Our synthetic goals for the fluorescent probe were to further simplify the binding motif and develop a cysteine-based monomer that could be easily incorporated into conventional solid phase peptide synthesis. A strategy employing differentially acid-sensitive protecting groups was developed to synthesize a monoacylated monomer with appropriately spaced and oriented synthons as elucidated in previous SAR work.

3.2 Results and Discussion

At the outset of this research project, the goal was to synthesize a monoacylated analog of a previously reported TLR2 ligand with a customized fluorescent dye to match the filter set of the imaging platform used by our collaborators. The peptide portion of molecule appeared amenable to conventional solid phase peptide synthesis, while some of the non-canonical monomers would have to be synthesized using organic chemistry techniques. Specifically the monoacylated L-cysteine and the fluorescent dye each required separate synthesis and characterization prior to peptide synthesis.

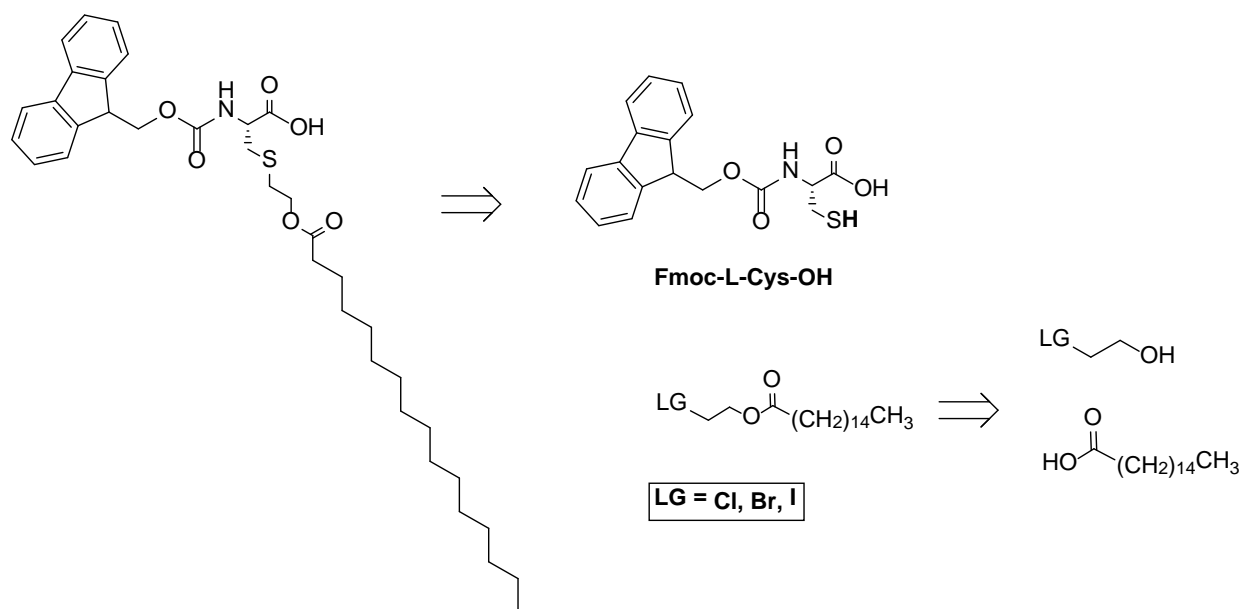
3.2.1 Fmoc-Cys(POE)-OH Synthesis

The amino acid monomer required for TL2RL synthesis was Fmoc-Cys(S-[palmitoyloxyethyl])-OH (Fmoc-Cys(POE)-OH). A simple retrosynthetic scheme was devised for this monomer and is shown in Scheme 3.1. The first disconnection would have resulted in two synthons, a commercially available Fmoc-Cys-OH and a palmitate ester with a terminal leaving group. The ester could further be disconnected to two other commercially available products: palmitic acid and a 2-halogenated ethanol.

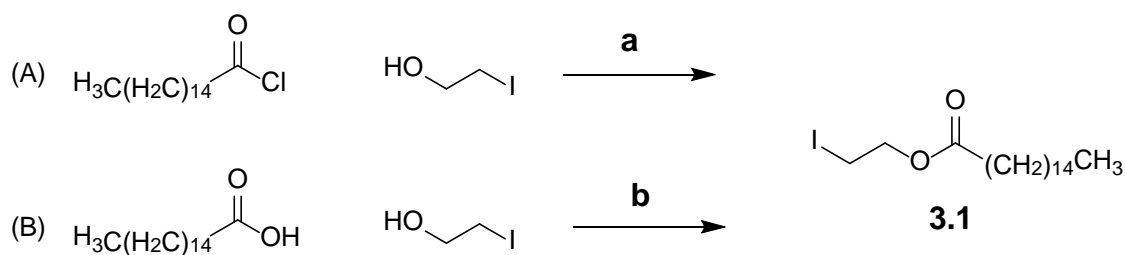
The palmitate ester was prepared in one step from either of two reactions. The schemes for both reactions are shown in Scheme 3.1. In reaction (A), palmitoyl chloride was reacted with 2-iodoethanol in DCM. In reaction (B), palmitic acid was condensed with 2-iodoethanol using dicyclohexylcarbodiimide (DCC) and catalytic 4-dimethylaminopyridine (DMAP) in DCM. Both products were purified by recrystallization and resulted in high yields. Reaction (A) was preferred

for the synthesis of compound **3.1** because of the dicyclohexylurea was difficult to remove from reaction (B).

From the retrosynthetic analysis, the next step in the forward route was to combine compound **3.1** with N^α-Fmoc protected L-Cysteine, which itself was prepared from treating Fmoc-Cys(Trt)-OH with TFA. This substitution reaction was attempted by deprotonation of the sulfhydryl on the cysteine and mixing with the palmitate ester, **3.1**. Unfortunately, very little of the correct sulfur alkylated product was observed by reaction monitoring with TLC and HPLC-MS. The majority product observed (Figure 3.2) was the result of substitution with the dibenzofulvene product of Fmoc deprotection. Many organic and inorganic bases were screened to find one that would balance the deprotonation of the sulfhydryl without removing the Fmoc protecting group. Unfortunately none were found that could produce reasonable yields of the desired product.



Scheme 3.1. Retrosynthetic analysis of Fmoc-Cys(POE)-OH.



(a) DCM, TEA, 92%
(b) DCC (1.2 eq), DMAP (5%), DCM, 95%

Scheme 3.2. Synthesis of 2-iodoethyl palmitate **3.1**.

Since the first approach to preparing Fmoc-Cys(POE)-OH failed due to the incompatibility of the base labile Fmoc PG, an alternative scheme (Scheme 3.3) was devised with orthogonal PGs. This scheme began with S-trityl protected *L*-cysteine and subsequently modified both the amino and carboxylic acid functional groups with PGs sensitive to hydrogenolysis. Next the S-trityl group was removed by treatment with TFA and compound **3.1** was substituted. Unfortunately the final step of removing the carboxybenzyl (Cbz) and benzyl (Bn) PGs failed. This failure was likely due to sulfur poisoning of the palladium catalyst. A Raney nickel catalyzed reduction was also attempted but resulted in compound desulfurization.

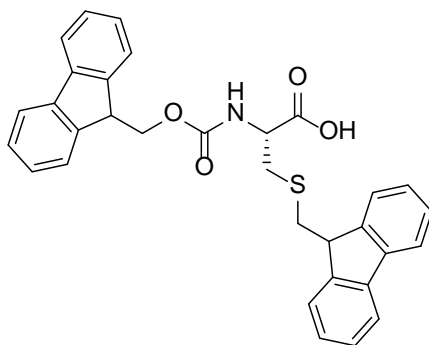
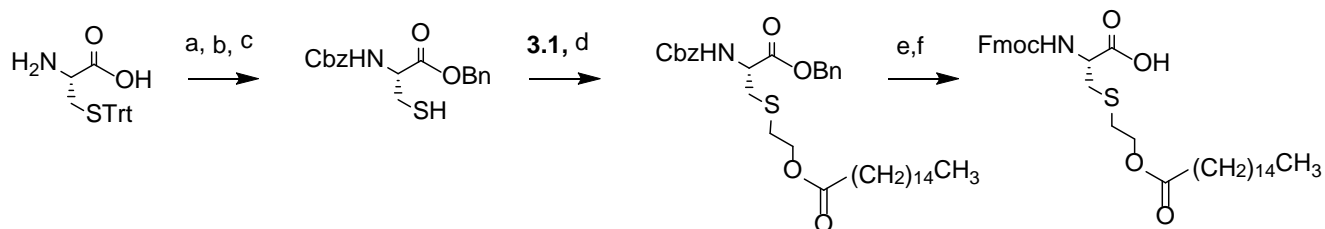


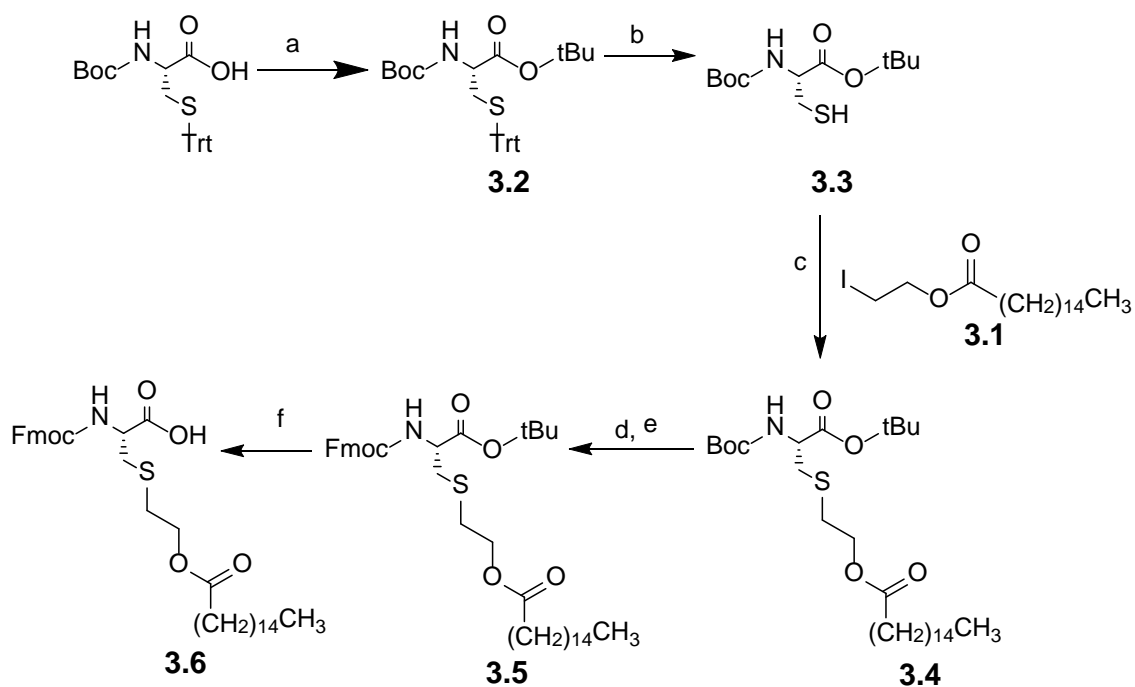
Figure 3.2. Structure of major product from the first attempt to synthesize Fmoc-Cys(POE)-OH.



(a) Cbz-OSu, (b) Benzyl-Bromide, (c) TFA (d) Cs₂CO₃ (e) H₂ Pd/C, (f) Fmoc-OSu

Scheme 3.3. Synthetic route for the preparation of Fmoc-Cys(POE)-OH via hydrogenolysis sensitive PGs.

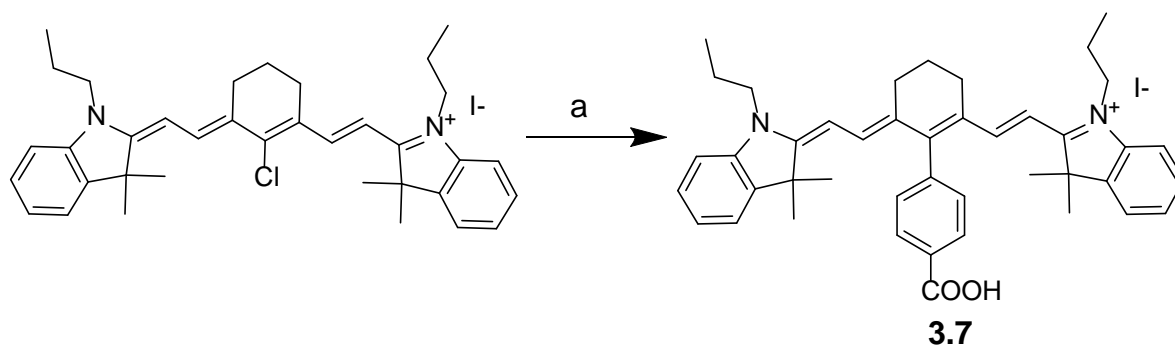
The next synthetic scheme made use of protecting groups that were differentially sensitive to acid. Scheme 3.4 depicts the route starting from Boc-Cys(Trt)-OH. First the carboxylic acid was esterified with *t*-butanol. Next the most acid-sensitive PG, S-trityl, was removed by treatment with 1% TFA in DCM at 0 °C. Next the substitution reaction was performed by stirring palmitate ester **3.1** with compound **3.3** and DIEA in peptide grade DMF at elevated temperature. The N-Boc group was removed by treatment with 10% TFA in DCM at 0 °C, and an N-Fmoc group was installed. Finally the OtBu ester was hydrolyzed in neat TFA to produce the final desired Fmoc-Cys(POE)-OH, **3.6**.



Scheme 3.4. Synthetic route for Fmoc-Cys(S-[palmitoyloxyethyl])-OH, **3.6**.

3.2.2 IR-780-COOH Synthesis

Many commercially available fluorescent dyes are tremendously expensive. For instance LI-COR sells a fluorescent dye (IRDye® 800CW) similar to one used in this project for \$1,990/50 mg. The precursor for our dye (IR780) was purchased from Sigma for \$74/1 g. To incorporate the dye into solid phase peptide synthesis (SPPS), a carboxylic acid was required. This functional group was attached to the acquired dye through Suzuki coupling with 4-carboxyphenyl boronic acid (Scheme 3.5). After silica gel chromatography, the purified dye was isolated in 56% yield.



(a) 4-CarboxyPhenyl Boronic Acid, K_2CO_3 , $Pd(PPh_3)_4$, Refluxing MeOH/ H_2O

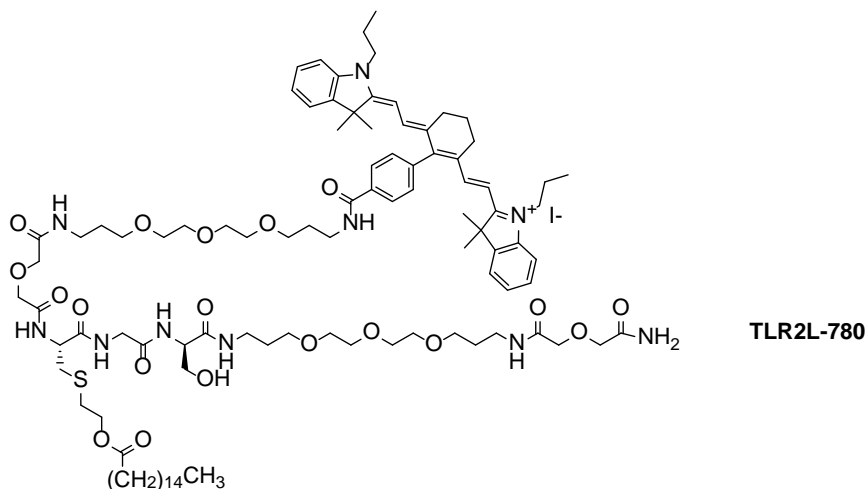
Scheme 3.5. Synthetic route for conjugated IR780 dye.

3.2.3 TLR2L Peptide Synthesis

Peptide synthesis was according to Scheme 3.6. TentaGel Rink amide resin (0.15 g, 0.036 mmol) was used as solid support and all amino acids were coupled using conventional N^{α} -Fmoc/tBu SPPS strategy and HCTU/NMM activation. An Fmoc-protected oligomeric PEG linker acid called PEGO was incorporated before and after the short pharmacophore (DSer-Gly-Cys(POE)) to help solubilize the final lipopeptide. After the completion of synthesis, the product was cleaved from resin using TFA cocktail. Instead of typical ether precipitation, the blue-green acid filtrate was reduced *in vacuo* and reconstituted in MeOH prior to HPLC purification. After purification and lyophilization, 33.4 mg (0.01753 mmol, 49%) of blue-green product was isolated.

NH₂⁻ Tentagel RAM 

- 1) a) Remove Fmoc, b) Couple 4 eq Fmoc-PEGO-OH, 4 eq HCTU, 15 eq NMM
- 2) a) Remove Fmoc, b) Couple 4 eq Fmoc-D-Ser(Trt)-OH, 4 eq HCTU, 15 eq NMM
- 3) a) Remove Fmoc, b) Couple 4 eq Fmoc-Gly-OH, 4 eq HCTU, 15 eq NMM
- 4) a) Remove Fmoc, b) Couple 4 eq Fmoc-Cys(POE)-OH, 4 eq HCTU
- 5) a) Remove Fmoc, b) Couple 4 eq Fmoc-PEGO-OH, 4 eq HCTU, 15 eq NMM
- 6) a) Remove Fmoc, b) Couple 4 eq IR₇₈₀-COOH, 4 eq HCTU, 15 eq NMM
- 7) TFA Cleavage
- 8) Lyophilization
- 9) RP-HPLC purification



Scheme 3.6. SPPS strategy used for TLR2L-780.

3.2.4 TLR2L Characterization

3.2.4.1 Product Purity and Identification. Figure 3.3 depicts the HPLC chromatogram of purified TLR2L-780 peptide. The purity of the compound was measured as a percentage of the total area under the curve of the HPLC trace. Purity was recorded as 96.4% with a retention time of 25.2 min. The peptide was also analyzed by MALDI-TOF; M⁺ was recorded as 1790.0989 (exp. 1790.0716).

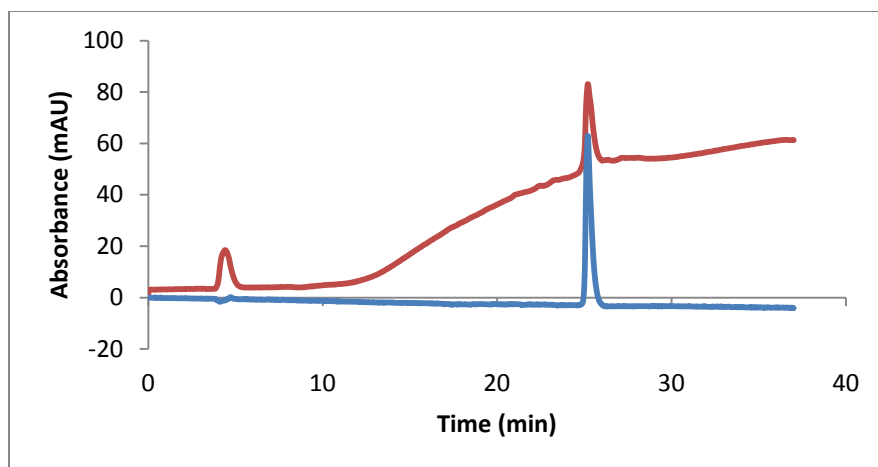


Figure 3.3. HPLC chromatogram of purified TLR2L-780. UV absorbance was monitored at 222 nm (red) and 300 nm (blue).

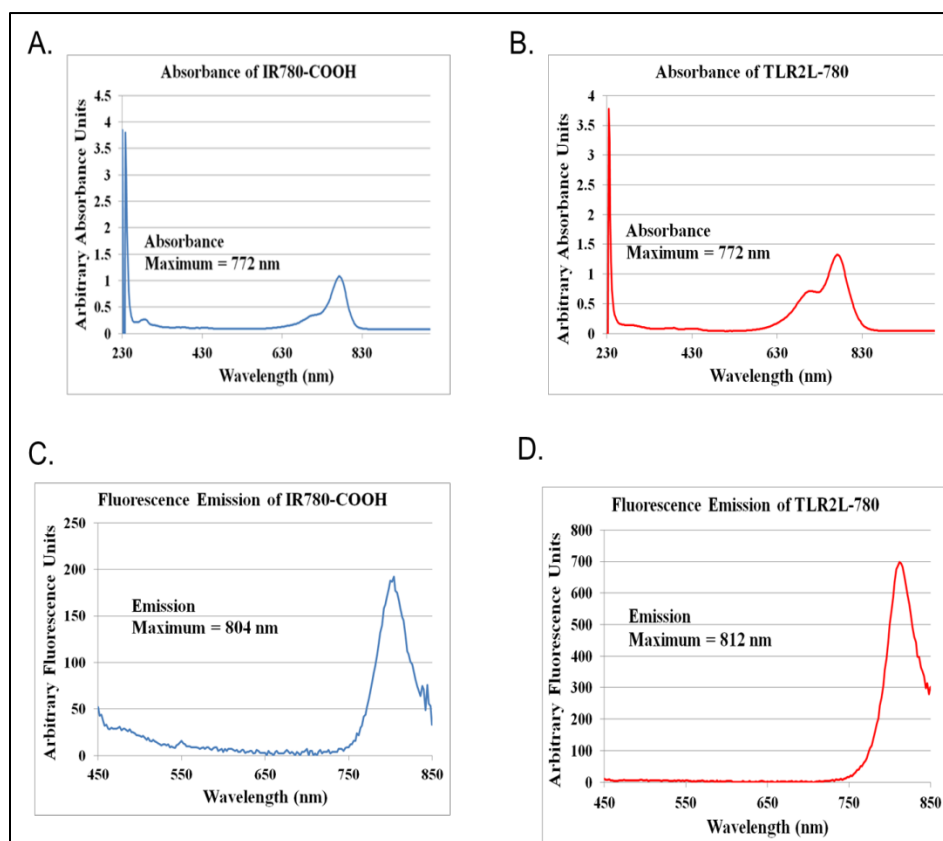


Figure 3.4. Optical characterization of IR780-COOH (3.7) and TLR2Li-780. Boxes A and C show absorbance and fluorescence emission spectra for IR780-COOH, 3.7, respectively. Boxes B and D show absorbance and fluorescence emission spectra for TLR2LI-780. Experiment and figure done with Dr. Allison Cohen (Morse Lab).

3.2.4.2 Optical Characterization. Both the IR780-COOH dye (3.7) and TLR2L-780 peptide were subjected to optical testing measuring both absorbance and fluorescence emission. Figure 3.4 shows the spectra recorded from these experiments. The Stokes shift of the peptide increased from the 32 nm of compound 3.7 to 40 nm. This shift is beneficial for imaging as a larger Stokes shift reduces the signal to noise due to the smaller overlap in emissions and absorption. This characteristic also has the effect of lessening photo quenching of the dye.

3.2.4.3 Lipophilicity Measurement. The lipophilicity of TLR2L-780 was determined by miniaturized shake flask method using an HPLC-triple quadruple-mass spectrometry for determining ligand concentrations, as was done in Chapter 2. The phosphate buffered solution was buffered to physiologic pH and the $\text{LogD}_{7.4}$ was measured as 2.05 ± 0.17 . This measurement of ligand lipophilicity is indicative of a compound with low aqueous solubility.

3.2.5 Biological Testing

The final fluorescent dye-conjugated peptidomimetic was tested by our collaborators in Dr. David Morse's group at the Moffitt Cancer Center. Amanda S. Huynh was the lead scientist for these experiments. First the compound was tested for *in cyto* binding affinity on a pancreatic tumor cell line with endogenous TLR2 surface expression (19,300 per cell). The binding affinity was measured using a time-resolved fluorescence (TRF) competition assay.¹⁸ Figure 3.5 shows the binding curve, $K_i = 16 \pm 1.4$ nM, $R^2 = 0.85$, $n=3$.

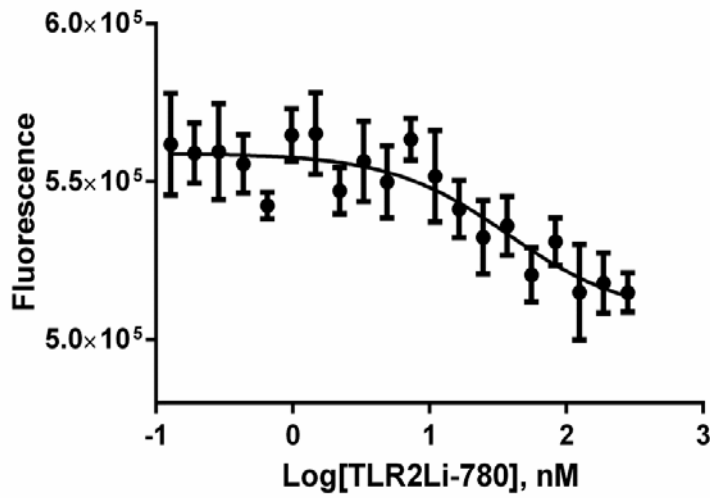


Figure 3.5. Competition binding assay SU.86.86 pancreatic tumor cells with endogenous TLR2 expression (n=3, $R^2=0.90$). Experiment and figure done by Amanda S. Huynh.

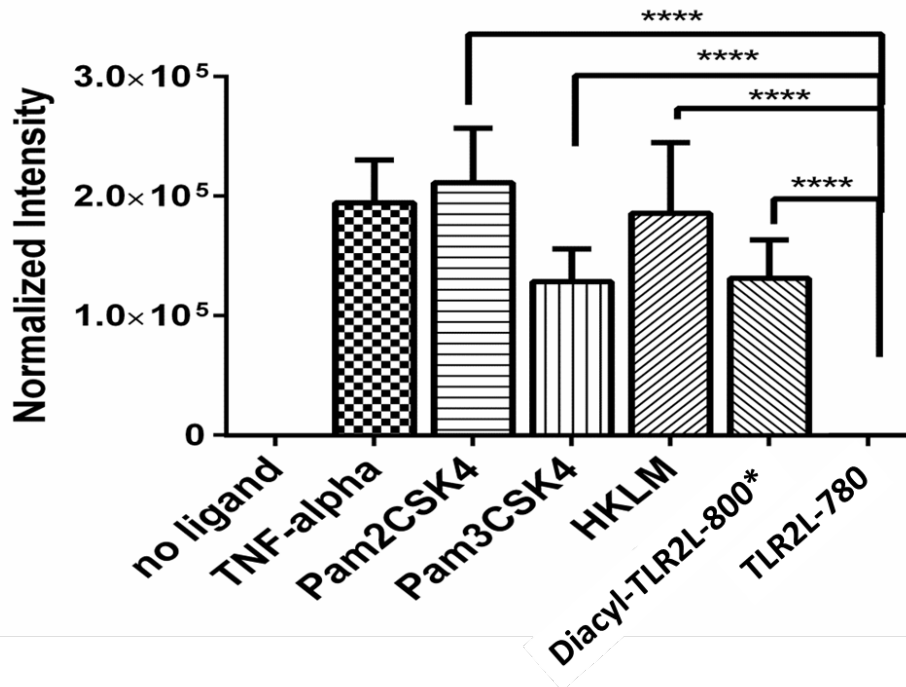


Figure 3.6. Functional bioassay measuring downstream signaling of TLR2 upon treatment with listed compound. Experiment and figure done by Amanda S. Huynh.

Next the Moffitt team tested the **TLR2L-780** peptide in a bioactivity functional assay. The compound was shown to inhibit receptor activity compared to the control agonists (Pam₂CSK₄, Pam₃CSK₄, HKLM) shown in Figure 3.6. The group's previously reported diacyl-TLR2L-800 compound (Figure 3.1)⁷ was also tested in this experiment and demonstrated comparable activity to the controls. The IC₅₀ of the new compound was measured at 361 nM. Further *in vitro* experiments were carried out to determine **TLR2L-780** selectivity for the TLR2. No agonistic activity was observed in human TLR3, TLR4, TLR5, TLR7, TLR8 or TLR9. Additionally, no inhibition of stimulation was measured for on the human TLR3, TLR5, TLR7, TLR8 or TLR9 receptors.

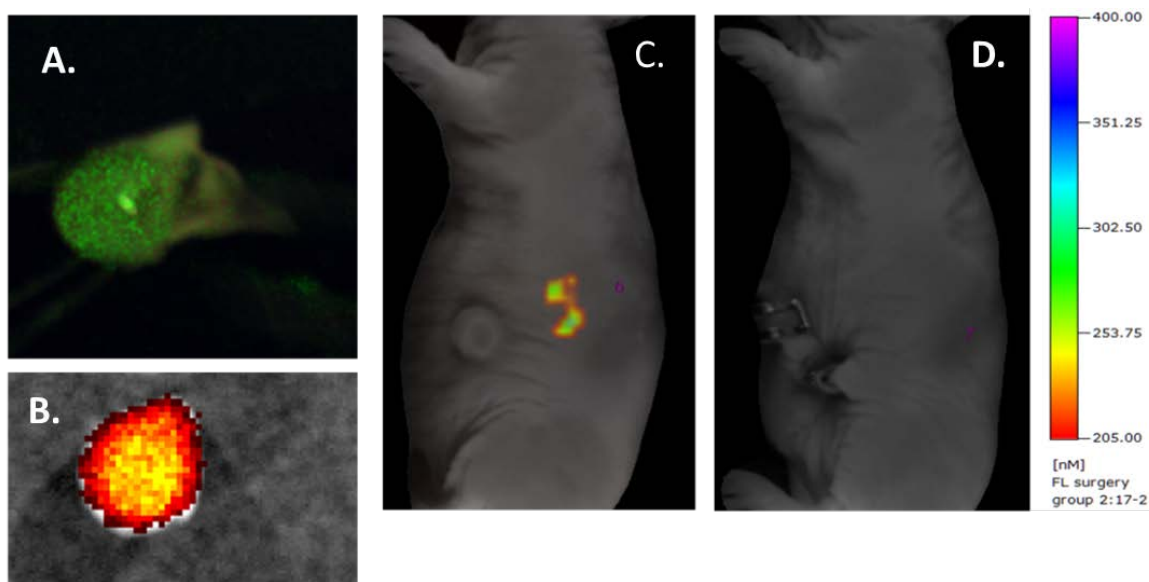


Figure. 3.7. *In vivo* and *ex vivo* near infrared (NIRF) guided imaging using **TLR2L-780**. A) Snapshot of real-time intraoperative fluorescence guided imagery of orthotopic pancreatic tumor. B) *Ex vivo* NIRF image of excised tumor. C) Pre-operative and post-operative (D) tomographic images of NIRF guided surgery. Experiment performed by Amanda S. Huynh.

Finally the Moffitt Team tested the TLR2L-780 peptide for in vivo tumor binding and in an intraoperative fluorescence guided surgery. Figure 3.7 highlights these experiments. The fluorescently labeled peptide ligand is shown to bind an orthotopic SU.86.86 pancreatic tumor (Figure 3.7, A). During a real-time image guided surgery the injected fluorescent peptide probe enabled the surgeon to remove the tumor cleanly at its margins. Figure 3.7, box C shows tomographic imagery of the tumor in place pre-surgery and box D shows complete resection of the tumor post-surgery.

3.3 Conclusions

A new toll-like receptor 2 binding peptide was designed and synthesized based upon structural modification of a previously reported agonist peptides. A synthetic scheme was developed to produce the cysteine-based monomer used in the ligand's pharmacophore. Additionally, a fluorescent tag with was designed and synthesized. Conventional peptide synthesis was used to prepare the final peptide-dye conjugate in good yields.

The new fluorescently labeled peptide targeting ligand was tested for biological function by our collaborators in the Moffitt Cancer Center. It was determined to be a highly selective ligand for human TLR2 with higher binding affinity than the diacyl version previously reported. The result of exchanging the diacyl-cysteine monomer with the new cysteine-palmitate ester and the IR-780 dye completely abrogated the biological effect seen in all previously reported TLR2 lipopeptide ligands. The novel antagonist, TLR2L-780, is the most potent TLR2 inhibitor reported to date and the only TLR2 antagonist-based fluorescence imaging probe. Finally the new imaging probe was

used in an intraoperative guided surgery and the orthotopic tumor was cleanly resected with guidance from the new probe.

3.4 Experimental

3.4.1 Materials and Instrumentation

N^α-Fmoc protected amino acids, and peptide synthesis reagents were purchased from ChemImpex (Wood Dale, IL). Rink amide TentaGel S resin (0.2 mmol/g) was acquired from Rapp Polymere (Tubingen, Germany). The *D*-serine amino acid was purchased with *t*-butyl and N^α-Fmoc protecting groups. An Fmoc-protected version of PEGO (20 atom linker: 19-amino-5-oxo-3,10,13,16-tetraoxo-6-azanonadecan-1-oic acid residue) was purchased from Novabiochem. IRDye780 and 4-carboxyphenylboronic acid was purchased from Sigma Aldrich (St. Louis, MO). Peptide synthesis solvents, dry solvents, and solvents for HPLC (reagent grade) were acquired from VWR (West Chester, PA), Sigma-Aldrich (Milwaukee, WI), or ChemImpex (Wood Dale, IL) and were used without further purification unless otherwise noted.

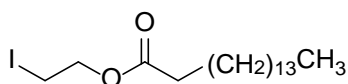
A Varian solvent delivery module with Dionex UVD340U diode array detector was used for preparative HPLC chromatography. Analytical scale HPLC was performed using a Dionex P680 system with quaternary pumps, autosampler, and diode array detector. Mass spectral analysis was performed with either Agilent 6540 QTOF with dual Jet-Stream ESI source, Agilent 6460 QQQ with Jet-Stream ESI source coupled to Agilent 1260 Infinity HPLC, Agilent LC/MSD VL single quadrupole with Agilent 1100 series HPLC, or Applied Biosystem 4700 MALDI-TOF-TOF proteomics analyzer with 355nm Nd:YAG laser. Peptide was assembled using a ChemGlass manual peptide vessel and lyophilized on a Labconco Freeze Dry/Shell Freeze System. Absorbance

and Fluorescence measurements were taken on a Tecan Infinite M-1000 PRO multimode microplate reader.

Nuclear Magnetic Resonance (NMR) experiments were carried out on either a 400 MHz Varian INOVA instrument with 5 mm ASW probe, a 500 MHz direct drive Agilent instrument with TR cryoprobe, or a 600 MHz Varian INOVA instrument with 5 mm BB rt probe. Spectra were analyzed by ACD labs NMR Workbook 2015. Chemical shifts (δ) were reported in parts per million (ppm) and corrected to residual solvent signals.

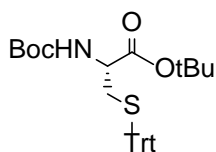
3.4.2 Experimental Procedures

3.4.2.1 Monomer Synthesis



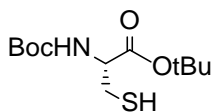
2-iodoethyl palmitate, 3.1

Palmitoyl chloride (3.33 mL, 10.9 mmol) and 2-iodoethanol (1.02 mL, 13.1 mmol) were combined in 300 mL dichloromethane. Triethylamine (3 mL, 22 mmol) was slowly added with mechanical stirring at room temperature. The reaction was concentrated after 1 hour. An off-white pure compound was isolated by recrystallization from DCM/MeOH (4.33 g, 10.9 mmol, 97%); ^1H NMR (400 MHz, CDCl_3) δ 4.33 (t, $J=6.81$ Hz, 2H), 3.30 (t, $J=6.78$ Hz, 2H), 2.34 (t, $J=7.52$ Hz, 2H), 1.58-1.70 (m, 2H), 1.21-1.34 (m, 24H), 0.89 (t, $J=6.76$ Hz, 3H); ^{13}C NMR (101 MHz, CDCl_3) δ 173.2, 64.3, 34.2, 31.9, 29.7, 29.6, 29.4, 29.3, 29.2, 29.1, 24.9, 22.7, 14.1, 0.5; GC-MS m/z [M^+] calcd for $\text{C}_{18}\text{H}_{35}\text{IO}_2$ 410.168, found 410.040.



tert-butyl N-(tert-butoxycarbonyl)-S-trityl-L-cysteinate, 3.2

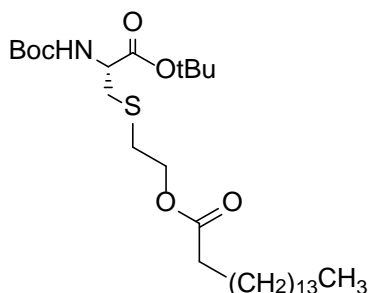
Boc-L-Cys(Trt)-OH (2.2 g, 4.78 mmol) was dissolved in 300 mL dichloromethane. N,N-dicyclohexylcarbodiimide (1.2 g, 5.7 mmol), *tert*-butanol (0.69 mL, 7.17 mmol), and 4-dimethylaminopyridine (0.0354 g, 0.23 mmol) were combined with the cysteine with mechanical stirring. The reaction was refluxed for 15 hours and the dicyclohexylurea by-product was filtered upon cooling (0 °C). The filtrate was washed with sat. aq. NaHCO₃ and brine. The organic layer was dried over anhydrous MgSO₄, the solvent was removed under vacuum. Crude residue was purified by silica gel chromatography (20% EtOAc/hexanes) to give **3.2** as a solid white powder after concentration (2.28 mg, 4.63 mmol, 97%). ¹H NMR (400 MHz, CDCl₃) δ 7.40 (br d, *J*=7.86 Hz, 5H), 7.12-7.34 (m, 13H), 5.08 (br d, *J*=7.26 Hz, 1H), 4.13-4.26 (m, 1H), 2.52 (br s, 2H), 1.41-1.46 (m, 15H); ¹³C NMR (101 MHz, CDCl₃) δ 169.7, 155.0, 144.4, 129.6, 128.3, 128.0, 127.7, 127.7, 129.5, 127.9, 126.7, 82.2, 79.7, 66.4, 52.9, 34.5, 28.3, 27.9 HRMS (ESI-QTOF) *m/z* [M + Na]⁺ calcd for C₃₁H₃₇NO₄S 542.2336, found 542.2347, 2.03ppm.



tert-butyl (tert-butoxycarbonyl)-L-cysteinate, 3.3

Compound **3.2** (1.3 g, 2.5 mmol) was dissolved in 1% TFA in DCM with triethylsilane (0.6 mL, 3.75 mmol). The deprotection was stirred at 0 °C, monitored by TLC with Ellman's

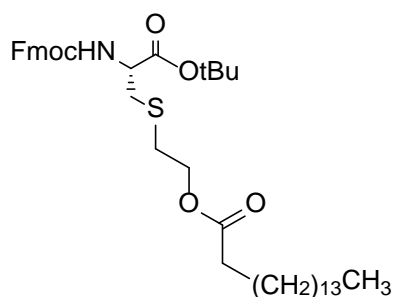
reagent as a developing agent. After 5 hours, the solvent was removed under vacuum yielding an oily residue. Crude residue was purified by silica gel chromatography (50% EtOAc/hexanes) to give **3.3** as a thick oil (0.544 g, 1.96 mmol, 78%). ¹H NMR (400 MHz, CDCl₃) 5.41 (br s, 1H), 4.47 (br s, 1H), 2.96 (br dd, J=3.80, 8.62 Hz, 1H), 1.48 (br s, 20H); ¹³C NMR (101 MHz, CHLOROFORM-d) δ 169.6, 155.0, 82.7, 79.9, 53.8, 42.0, 29.7, 27.9, 28.3, 18.1; HRMS (ESI-QTOF) m/z [M + Na]⁺ calcd for C₁₂H₂₃NO₄S 300.1240, found 300.1246, 2.00ppm.



(R)-2-((3-(tert-butoxy)-2-((tert-butoxycarbonyl)amino)-3-oxopropyl)thio)ethyl palmitate, 3.4

Compound **3.3** (126.6 mg, 0.4564 mmol) was dissolved in peptide grade DMF with compound **4** (229.2 mg, 0.5592 mmol). Diisopropylethylamine (0.159 mL, 0.9128 mmol) was added to the reaction with stirring and the reaction was heated to 80 °C. The reaction was monitored by TLC and iodine chamber for 15 h and then solvent was removed under vacuum. Crude residue was purified by silica gel chromatography (25% EtOAc/hexanes) to give **3.4** as a colorless oil (243 mg, 0.434 mmol, 95%). ¹H NMR (500 MHz, CDCl₃) δ 5.34 (br d, J=6.97 Hz, 1H), 4.41 (br d, J=6.83 Hz, 1H), 4.28-4.35 (m, 1H), 4.21 (dt, J=1.97, 6.73 Hz, 1H), 3.64-3.71 (m, 1H), 2.91-3.07 (m, 1H), 2.78 (t, J=6.72 Hz, 1H), 2.27-2.40 (m, 2H), 1.56 (br s, 9H), 1.48 (s, 7H), 1.45 (s, 7H), 1.25 (s, 22H), 0.88 (s, 3H); ¹³C NMR (151 MHz, CDCl₃) δ 173.5, 169.8, 155.1, 82.6, 79.9, 77.3, 63.7, 63.1, 53.9, 41.6, 34.9, 34.2, 34.1, 31.9, 31.3, 29.6, 29.6, 29.6, 29.3, 28.3, 27.9,

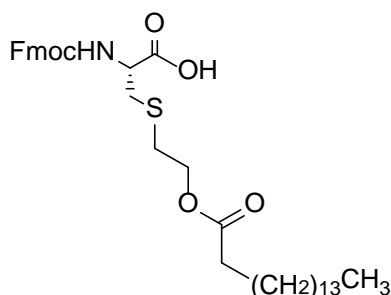
24.9, 22.6, 14.1; HRMS (ESI-QTOF) m/z $[M + H]^+$ calcd for $C_{30}H_{57}NO_6S$ 560.3979 ($[M+Na]^+$ 582.3799), found 560.3997, 3.21 ppm (582.3818, 3.26 ppm).



(R)-2-((2-(((9H-fluoren-9-yl)methoxy)carbonyl)amino)-3-(tert-butoxy)-3-oxopropyl)thio)ethyl palmitate, 3.5

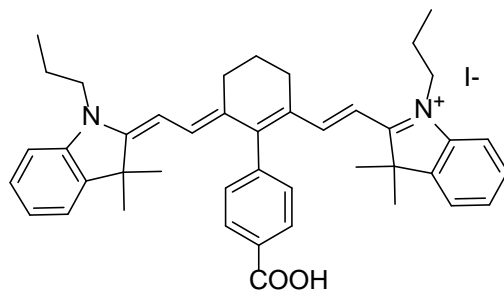
Compound **3.4** (243 mg, 0.434 mmol) was dissolved with 10% TFA in DCM at 0 °C. The deprotection was monitored by TLC with ninhydrin reagent developing. After 4 hours, the solvent was removed under vacuum and diisopropylethylamine (0.151 mL, 0.868 mmol) was added with Fmoc-OSu (176 mg, 0.521 mmol) in anhydrous DCM. After 2 hours the reaction was concentrated until reduced pressure and the crude residue was purified by silica gel chromatography (30% EtOAc/hexanes) to give **3.5** as an off-white semisolid (0.2072 mg, 0.3038 mmol, 70%). 1H NMR (500 MHz, $CDCl_3$) δ 7.78 (br d, $J=7.52$ Hz, 2H), 7.62 (br d, $J=7.40$ Hz, 1H), 7.41 (br t, $J=7.46$ Hz, 2H), 7.29-7.37 (m, 2H), 6.05-6.13 (m, 1H), 6.09 (s, 1H), 5.66 (br d, $J=7.46$ Hz, 1H), 4.52 (br d, $J=5.32$ Hz, 1H), 4.31-4.47 (m, 1H), 4.31-4.47 (m, 1H), 4.09-4.30 (m, 2H), 3.70 (d, $J=5.75$ Hz, 1H), 3.05 (br dd, $J=4.62, 17.03$ Hz, 1H), 2.79 (br t, $J=6.48$ Hz, 1H), 2.33-2.41 (m, 1H), 2.36 (t, $J=7.55$ Hz, 1H), 2.30 (br t, $J=7.58$ Hz, 1H), 1.57 (br s, 5H), 1.51 (s, 7H), 1.20-1.38 (m, 23H), 0.89 (br t, $J=6.91$ Hz, 3H); ^{13}C NMR (151 MHz, $CDCl_3$) δ 173.5, 173.3, 143.7, 143.7, 141.3, 127.7, 127.0, 125.1, 119.9, 83.0, 67.4, 67.1, 63.0, 56.7, 54.3, 53.7, 47.1,

34.9, 34.1, 34.0, 32.4, 31.9, 31.4, 30.4, 29.6, 29.6, 29.6, 29.4, 29.3, 29.2, 29.1, 28.0, 27.9, 25.8, 25.4, 25.3, 25.0, 24.9, 24.7, 24.6, 22.6, 18.6, 17.4, 14.1, 12.0; HRMS (ESI-QTOF) m/z $[M + H]^+$ calcd for $C_{40}H_{59}NO_6S$ 682.4136 ($[M+Na]^+$ 704.3955), found 682.4156 2.93 ppm (704.3978 3.27 ppm).



N-(((9H-fluoren-9-yl)methoxy)carbonyl)-S-(2-(palmitoyloxy)ethyl)-L-cysteine, 3.6

Compound 3.5 (74.2 mg, 0.109 mmol) was dissolved in 50% TFA in DCM. Solvent was removed under reduced pressure after 2 h. Final product was allowed to dry overnight under high-vacuum, yielding off-white semisolid compound 3.6. 1H NMR (500 MHz, $CDCl_3$) δ 7.77 (br d, $J=7.14$ Hz, 2H), 7.61 (br s, 2H), 7.41 (br t, $J=6.86$ Hz, 2H), 7.29-7.37 (m, 2H), 5.73 (br s, 1H), 4.66 (br s, 1H), 4.43 (br s, 1H), 4.34 (br t, $J=5.63$ Hz, 1H), 4.24 (br d, $J=6.86$ Hz, 2H), 3.65-3.73 (m, 2H), 2.95-3.23 (m, 1H), 2.79 (br s, 1H), 2.20-2.42 (m, 2H), 1.53-1.72 (m, 2H), 1.26 (br s, 26H), 0.89 (br t, $J=6.45$ Hz, 3H); ^{13}C NMR (126 MHz, $CDCl_3$) δ 174.3, 174.1, 156.0, 143.6, 143.6, 141.3, 127.8, 127.1, 125.1, 120.0, 67.5, 63.1, 53.5, 47.0, 34.3, 34.2, 31.9, 31.2, 29.7, 29.6, 29.6, 29.5, 29.4, 29.2, 29.1, 24.9, 22.7, 14.1; HRMS (ESI-QTOF) m/z $[M + H]^+$ calcd for $C_{36}H_{51}NO_6S$ 626.3510 ($[M+Na]^+$ 648.3329) found 626.3538, 4.47 ppm (648.3345, 2.47 ppm).



IR₇₈₀-COOH, 3.7

Commercially available IR780 dye (330 mg, 0.5 mmol) was refluxed in MeOH/H₂O (v/v) with 4-carboxyphenyl boronic acid (150 mg, 0.9 mmol) and Pd(PPh₃)₄ (5 mol%). The reaction was allowed to progress overnight and then dried *in vacuo* which produces solid, blue-green flakes. The crude product was purified with silica gel chromatography (50% MeOH/DCM) to yield compound 3.7 as blue-green crystalline solid (210 mg, 0.279 mmol, 56%). ¹H NMR (400 MHz, DMSO-d₆) δ 8.07 (d, J=8.12 Hz, 2H), 7.45 (d, J=7.45 Hz, 2H), 7.31 (d, J=3.86 Hz, 4H), 7.02-7.21 (m, 6H), 6.18 (d, J=14.13 Hz, 2H), 4.06 (br t, J=7.13 Hz, 4H), 2.65 (br t, J=6.29 Hz, 4H), 1.92 (br s, 2H), 1.58-1.80 (m, 4H), 1.10 (s, 12H), 0.90 (s, 6H); ¹³C NMR (151 MHz, CDCl₃) δ 172.1, 148.6, 142.1, 140.9, 131.1, 130.4, 128.4, 124.9, 122.3, 110.2, 99.4, 48.8, 45.7, 27.7, 24.7, 21.2, 20.7, 11.6; HRMS (ESI-QTOF) *m/z* [M]⁺ calcd 625.3789 for C₄₃H₄₉N₂O₂, found 625.3811, 3.52 ppm.

3.4.2.2 Ligand Synthesis, Purification, and Characterization. TLR2L-780 was synthesized by SPPS strategy following the outline given in Scheme 3.6. Resin was initially swollen in DCM for 20 min (2x), washed with NMP (2x), and then the Fmoc-protecting group removed with 20% piperidine, 2% DBU in DMF (2 x 20 min). Next the resin was washed with NMP (3x), DCM (3x), and finally with NMP (3x). The subsequent residue was coupled using 4 eq. of Fmoc-protected

amino acid, 4 eq. of HCTU and 15 eq. of NMM in NMP. Kaiser Assay was used to qualitatively test for reaction completion. The washing, Fmoc-deprotection, and coupling steps were repeated as indicated in Scheme 3.6 for each subsequent monomer.

Infrared dye 780 was reacted through Suzuki coupling with 4-carboxyphenylboronic acid as shown in Scheme 3.6 to produce the IR₇₈₀-COOH monomer. The dye conjugate was then coupled to the N-terminus of TLR2Li on-resin intermediate with HCTU activation (3 eq. IR₇₈₀-COOH, 3 eq. HCTU and 6 eq. DIEA in DMF). Crude peptide was cleaved from the resin with a cocktail (10 mL) of TFA, water, and TIS (95:2.5:2.5, v/v). Resin agitation was accomplished by N₂ gas bubbling over 4 h at room temperature. The filtrate was concentrated *in vacuo*. The residue from cleavage was dissolved in 50/50 MeOH, H₂O (v/v) and purified with the MeOH HPLC method described below. Blue-green solid product was isolated as crude TLR2L-780 compound.

Purity of the peptide was ensured using analytical HPLC. The peptide was chromatographed on an AAPPTEc Spirit Protein C-8 column, 250 x 46 mm, 5 µm with a linear gradient of 25-100 % B over 50 min, where A was H₂O + 0.1% TFA and B was MeOH + 0.1% TFA. Pure peptide was dissolved (1 mg/mL) in DMSO, stored at -20°C, and protected from light. Working solutions of 10 µg/mL were prepared from dilutions of the DMSO stocks in deionized water.

3.4.2.3 Mass Spectral Analysis: QToF and MALDI-TOF. MALDI-TOF experiments were used to analyze both crude and pure peptides. Samples were premixed 1:1 (v/v) with a saturated solution of α-cyano-4-hydroxycinnamic acid and then 500 nL was spotted on the MALDI plate. The instrument was run in positive, reflective mode.

For QToF characterization of purified peptides, the samples were introduced to the mass spectrometer as a direct infusion from the HPLC. The instrument was set to high resolution mode in extended dynamic range. Only positive polarity was measured. Real-time reference masses were infused in the second nebulizer during the acquisition.

3.4.2.4 Lipophilicity Measurement. First, the triple quadrupole mass spectrometer was set up as described in Chapter 2. The deviation from the procedure outlined in Chapter two is that an Alltech Alltima Cyano 100Å 5 µm (4.6 mm x 250 mm) HPLC column was used to chromatograph the peptide ligand into the spectrometer. Transitions of double charged pre-cursor ion (the most abundant) were mapped and optimized for the TLR2L. A standard curve was setup to measure unknown peptide concentrations. A 2.5 µM solution of ligand in sodium phosphate (25 mM, pH 7.4) was vortexed with three ratios of n-octanol and centrifuged to better partition the separated layers. Triplicate measurements of ligand concentration in each layer were used to calculate the LogD_{7.4}.

3.5 References

- (1) Society, A. C.; Society, A. C., Ed. Atlanta, GA, 2016.
- (2) Kim, C. B.; Ahmed, S.; Hsueh, E. C. *Journal of Gastrointestinal Oncology* 2011, 2, 126.
- (3) Ujiki, M. B.; Talamonti, M. S. *Semin Oncol* 2007, 34, 311.
- (4) Akira, S.; Takeda, K. *Nat Rev Immunol* 2004, 4, 499.
- (5) Takeuchi, O.; Akira, S. *Immunol Rev* 2009, 227, 75.
- (6) Morse, D. L.; Balagurunathan, Y.; Hostetter, G.; Trissal, M.; Tafreshi, N. K.; Burke, N.; Lloyd, M.; Enkemann, S.; Coppola, D.; Hruby, V. J.; Gillies, R. J.; Han, H. *Biochemical Pharmacology* 2010, 80, 748.
- (7) Huynh, A. S.; Chung, W. J.; Cho, H.-I.; Moberg, V. E.; Celis, E.; Morse, D. L.; Vagner, J. *Journal of Medicinal Chemistry* 2012, 55, 9751.
- (8) Zhou, S.; Cerny, A. M.; Bowen, G.; Chan, M.; Knipe, D. M.; Kurt-Jones, E. A.; Finberg, R. W. *Antiviral Research* 2010, 87, 295.

- (9) Zhong, Z.; Liu, L.-J.; Dong, Z.-Q.; Lu, L.; Wang, M.; Leung, C.-H.; Ma, D.-L.; Wang, Y. *Chemical Communications* 2015, 51, 11178.
- (10) Cheng, K.; Wang, X.; Zhang, S.; Yin, H. *Angewandte Chemie International Edition* 2012, 51, 12246.
- (11) Mistry, P.; Laird, M. H. W.; Schwarz, R. S.; Greene, S.; Dyson, T.; Snyder, G. A.; Xiao, T. S.; Chauhan, J.; Fletcher, S.; Toshchakov, V. Y.; MacKerell, A. D.; Vogel, S. N. *Proceedings of the National Academy of Sciences of the United States of America* 2015, 112, 5455.
- (12) Celis, E. *Cancer research* 2007, 67, 7945.
- (13) Farnebo, L.; Shahangian, A.; Lee, Y.; Shin, J. H.; Scheeren, F. A.; Sunwoo, J. B. *OncoTarget* 2015, 6, 9897.
- (14) Agnihotri, G.; Crall, B. M.; Lewis, T. C.; Day, T. P.; Balakrishna, R.; Warshakoon, H. J.; Malladi, S. S.; David, S. A. *Journal of Medicinal Chemistry* 2011, 54, 8148.
- (15) Seyberth, T.; Voss, S.; Brock, R.; Wiesmüller, K.-H.; Jung, G. *Journal of Medicinal Chemistry* 2006, 49, 1754.
- (16) Salunke, D. B.; Shukla, N. M.; Yoo, E.; Crall, B. M.; Balakrishna, R.; Malladi, S. S.; David, S. A. *Journal of Medicinal Chemistry* 2012, 55, 3353.
- (17) Agnihotri, G.; Crall, B. M.; Lewis, T. C.; Day, T. P.; Balakrishna, R.; Warshakoon, H. J.; Malladi, S. S.; David, S. A. *Journal of Medicinal Chemistry* 2011, 54, 8148.
- (18) Josan, J. S.; De Silva, C. R.; Yoo, B.; Lynch, R. M.; Pagel, M. D.; Vagner, J.; Hruby, V. J. *Methods Mol Biol* 2011, 716, 89.
- (19) Möller, I.; Thomas, A.; Geyer, H.; Schänzer, W.; Thevis, M. *Rapid Communications in Mass Spectrometry* 2011, 25, 2115.

CHAPTER FOUR:
DEVELOPMENT OF NOVEL TARGETED IMMUNOCONJUGATES FOR USE AS
PEPTIDE-TARGETED IMMUNE EFFECTORS

4.1 Introduction

The adaptive immune system is an immensely complex system of checks and balances that simultaneously protects against pathogens as well as aberrant cells while maintaining self-tolerance. Briefly, T cells are able to molecularly recognize and identify abnormal cells or pathogens via antigens expressed on the cell surface (Figure 4.1). In response to this recognition, T helper (T_h) cells release an array of cytokines to attract other immune modulators such as natural killer cells and B cells to the affected area. Additionally, T_h cells will attract and activate cytotoxic T cells, all of which, in concert with other immune modulators, will destroy the targeted cell. Inherent in this process are many molecular recognition events, or immune checkpoints, that can either enhance or dampen the immune response. Cancer cells use many different immune suppression strategies including the expression of proteins that prompt the downregulation of the immunologic response.¹ Disrupting this evasion by using so-called immune checkpoint inhibitors to blockade the signals has been a revolutionary idea in cancer treatment, and is currently a promising research target.^{2,5}

Ipilimumab was the first and still only FDA approved anti-cytotoxic T-lymphocyte antigen-4 (α CTLA4) immune effector. It was the first approved checkpoint inhibitor for treatment of metastatic melanomas in 2011.⁶ This drug was the first non-standard chemotherapeutic to substantially increase survival outcomes for advanced, surgically unresectable melanomas.⁷ A few years later, two new immune effectors targeting the programmed cell death protein-1 (α PD-1) were approved for metastatic melanomas in 2014.⁸ Nivolumab and pembrolizumab are both α PD-1 antibodies used for analogous blockade therapy, and both received new indications for metastatic squamous non-small cell lung cancer (NSCLC) in 2015. In fact, lung cancer indications are more frequently being assigned to these immunotherapeutics.⁹⁻¹¹ Many additional new immune effectors are currently being researched and several have made their way to various stages of preclinical and clinical trials.¹²

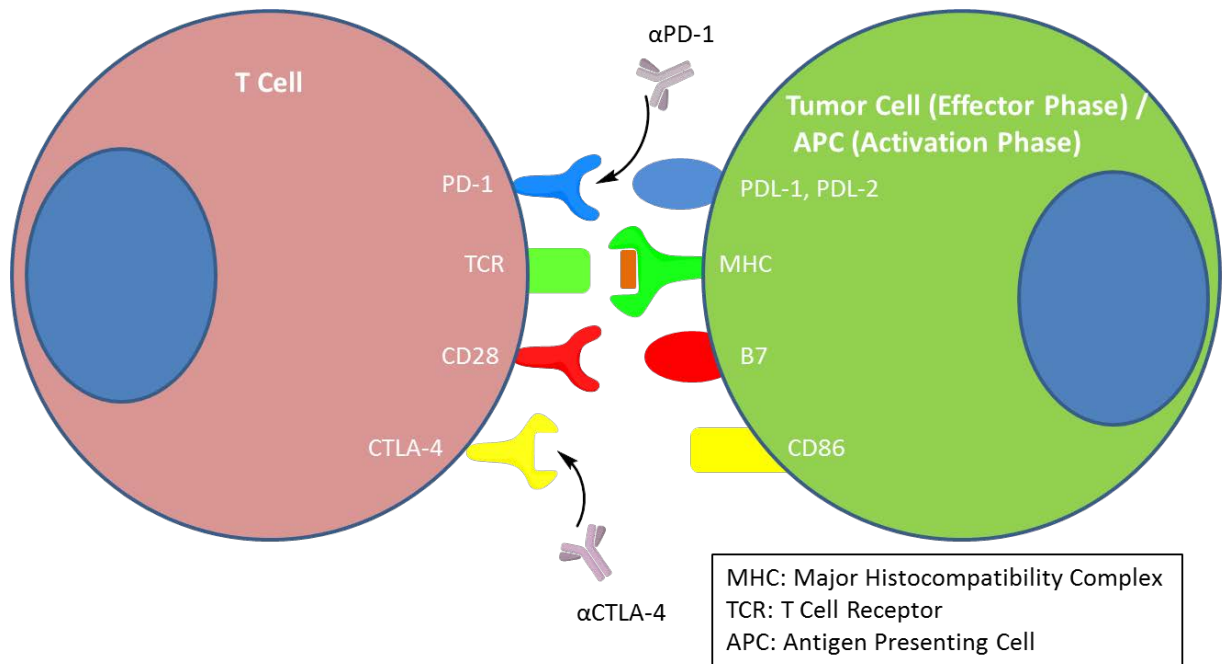


Figure 4.1. Key cell surface molecular interactions in T cell signaling.

The downside to these new armaments of antibody drugs comes from an over-activation of the systemic immune system; almost all toxicity seen from these new drugs is termed immune related adverse effects (irAE). Typical issues include dermatitis 40%,¹³ diarrhea/colitis 30%,¹⁴ and sometimes hepatitis.¹⁵ Clinical evidence suggests that the irAE from the α PD1 class of antibodies is not as bad as that from the α CTLA4, however typical combinations and sequential protocols make use of both.^{16,17} Once irAEs are observed in the clinical setting, the immunotherapy is often discontinued, until the treatment of the side effects through the administration of steroids, tumor necrosis factor- α inhibitors (infliximab), and immunosuppression.¹⁵ Not only do these interventions cost time and money, the patient loses critical time without the immunotherapy.

Because immune checkpoint inhibitors are antibodies with an affinity for proteins on the surface of immune cells, they are technically a type of targeted therapy. However these current checkpoint inhibitors have little discrimination for tumor cells. The vision of the current study was to reduce the immune related adverse events (irAEs) and increase potency by targeting the PD-1 blockade using established tumor cell surface, targeted ligand (TL) technology to concentrate the immune effectors in the tumor microenvironment.

Although the incidence of lung cancer in the US has declined in recent decades (due to fewer smokers), the American Cancer Society still lists lung cancers as the second most frequently diagnosed cancers among both men and women.¹⁸ Owing to both its severity and the large number of affected people, this insidious disease also boasts the highest cancer death rates in the US with one and five year survival rates at 44% and 17% respectively.¹⁸ Unfortunately, the rest of world has an increasing number of smokers and the WHO data reports 1.6 million people died of lung cancer worldwide in 2015. Treatment options depend on the subtype and stage of disease but

most often include surgery, radiation therapy, and chemotherapy. Patients with advanced stages of the largest subtype, non-small cell (83%), can benefit from recent advances in immunotherapy.

The δ -opioid receptor (DOR) is characterized as a 7-transmembrane GPCR that has normal expression in brain tissue, where it is understood to be involved with analgesic effects upon agonistic binding. In the 1990s this extracellular receptor was found to be overexpressed on the surface of NSCLC tumors.^{19,20} The use of this receptor for imaging and characterization of lung cancer tumors demonstrated in subsequent research.^{21,22} Previous work in our group capitalized on this overexpression through the synthesis of a dipeptide antagonist for the delta-opioid receptor and coupling fluorescent dyes with the goal of real-time intraoperative guided surgical resections.^{23,24}

Combining the group's previous work with the novel idea of target immunotherapy led to the goal of the current research project: to synthesize bifunctional molecules that target tumor cells through overexpressed extracellular receptors and subsequently effect a local immune response in the tumor micro environment. Because these biomolecules can target and concentrate at the tumor, the resulting immunoconjugate should have a larger therapeutic window than current analogous therapies. The reduction of systemic toxicities would also likely require the use of lower levels of systemically circulating drug. Finally this new class of immune modulators could be more pharmaco-economic since doses of costly antibodies might be reduced.

4.2 Results and Discussion

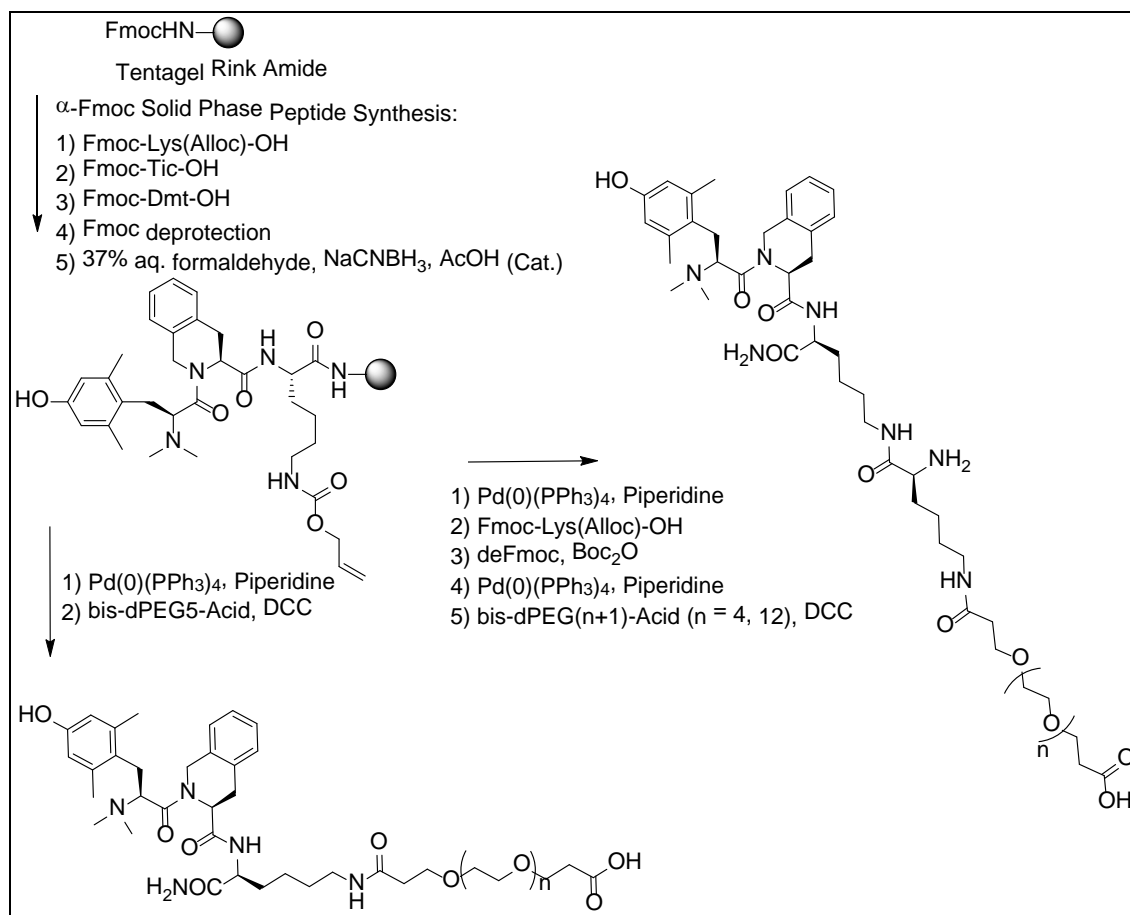
4.2.1 Targeting Ligand Design and Synthesis

Often referred to simply as 'DmtTic,' the delta opioid receptor (DOR) targeting peptide ligand is a logical first choice to test the viability of peptide-targeted checkpoint inhibitors. The

pharmacophore is well characterized as a selective, high affinity ligand for the δ -opioid receptor.^{25,26}

The synthesis is facile with conventional peptide synthesis techniques, and is amenable to bioconjugations with simple modifications. While the DOR is understood to be a bonafide cell surface marker of NSCLC, its expression in normal tissues is mostly limited to the CNS. DmtTic's peptidic nature limits its permeation of the blood brain barrier, especially once covalently attached to a 150 kDa antibody.

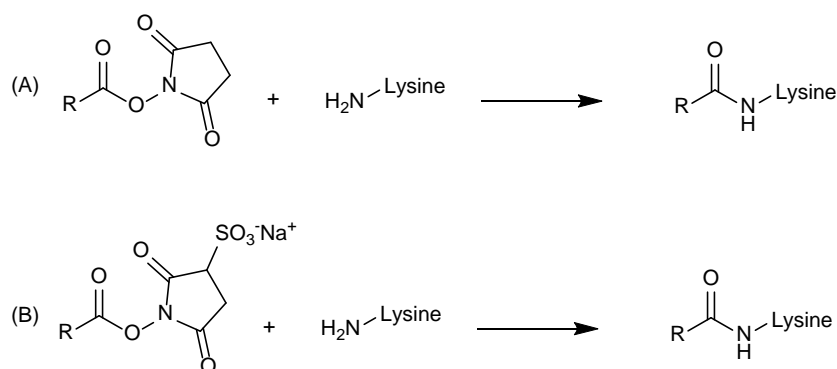
Peptide synthesis was performed using conventional 9-fluorenylmethoxycarbonyl (Fmoc) based solid-phase peptide synthesis (SPPS). TentaGel MB NH₂ resin was chosen as an appropriate resin due to the swelling characteristics of the polyethylene glycol (PEG) linker in a variety of both aqueous and polar organic solvents. For these reasons the resin was found to be efficient for the peptide synthesis steps, including a reductive amination step using aqueous formaldehyde. Scheme 4.1 outlines the synthesis of the DmtTic targeting ligand. As in previous research projects, the C-terminal lysine of each of the targeting ligand analogs was an important synthetic tool which allowed for creating a branched structure. By employing an orthogonal protecting group (Alloc) on the ϵ -amino group, the linear portion of the peptide was completed first. Then the structure was branched after alloc deprotection to incorporate the PEG oligomer (Scheme 4.1, bottom product). To incorporate two branched elements, a second lysine(Alloc) amino acid was coupled to the first's ϵ -amino group. The right product on Scheme 4.1 shows this branched TL. This scaffold was used to incorporate both a fluorescent dye and an oligomeric PEG monomer.



Scheme 4.1. SPPS strategy used to synthesize the DmtTic targeting ligand. The bottom and right products depict how products could have no branching or branching from a C-terminal lysine residue in order to incorporate extra elements into the targeting ligand via the remaining primary of the terminal lysine.

Methods for conjugating peptides and drugs to biomolecules are described in many primary texts, including Hermanson's *Bioconjugate Techniques*.²⁷ Scheme 4.2 depicts two strategies to conjugate the ϵ -amine of ubiquitous lysine side chains. By pre-activating the DmtTic ligand with an ester leaving group, like N-hydroxysuccinimide or N-hydroxysulfosuccinimide (Scheme 4.2, (A) and (B) respectively), coupling of ligand with antibody could be affected. These coupling strategies were a strategic choice for DmtTic due to its lack of nucleophilic side chains. For instance, amino acid side chains containing amines or sulfhydryls could intramolecularly compete with the lysines

on the proteins for the activated ester of DmtTic. The most nucleophilic functional group on the DmtTic targeting ligand was the primary amine on the N-terminus. Salvadoria et al. have previously reported SAR indicating that the N-terminal dimethylated analog of DmtTic retained comparable binding affinity and selectivity for the DOR.²⁶ To this end, the N-terminus of DmtTic was dimethylated to limit any other competing coupling chemistry of the ligand that could lead oligomerization of the DmtTic ligand as well antibody coupling. As shown in Scheme 4.1, the dimethylation reaction was done on solid support before alloc deprotection. Initial experiments involved reductive amination using 1,3,5-trioxane as a source of formaldehyde, and several reductants were surveyed. Optimal reductive amination was accomplished with aqueous formaldehyde (37%), fresh NaBH₃CN, and catalytic AcOH.



Scheme 4.2. Common conjugation chemistries used to functionalize bio molecules. Rows (a) and (b) show activated NHS and Sulfo-NHS esters reacting to form native amide bonds with lysine side chains from a biomolecule.

Another crucial design element in the TL was the inclusion of a water soluble linker. The appropriate space between the TL and the antibody is critical for the functionality of both components. A relationship is known to exist between linker length, flexibility and increased

avidity for the target receptor.^{28,29} Linker length and composition, and also receptor number and spacing/relative distance, are critical factors to balance when designing linkers. The linker chosen for this DmtTic ligand was an oligomeric polyethylene glycol monomer, or discrete PEG (dPEG), that can be purchased in various lengths. Additionally, the polyethylene glycol monomers of the linker were intended to enhance aqueous solubility of the relatively hydrophobic DmtTic pharmacophore.

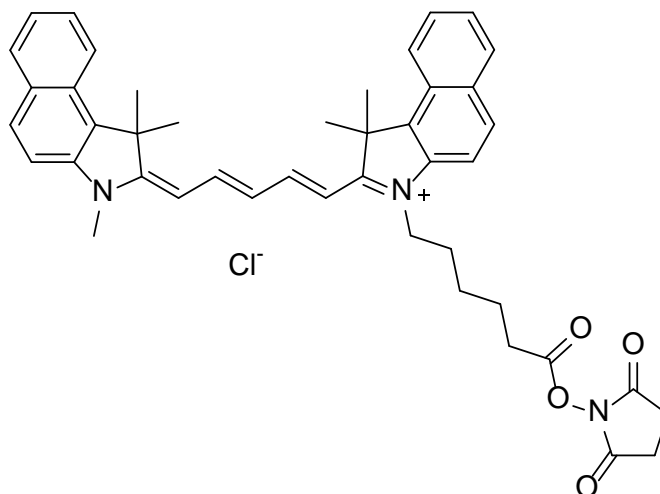


Figure 4.2. Structure of Cyanine Dye 5.5, NHS-ester.

One final contribution to the design of the targeting ligand was the inclusion of a fluorescent dye. For purposes of monitoring biodistribution and pharmacokinetics, a commercially available indocyanine green (ICG) derivative dye, named Cy5.5 was purchased. Figure 4.2 illustrates the structure of the dye as it was purchased from Lumiprobe. The dye was chosen both for its emission and excitation characteristics (678/694 nm respectively) and for its NHS-ester. For economic reasons, the dye was not coupled to the peptide while on solid support.

Instead the NHS-ester dye was coupled in solution with the purified peptide as shown in Figure 4.3.

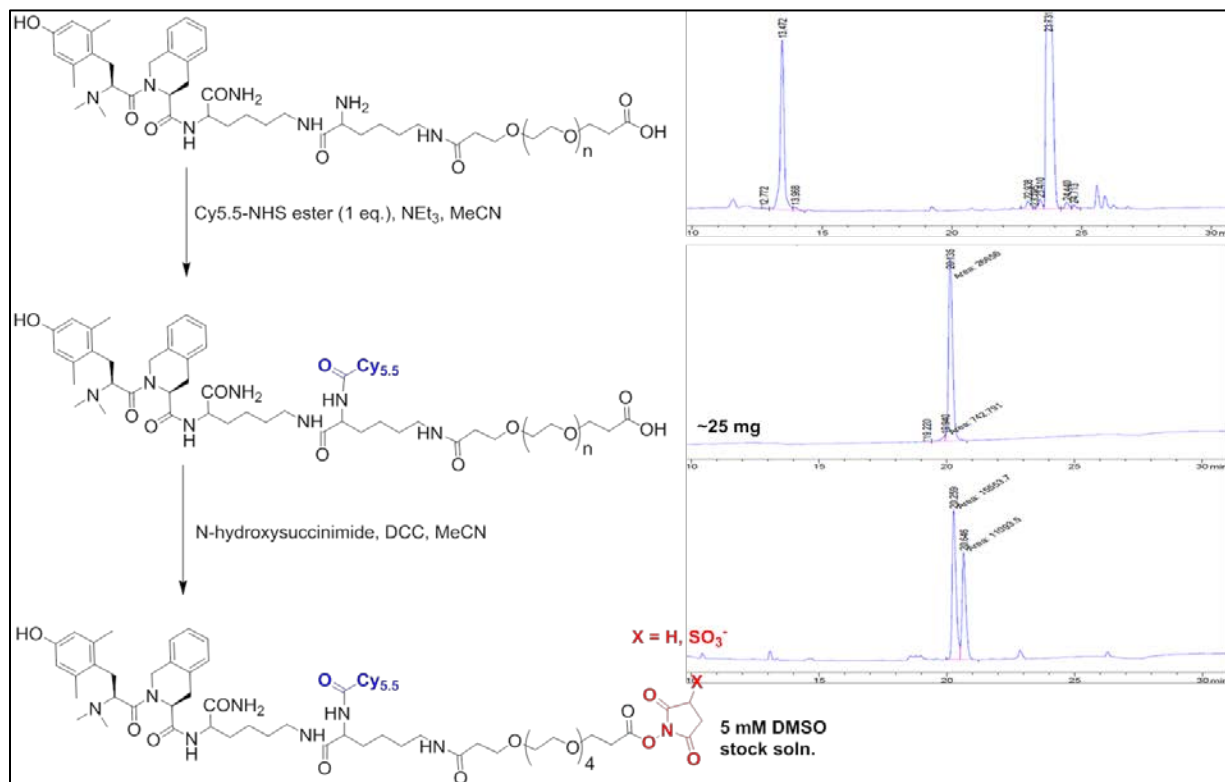


Figure 4.3. Solution-phase modifications to targeting peptide ligand. (a) Cy5.5-NHS ester (1 equiv.), NEt_3 (5 equiv.), MeCN (b) N-hydroxysuccinimide (3 equiv.) DCC (3 equiv.), MeCN. The inset HPLC traces (right of reaction scheme) demonstrate how the reaction was monitored for completion of each step.

In summary, different versions of DmtTic TL were synthesized. The structures of these compounds are shown at the end of this chapter and pertinent information is summarized in Table 4.1. Variations included length of dPEG linker, the inclusion of cyanine dye, and type of NHS leaving group. One final compound (4.5) was made with a scrambled pharmacophore by reversing the order of amino acids in the pharmacophore. The purpose of this compound was to prepare negative-binding control immunoconjugates. After each targeting ligand was synthesized,

pre-activated, and lyophilized, they were each fully characterized by HPLC and MALDI-TOF. Prior to use, each compound was reconstituted in DMSO to 5 mM. These targeting ligand stock solutions were then used for immunoconjugate synthesis. Unused DMSO solutions were frozen to -20 °C and were assayed by HPLC for hydrolysis before use in later immunoconjugate reactions.

Table 4.1 Summary of peptide targeting ligands prepared for subsequent immunoconjugation.

	Targeting Ligand	Linker	Dye	Activated LG
4.1	N,N-DiMethyl-Dmt-Tic-Lys-CONH ₂	dPEG5	~	NHS
4.2	N,N-DiMethyl-Dmt-Tic-Lys-CONH ₂	dPEG5	Cy5.5	NHS
4.3	N,N-DiMethyl-Dmt-Tic-Lys-CONH ₂	dPEG5	Cy5.5	SulfoNHS
4.4	N,N-DiMethyl-Dmt-Tic-Lys-CONH ₂	dPEG13	Cy5.5	NHS
4.5	N,N-DiMethyl-Lys-Tic-Dmt-CONH ₂	dPEG5	Cy5.5	NHS

4.2.2 Immunoconjugate Synthesis

The bioconjugation reaction of activated targeting ligand with antibody is shown in Figure 4.4. This cartoon represents the stochastic reaction where the roughly 60 surface accessible lysine side chains may react with the activated targeting ligand (presented as blue spheres). A characteristic of this reaction was the random assortment of potential products. Due to differences in concentration, pH, temperature, salt concentration, etc., this reaction produced slightly different combinations of products with each batch.

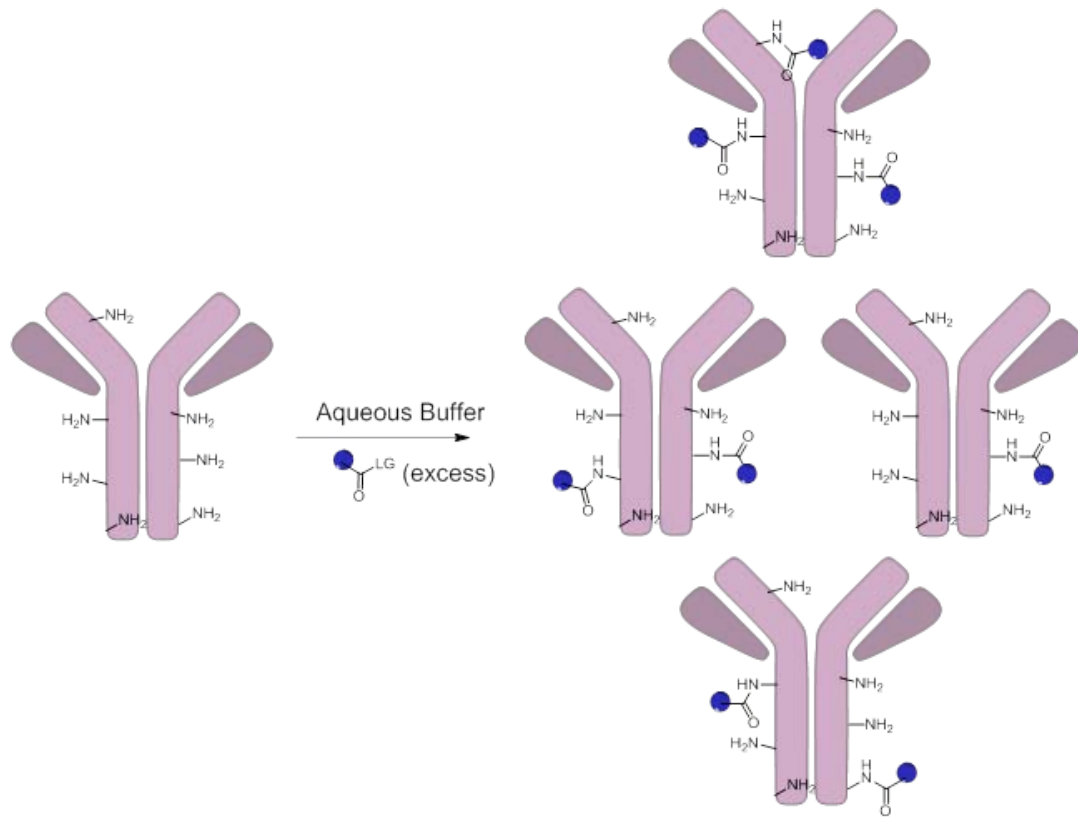


Figure 4.4. Bioconjugation reaction for the addition of targeting ligand to immune effector antibody. This cartoon is only a representation of possible products of lysine side chains (-NH_2) and targeting ligand (blue spheres).

Similar batch-wise differences were seen in first-generation antibody-drug conjugates, or ADCs. These targeted therapeutics attach a cytotoxic drug payload to a targeting antibody. Typically the drug is linked to the antibody through a cleavable linker which releases the cytotoxic payload once the antibody is internalized to its cellular target. While developments in this field have elucidated methods to specifically attach payloads to antibodies, the earliest conjugates were either lysine or cysteine linked conjugates. An important trait of ADCs is the so-called drug-to-antibody ratio, or DAR. As the name implies, this value is a measure of the number of drug molecules given as a ratio to the number of antibodies. Even with tight production controls this value could change slightly for each batch of immunoconjugates.³⁰

Because our targeted immunoconjugate scheme reverses the paradigm of ADCs by targeting the antibody with its payload, we thought it would be appropriate to rename the payload-to-antibody ratio. Hence the name, targeted ligand-to-antibody ratio, or TAR. Analogously to the first generation ADCs, our TAR changes slightly between batches but can generally be controlled through the conditions set during each conjugation reaction. It serves as one measurable output to be used in tracking the efficiency of the conjugation reaction.

A series of initial experiments were performed to optimize the bioconjugation reaction. Table 4.2 lists the tested conditions. First the pH of the conjugation buffer was varied. A trend of increasing TAR followed from increasing the pH of solution to 8.5 in 50 mM HEPES buffer. Changing the buffer component from HEPES to phosphate also served to increase the TAR of the resulting conjugate. Finally the effects of salt concentration and organic modifier were tested. Increased salt concentration had large deleterious effects to the TAR, reducing from 3.63 to 1.46.

Table 4.2. Targeting Ligand to Antibody Ratio (TAR) observed from various buffers during immunoconjugation.

	HEPES pH 7.5	HEPES pH 8	HEPES pH 8.5	Phosphate pH 8	HEPES pH 8 10% EtOH	HEPES pH 8 50mM NaCl	HEPES pH 8, 10% EtOH, 50mM NaCl
NHS ester	4.01	3.63	4.76	5.13	3.23	1.46	1.72
Sulfo-NHS ester	ND	0.62	ND	ND	1.96	1.46	ND

The addition of an organic modifier to the reaction buffer was tested due to poor aqueous solubility of the TL. Without organic modifier in the conjugation reaction, DmtTic didn't mix

well in the aqueous solution. The addition of up to 10% ethanol was qualitatively observed to increase solubility. However the resulting TAR was actually lower with the ethanol. Due the compatibility with antibodies and typical use as a cryoprotectant, later tests using ethylene glycol as organic modifier yielded high TAR values.

Table 4.3 shows another measure of reaction efficiency under the given optimization conditions: protein recovery. Due to the measurement error when determining final volumes, one of the values was recorded over 100%. However the clear trend suggests that the 10% ethanol solution promotes protein recovery. The use of organic modifier was therefore continued in further experiments.

A final variable tested during the optimization experiments was the leaving group (LG). Up to this point the DmtTic targeting ligand was preactivated as the N-hydroxysuccinimide ester. Due to the previously mentioned solubility issues, a similar leaving group with a single appended sulfonate group was synthesized. This N-hydroxysulfosuccinimide imparted an additional negative charge to targeting ligand and was designed to help solubilize the compound during the bioconjugation reaction. Unexpectedly the sulfo-NHS activated compounds failed to increase either the TAR or protein recovery measurements.

Table 4.3. Recovered protein as a result of the varied immunoconjugation conditions.

	HEPES pH 7.5	HEPES pH 8	HEPES pH 8.5	Phosphate pH 8	HEPES pH 8 10% EtOH	HEPES pH 8 50mM NaCl	HEPES pH 8, 10% EtOH, 50mM NaCl
NHS ester	75%	55%	68%	75%	102%	53%	68%
Sulfo-NHS ester	ND	14%	ND	ND	64%	68%	ND

Ultimately the TAR of each batch was controlled through the amount of excess TL in the reaction. Most reactions with ten equivalents TL yielded a TAR of ~ 5 . Doubling the amount of TL in the reaction proportionately increased resulting TAR. Table 4.4 illustrates these trends by listing the completed immunoconjugates. Both conjugates D13A and D26A were conjugation reactions with 10 equivalent TL on 10 mg antibody, and the TAR for each were measured at 4.58 and 4.20 respectively. Reactions D13B and D26B were completed in parallel, only varying the excess TL (20 equivalents each). Both D13B and D26B had a TAR of roughly 12. In this manner the control over TAR was followed for subsequent batches of immunoconjugates summarized in Table 4.4.

4.2.3 Immunoconjugate Workup and Characterization: Size Exclusion

After the bioconjugation reaction of targeting ligand and antibody, the new conjugates were concentrated in Vivaspin 30 kDa MWCU centrifuge tubes. Unfortunately this method failed to adequately separate the excess, hydrolyzed targeting ligand from the substantially larger immunoconjugates. Instead, some of the excess targeting ligand was observed to stick to the membrane of the filter as a blue precipitate.

A subsequent step of passing the concentrated immunoconjugate through a size exclusion column was necessary to remove the excess targeting ligand. Due to the blue color of the targeting ligand, it was possible to observe the separation of immunoconjugates from the targeting ligand. The larger immunoconjugates eluted first, leaving a blue band of targeting ligand on the PD-10 SEC column. The collected fractions with immunoconjugate were concentrated and exchanged into 1x DPBS buffer using a Vivaspin column.

Finally the purified immunoconjugates were run on an analytical scale SEC-HPLC column (TSKgel SuperSW3000) to confirm product homogeneity. Examples of the separation observed between free antibody (A), free targeting ligand (B), and immunoconjugate (D) are shown in Figure 4.5. Box (C) also shows a coinjection of free targeting ligand and free antibody, demonstrating adequate separation using this method. Final immunoconjugates were analyzed with this technique before going forward with further testing.

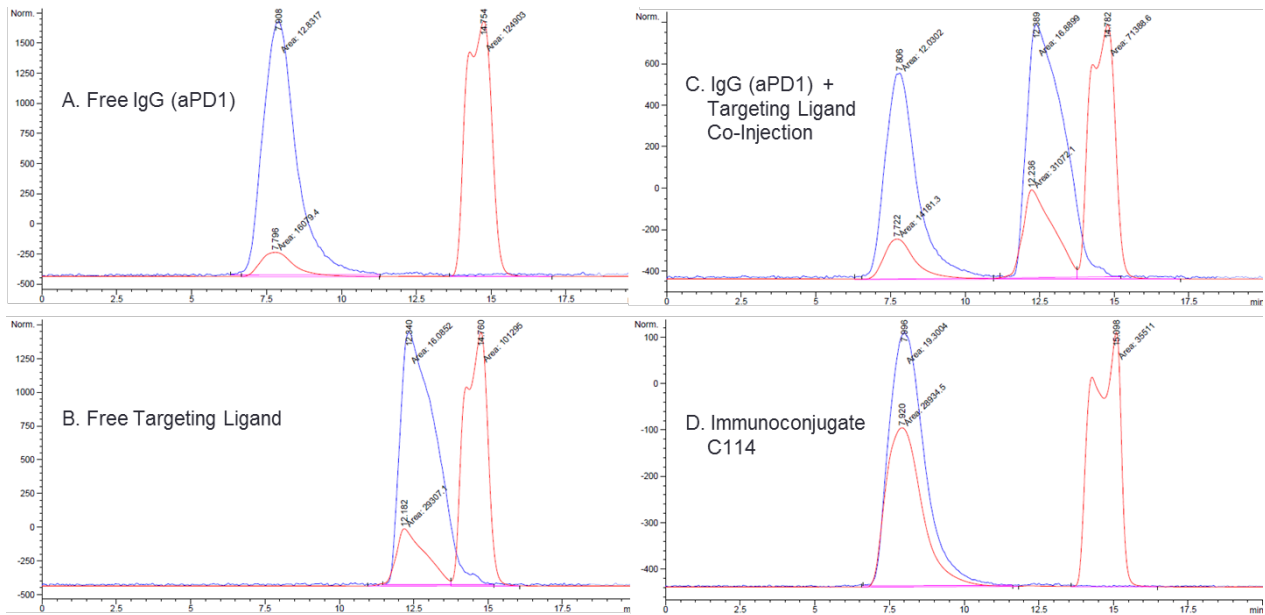


Figure 4.5. Size exclusion experiment demonstrating the separation of conjugated and unconjugated immune effectors.

4.2.4 Immunoconjugate Characterization: UV/Vis TAR Determination

The most successful method of determining the TAR of the immunoconjugates used the UV/Vis absorbance of the final products. Because the chromophores on the TL and the antibodies are different, maximally absorbing at 688 and 280 nm respectively, extinction coefficients (ϵ) for both components were determined experimentally (See Figure 4.6 for the linear

regressions used to calculate ϵ). Through application of the Beer-Lambert equation, the absolute concentrations of each component in the immunoconjugate solution were determined. Finally, since the SEC analysis suggested that the components in the final immunoconjugate solution were attached, the relative concentrations of each were used to provide the average ratio of targeting ligand to antibody, or TAR.

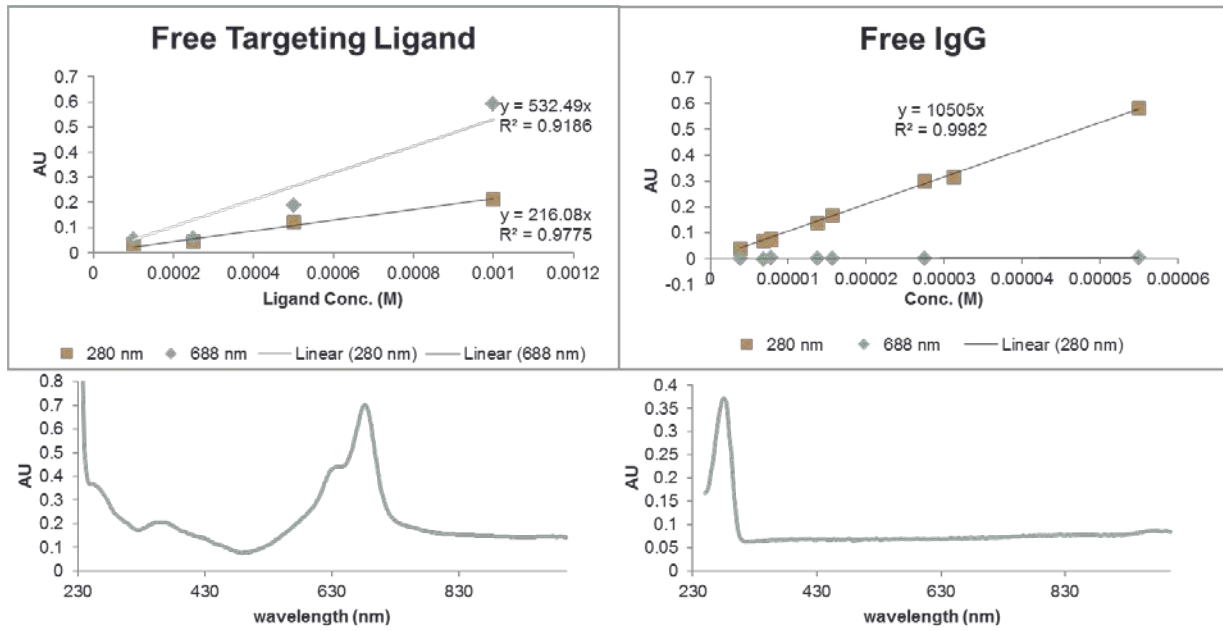


Figure 4.6. Experimental UV/Vis extinction coefficients for TAR calculations.

The results of UV/Vis TAR determination for each completed immunoconjugate are listed in Table 4.4. The majority of entries are conjugations with the α PD-1 antibody since the efficacy models of our collaborator (Dr. Amer Beg) were most pertinent to this immune effector. However, these modifications can be extended to other immune effectors as shown at the bottom of the table. For instance, immunoconjugates of another checkpoint inhibitor class, α CD137, were also prepared (C119, D19). Additionally, another antibody designed to blockade a cognate receptor of T_h expressed PD-1, α PDL-L, was also conjugated with TL. Other immunoconjugates

prepared and listed in the table contain the scrambled TL (4.5). These conjugates were designed to be used as a non-targeting control in the efficacy model. Finally an α -trinitrophenol isotype control antibody was prepared for use as negative immune modulator conjugate.

Table 4.4. Summary of immunoconjugates prepared.

Notebook Entry	Targeting Ligand	mAb	TAR	Conc. (mg/mL)	Comment
C100	4.1	α PD-1	ND	2.07	
C106	4.2	α PD-1	5.18	9.11	
C114	4.3	α PD-1	6.20	7.28	
D9A	4.2	α PD-1	4.05	1.90	
D9B	4.2	α PD-1	9.03	6.59	
D13A	4.2	α PD-1	4.58	8.25	
D13B	4.2	α PD-1	12.9	6.36	
D26A	4.2	α PD-1	4.20	8.0	
D26B	4.2	α PD-1	11.0	8.0	
D40	4.5	α PD-1	30.5	2.6	Negative binding control
D46	4.5	α PD-1	8.97	5.34	Negative binding control
D49	4.2	α PD-1	10.9	4.00	
D51	4.4	α PD-1	9.51	5.08	
C119	4.3	α CD137	1.70	3.70	
D39	4.2	α CD137	4.20	8.21	
D38	4.2	α PD-L1	5.23	6.11	
D41	4.2	α TNP	5.43	3.26	Isotype control

4.2.5 Immunoconjugate Characterization: Mass Spec TAR Determination

A secondary method useful for determining the TAR of immunoconjugates is mass spectrometry (MS). Initial efforts to characterize the immunoconjugates by MS for this project began with MALDI-TOF. The results (not shown) were encouraging but peak shapes were too broad to be of real use in calculating TAR. In the ADC field, HPLC-MS is becoming more common place but is still an area of active research. After studying previously reported electrospray ionization experiments in the literature,³¹⁻³⁴ HPLC-QToF experiments were executed with the goal of determining the final immunoconjugate TAR and corroborating the UV/Vis data.

One of the biggest challenges of measuring lysine-linked monoclonal antibody (mAb) immunoconjugates is the heterogeneity. Aside from the stochastic nature of the bioconjugation reactions, the starting mAbs have a large degree of glycosylation. These N-glycans are particularly pronounced in the Fc region of the antibodies and have been shown to be important for both the structural stability and function of the antibodies.³⁵ Although fully intact antibodies were tested by HPLC-MS in this project, it was found that deglycosylating the immunoconjugates prior to MS analysis produced the cleanest spectra. Two enzymes were used for deglycosylation in the project: IgGZero (Endo S) and PNGase F. Both of these products are commercially available with the former marketed as a specific endoglycosidases for the Fc region of antibodies and the later a general purpose glycoprotein endoglycosidases.

During the course of HPLC-QToF method development many different conditions, buffers, sample preps, and mass spectrometer conditions were tested. Samples were worked up by either ZipTip, desalting Vivaspin columns, or miniature scale Sephadex G-25 packed syringes prior to being directly infused or injected on the HPLC front end of the MS instrument. Both a C8

protein (300 Å) RP-HPLC column and analytical scale SEC column were tested for chromatographing the analyte into the MS instrument. Various mobile phases consisting of water and acetonitrile were tested under buffered conditions ranging from trifluoroacetic acid (TFA), formic acid (FA), and ammonium formate. Finally antibodies and immunoconjugates were tested as either intact molecules or as fragments that were reduced with TCEP and alkylated with iodoacetamide. The optimized method that produced the highest quality spectrum consisted of the analytical scale SEC column using an isocratic mobile phase of ACN/H₂O (50% + 0.1% TFA). The intact biomolecules were injected in their deglycosylation buffers and the MS instrument was cycled to waste when the buffer salts were eluted from the SEC method.

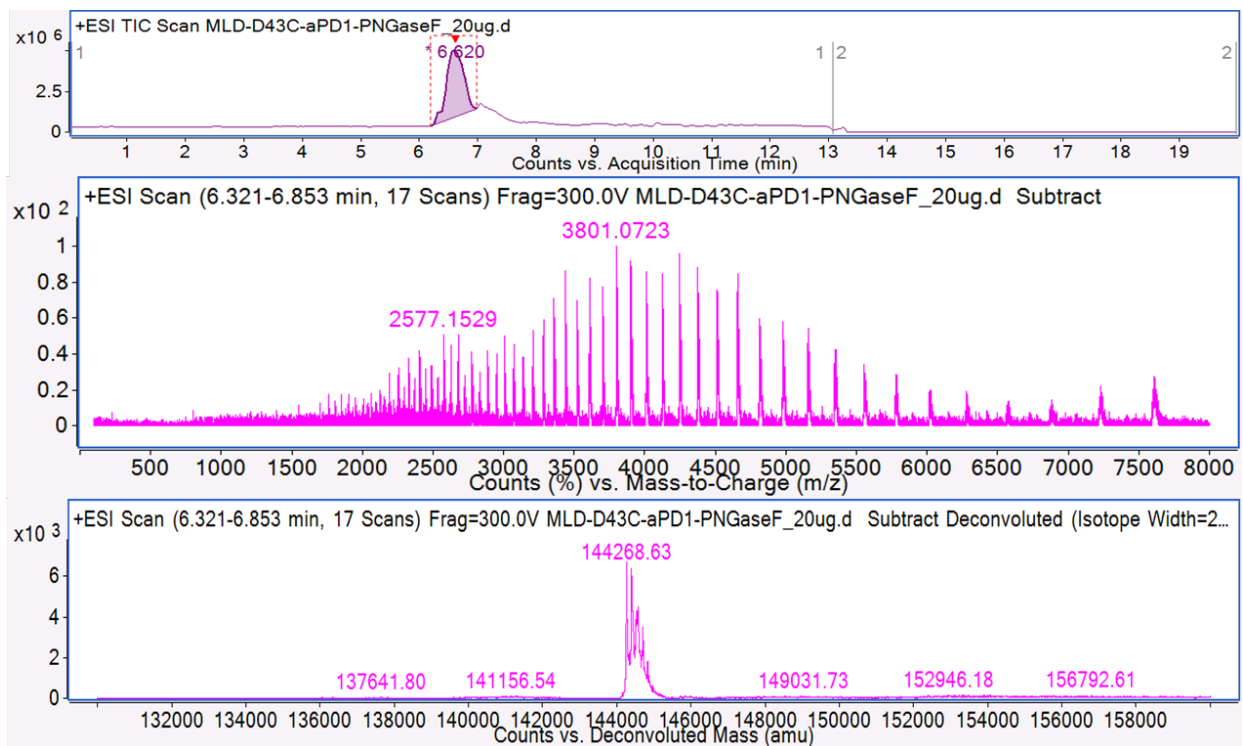


Figure 4.7. MS analysis of deglycosylated α PD-1.

Once the analyte eluted into the mass spectrometer, the area under each total ion chromatogram (TIC) was integrated and a summed mass spectrum was produced. A maximum entropy algorithm was then applied to produce a deconvoluted spectrum for each sample. Figures 4.7 and 4.8 show representative mass spectra for deglycosylated α PD-1 and an immunoconjugate consisting of α PD-1 and 4.5, respectively.

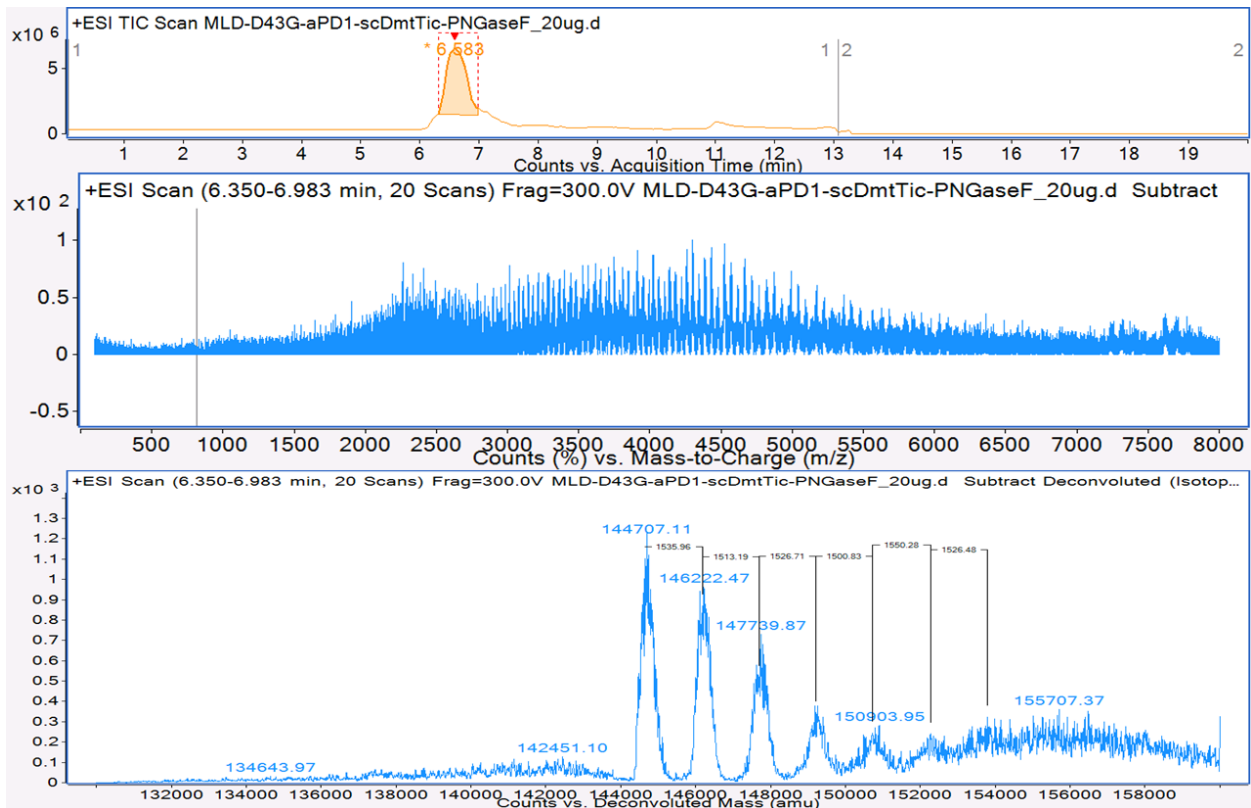


Figure 4.8. MS analysis of deglycosylated immunoconjugate α PD-1 + 4.5 (D43).

While the deconvoluted spectrum in Figure 4.8 shows successive peaks with repeating units corresponding to the mass of TL, it fails to corroborate the TAR calculated from the UV/Vis experiments. Due to the nature of the bioconjugation reaction, a Gaussian distribution of deconvoluted peaks centered on the TAR was expected. Instead the deconvoluted peaks decay

from a peak corresponding to the unconjugated mAb mass. These results may be linked to the sample preparation with the endoglycosidases, settings on the instrument itself, inherent differences in ionization potentials, or some other unknown factor. Therefore the take away from these experiments was that the immunoconjugates consist of some covalently attached targeting ligands to mAbs. Since the analytical scale SEC experiments demonstrated that unbound targeting ligand was successfully removed during the workup, the UV/Vis analysis remains the most reliable method for TAR determination.

4.2.6 Biological Testing of Immunoconjugates

This research wouldn't be complete without a discussion on the biological testing of many of the newly created immunoconjugates. As with the previous research projects described in this dissertation, the novel compounds discussed in this chapter were tested in collaboration with research labs at the Moffitt Cancer Center. Biological testing of the immunoconjugates was done by two groups; each with a different specialty. Dr. Allison Cohen in the Morse group performed whole cell binding assays, engineered tumor cell lines to express mouse and human DOR, and performed *in vivo* fluorescence imaging studies. Dr. Hong Zheng in the Beg group developed the *in vivo* mouse efficacy studies.

Figure 4.9 shows the binding assay results of two immunoconjugates, D13A and D13B, for whole cells expressing the DOR. These two immunoconjugates had TARs of 4.6 and 12.9 respectively. The assay not only demonstrates that the TL immunoconjugates retain the high binding affinities (18 and 4 nM respectively) of the TLs, but that they do so in a TAR dependent

fashion. The experiment further validates the postulate that higher TARs resulted in increased avidity of the immunoconjugate for the targeted receptor.

Box A in Figure 4.10 shows a representative *in vivo* image at 96 h post intravenous immunoconjugate injection to a mouse (n=4) with two flank xenografts. Immunoconjugate was observed by fluorescence in both denuded tumor implant areas and through the soles of the mouse's feet. The right tumor was engineered to express DOR(+) on the cell surface, and this tumor is shown to have substantially higher uptake of immunoconjugate than the DOR(-) tumor, left. Box B of the figure shows the same tumors, excised, after 168 hours. Box C of Figure 4.10 quantifies the fluorescence uptake in the positive and negative tumors over the 168 h time course. In addition to higher levels of immunoconjugate in the positive tumor, Box C also indicates that free immunoconjugate was cleared from circulation after 96 h and a substantial portion remained at the positive tumors.

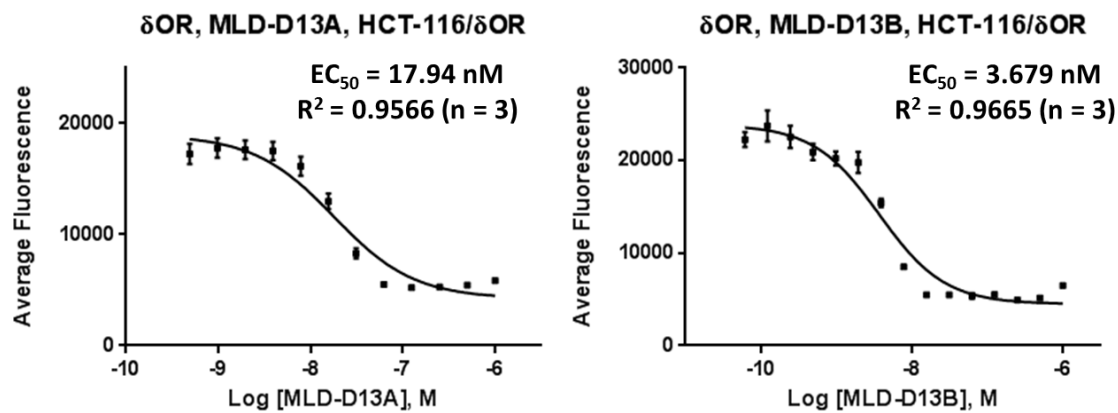


Figure 4.9. Immunoconjugate competition binding assays for DOR expressing cells. Experiment performed by Allison Cohen (Morse Lab).

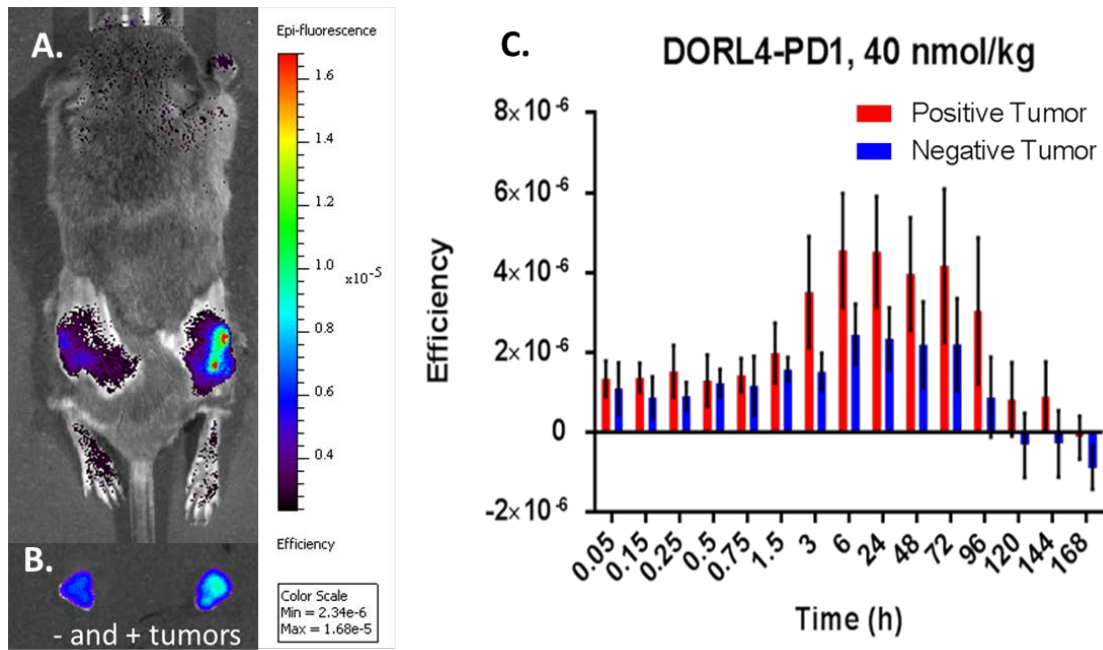


Figure 4.10. Differential uptake of immunoconjugate (D26A TAR 4.2) in DOR(-) and DOR(+) tumors. Experiment performed by Allison Cohen (Morse Lab).

Figure 4.11 reports the findings of an initial *in vivo* murine efficacy experiment performed by the Dr. Hong Zheng in the Beg lab. The mice in this experiment had xenografted LKR tumors that did not express DOR. Box A in the figure shows tumor volume as a function of time for untreated animals (UT), and all tumors increased without inhibition. The three other boxes that comprise Figure 4.11 have similar trends with plateaued and decreased tumor growth after treatments. Boxes B and C show animals that had been treated with immunoconjugates of TARs 4.58 and 12.9, respectively. Box D in the bottom right shows animals that were treated with untargeted α PD-1. The critical finding from this experiment was that the TL immunoconjugates retained functionality as immune modulators.

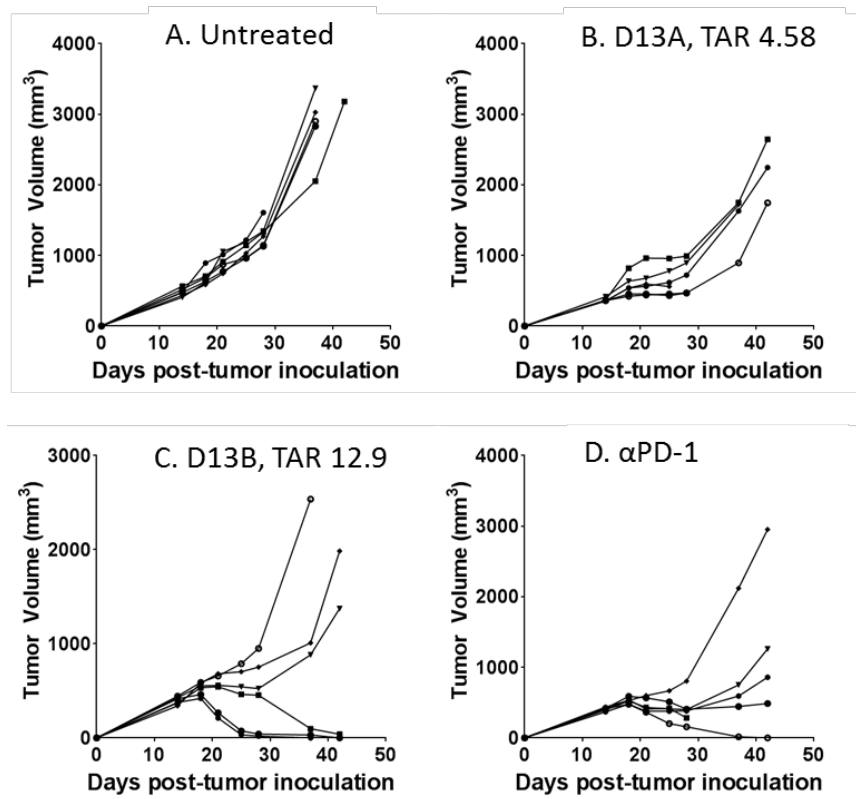


Figure 4.11. Comparison of immune modulator efficacy with and without TL in a mouse model. Experiment performed by Hong Zheng (Beg Lab).

4.3 Conclusions

In summary, we have shown how simple modifications to a known peptide TL can make them amenable to bioconjugations with proteinaceous molecules. Furthermore, the addition of fluorescent dye was shown to aide synthesis ease and characterization of products. The dye also yielded information about biodistribution and pharmacokinetics of the final immunoconjugates. This work outlines how TARs can be controlled through simple manipulations of buffers and targeting ligands. Finally, peptide ligands were shown to be able to target biomolecules 100 times

larger than themselves to extracellular targets, while retaining the functionality of the biomolecules.

The experiments and immunoconjugates in this chapter demonstrate a novel manner in which peptide ligands can be used to deliver and concentrate immunomodulators to targeted cells. Not only does this project expand upon currently approved therapies for devastating diseases, but these conjugates open up a new platform technology. Going forward peptide, TL could be coupled not only with checkpoint inhibitors, but other immune modulators like interleukins or even engineered antibody fragments. Other advances in this field might include site-specific modifications to the biomolecules. Ultimately this pioneering work holds much promise for improving current immunotherapies.

4.4 Experimental

4.4.1 Materials and Instrumentation

All purchased solvents and reagents were obtained at ACS grade or higher purity level and used without further purification unless specified otherwise. Antibodies were purchased from BioXCell (www.bxcell.com). Fluorescent dye was purchased from Lumiprobe. Peptide coupling reagents and amino acids were obtained from either Chem-Impex or AnaSpec. Distilled NMP (99.96%) was purchased from Chem-Impex. Tentagel Resin was obtained from Rapp Polymere. HPLC grade Acetonitrile was purchased from or Fisher was used for HPLC and de-ionized water was processed by Millipore Milli-Q water purifier for HPLC.

A Varian solvent delivery module with Dionex UVD340U diode array detector was used for preparative HPLC chromatography. Analytical scale HPLC was performed using either a

Dionex P680 system or an Agilent 1200 system, both with quaternary pumps, autosamplers, and diode array detectors. Mass spectral analysis was performed with either Agilent 6540 QTOF with dual Jet-Stream ESI source coupled to Agilent 1260 Infinity HPLC, Agilent LC/MSD VL single quadrupole with Agilent 1100 series HPLC, or Applied Biosystem 4700 MALDI-TOF-TOF proteomics analyzer with 355nm Nd:YAG laser. Peptides were lyophilized on a Labconco Freeze Dry/Shell Freeze System. Absorbance and Fluorescence measurements were taken on a Tecan Infinite M-1000 PRO multimode microplate reader.

4.4.2 Experimental Procedures

4.4.2.1 Targeting Ligand (TL) Synthesis. Peptide TLs were synthesized with conventional N^α-Fmoc solid phase peptide synthesis according to Scheme 4.1. Standard TentaGel Rink amide resin (0.5-1 g) with substitution of 0.24 mmol/g was swollen in DCM (10-15 mL) followed by N-methyl-2-pyrrolidinone (10-15 mL). All mixing resulted from gentle agitation of bubbled Ar (g) in a glass-fritted peptide reaction vessel. Fmoc-protecting groups were removed by reaction with 20% piperidine, 2% DBU in NMP for 15min (x2). Following Fmoc deprotection, a typical washing step consisting of 15 mL each: NMP (3x), DCM (3x), NMP (3x) was performed. Next Fmoc-Lys(Alloc)-OH (5x eq) was coupled for 2 h with activation from HCTU (5 eq) and NMM (15 eq). Qualitative Kaiser Assay was performed on several resin beads to ensure complete reaction. This cycle of washing, Fmoc-deprotection, washing, and coupling was repeated for the Fmoc-1,2,3,4-tetrahydroisoquinoline-3-OH (TIC). The next amino acid (4 eq), Fmoc-(2,6-diMethyl)Tyrosine-OH (Dmt), was coupled for 2 h after preparing the symmetric anhydride with DCC (2 eq). The

scrambled TL was synthesized in an analogous fashion by reversing the order of amino acids: Fmoc-Dmt-OH, Fmoc-Tic-OH, Fmoc-Lys(Alloc)-OH.

The N-terminus of each on-resin intermediate was dimethylated through reductive amination in Ar (g) agitated NMP. Three hundred microliters of 37% formaldehyde per gram of resin was added to the reaction along with NaCNBH₃ (5eq). Catalytic AcOH was added dropwise and the reaction was left for 4 hours.

After methylation, the alloc protection group was removed by treatment with Pd(0)(PPh₃)₄ (5 mol%), 5 drops of piperidine, and 10 mL DCM for 1 hour. The resin was washed in the typical manner, with the addition of 2x 15 mL, 5 mol% sodium diethyldithiocarbamate in NMP and 10% DIEA. Qualitative Kaiser assay and a small-test cleavage for MALDI-TOF analysis were used to test peptide purity. At this stage, the peptide was either branched once more with the HCTU activated coupling of Fmoc-Lys(Alloc)-OH or capped by discrete PEG monomer. After the former, the alloc group was removed as previously described. The symmetric anhydride of dPEG monomer was synthesized as described by DCC condensation and coupled to the resin. Finally, peptides were cleaved from the resin with a cocktail of TFA, H₂O, and triisopropylsilane (95:2.5:2.5, v/v).

Peptides were characterized and purified by RP-HPLC, followed by MALDI-TOF analysis and lyophilization as described in chapter 2. For compounds **4.2** - **4.5**, pure peptide powder was reconstituted in acetonitrile (1 mL) with Cyanine5.5 NHS ester (1.2 eq) and TEA (10 eq). The reactions were monitored for completion by linear gradient HPLC. Once starting material was consumed, the acetonitrile was diluted with H₂O, frozen, and lyophilized. The resulting blue powder was purified by semi-preparative HPLC with a linear gradient of H₂O and ACN with 0.1% TFA. Fractions with purity greater than 95% were collected by hand, frozen and lyophilized.

Finally, dried blue powder was activated with either N-hydroxysuccinimide or N-hydroxysulfosuccinimide. This reaction was carried out in minimal ACN with EDAC (5 eq) and NHS/sulfo-NHS (5 eq). Once again the reaction was monitored by retention time shift on a linear gradient of HPLC and once complete, purified by HPLC and lyophilized. The final, activated, peptide TLs (Table 4.1) were dissolved in dry DMSO to make 5 mM stock solutions. They were protected from UV light and kept at -20 °C until use.

4.4.3.2 General Antibody Conjugation Protocol. Immunoconjugates were prepared in buffered aqueous solutions with organic solvent modifiers. The generalized reaction media that resulted in the most efficient reactions consisted of 50 mM phosphate buffered to pH 8 with 50% ethylene glycol. Purchased antibodies were first exchanged (2x) into phosphate buffer by centrifugation in Vivaspin 6 or 20, 30kDa MWCO tubes (GE Healthcare). Then the antibodies were reconstituted to 4 mg/mL in the 50% ethylene glycol, phosphate buffer. Ten to twenty equivalents of activated TL stock solution (5 mM) were added dropwise to the mechanically stirred solutions. The reactions were protected from light and stirred overnight at room temperature.

4.4.3.3 General Immunoconjugate Purification Protocol. The crude reaction solution was first concentrated by centrifugation in Vivaspin 20, 30kDa MWCO tubes. Samples were loaded into the upper section of the tube and diluted with 1x DPBS; then spun at 4000 for 40 min at 25 min. This resulted in a concentrated solution of about 2 mL to load onto the size exclusion columns.

PD-10 (GE Healthcare) desalting columns containing 8.3 mL of prepacked Sephadex™ G-25 size exclusion gel were used to separate conjugated antibodies from excess targeting ligand. Prior to loading, the columns were equilibrated with 25 mL mobile phase, 10% ethanol in 1x DPBS. The crude samples were loaded onto PD-10 column as a concentrated band and allowed to penetrate the column bed before the addition of more mobile phase. Then the column was allowed to run by gravity and ~ 1 mL fractions were collected manually. Two sets fractions with clear blue tint were collected for each respective immunoconjugate.

Due to its larger molecular weight, the first band of blue fractions was combined and further characterized by SEC-HPLC. The Agilent analytical HPLC system was coupled with TSKgel SuperSW3000 size exclusion column (30cm x 4.6mm, 4µm) to assay components in eluted fractions. Analysis was done by injecting 50 µg of compound on an isocratic elution of 50% ACN/H₂O and 0.1% TFA at 0.3 mL/min flow rate. Eluent was monitored by absorbance at 280 nm and fluorescence at 352/708 nm (emission and excitation respectively). Figure 4.5 shows typical separation of free targeting ligand, free antibody, and immunoconjugates. The combined fractions were then exchanged into 1x DPBS through 3 centrifugation steps with Vivaspin 20, 30kDa MWCO tubes. Final immunoconjugates were stored at 4 °C and protected from UV light.

4.4.3.4 Immunoconjugate TAR Determination: UV/Vis. Absorbance and fluorescence emission spectra were measured for TL, antibodies, and immunoconjugates. Samples were spotted (4 µL) in triplicate on a Tecan Nanoquant plate with a pathlength of 0.05 cm. Blanks were subtracted from sample measurements. Absorbance measurements were collected from 230 to 1000 nm with a 2 nm step size. Emission spectra were collected from 500 to 850 nm with 2 nm

step size and 361 nm excitation wavelength. Extinction coefficients were calculated at 280 nm and 688 nm by plotting the linear regression of serially diluted samples from 0.1 – 2 mM.

Manipulation of the Beer-Lambert equation, $A = \epsilon \times c \times l$ (A , absorbance at specified wavelength; ϵ , extinction coefficient; c , concentration; l , path length) was used to give the following systems of equations where the TAR could be solved for by determining the ratio of concentrations of peptide to mAb.

$$A_{280\text{nm}} = (\epsilon_{280\text{nm, Pep}} \times C_{\text{pep}} + \epsilon_{280\text{nm, mAb}} \times C_{\text{mAb}})$$

$$A_{680\text{nm}} = (\epsilon_{680\text{nm, Pep}} \times C_{\text{pep}} + \epsilon_{680\text{nm, mAb}} \times C_{\text{mAb}})$$

$$\text{TAR} = C_{\text{pep}} / C_{\text{mAb}}$$

4.4.3.5 Immunoconjugate TAR Determination: Mass Spectrometry. Antibodies and immunoconjugates were prepared for mass spectral analysis by deglycosylation using PNGase F enzyme. Proteins were exchanged into 40 mM HEPES buffer, pH 7.5, at concentration of 2 mg/mL. Enzyme was added (500 units/100 μg) and each solution was incubated at 37 °C for 24 h. Finally the solution was diluted 1:1 with mobile phase from the SEC separation (50% ACN + 0.1% TFA).

The QToF instrument was coupled with the SEC column on the front end HPLC as previously described. The dual Jet Stream ESI mass spectrometer source was set according to the parameters in Table 4.5. Antibody and immunoconjugates were injected 20 μg per experiment and eluted under isocratic condition of 50% ACN + 0.1% TFA at 0.3 mL/min. Data was collected

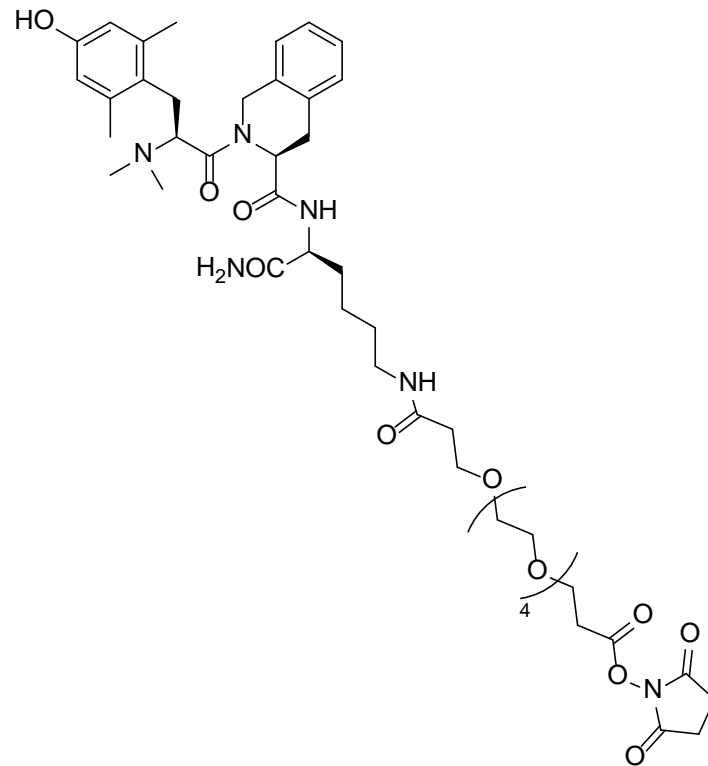
in 2 GHz extended mass range mode (1000-8000 m/z) using MassHunter Workstation Version B.05.01.

Analysis of antibodies and immunoconjugates was performed with Agilent MassHunter Qualitative Analysis version B.05.00 with Bioconfirm. The analysis method was set to BioConfirmIntactProteinHighMass-default. Regions of protein elution in the TIC (total ion chromatogram) were manually integrated, extracted, and background subtracted. Each resulting spectrum was subsequently deconvoluted using the Maximum Entropy feature. The mass range was set to 130-160 kDa with a mass step of 1 Da and a S/N threshold of 1.0. Proton adducts with an average mass of 25% peak height were specified.

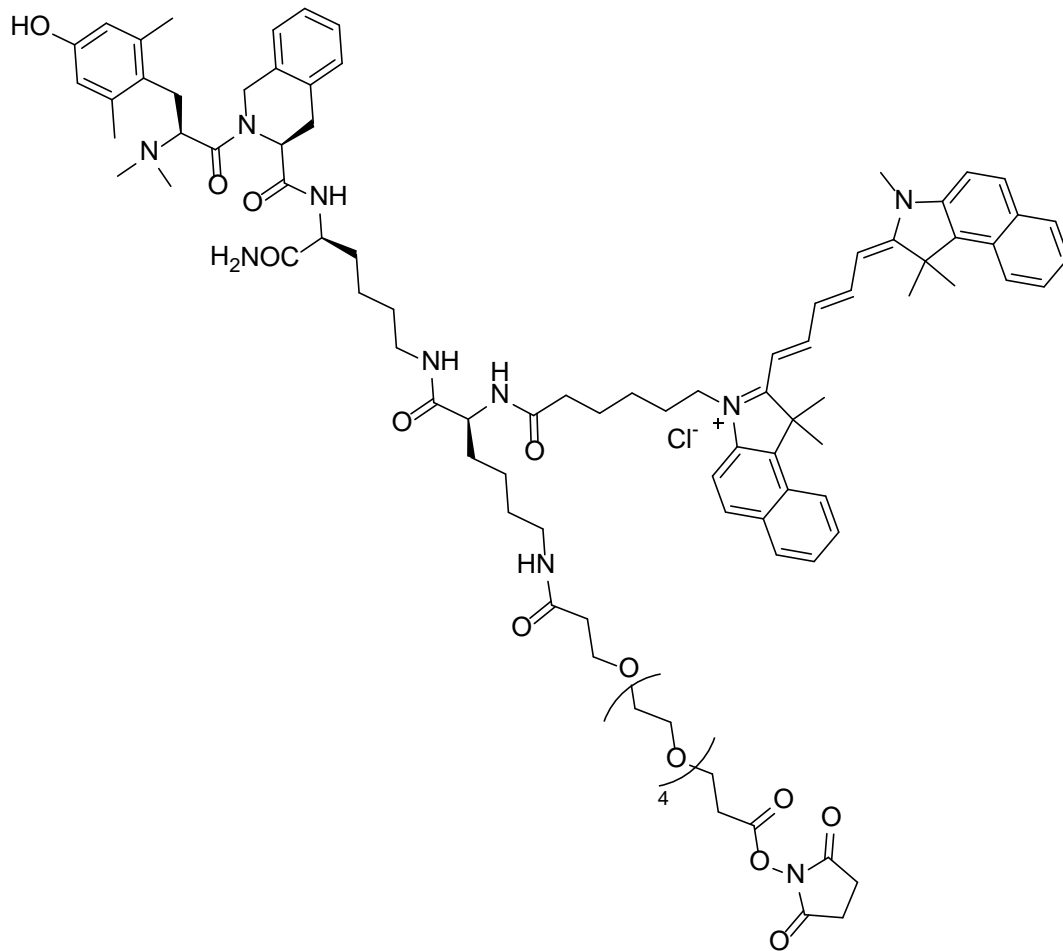
Table 4.5. Source and TOF parameters used for antibody and immunoconjugate MS analysis.

Parameter	Setting
Gas Temperature	300 °C
Drying Gas	13 L/min
Nebulizer	45 psig
Sheath Gas Temp	400 °C
Sheath Gas Flow	12 L/min
Capillary Voltage	5500 V
Fragmentor Voltage	300 V
Skimmer Voltage	250 V
Octopole RF Peak	750 V

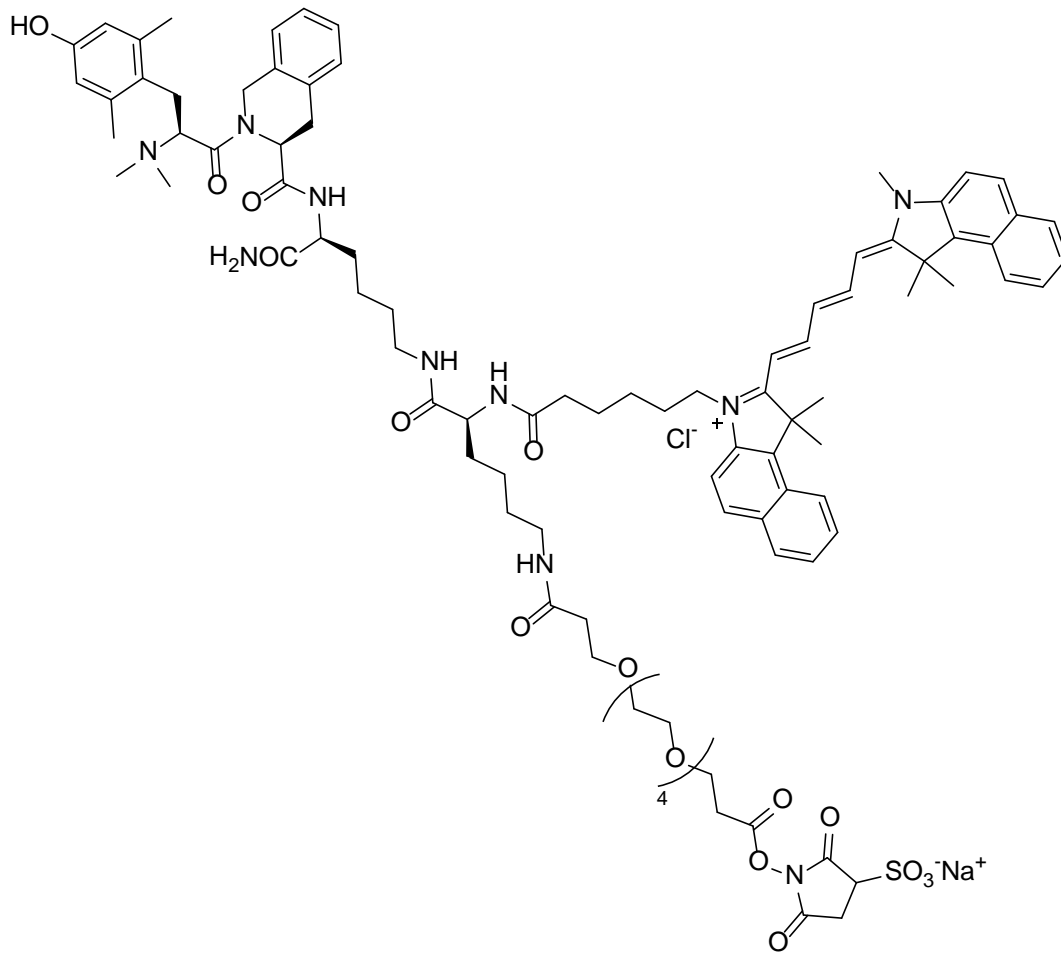
4.5 Targeting Ligand Structures



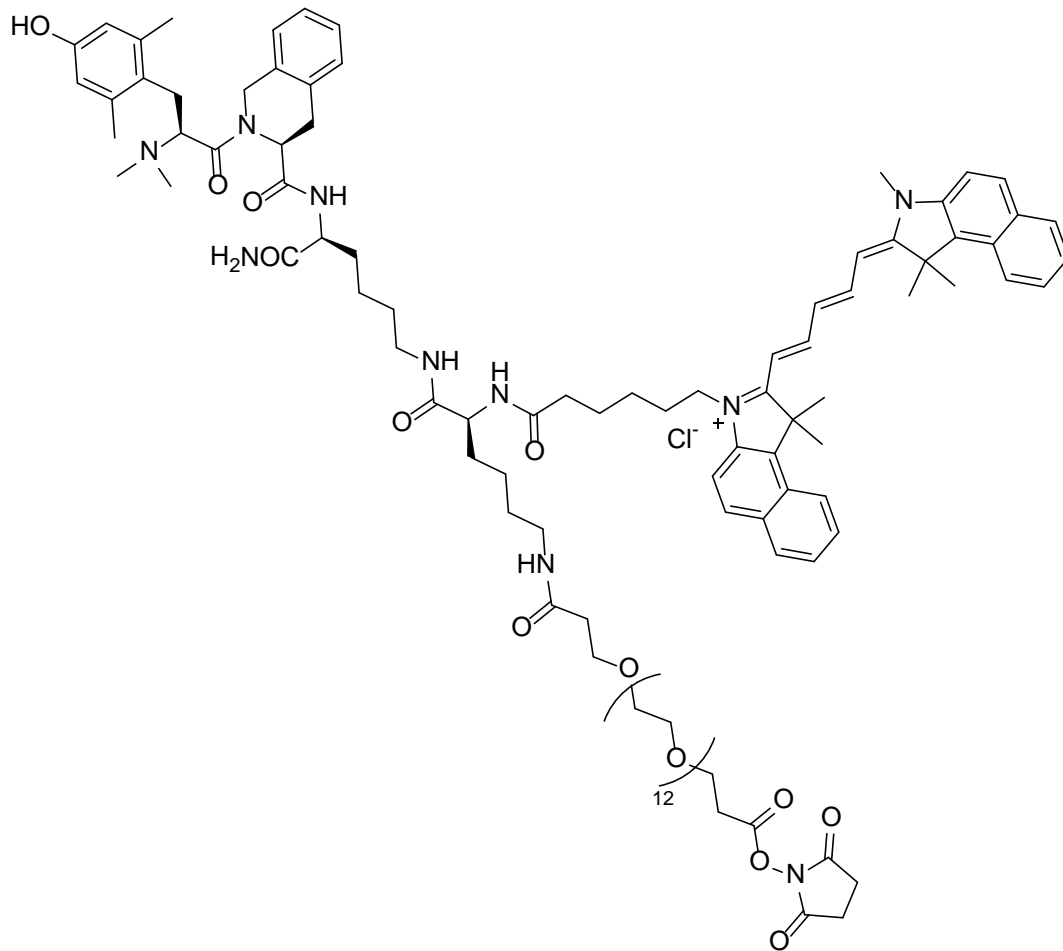
N,N-DiMethyl-Dmt-Tic-Lys(dPEG5-NHS)-CONH₂ Targeting Ligand, 4.1



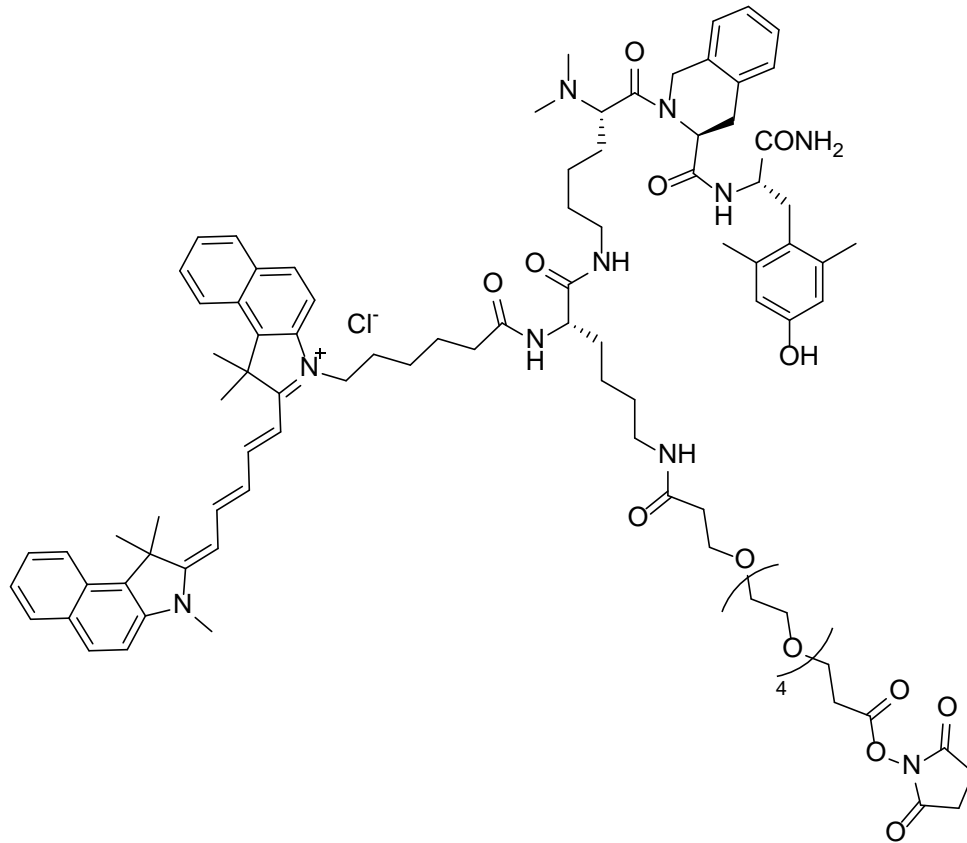
N,N-DiMethyl-Dmt-Tic-Lys(Lys(Cy5.5)-dPEG5-NHS)-CONH₂ Targeting Ligand, 4.2



N,N-Dimethyl-Dmt-Tic-Lys(Lys(Cy5.5)-dPEG5-SulfoNHS)-CONH₂ Targeting Ligand, 4.3



N,N-DiMethyl-Dmt-Tic-Lys(Lys(Cy5.5)-dPEG13-NHS)-CONH₂ Targeting Ligand, 4.4



N,N-DiMethyl-Lys(Lys(Cy5.5)-dPEG5)-Tic-Dmt-CONH₂, Scrambled Targeting Ligand, 4.5

4.6 References

- (1) Pardoll, D. *Annual Review of Immunology* **2003**, *21*, 807.
- (2) Pardoll, D. M. *Nat Rev Cancer* **2012**, *12*, 252.
- (3) Garon, E. B. *The Lancet Oncology* **2016**, *17*, 259.
- (4) Nirschl, C. J.; Drake, C. G. *Clin Cancer Res* **2013**, *19*, 4917.
- (5) Forde, P. M.; Kelly, R. J.; Brahmer, J. R. *Clin Cancer Res* **2014**, *20*, 1067.
- (6) Hoos, A.; Ibrahim, R.; Korman, A.; Abdallah, K.; Berman, D.; Shahabi, V.; Chin, K.; Canetta, R.; Humphrey, R. *Seminars in Oncology* **2010**, *37*, 533.
- (7) Schadendorf, D.; Hodi, F. S.; Robert, C.; Weber, J. S.; Margolin, K.; Hamid, O.; Patt, D.; Chen, T. T.; Berman, D. M.; Wolchok, J. D. *J Clin Oncol* **2015**, *33*, 1889.
- (8) Luke, J. J.; Ott, P. A. *OncoTarget* **2015**, *6*, 3479.
- (9) Scagliotti, G. V.; Bironzo, P.; Vansteenkiste, J. F. *Cancer Treatment Reviews* **2015**, *41*, 465.
- (10) Reck, M.; Paz-Ares, L. *Seminars in Oncology* **2015**, *42*, 402.
- (11) Brahmer, J. R.; Pardoll, D. M. *Cancer Immunology Research* **2013**, *1*, 85.
- (12) Linch, S. N.; McNamara, M. J.; Redmond, W. L. *Front Oncol* **2015**, *5*.
- (13) Joseph, R. W.; Cappel, M.; Goedjen, B.; Gordon, M.; Kirsch, B.; Gilstrap, C.; Bagaria, S.; Jambusaria-Pahlajani, A. *Cancer Immunol Res* **2015**, *3*, 18.
- (14) Weber, J. S.; Dummer, R.; de Pril, V.; Lebbe, C.; Hodi, F. S. *Cancer* **2013**, *119*, 1675.
- (15) Weber, J. S.; Kahler, K. C.; Hauschild, A. *J Clin Oncol* **2012**, *30*, 2691.
- (16) Postow, M. A.; Chesney, J.; Pavlick, A. C.; Robert, C.; Grossmann, K.; McDermott, D.; Linette, G. P.; Meyer, N.; Giguere, J. K.; Agarwala, S. S.; Shaheen, M.; Ernstoff, M. S.; Minor, D.; Salama, A. K.; Taylor, M.; Ott, P. A.; Rollin, L. M.; Horak, C.; Gagnier, P.; Wolchok, J. D.; Hodi, F. S. *New England Journal of Medicine* **2015**, *372*, 2006.
- (17) Weber, J. S.; D'Angelo, S. P.; Minor, D.; Hodi, F. S.; Gutzmer, R.; Neyns, B.; Hoeller, C.; Khushalani, N. I.; Miller, W. H., Jr.; Lao, C. D.; Linette, G. P.; Thomas, L.; Lorigan, P.; Grossmann, K. F.; Hassel, J. C.; Maio, M.; Sznol, M.; Ascierto, P. A.; Mohr, P.; Chmielowski, B.; Bryce, A.; Svane, I. M.; Grob, J. J.; Krackhardt, A. M.; Horak, C.; Lambert, A.; Yang, A. S.; Larkin, J. *Lancet Oncol* **2015**, *16*, 375.
- (18) Society, A. C.; Society, A. C., Ed. Atlanta, GA, 2016.
- (19) Maneckjee, R.; Minna, J. D. *Proceedings of the National Academy of Sciences of the United States of America* **1990**, *87*, 3294.
- (20) Schreiber, G.; Campa, M. J.; Prabhakar, S.; O'Briant, K.; Bepler, G.; Patz, E. F., Jr. *Anticancer Res* **1998**, *18*, 1787.
- (21) Campa, M. J.; Schreiber, G.; Bepler, G.; Bishop, M. J.; McNutt, R. W.; Chang, K. J.; Patz, E. F., Jr. *Cancer research* **1996**, *56*, 1695.
- (22) Madar, I.; Bencherif, B.; Lever, J.; Heitmiller, R. F.; Yang, S. C.; Brock, M.; Brahmer, J.; Ravert, H.; Dannals, R.; Frost, J. J. *J Nucl Med* **2007**, *48*, 207.
- (23) Josan, J. S.; Morse, D. L.; Xu, L.; Trissal, M.; Baggett, B.; Davis, P.; Vagner, J.; Gillies, R. J.; Hruby, V. J. *Org. Lett.* **2009**, *11*, 2479.
- (24) Cohen, A. S.; Patek, R.; Enkemann, S. A.; Johnson, J. O.; Chen, T.; Toloza, E.; Vagner, J.; Morse, D. L. *Bioconjugate Chemistry* **2016**, *27*, 427.
- (25) Salvadori, S.; Guerrini, R.; Balboni, G.; Bianchi, C.; Bryant, S. D.; Cooper, P. S.; Lazarus, L. H. *J Med Chem* **1999**, *42*, 5010.

- (26) Salvadori, S.; Balboni, G.; Guerrini, R.; Tomatis, R.; Bianchi, C.; Bryant, S. D.; Cooper, P. S.; Lazarus, L. H. *Journal of Medicinal Chemistry* **1997**, *40*, 3100.
- (27) Hermanson, G. T. *Bioconjugate Techniques*; Third Edition ed.; Academic Press, 2013.
- (28) Xu, L.; Josan, J. S.; Vagner, J.; Caplan, M. R.; Hruby, V. J.; Mash, E. A.; Lynch, R. M.; Morse, D. L.; Gillies, R. J. *Proceedings of the National Academy of Sciences of the United States of America* **2012**, *109*, 21295.
- (29) Xu, L.; Vagner, J.; Josan, J.; Lynch, R. M.; Morse, D. L.; Baggett, B.; Han, H.; Mash, E. A.; Hruby, V. J.; Gillies, R. J. *Molecular Cancer Therapeutics* **2009**, *8*, 2356.
- (30) Marie-Priscelle Brun, L. G.-L. In *Antibody-Drug Conjugates*; Ducry, L., Ed.; Humana Press: 2013; Vol. 1045, p 173.
- (31) Lazar, A. C.; Wang, L.; Blättler, W. A.; Amphlett, G.; Lambert, J. M.; Zhang, W. *Rapid Communications in Mass Spectrometry* **2005**, *19*, 1806.
- (32) Valliere-Douglass, J. F.; Hengel, S. M.; Pan, L. Y. *Molecular Pharmaceutics* **2015**, *12*, 1774.
- (33) Wagner-Rousset, E.; Janin-Bussat, M.-C.; Colas, O.; Excoffier, M.; Ayoub, D.; Haeuw, J.-F.; Rilatt, I.; Perez, M.; Corvaia, N.; Beck, A. *mAbs* **2014**, *6*, 173.
- (34) Basa, L. In *Antibody-Drug Conjugates*; Ducry, L., Ed.; Humana Press: 2013; Vol. 1045, p 285.
- (35) Hayes, J. M.; Cosgrave, E. F.; Struwe, W. B.; Wormald, M.; Davey, G. P.; Jefferis, R.; Rudd, P. M. *Curr Top Microbiol Immunol* **2014**, *382*, 165.

APPENDIX A:
SELECTED MASS SPECTRA AND HPLC CHROMATOGRAMS OF PEPTIDE TARGETING
LIGANDS

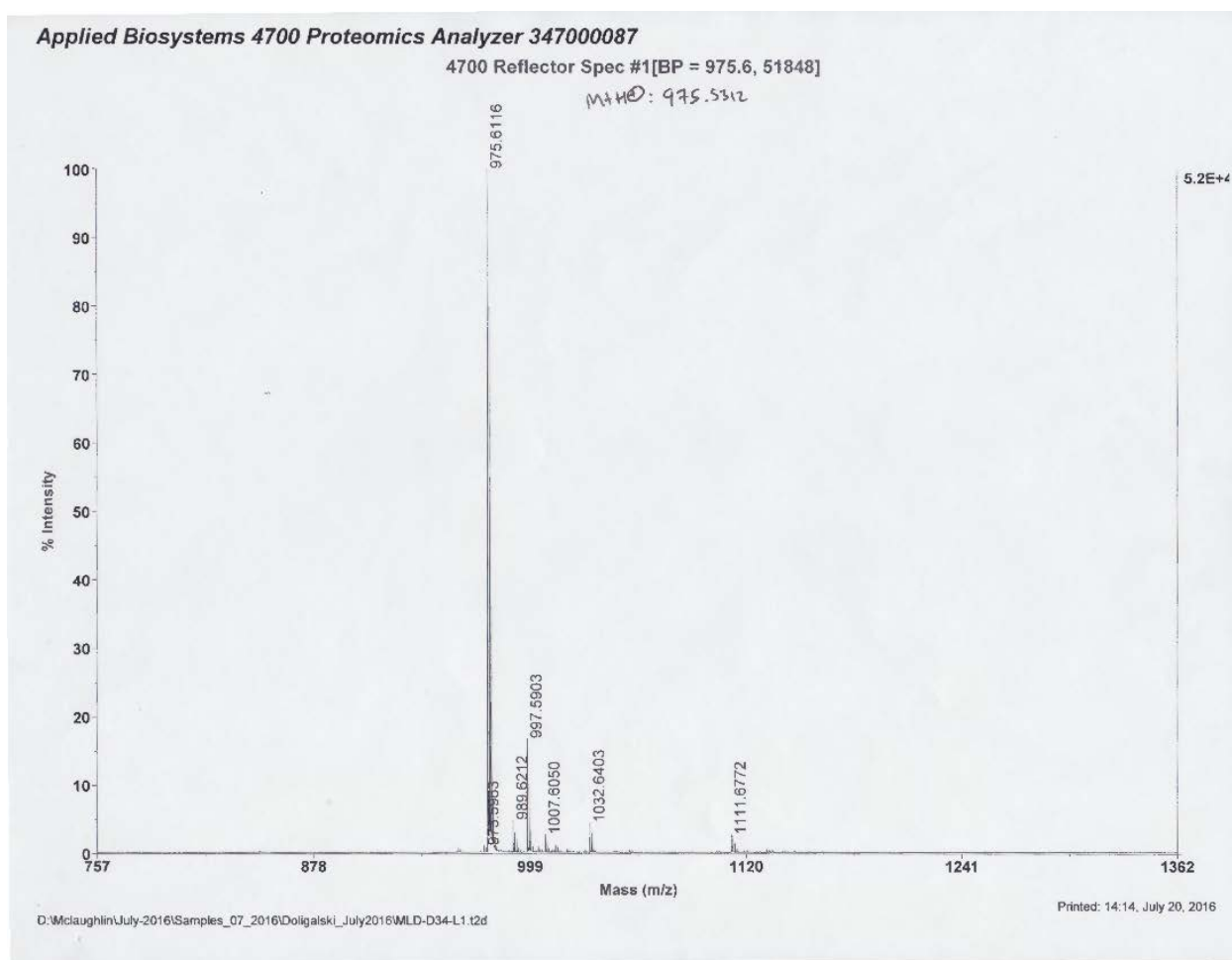


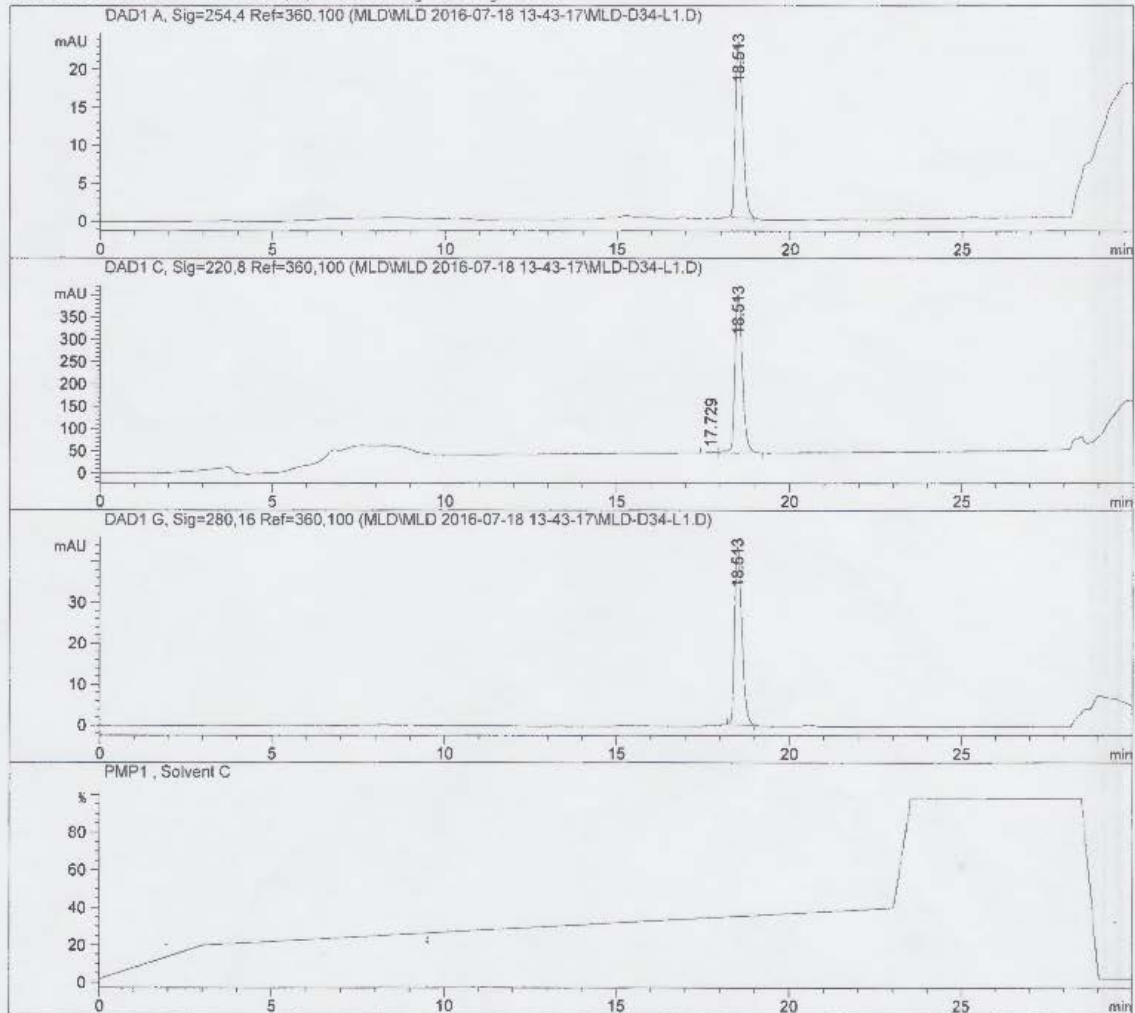
Figure A2.1 MC1RL; Mass Spectrum

Data File C:\CHEM32\1\DATA\MLD\MLD 2016-07-18 13-43-17\MLD-D34-L1.D
Sample Name: MLD-D34-L1

=====

Acq. Operator :	Instrument 1	Seq. Line :	1
Acq. Instrument :	Instrument 1	Location :	Vial 62
Injection Date :	7/18/2016 1:43:35 PM	Inj :	1
		Inj Volume :	10.0 µl

Acq. Method : C:\CHEM32\1\DATA\MLD\MLD 2016-07-18 13-43-17\MLD-2-20-40_20MIN_1.M
Last changed : 1/25/2016 6:12:07 PM
Analysis Method : C:\CHEM32\1\METHODS\MLD-10-40-85_20MIN_1.M
Last changed : 2/1/2016 3:16:23 PM
Additional Info : Peak(s) manually integrated



=====
Fraction Information
=====

Fraction collection off

No Fractions found.

Instrument 1 7/21/2016 9:32:29 AM

Page 1 of 2

Figure A2.2 MC1RL; HPLC Trace

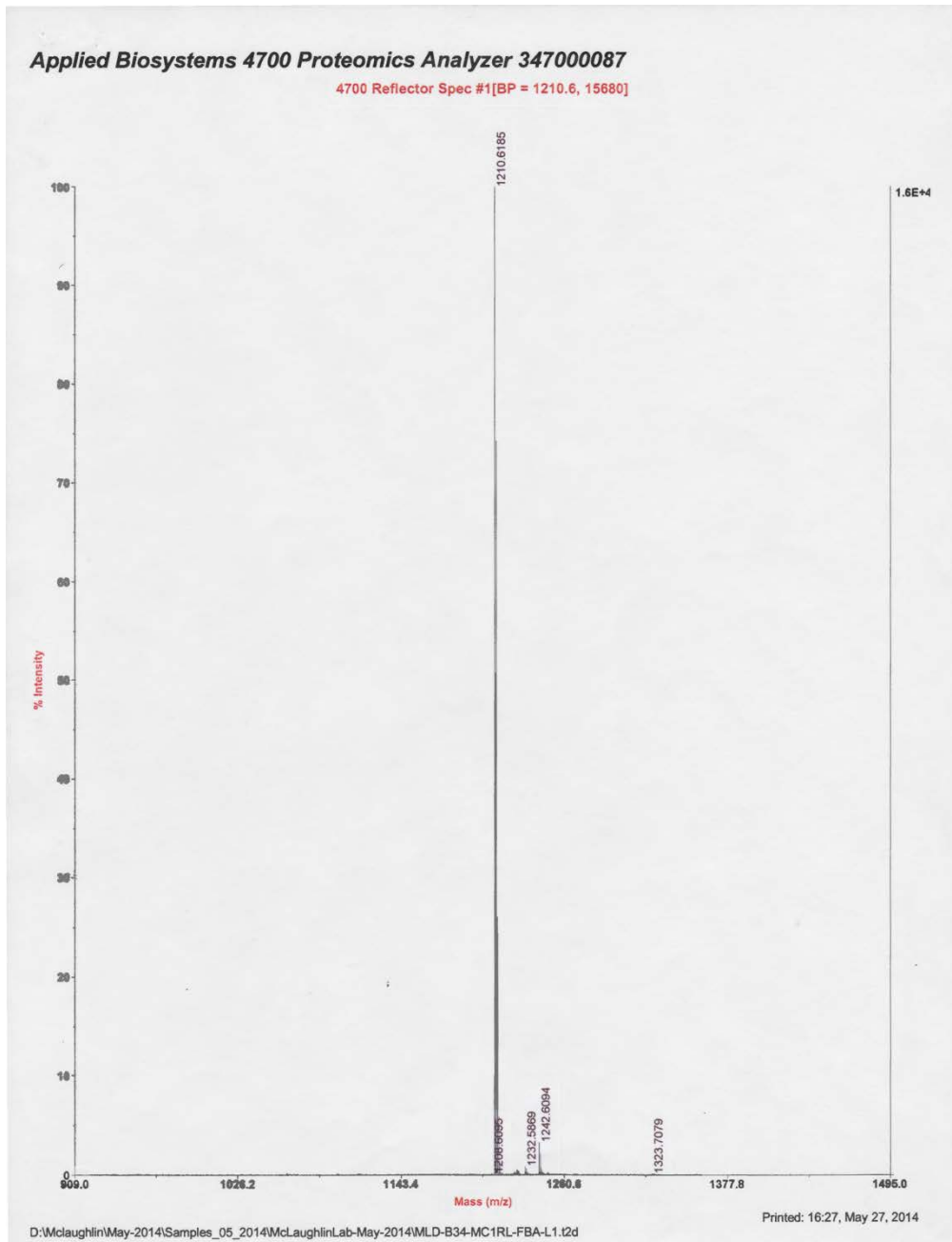
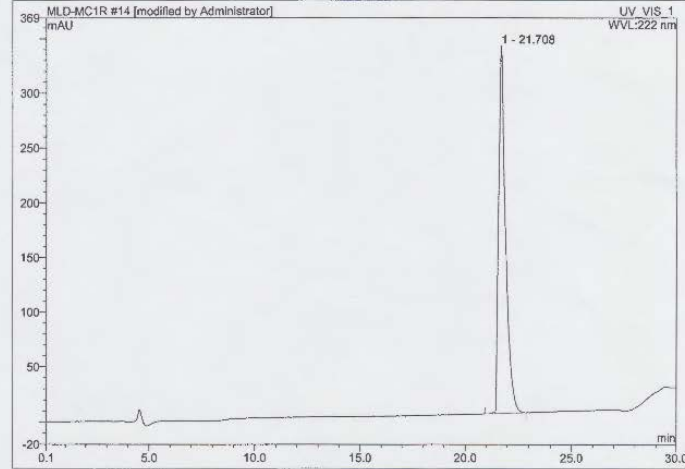


Figure A2.3 MC1RL-Ahx-FBA; Mass Spectrum

14 MLD-B34-B34-MC1RL-Ahx-FBA_F7

Sample Name:	MLD-B34-B34-MC1RL-Ahx-FBA_F7	Injection Volume:	50.0
Vial Number:	RB7	Channel:	UV_VIS_1
Sample Type:	unknown	Wavelength:	222
Control Program:	Exploratory gradient_MLD-2-60_20min	Bandwidth:	1
Quantif. Method:	default	Dilution Factor:	1.0000
Recording Time:	4/23/2014 14:39	Sample Weight:	1.0000
Run Time (min):	37.00	Sample Amount:	1.0000



No.	Ret.Time min	Peak Name	Height mAU	Area mAU*min	Rel.Area %	Amount n.a.	Type
1	21.71	n.a.	335.413	125.901	100.00	n.a.	BMB*
Total:			335.413	125.901	100.00	0.000	

default/integration

Chromeleon (c) Dionex 1996-2001
Version 6.50 SP3a Build 986

Figure A2.4 MC1RL-Ahx-FBA; HPLC Trace

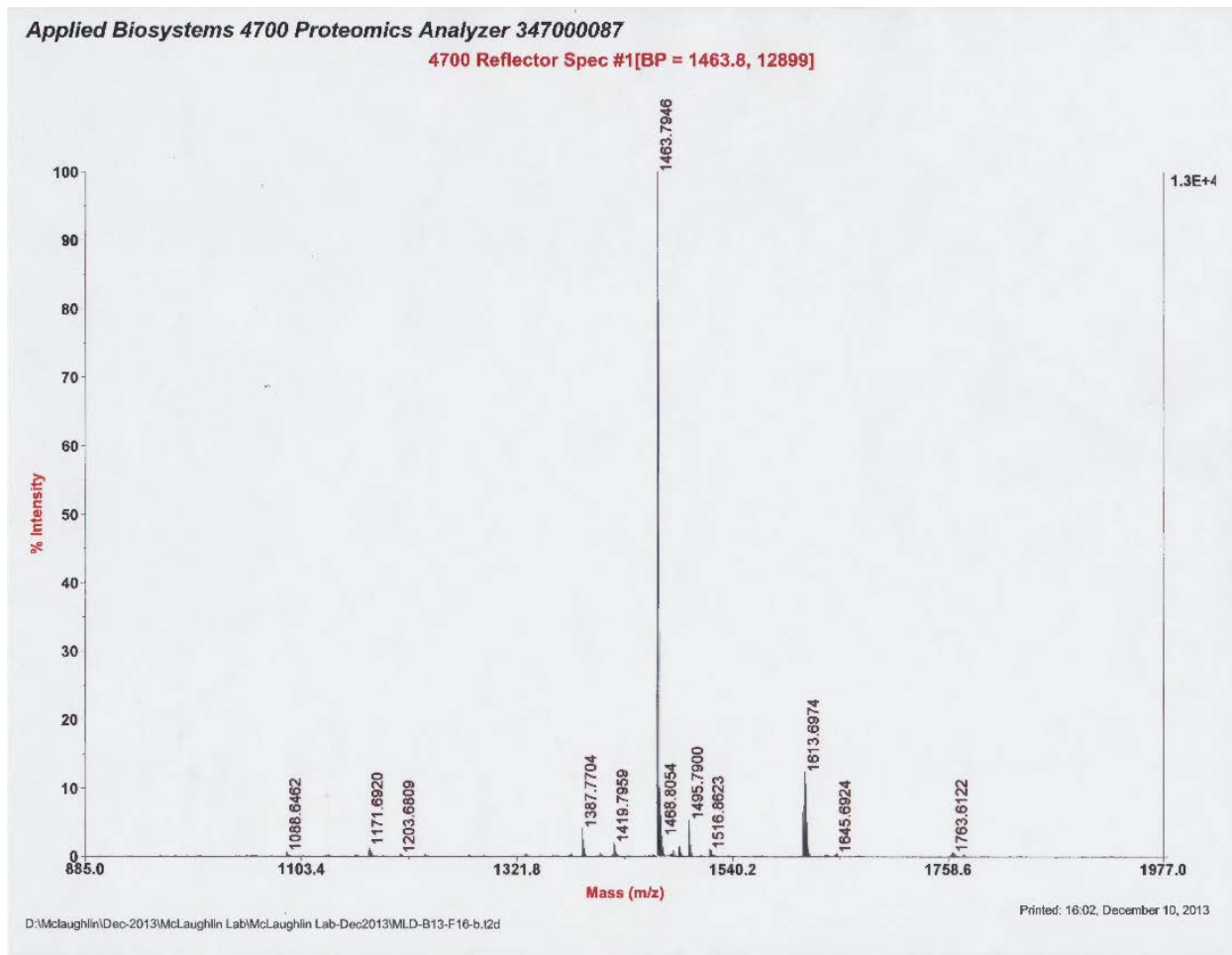


Figure A2.5 MC1RL-Ahx-DTPA; Mass Spectrum

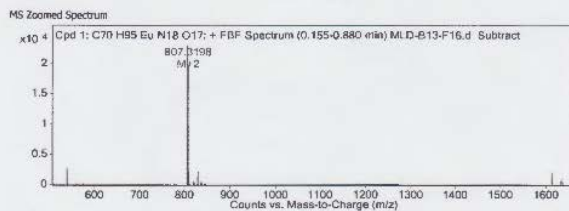
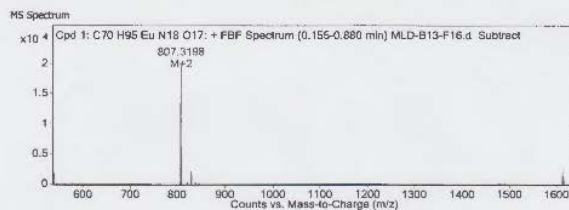
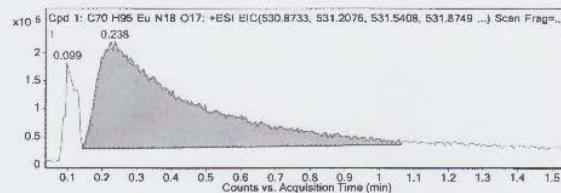
Qualitative Compound Report

Data File	MLD-B13-F16.d	Sample Name	Unavailable
Sample Type	Unavailable	Position	Unavailable
Instrument Name	Unavailable	User Name	Unavailable
Acq Method		Acquired Time	Unavailable
IRM Calibration Status	8/21/11	DA Method	Default.m
Comment	Sample information is unavailable		

Compound Table

Compound Label	RT	Mass	Abund	Formula	Tgt Mass	Diff (ppm)	MFG Formula	DB Formula
Cpd 1: C70 H95 Eu N18 O17	0.238	1610.6323	19818	C70 H95 Eu N18 O17	1610.6321	0.11	C70 H95 Eu N18 O17	C70 H95 Eu N18 O17

Compound Label	m/z	RT	Algorithm	Mass
Cpd 1: C70 H95 Eu N18 O17	807.3198	0.238	Find By Formula	1610.6323



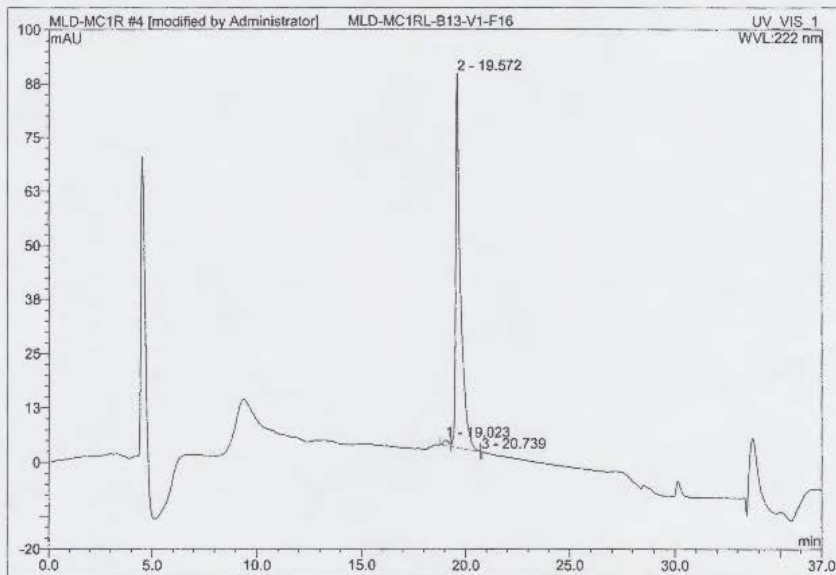
MS Spectrum Peak List

m/z	z	Abund	Formula	Ion
537.8812	3	1672.4	C70H98EuN18O17	(M+3H)+3
560.5093	3	146.83	C70H95EuN18Na3O17	(M+3Na)+3
576.5028	3	230.09	C70H95EuK3N18O17	(M+3K)+3
806.3185	2	13435.14	C70H95EuN18O17	M+2
820.3125	2	365.25	C70H93EuN18Na2O16	(M+2Na)+2(-H2O)
828.801	2	1232.07	C70H95EuN18Na2O17	(M+2Na)+2
836.7806	2	248.28	C70H93EuK2N18O16	(M+2K)+2(-H2O)
844.2706	2	31.12	C70H95EuK2N18O17	(M+2K)+2
1611.6372	1	1376.72	C70H95EuN18O17	M+

Figure A2.6 MC1RL-Ahx-DTPA:Eu; Mass Spectrum

4 MLD-MC1RL-B13-V1-F16

Sample Name:	MLD-MC1RL-B13-V1-F16	Injection Volume:	100.0
Vial Number:	RA4	Channel:	UV_VIS_1
Sample Type:	unknown	Wavelength:	222
Control Program:	Exploratory gradient_MLD-2-60_20min	Bandwidth:	1
Quantif. Method:	default	Dilution Factor:	1.0000
Recording Time:	12/2/2013 16:30	Sample Weight:	1.0000
Run Time (min):	37.00	Sample Amount:	1.0000



No.	Ret.Time min	Peak Name	Height mAU	Area mAU*min	Rel.Area %	Amount n.a.	Type
1	19.02	n.a.	1.289	0.401	1.88	n.a.	BM *
2	19.57	n.a.	86.499	23.530	98.31	n.a.	MB*
3	20.74	n.a.	0.069	0.003	0.01	n.a.	BMB
Total:			87.856	23.934	100.00	0.000	

default/Integration

Chromleon (c) Dionex 1996-2001
Version 6.50 SP3a Build 986

Figure A2.7 MC1RL-Ahx-DTPA:Eu; HPLC Trace

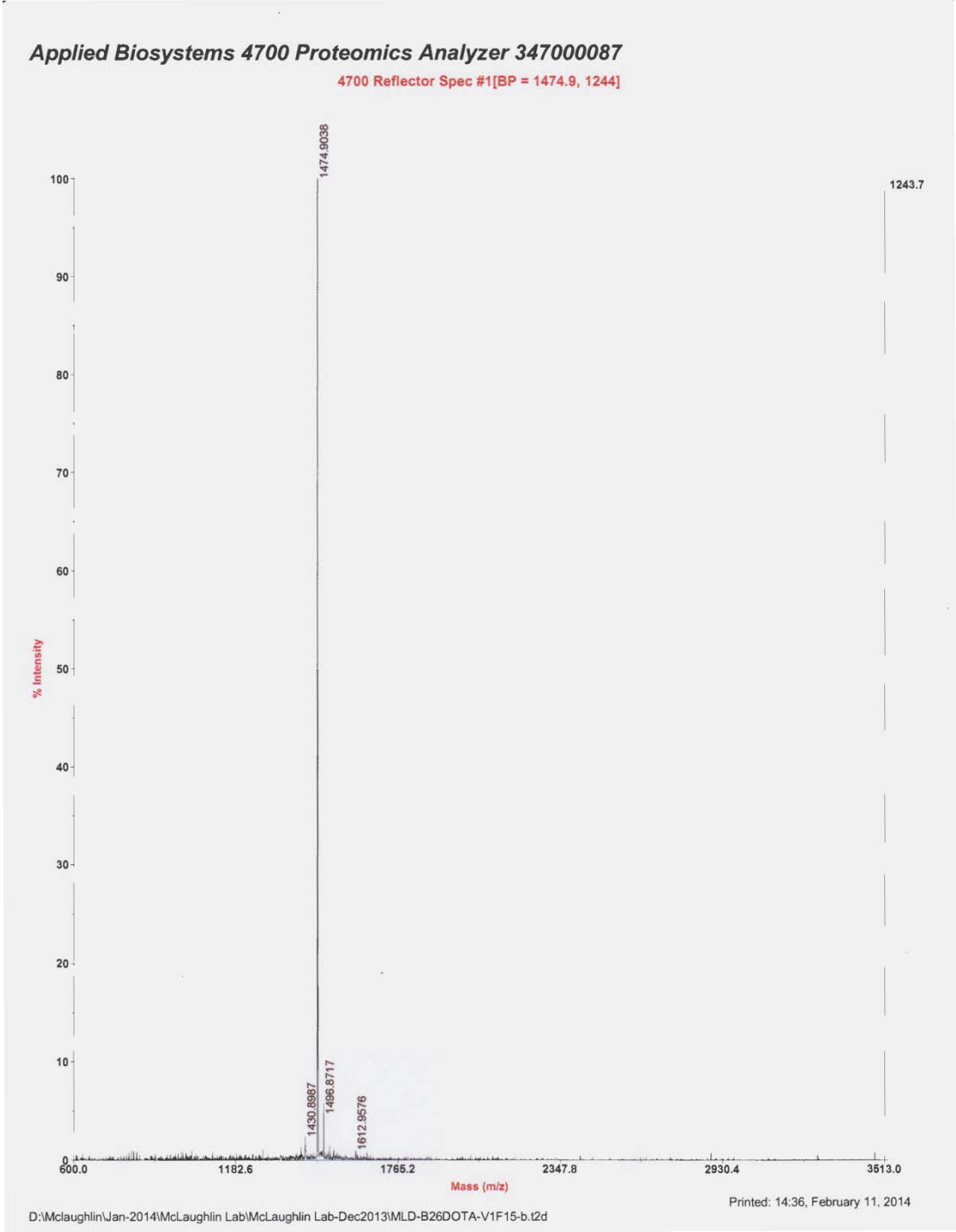
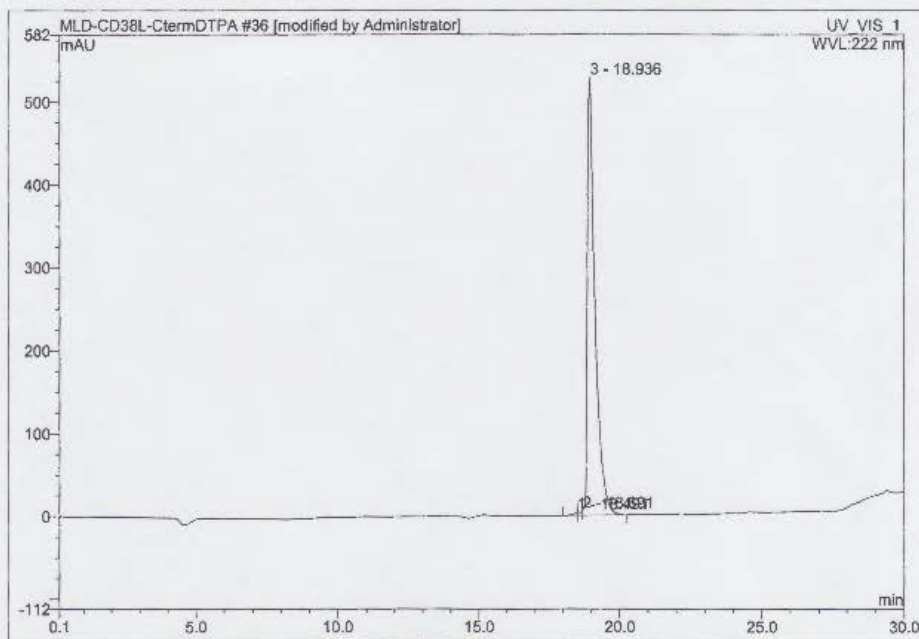


Figure A2.8 MC1RL-Ahx-DOTA; Mass Spectrum

36 MLD-B26-DOA-L1

Sample Name:	MLD-B26-DOA-L1	Injection Volume:	100.0
Vial Number:	GA1	Channel:	UV_VIS_1
Sample Type:	unknown	Wavelength:	222
Control Program:	Exploratory gradient_MLD-2-60_20min	Bandwidth:	1
Quantif. Method:	default	Dilution Factor:	1.0000
Recording Time:	2/15/2014 13:29	Sample Weight:	1.0000
Run Time (min):	37.00	Sample Amount:	1.0000



No.	Ret.Time min	Peak Name	Height mAU	Area mAU*min	Rel.Area %	Amount n.a.	Type
1	18.49	n.a.	3.481	0.708	0.43	n.a.	BM *
2	18.69	n.a.	5.362	0.643	0.39	n.a.	M *
3	18.94	n.a.	528.364	164.735	99.19	n.a.	MB*
Total:			537.208	166.086	100.00	0.000	

default/Integration

Chromeleon (c) Dionex 1996-2001
Version 6.50 SP3a Build 986

Figure A2.9 MC1RL-Ahx-DOA; HPLC Trace

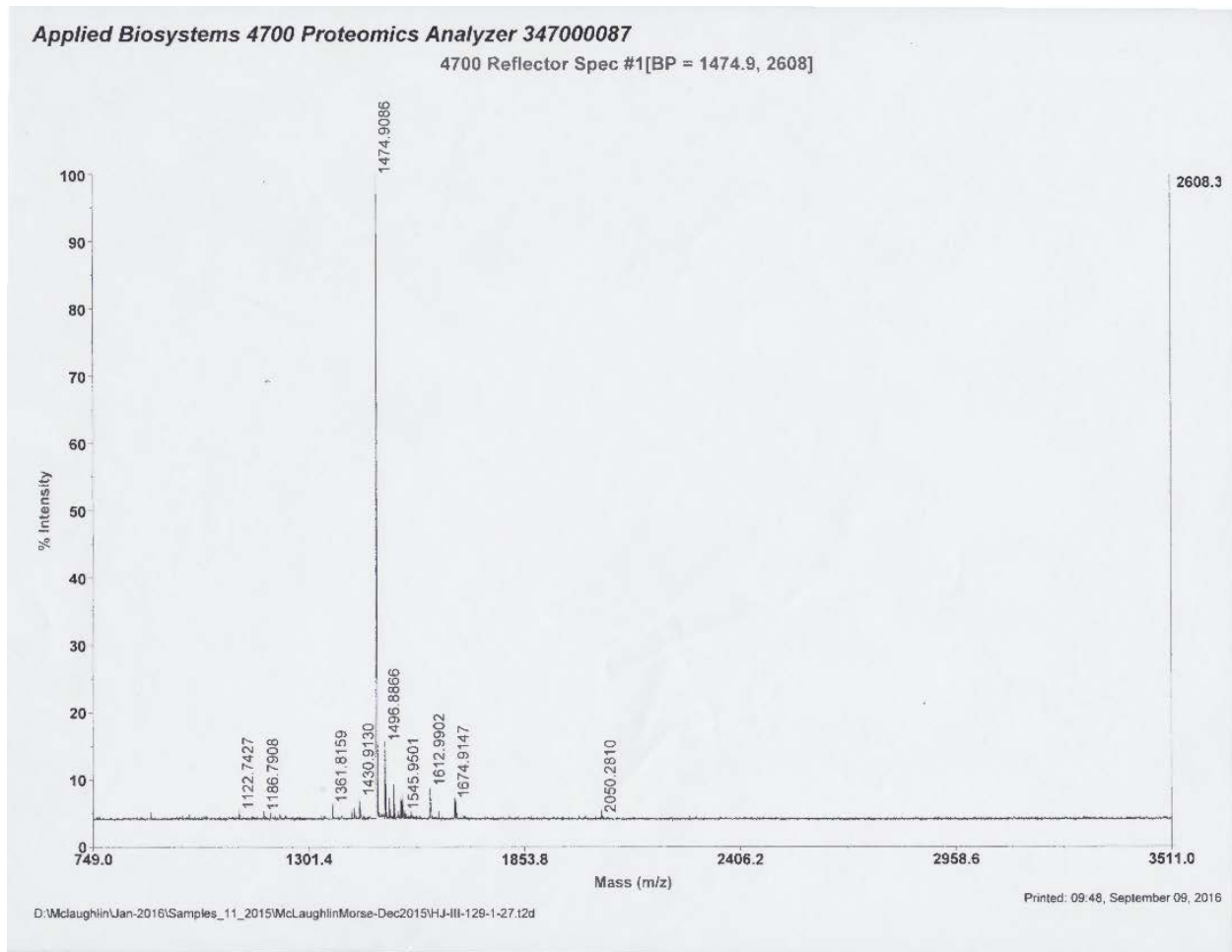
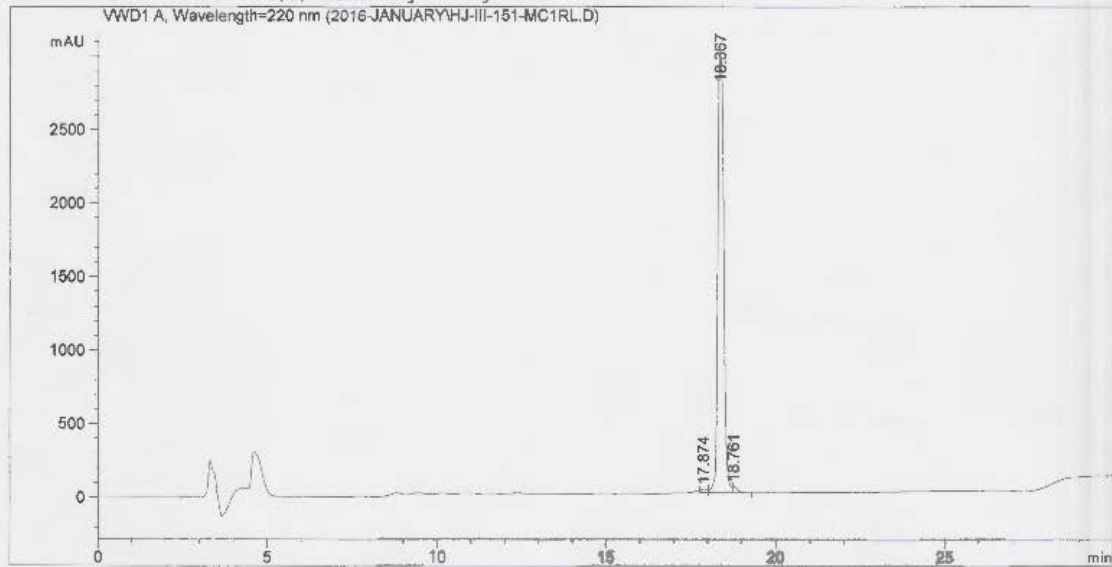


Figure A2.10 Scrambled-MC1RL-Ahx-DOTA; Mass Spectrum (prepared by Dr. Hunjoo Kil)

Data File C:\CHEM32\1\DATA\2016-JANUARY\HJ-III-151-MC1RL.D
Sample Name: HJ-III-151-MC1RL

=====
Acq. Operator : SYSTEM
Acq. Instrument : 1260 HPLC Location : -
Injection Date : 1/20/2016 11:22:23 AM Inj Volume : No inj
Acq. Method : C:\CHEM32\1\METHODS\MLD-2-2-60_20MIN_1ML.M
Last changed : 1/15/2016 11:07:02 AM by SYSTEM
Analysis Method : C:\CHEM32\1\METHODS\DEF_LC.M
Last changed : 9/9/2016 9:42:32 AM by SYSTEM
Sample Info : HJ-III-151-MC1RL

Additional Info : Peak(s) manually integrated



=====
Area Percent Report
=====

Sorted By : Signal
Multiplier: : 1.0000
Dilution: : 1.0000
Use Multiplier & Dilution Factor with ISTDs

Signal 1: WVD1 A, Wavelength=220 nm

Peak #	RetTime [min]	Type	Width [min]	Area [mAU*s]	Height [mAU]	Area %
1	17.874	VV	0.1718	294.67816	24.58476	0.7953
2	18.367	VV	0.1960	3.63469e4	2966.29150	98.1011
3	18.761	VB	0.1388	408.86725	42.67663	1.1035

Totals : 3.70505e4 3033.55289

Figure A2.11 Scrambled-MC1RL-Ahx-DOTA; HPLC Trace (prepared by Dr. Hunjoo Kil)

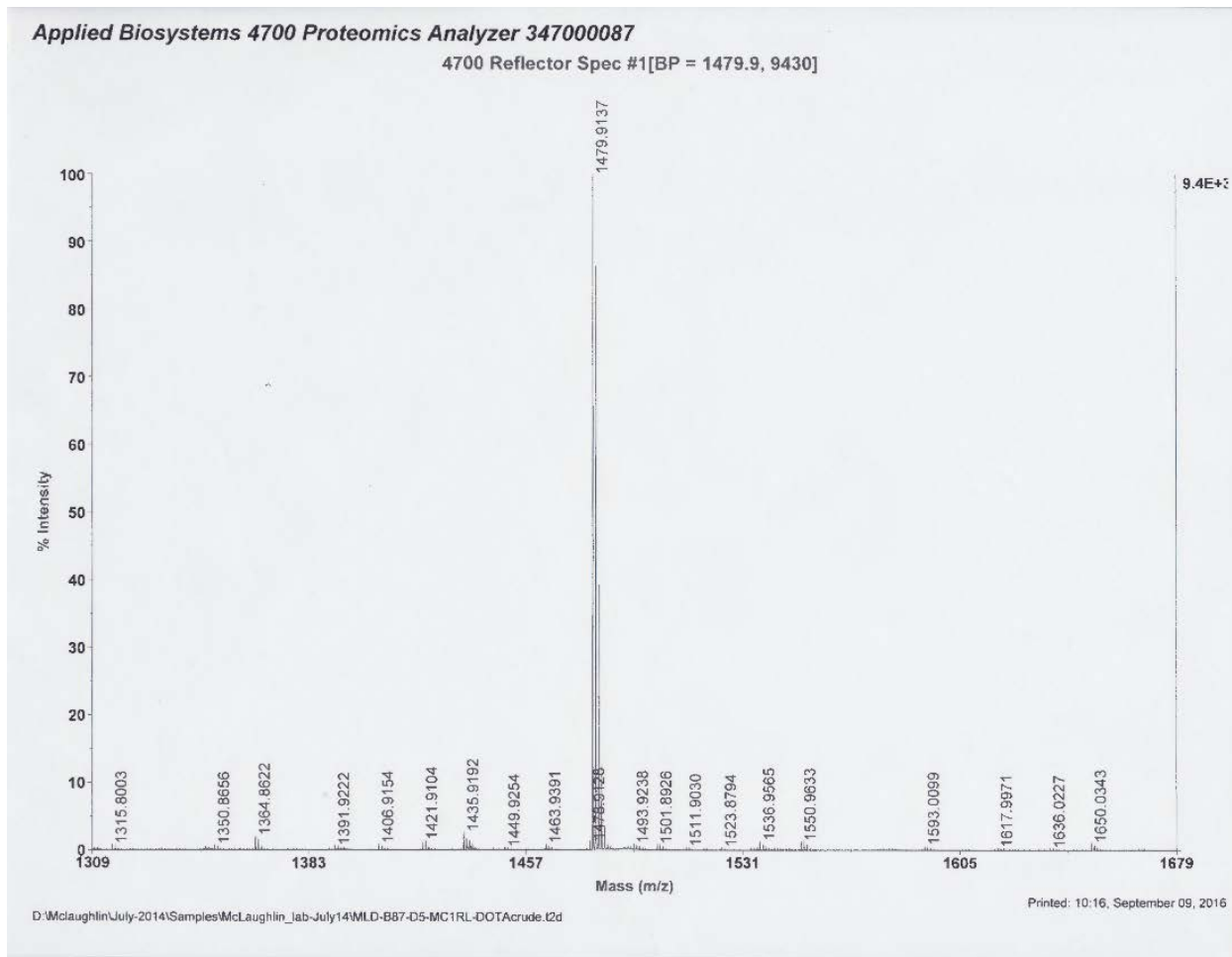
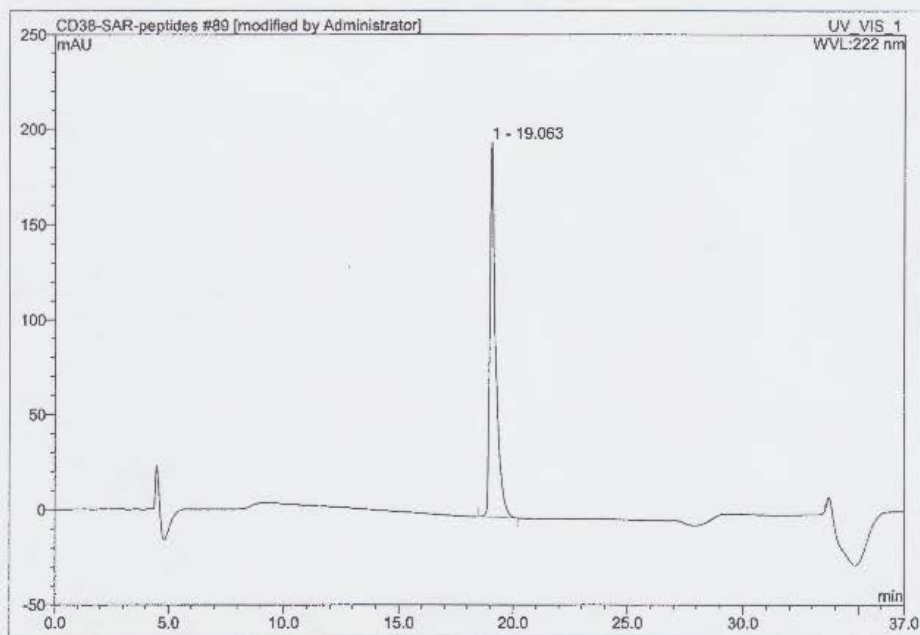


Figure A2.12 MC1RL(D5)-Ahx-DOTA; Mass Spectrum

LI

89 MLD-B87-D5MC1RLDOTA-F18		
Sample Name:	MLD-B87-D5MC1RLDOTA-F18	Injection Volume: 100.0
Vial Number:	RA3	Channel: UV_VIS_1
Sample Type:	unknown	Wavelength: 222
Control Program:	MLD-2-60_20min	Bandwidth: 1
Quantif. Method:	default	Dilution Factor: 1.0000
Recording Time:	8/9/2014 17:17	Sample Weight: 1.0000
Run Time (min):	37.00	Sample Amount: 1.0000



No.	Ret.Time min	Peak Name	Height mAU	Area mAU*min	Rel.Area %	Amount n.a.	Type
1	19.06	n.a.	197.144	58.528	100.00	n.a.	BMB
Total:			197.144	58.528	100.00	0.000	

default/Integration

Chromeleon (c) Dionex 1996-2001
Version 6.50 SP3a Build 986

Figure A2.13 MC1RL(D5)-Ahx-DOTA; HPLC Trace

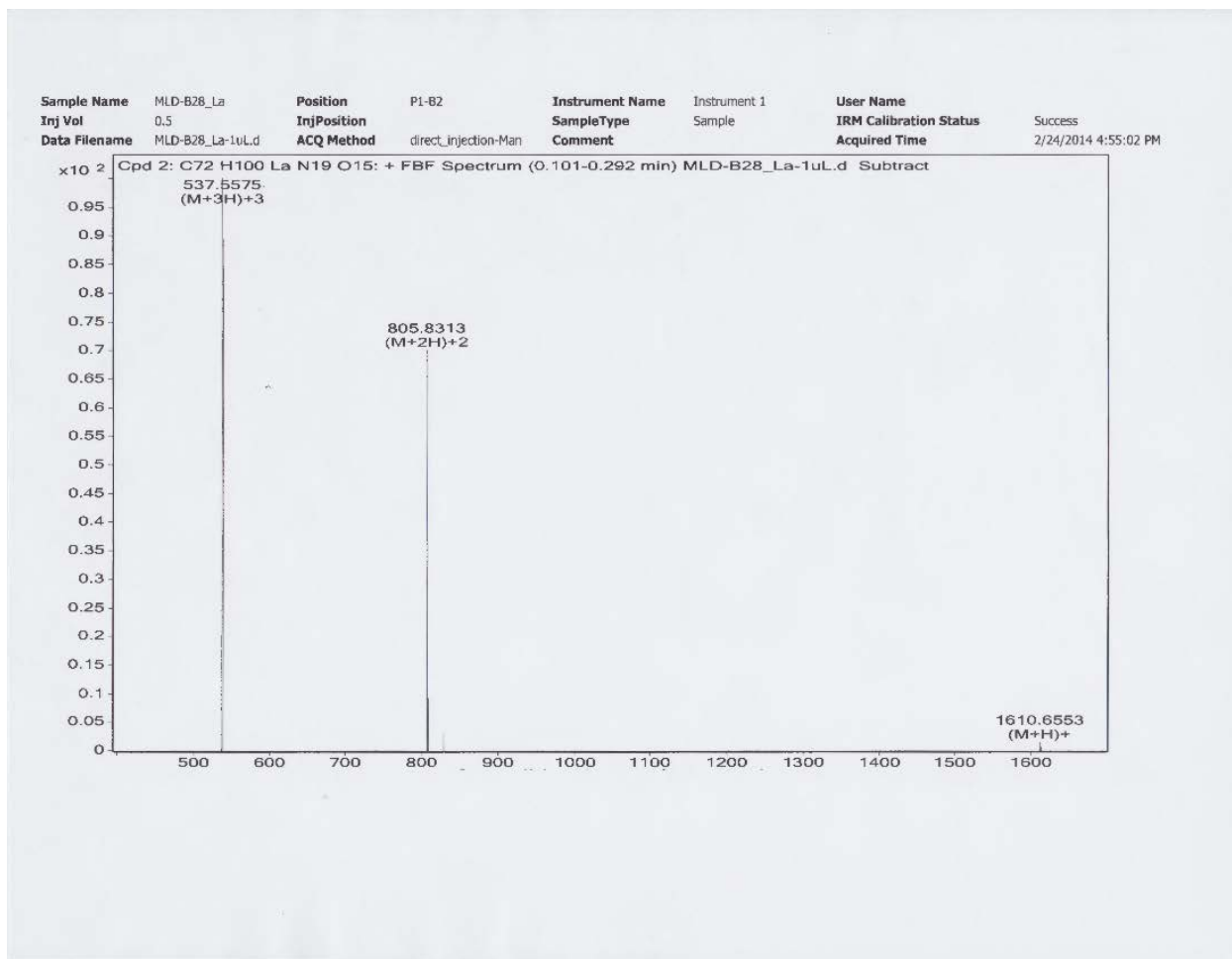
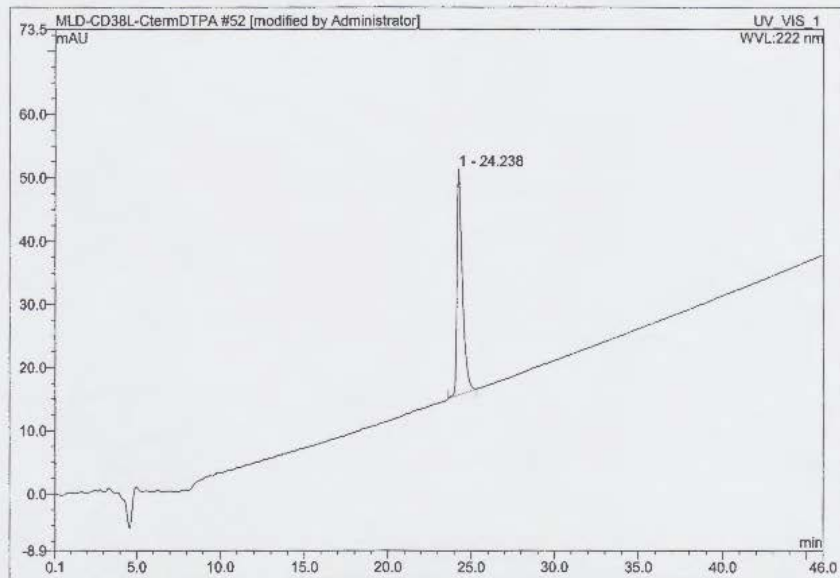


Figure A2.14 MC1RL-Ahx-DOTA:La; Mass Spectrum

52 MLD-B28-MC1RL-DOTA-La

Sample Name:	MLD-B28-MC1RL-DOTA-La	Injection Volume:	100.0
Vial Number:	BB4	Channel:	UV_VIS_1
Sample Type:	unknown	Wavelength:	222
Control Program:	MLD-10-60_40min	Bandwidth:	1
Quantif. Method:	default	Dilution Factor:	1.0000
Recording Time:	2/20/2014 19:50	Sample Weight:	1.0000
Run Time (min):	57.00	Sample Amount:	1.0000



No.	Ret.Time min	Peak Name	Height mAU	Area mAU*min	Rel.Area %	Amount n.a.	Type
1	24.24	n.a.	35.746	13.687	100.00	n.a.	BMB*
Total:			35.746	13.687	100.00	0.000	

default/Integration

Chromeleon (c) Dionex 1996-2001
Version 6.50 SP3a Build 986

Figure A2.15 MC1RL-Ahx-DOTA:La; HPLC Trace

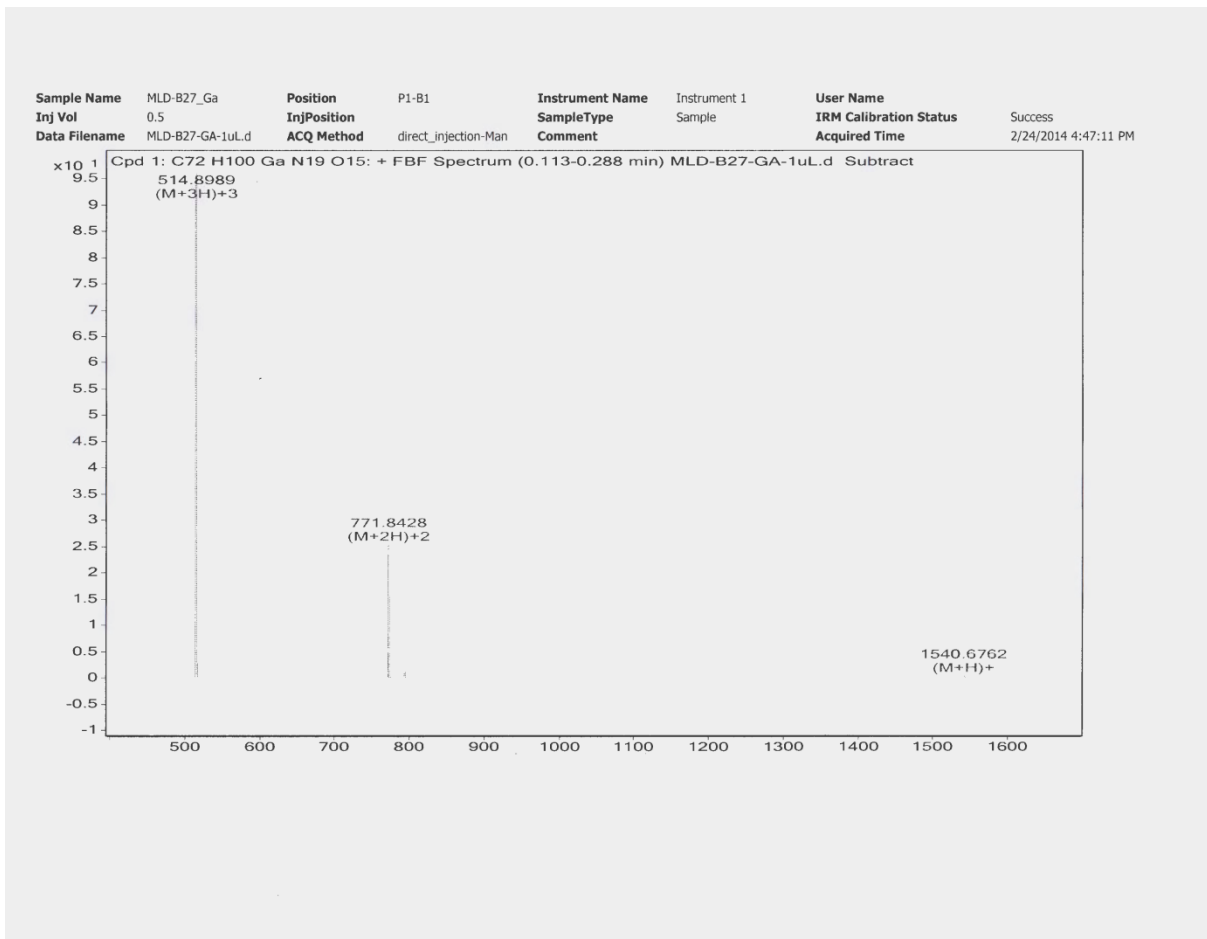
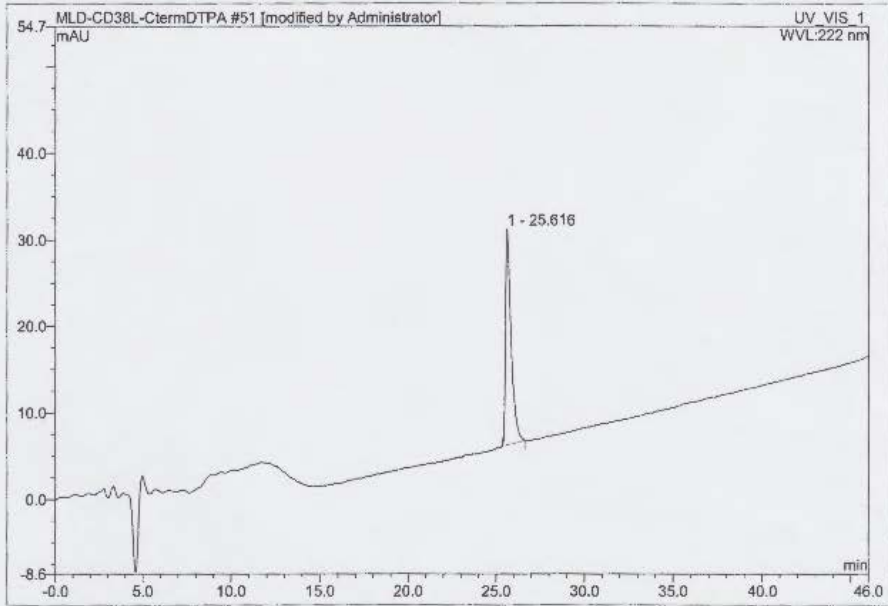


Figure A2.16 MC1RL-Ahx-DOTA:Ga; Mass Spectrum

51 MLD-B27-MC1RL-DOTA-Ga

Sample Name:	MLD-B27-MC1RL-DOTA-Ga	Injection Volume:	100.0
Vial Number:	BB3	Channel:	UV_VIS_1
Sample Type:	unknown	Wavelength:	222
Control Program:	MLD-10-60_40min	Bandwidth:	1
Quantif. Method:	default	Dilution Factor:	1.0000
Recording Time:	2/20/2014 18:50	Sample Weight:	1.0000
Run Time (min):	57.00	Sample Amount:	1.0000



No.	Ret.Time min	Peak Name	Height mAU	Area mAU*min	Rel.Area %	Amount n.a.	Type
1	25.62	n.a.	25.020	9.088	100.00	n.a.	BMB*
Total:			25.020	9.088	100.00	0.000	

default/Integration

Chromeleon (c) Dionex 1996-2001
Version 6.50 SP3a Build 986

Figure A2.17 MC1RL-Ahx-DOTA:Ga; HPLC Trace

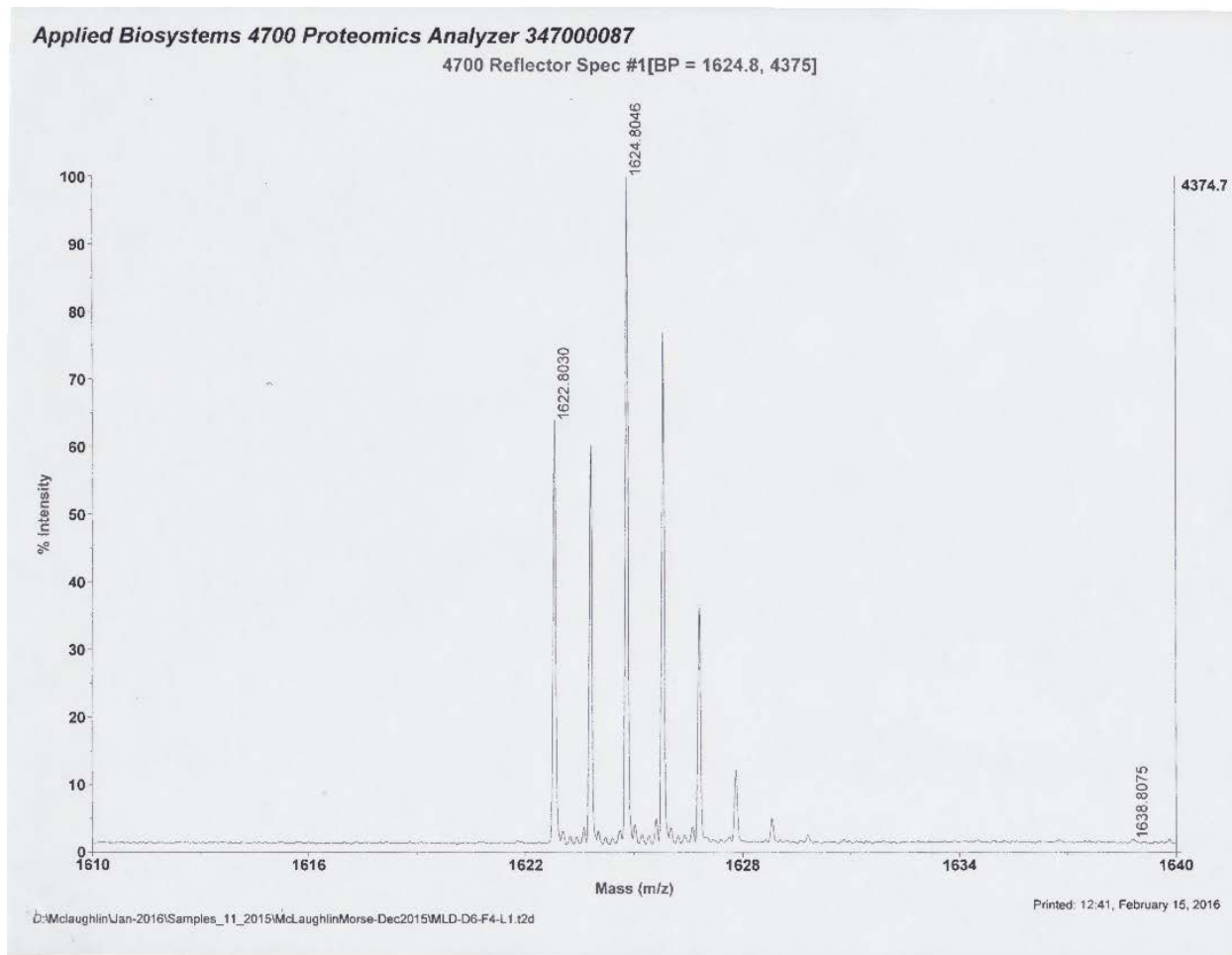


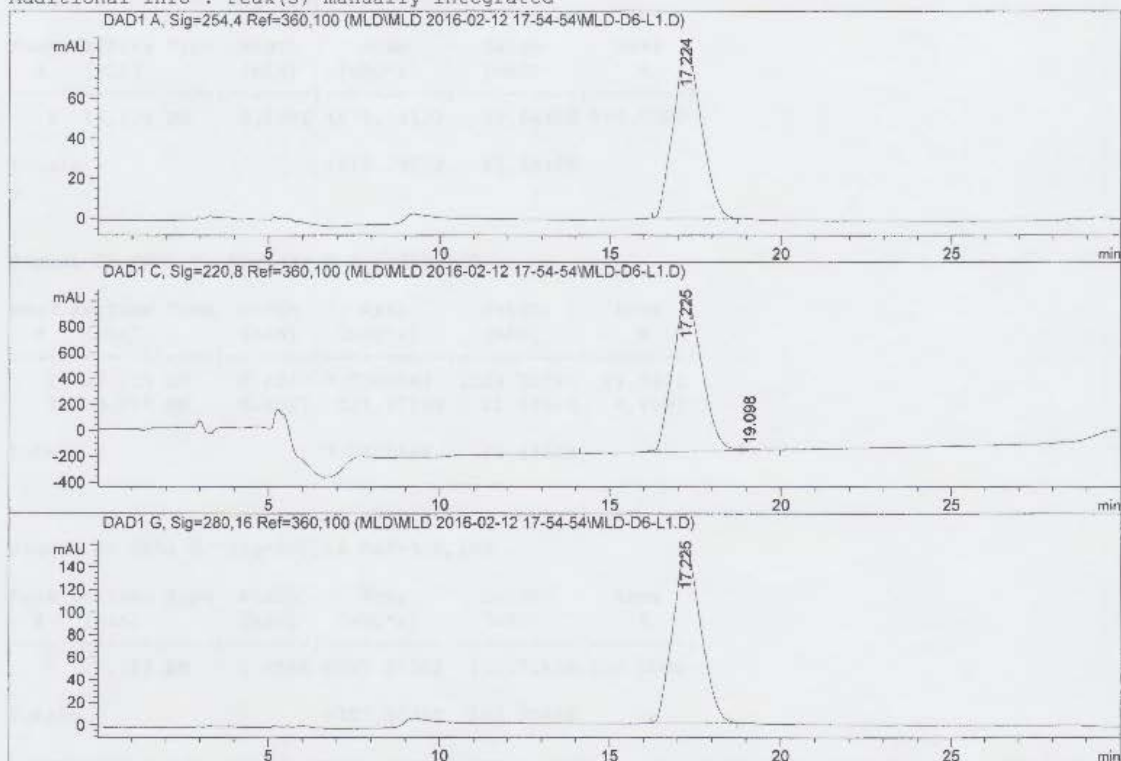
Figure A2.18 MC1RLAhx-DOTA:Eu; Mass Spectrum

Data File C:\CHEM32\1\DATA\MLD\MLD 2016-02-12 17-54-54\MLD-D6-L1.D
Sample Name: MLD-D6-L1

=====

Acq. Operator :	Instrument 1	Seq. Line :	2
Acq. Instrument :	Instrument 1	Location :	Vial 52
Injection Date :	2/12/2016 6:33:15 PM	Inj :	1
		Inj Volume :	10.0 µl
		Actual Inj Volume :	20.0 µl

Different Inj Volume from Sequence !
Acq. Method : C:\CHEM32\1\DATA\MLD\MLD 2016-02-12 17-54-54\MLD-2-15-60_20MIN_1-PH6.M
Last changed : 2/10/2016 7:23:47 PM
Analysis Method : C:\CHEM32\1\METHODS\MLD-2-20-40_20MIN_1.M
Last changed : 1/25/2016 6:12:07 PM
Additional Info : Peak(s) manually integrated



=====
Fraction Information
=====

Fraction collection off

No Fractions found.
=====

Instrument 1 2/15/2016 10:25:32 AM

Page 1 of 2

Figure A2.19 MC1RL-Ahx-DOTA:Eu; HPLC Trace

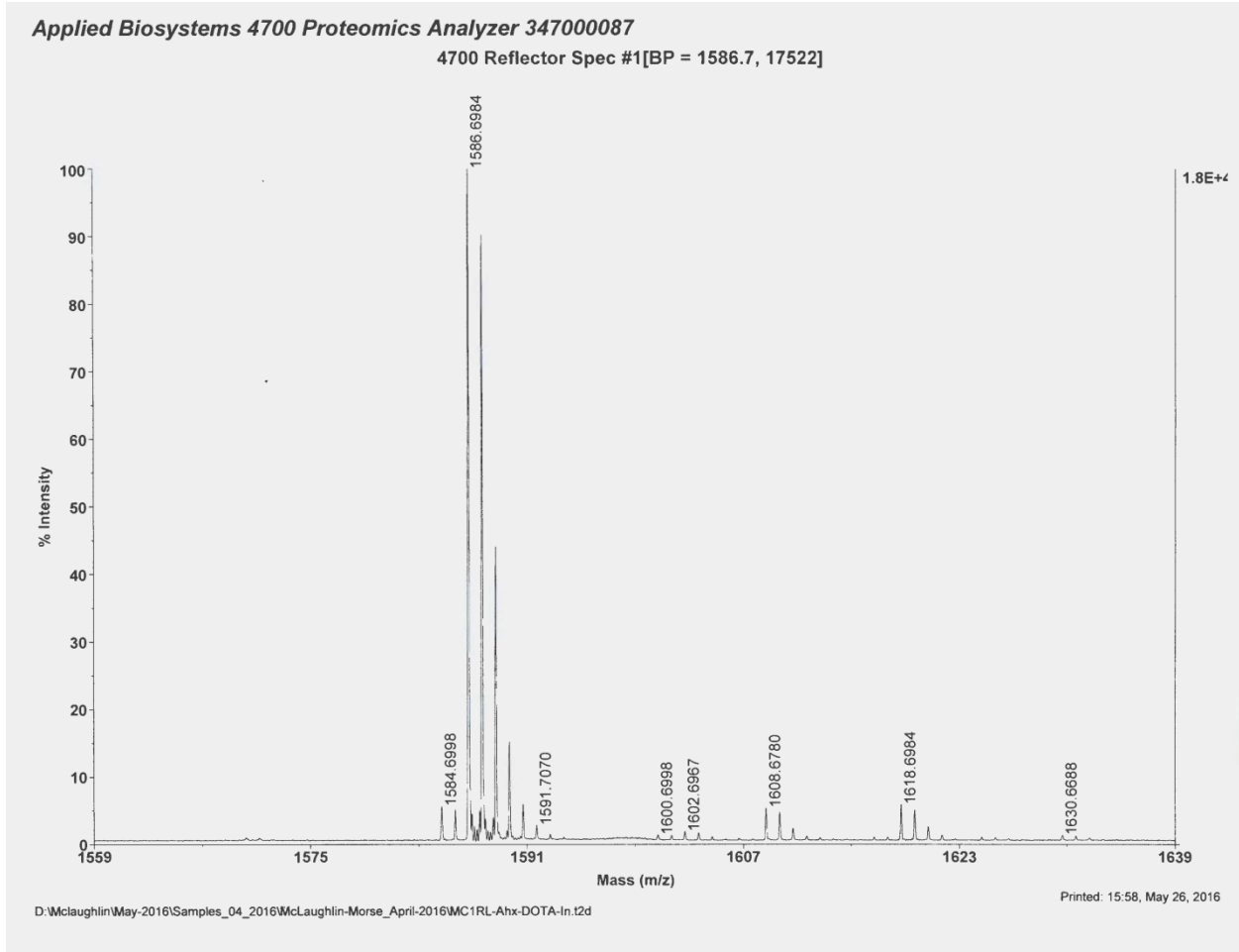
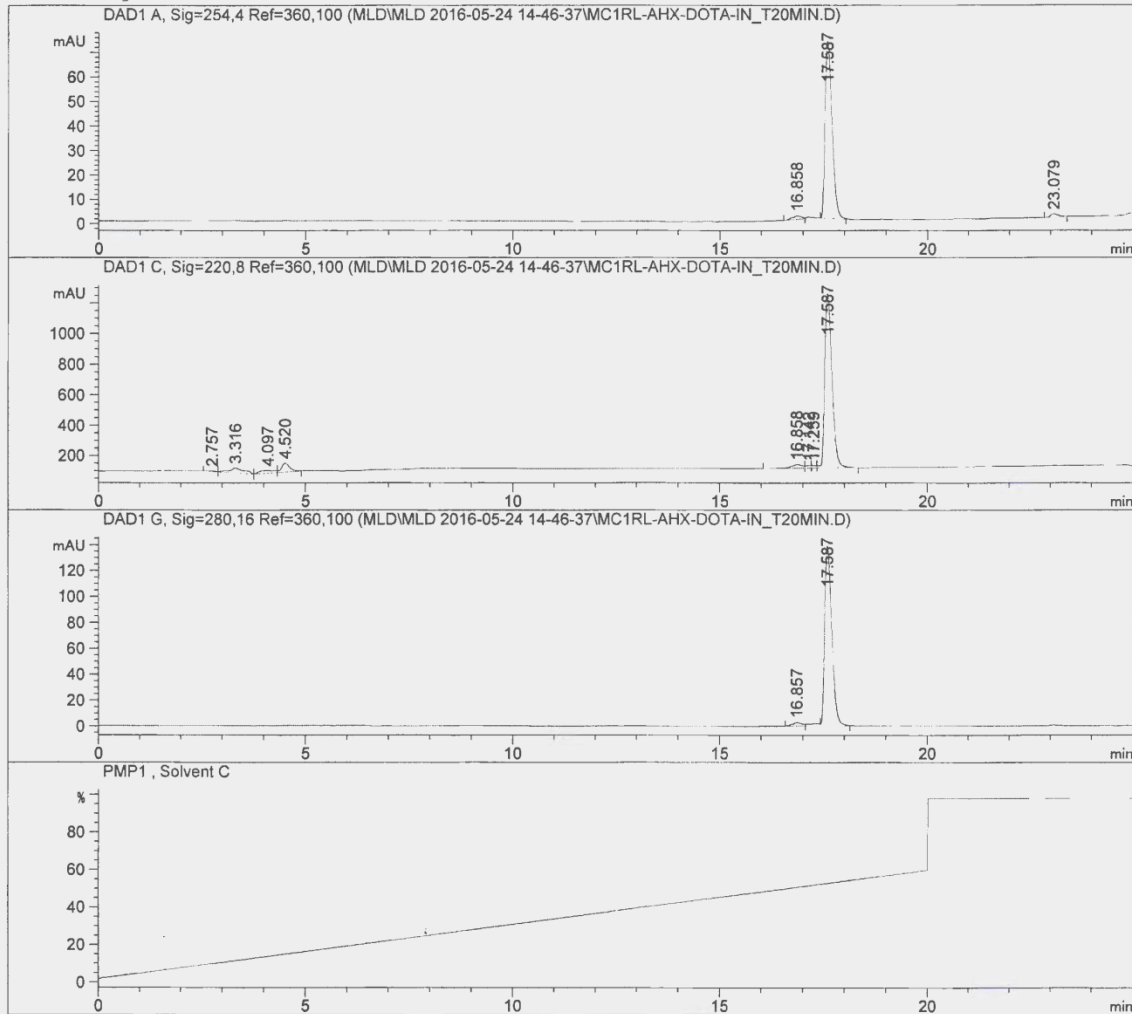


Figure A2.20 MC1RL-Ahx-DOTA:In; Mass Spectrum

Data File C:\CHEM32\1\DATA\MLD\MLD 2016-05-24 14-46-37\MC1RL-AHX-DOTA-IN_T20MIN.D
 Sample Name: MC1RL-Ahx-DOTA-In_T20min

```

=====
Acq. Operator   :                               Seq. Line :    4
Acq. Instrument : Instrument 1                  Location  : Vial 62
Injection Date  : 5/24/2016 4:25:55 PM        Inj       :    1
                                                Inj Volume: 10.0 µl
Different Inj Volume from Sequence ! Actual Inj Volume : 5.0 µl
Acq. Method    : C:\CHEM32\1\DATA\MLD\MLD 2016-05-24 14-46-37\MLD-2-60_20MIN_1.M
Last changed   : 5/24/2016 2:38:53 PM
Analysis Method : C:\CHEM32\1\METHODS\MLD-2-100_10MIN_1.M
Last changed   : 4/19/2016 10:19:54 AM
=====
  
```



```

=====
Fraction Information
=====
Fraction collection off
=====
No Fractions found.
=====
  
```

Instrument 1 5/24/2016 5:16:16 PM

Page 1 of 2

Figure A2.21 MC1RL-Ahx-DOTA:In; HPLC Trace

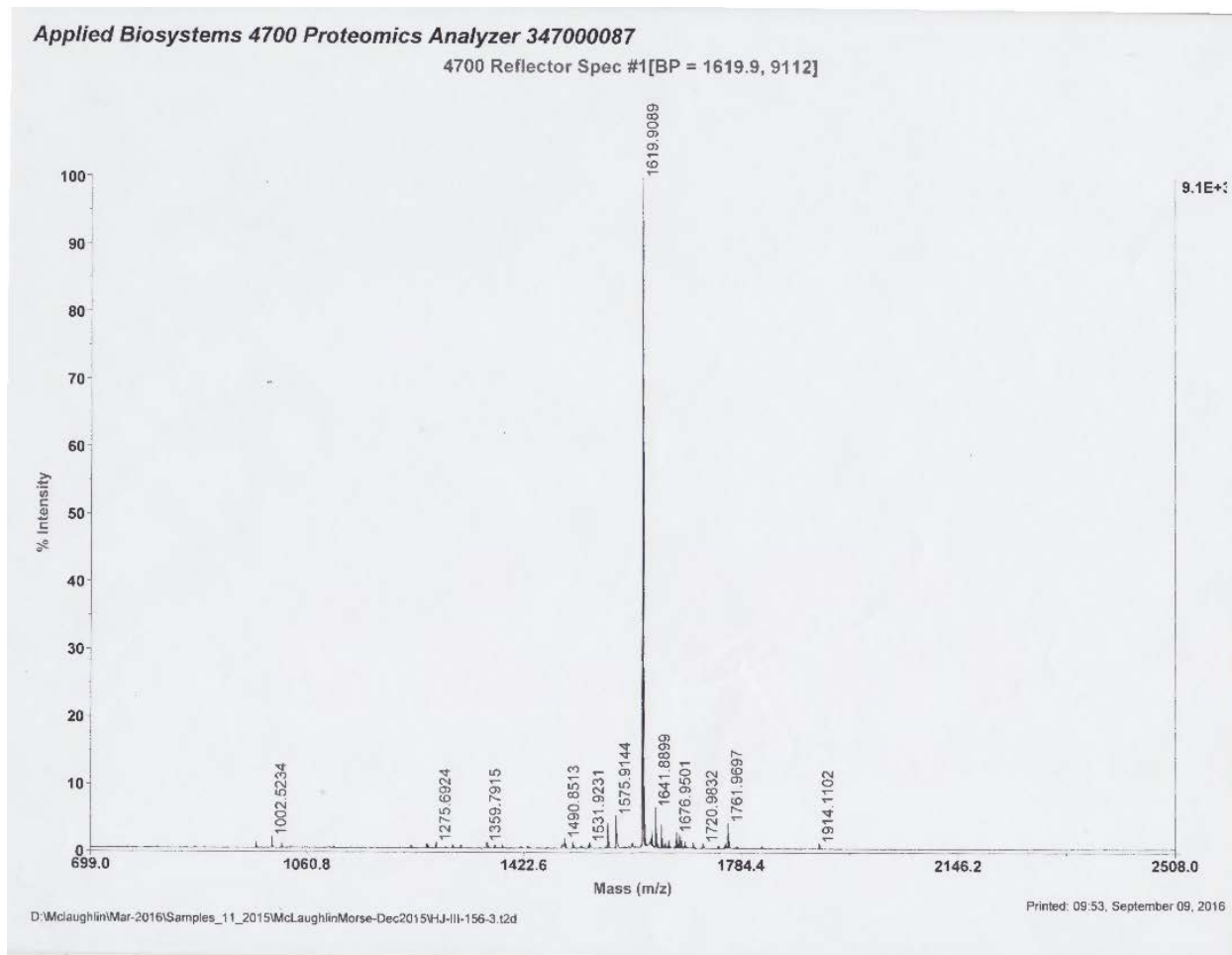
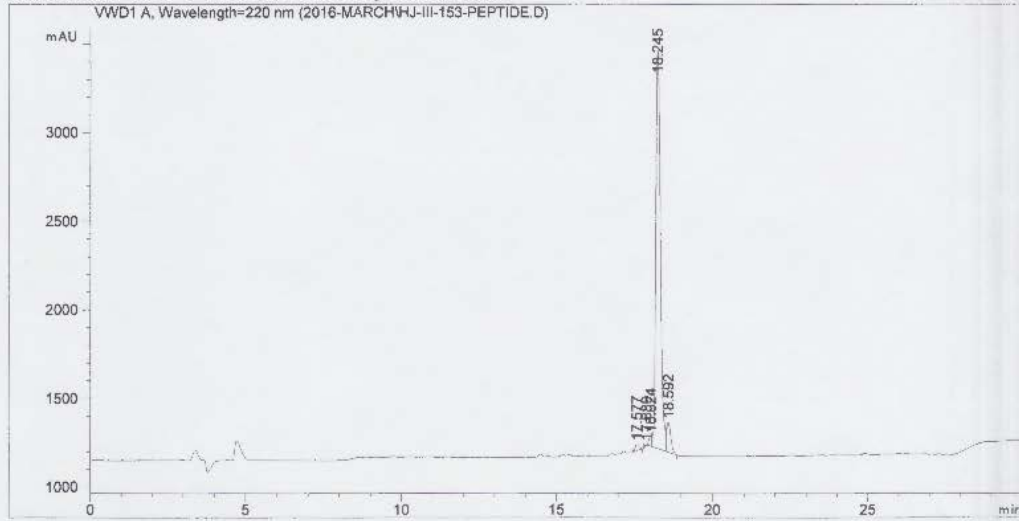


Figure A2.22 MC1RL-diDGlu-DOTA; Mass Spectrum (prepared by Dr. Hunjoo Kil)

Data File C:\CHEM32\1\DATA\2016-MARCH\HJ-III-153-PEPTIDE.D
Sample Name: HJ-III-153-PEPTIDE

=====
Acq. Operator : SYSTEM
Acq. Instrument : 1260 HPLC Location : -
Injection Date : 3/21/2016 6:05:40 PM Inj Volume : No inj
Acq. Method : C:\CHEM32\1\METHODS\MLD-2-2-60_20MIN_1ML.M
Last changed : 3/21/2016 4:52:31 PM by SYSTEM
(modified after loading)
Analysis Method : C:\CHEM32\1\METHODS\DEF_LC.M
Last changed : 9/9/2016 9:42:32 AM by SYSTEM
Sample Info : HJ-III-153-PEPTIDE

Additional Info : Peak(s) manually integrated



=====
Area Percent Report
=====

Sorted By : Signal
Multiplier: : 1.0000
Dilution: : 1.0000
Use Multiplier & Dilution Factor with ISTDs

Signal 1: VWD1 A, Wavelength=220 nm

Peak #	RetTime [min]	Type	Width [min]	Area [mAU*s]	Height [mAU]	Area %
1	17.577	BB	0.1199	283.16037	35.18645	1.1279
2	17.889	BB	0.1219	17.82671	2.04042	0.0710
3	18.024	BV	0.0867	298.69257	53.06313	1.1898
4	18.245	VV	0.1609	2.29380e4	2249.92261	91.3687
5	18.592	VB	0.1385	1567.20288	166.95795	6.2426

1260 HPLC 9/9/2016 9:58:49 AM SYSTEM

Page 1 of 2

Figure A2.23 MC1RL-diDGlu-DOTA; HPLC Trace (prepared by Dr. Hunjoo Kil)

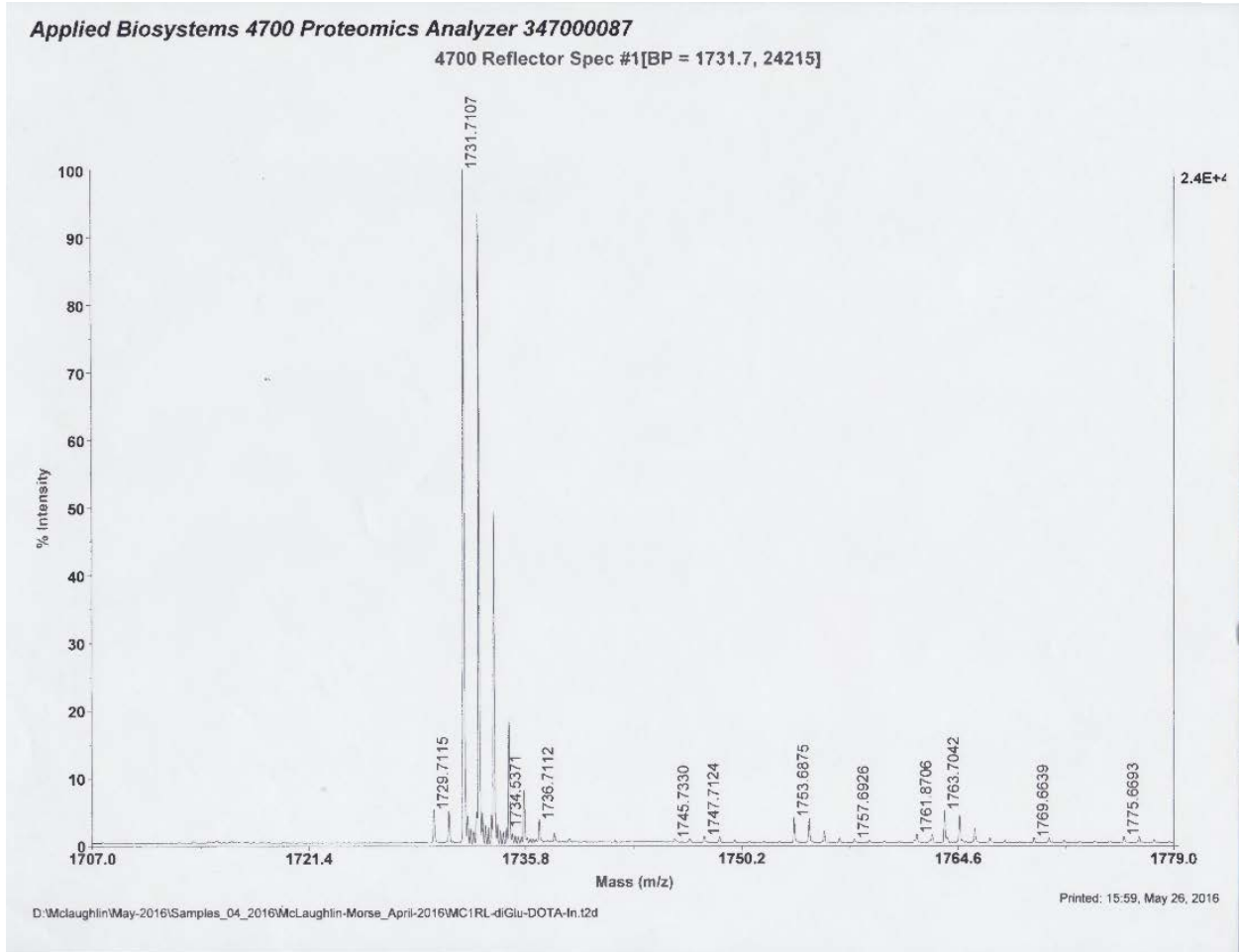


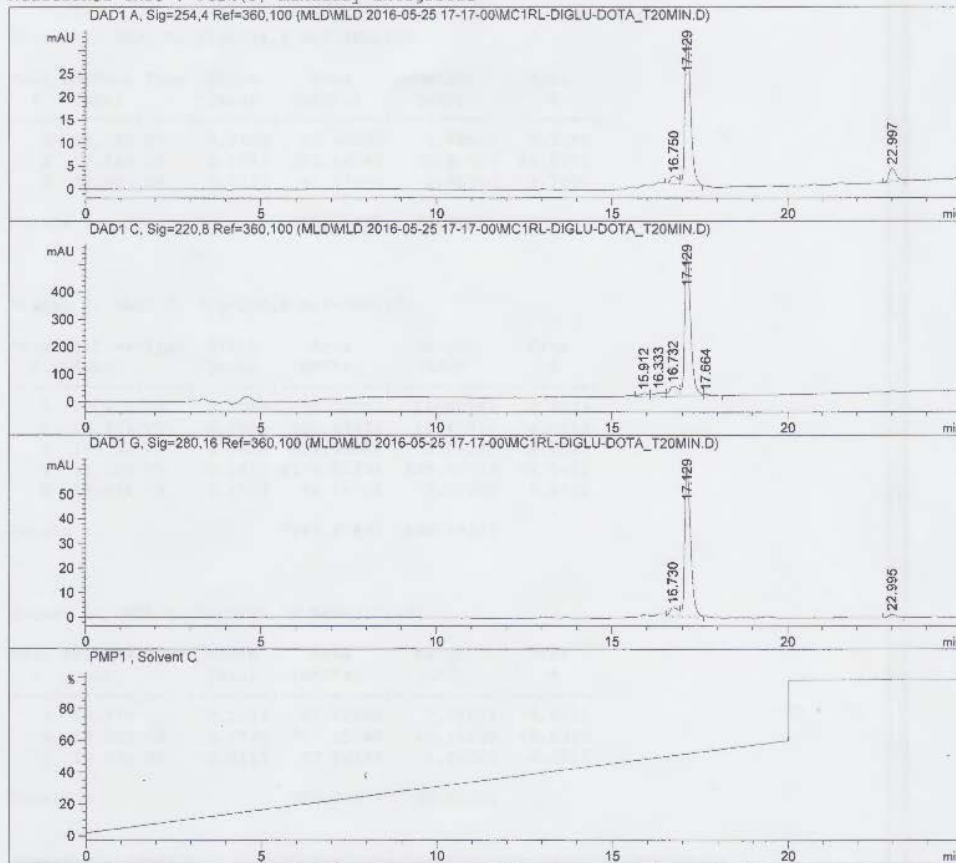
Figure A2.24 MC1RL-diDGLu-DOTA:In; Mass Spectrum (Precursor prepared by Dr. Hunjoo Kil)

Data File C:\CHEM32\1\DATA\MLD\MLD 2016-05-25 17-17-00\MC1RL-DIGLU-DOXA_T20MIN.D
Sample Name: MC1RL-diGlu-DOXA

=====

Acq. Operator	:	Seq. Line	:	1	
Acq. Instrument	:	Instrument 1	Location	:	Vial 64
Injection Date	:	5/25/2016 5:17:18 PM	Inj	:	1
			Inj Volume	:	10.0 µl

Different Inj Volume from Sequence ! Actual Inj Volume : 5.0 µl
Acq. Method : C:\CHEM32\1\DATA\MLD\MLD 2016-05-25 17-17-00\MLD-2-60_20MIN_1.M
Last changed : 5/24/2016 2:38:53 PM
Analysis Method : C:\CHEM32\1\METHODS\MLD-2-100_10MIN_1.M
Last changed : 4/19/2016 10:19:54 AM
Additional Info : Peak(s) manually integrated



=====

Fraction Information

=====

Fraction collection off

=====

Instrument 1 5/25/2016 5:52:21 PM

Page 1 of 2

Figure A2.25 MC1RL-diDGlu-DOXA:In; HPLC Trace (Precursor prepared by Dr. Hunjoo Kil)

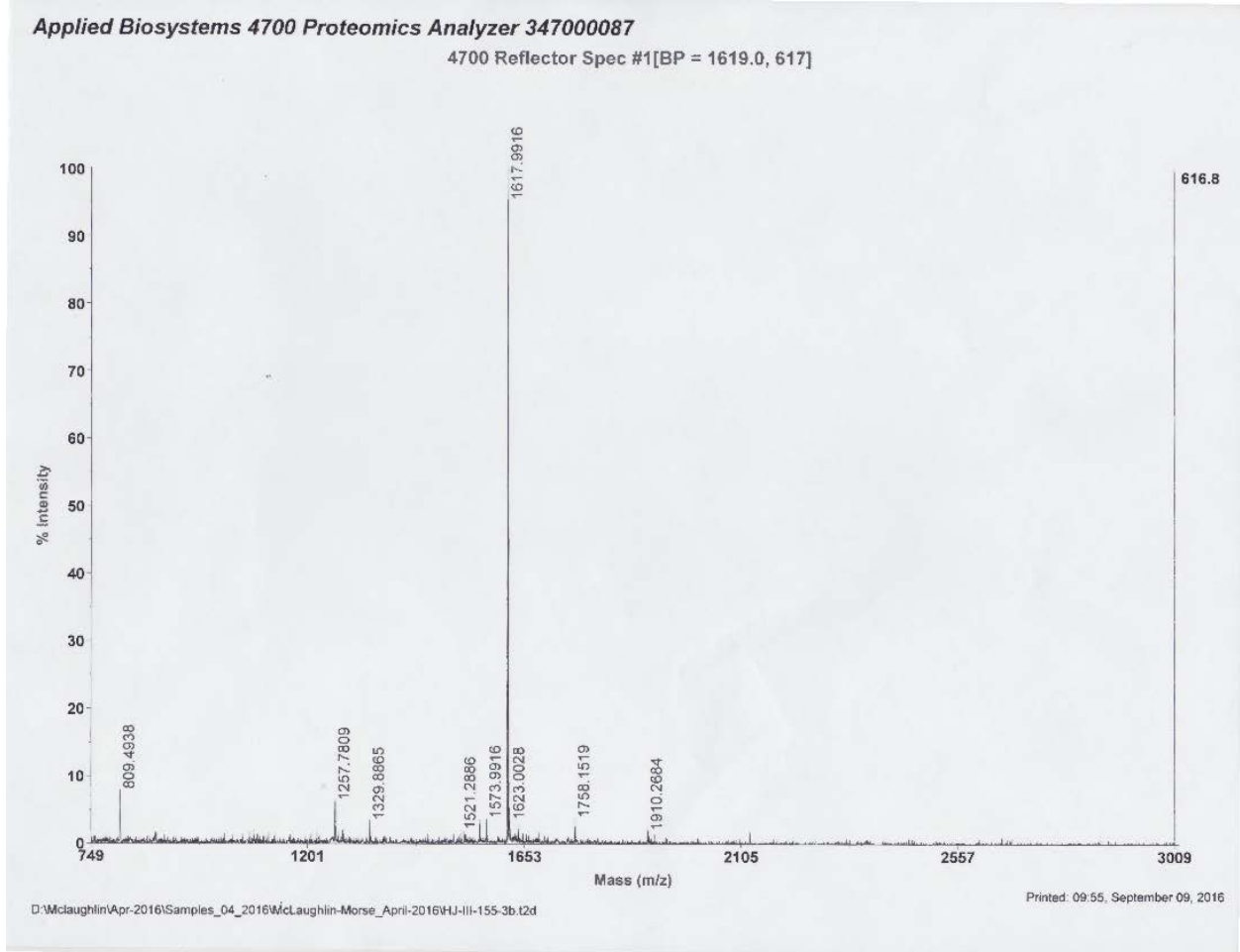


Figure A2.26 MC1RL-diDLys-DOTA; Mass Spectrum (Precursor prepared by Dr. Hunjoo Kil)

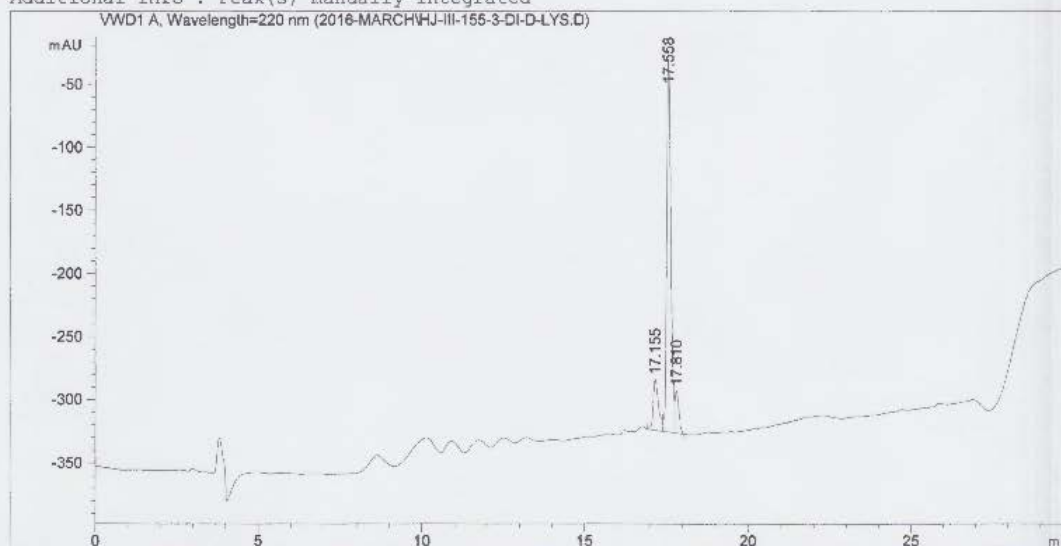
Data File C:\CHEM32\1\DATA\2016-MARCH\HJ-III-155-3-DI-D-LYS.D
 Sample Name: HJ-III-155-3-Di-D-Lys.D

```

=====
Acq. Operator   : SYSTEM
Acq. Instrument : 1260 HPLC
Injection Date  : 4/26/2016 10:48:57 AM
Location       : -
Inj Volume     : No inj

Acq. Method    : C:\CHEM32\1\METHODS\MLD-2-2-60_20MIN_1ML.M
Last changed   : 1/15/2016 11:07:02 AM by SYSTEM
Analysis Method : C:\CHEM32\1\METHODS\DEF_IC.M
Last changed   : 9/9/2016 9:42:32 AM by SYSTEM
Sample Info    : HJ-III-155-3-Di-D-Lys.D
=====
  
```

Additional Info : Peak(s) manually integrated



Area Percent Report

```

=====
Sorted By      :      Signal
Multiplier:    :      1.0000
Dilution:      :      1.0000
Use Multiplier & Dilution Factor with ISTDs
=====
  
```

Signal 1: WVD1 A, Wavelength=220 nm

Peak #	RetTime [min]	Type	Width [min]	Area [mAU*s]	Height [mAU]	Area %
1	17.155	BV	0.1723	457.02029	40.60275	13.7297
2	17.558	VV	0.1353	2592.70215	295.61655	77.8895
3	17.810	VB	0.1208	278.97110	33.97034	8.3808

Totals : 3328.69354 370.18963

1260 HPLC 9/9/2016 9:57:29 AM SYSTEM

Page 1 of 2

Figure A2.27 MC1RL-diDLys-DOTA; HPLC Trace (Precursor prepared by Dr. Hunjoo Kil)

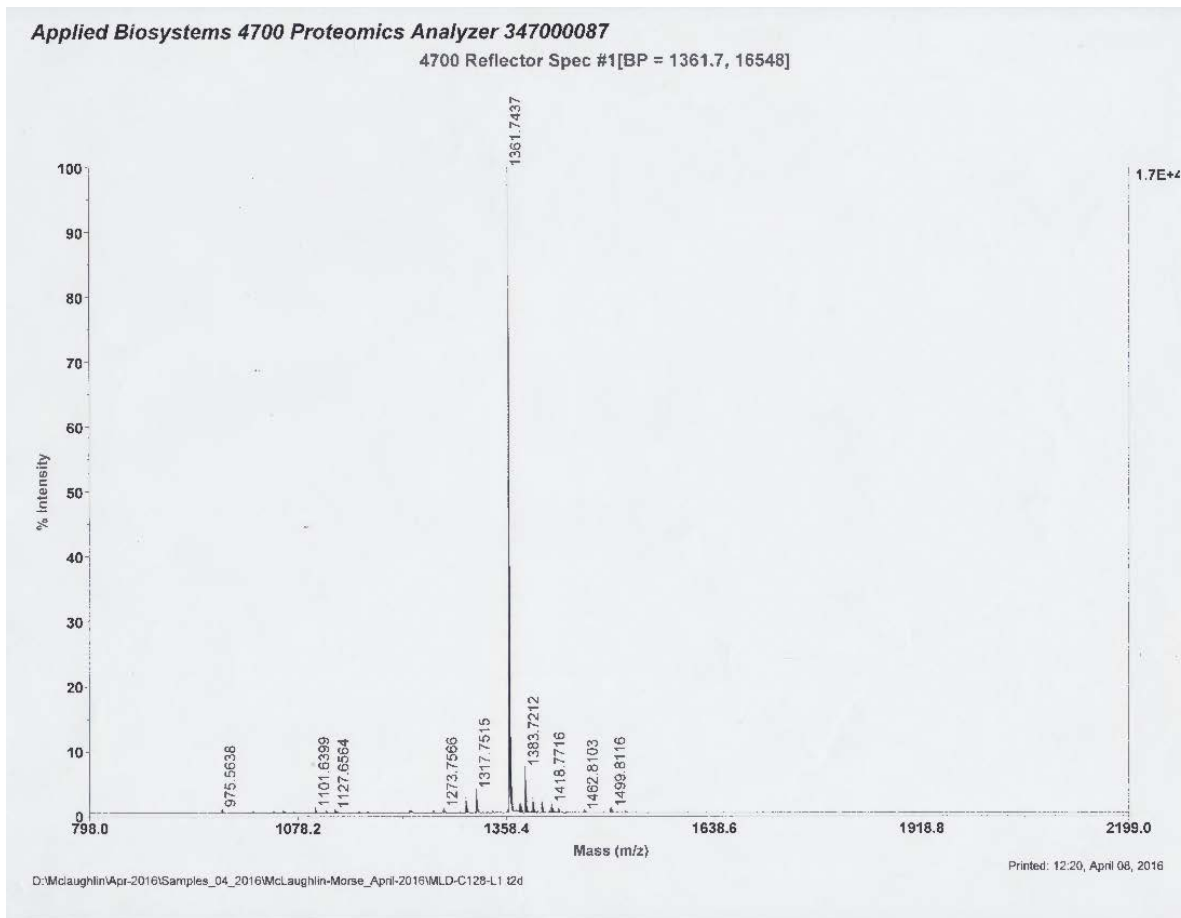


Figure A2.28 MC1RL-DOTA; Mass Spectrum

Data File C:\CHEM32\1\DATA\MLD\MLD 2016-01-26 11-15-57\MLD-C128-F8.D
Sample Name: MLD-C128-F8

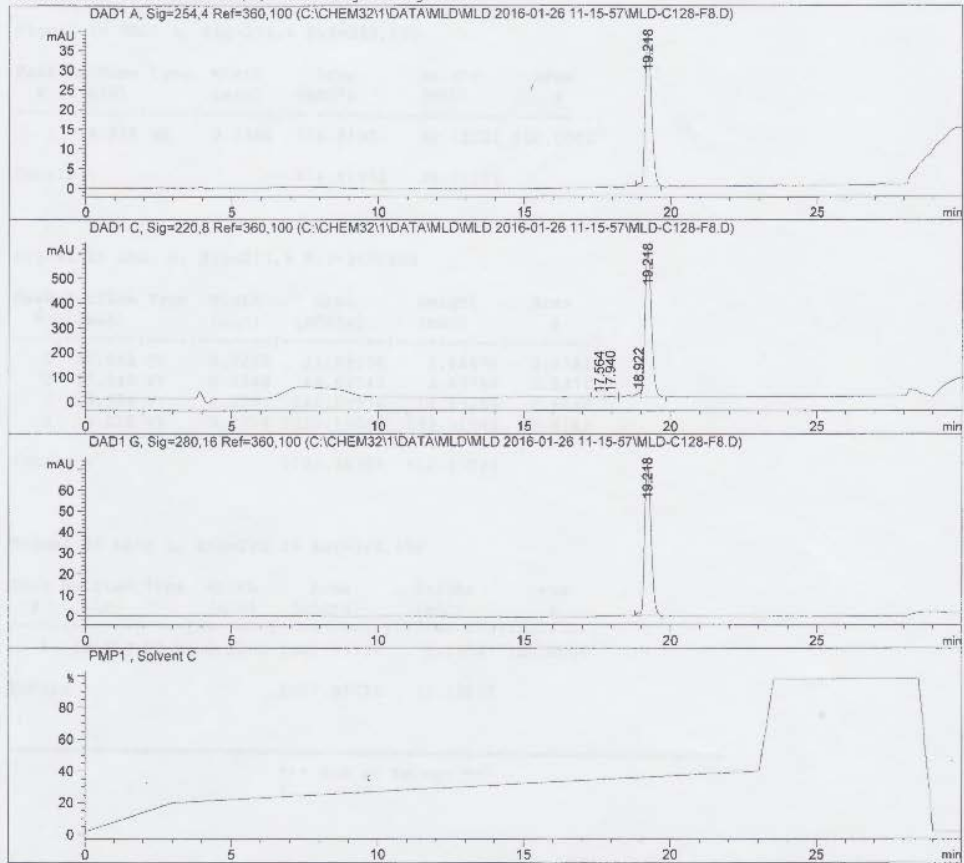
=====

Acq. Operator :	Seq. Line : 5
Acq. Instrument : Instrument 1	Location : Vial 5
Injection Date : 1/26/2016 1:49:09 PM	Inj : 1
	Inj Volume : 10.0 µl
	Actual Inj Volume : 20.0 µl

Different Inj Volume from Sequence !

Acq. Method :	C:\CHEM32\1\DATA\MLD\MLD 2016-01-26 11-15-57\MLD-2-20-40_20MIN_1.M
Last changed :	1/25/2016 6:12:07 PM
Analysis Method :	C:\CHEM32\1\METHODS\MLD-2-20-40_20MIN_1.M
Last changed :	1/25/2016 6:12:07 PM

Additional Info : Peak(s) manually integrated



=====
Fraction Information
=====

Fraction collection off
=====

Instrument 1 1/27/2016 12:41:50 PM

Page 1 of 2

Figure A2.29 MC1RL-DOTA; HPLC Trace

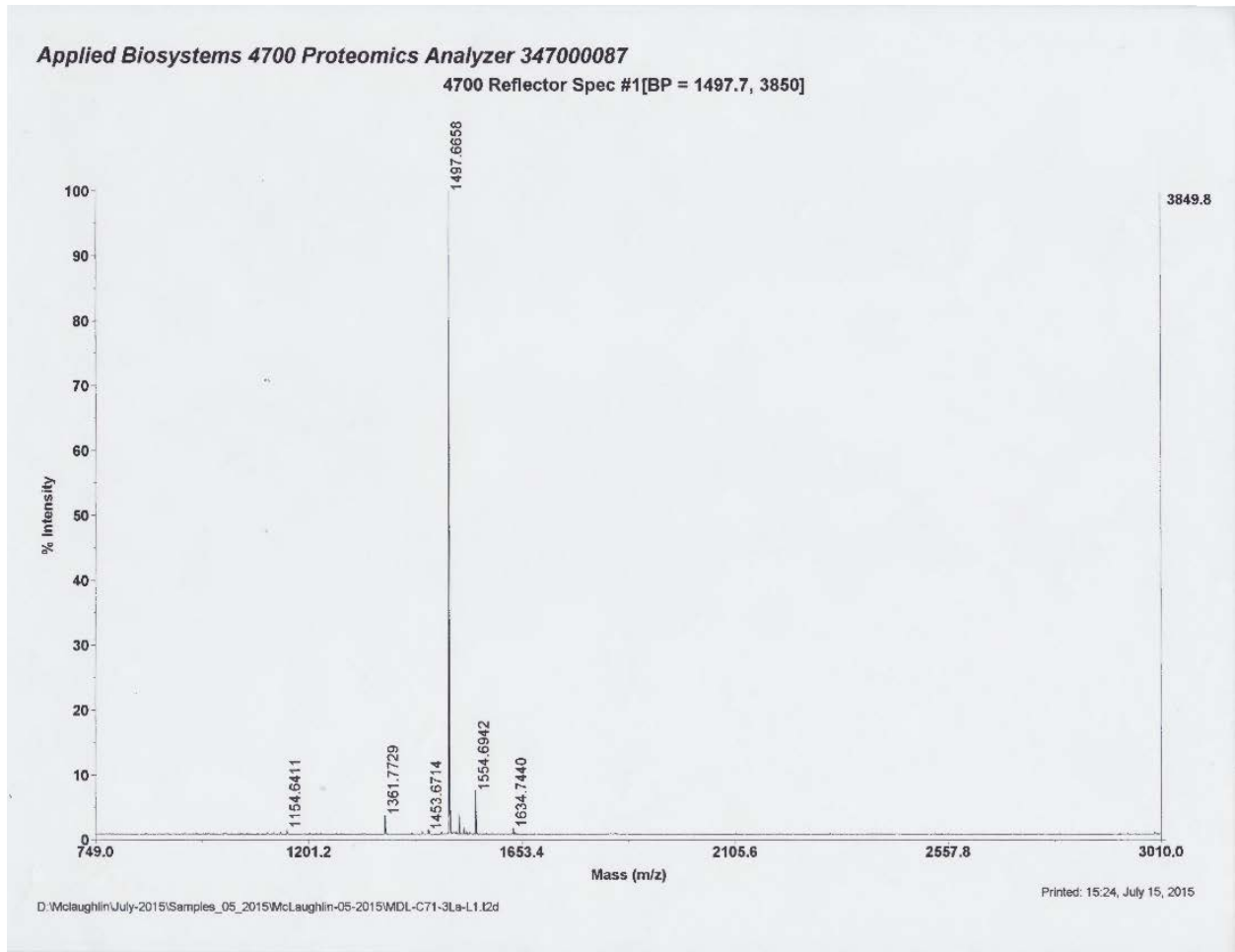
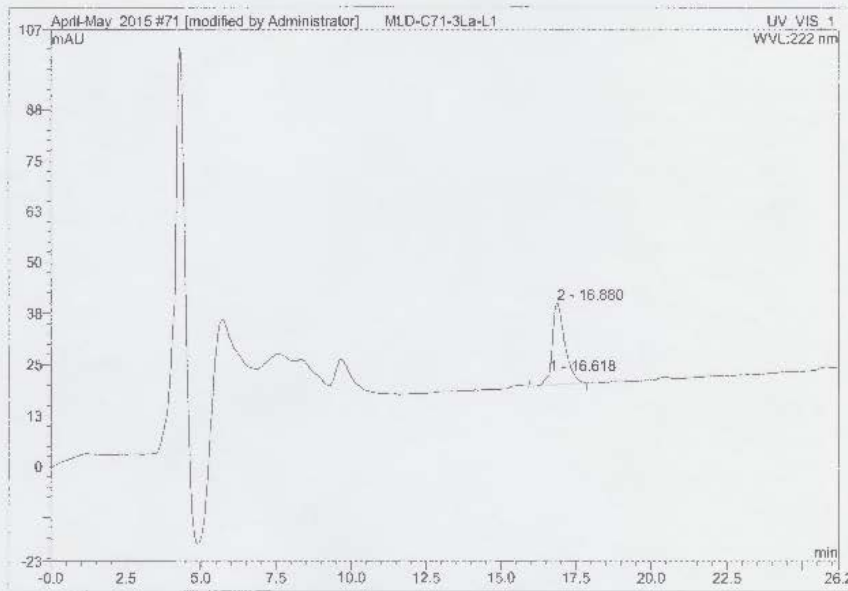


Figure A2.30 MC1RL-DOTA:La; HPLC Trace

71 MLD-C71-3La-L1

Sample Name:	MLD-C71-3La-L1	Injection Volume:	75.0
Vial Number:	BC4	Channel:	UV_VIS_1
Sample Type:	unknown	Wavelength:	222
Control Program:	MLD-2-20-40_20min	Bandwidth:	1
Quantif. Method:	default	Dilution Factor:	1.0000
Recording Time:	7/13/2015 20:13	Sample Weight:	1.0000
Run Time (min):	37.00	Sample Amount:	1.0000



No.	Ret.Time min	Peak Name	Height mAU	Area mAU*min	Rel.Area %	Amount n.a.	Type
1	16.62	n.a.	2.828	0.469	4.78	n.a.	BM *
2	16.88	n.a.	20.005	9.346	95.22	n.a.	MB*
Total:			22.833	9.815	100.00	0.000	

default/Integration

Chromeleon (c) Dionex 1996-2001
Version 6.50 SP3a Build 986

Figure A2.31 MC1RL-DOTA:La; HPLC Trace

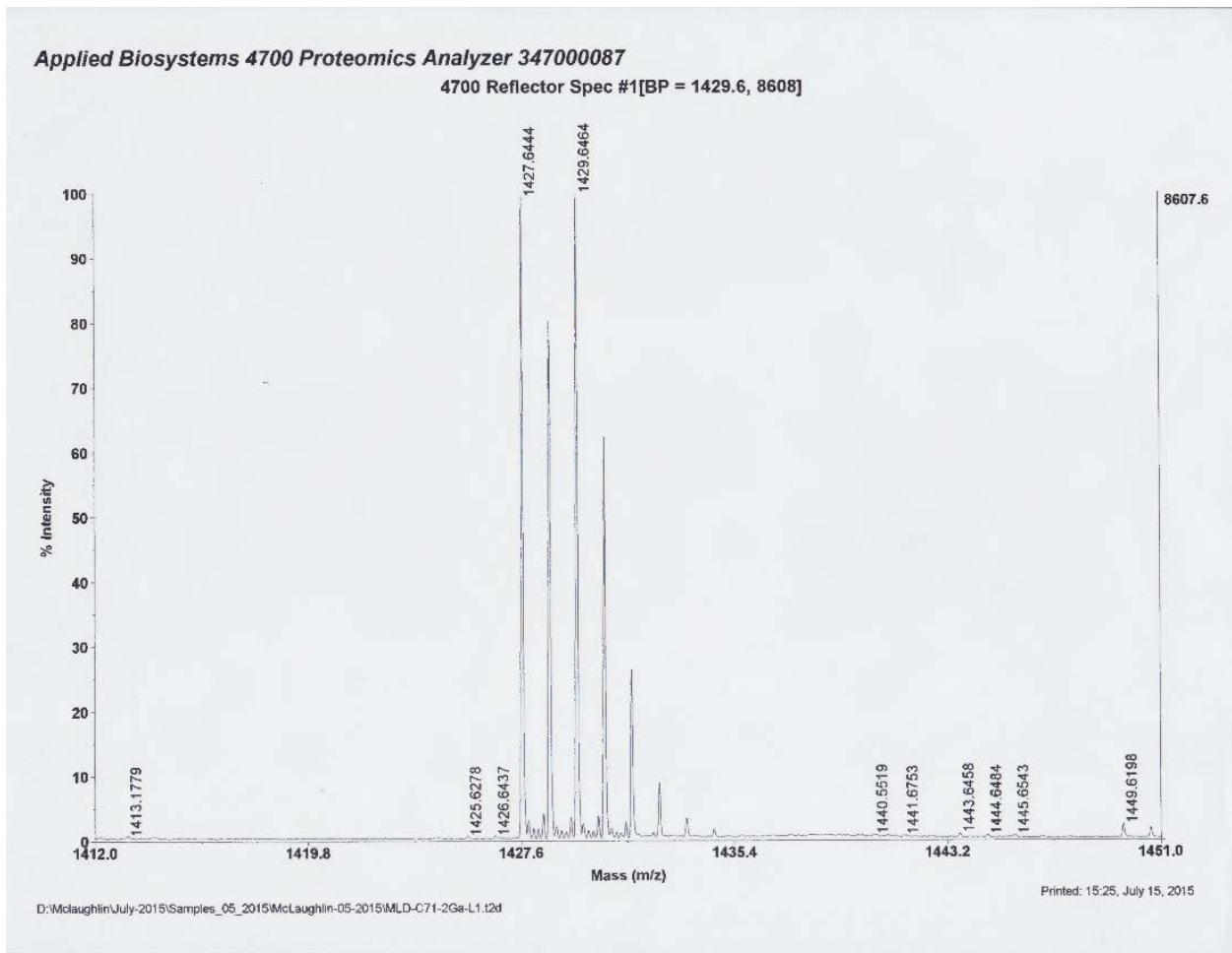
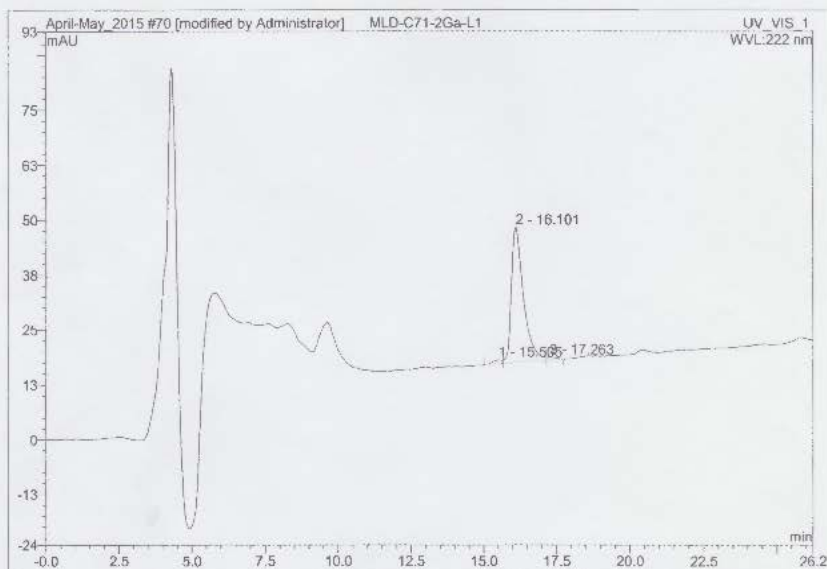


Figure A2.32 MC1RL-DOTA:Ga; Mass Spectrum

70 MLD-C71-2Ga-L1

Sample Name:	MLD-C71-2Ga-L1	Injection Volume:	75.0
Vial Number:	BC3	Channel:	UV_VIS_1
Sample Type:	unknown	Wavelength:	222
Control Program:	MLD-2-20-40_20min	Bandwidth:	1
Quantif. Method:	default	Dilution Factor:	1.0000
Recording Time:	7/13/2015 19:33	Sample Weight:	1.0000
Run Time (min):	37.00	Sample Amount:	1.0000



No.	Ret.Time min	Peak Name	Height mAU	Area mAU*min	Rel.Area %	Amount n.a.	Type
1	15.50	n.a.	0.890	0.334	2.18	n.a.	BM *
2	16.10	n.a.	30.764	14.739	96.29	n.a.	M *
3	17.26	n.a.	0.668	0.234	1.53	n.a.	MB *
Total:			32.322	15.307	100.00	0.000	

default/Integration

Chromeleon (c) Dionex 1996-2001
Version 6.50 SP3a Build 986

Figure A2.33 MC1RL-DOTA:Ga; HPLC Trace

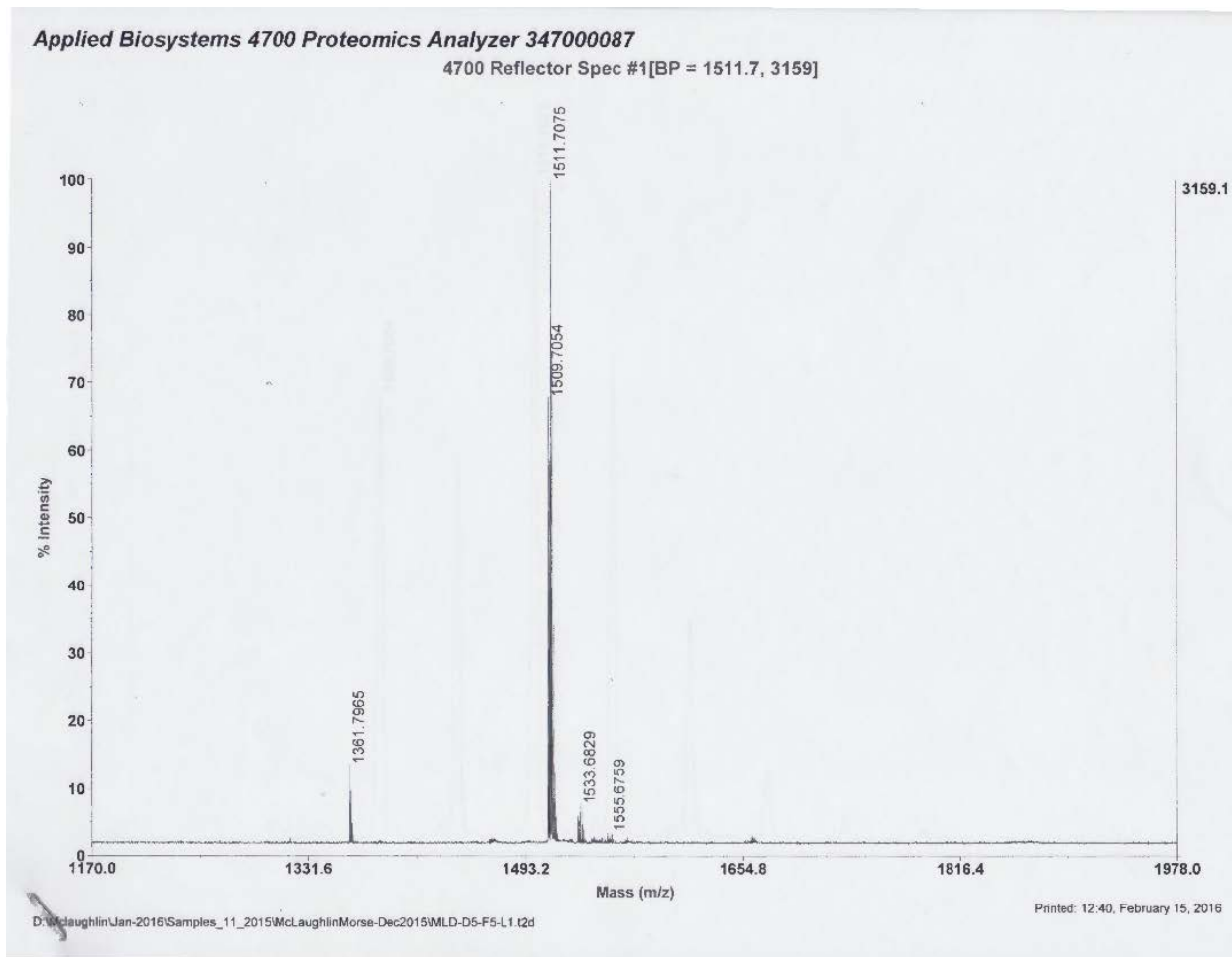


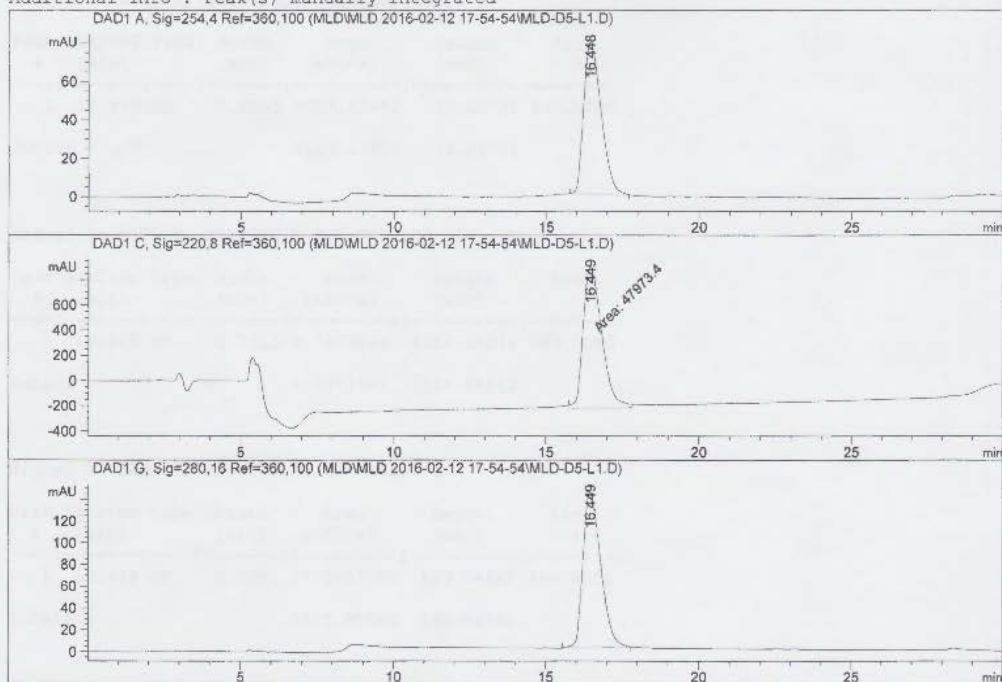
Figure A2.34 MC1RL-DOTA:Eu; Mass Spectrum

Data File C:\CHEM32\1\DATA\MLD\MLD 2016-02-12 17-54-54\MLD-D5-L1.D
Sample Name: MLD-D5-L1

=====

Acq. Operator :	Instrument 1	Seq. Line :	1
Acq. Instrument :	Instrument 1	Location :	Vial 51
Injection Date :	2/12/2016 5:55:12 PM	Inj :	1
		Inj Volume :	10.0 µl
		Actual Inj Volume :	20.0 µl

Different Inj Volume from Sequence !
Acq. Method : C:\CHEM32\1\DATA\MLD\MLD 2016-02-12 17-54-54\MLD-2-15-60_20MIN_1-PH6.M
Last changed : 2/10/2016 7:23:47 PM
Analysis Method : C:\CHEM32\1\METHODS\MLD-2-20-40_20MIN_1.M
Last changed : 1/25/2016 6:12:07 PM
Additional Info : Peak(s) manually integrated



=====

Fraction Information

=====

Fraction collection off

No Fractions found.

=====

Figure A2.35 MC1RL-DOTA:Eu; HPLC Trace

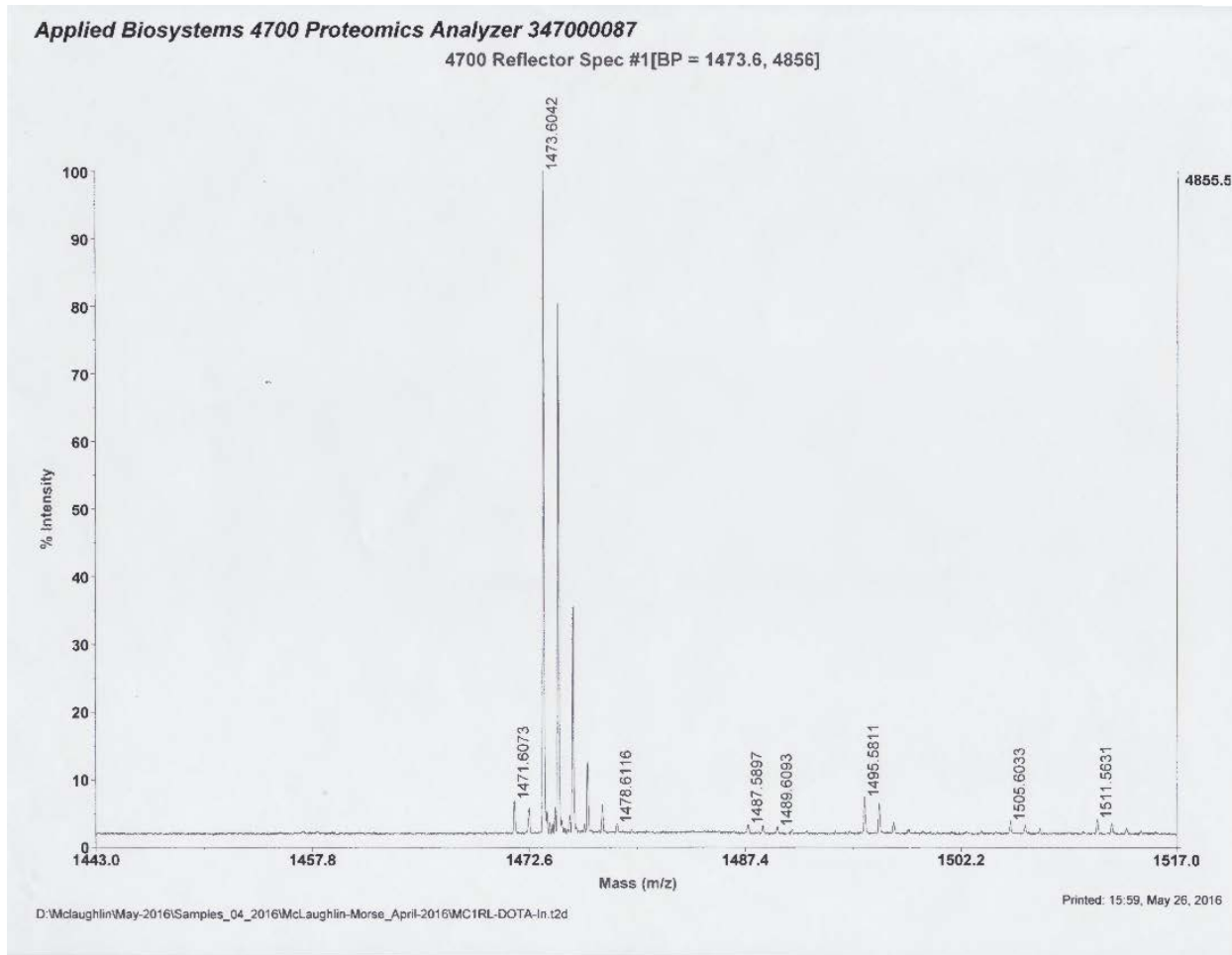
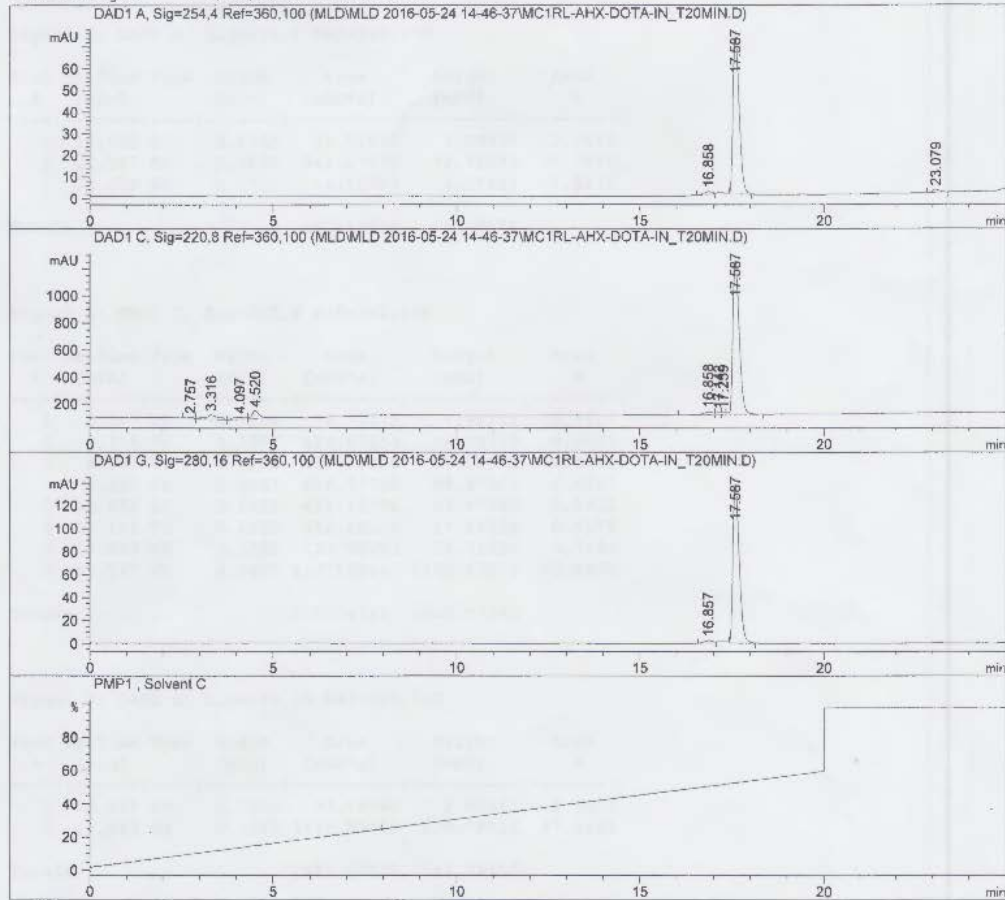


Figure A2.36 MC1RL-DOTA:In; Mass Spectrum

Data File C:\CHEM32\1\DATA\MLD\MLD 2016-05-24 14-46-37\MC1RL-AHX-DOA-IN_T20MIN.D
Sample Name: MC1RL-Ahx-DOA-In_T20min

=====

Acq. Operator :	Seq. Line : 4
Acq. Instrument : Instrument 1	Location : Vial 62
Injection Date : 5/24/2016 4:25:55 PM	Inj : 1
	Inj Volume : 10.0 µl
Different Inj Volume from Sequence !	Actual Inj Volume : 5.0 µl
Acq. Method : C:\CHEM32\1\DATA\MLD\MLD 2016-05-24 14-46-37\MLD-2-60_20MIN_1.M	
Last changed : 5/24/2016 2:38:53 PM	
Analysis Method : C:\CHEM32\1\METHODS\MLD-2-100_10MIN_1.M	
Last changed : 4/19/2016 10:19:54 AM	



=====

Fraction Information

=====

Fraction collection off
No Fractions found.

Instrument 1 5/24/2016 5:16:16 PM

Page 1 of 2

Figure A2.37 MC1RL-DOA:In; HPLC Trace

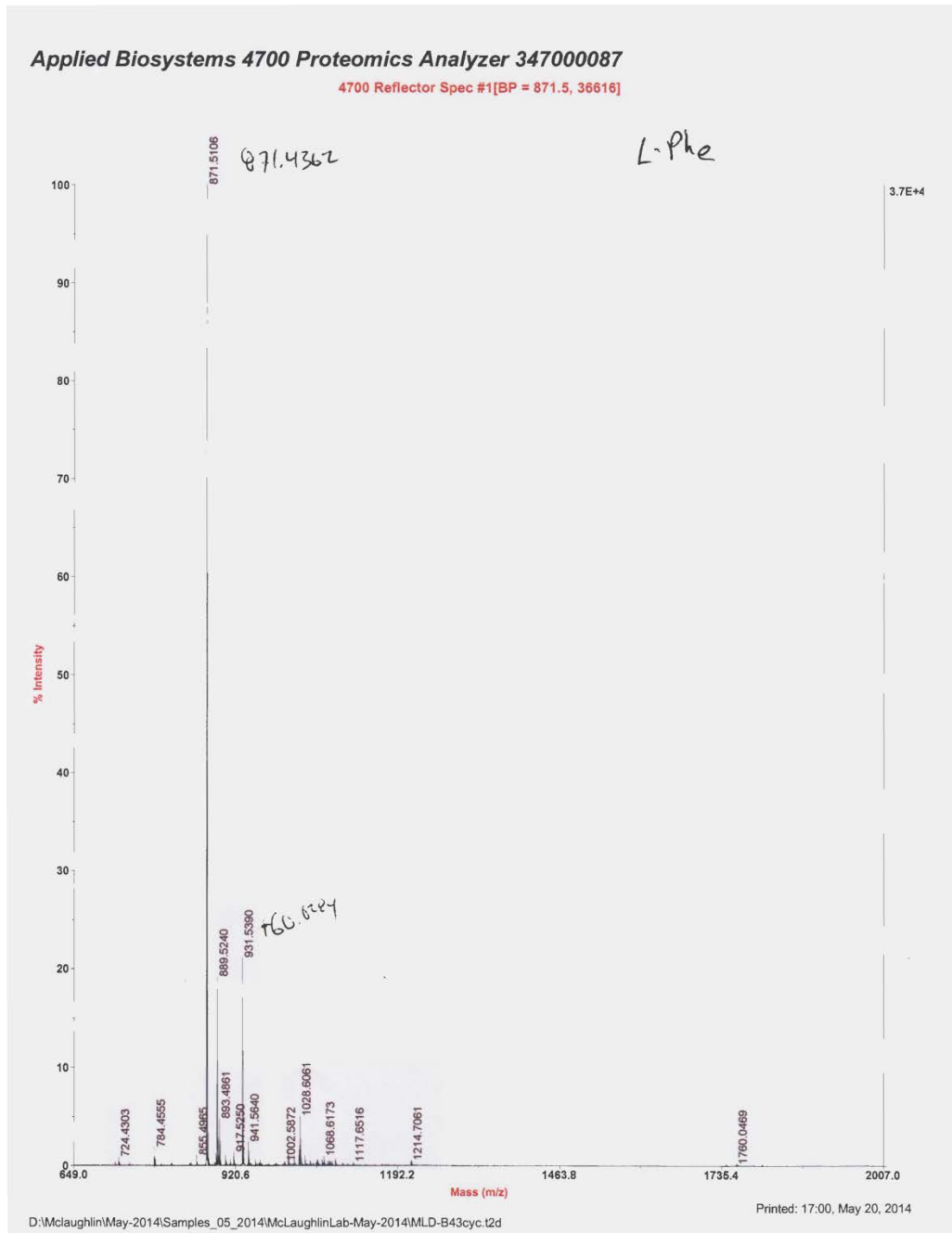
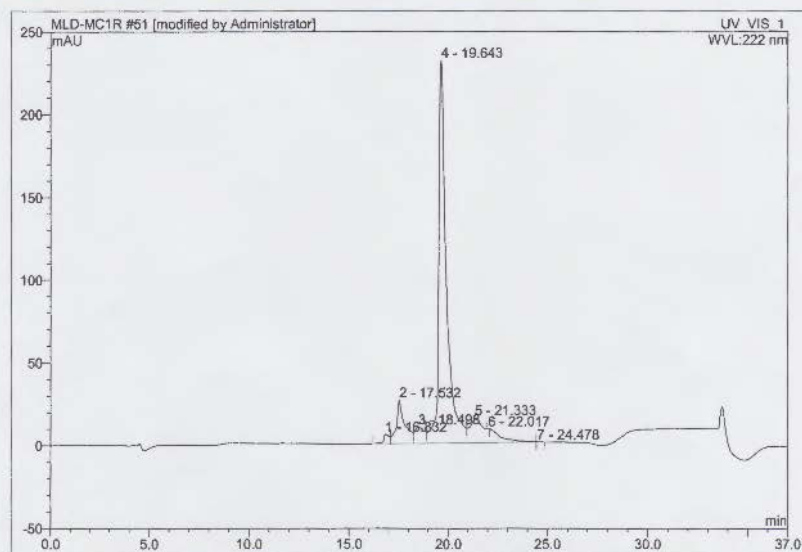


Figure A2.38 cMC1RL-B43-cyclic; Mass Spectrum

51 MLD-B43cyc-cMC1RL-L-Phe

Sample Name:	MLD-B43cyc-cMC1RL-L-Phe	Injection Volume:	75.0
Vial Number:	RA9	Channel:	UV_VIS_1
Sample Type:	unknown	Wavelength:	222
Control Program:	Exploratory gradient_MLD-2-60_20min	Bandwidth:	1
Quantif. Method:	default	Dilution Factor:	1.0000
Recording Time:	5/20/2014 17:42	Sample Weight:	1.0000
Run Time (min):	37.00	Sample Amount:	1.0000



No.	Ret.Time min	Peak Name	Height mAU	Area mAU*min	Rel.Area %	Amount n.a.	Type
1	16.83	n.a.	5.702	2.027	1.41	n.a.	BM
2	17.53	n.a.	26.343	12.935	8.97	n.a.	M
3	18.50	n.a.	10.012	5.677	3.93	n.a.	M
4	19.64	n.a.	231.092	105.514	73.13	n.a.	M
5	21.33	n.a.	15.199	18.067	12.52	n.a.	M
6	22.02	n.a.	0.184	0.017	0.01	n.a.	Rd
7	24.48	n.a.	0.160	0.043	0.03	n.a.	MB
Total:			288.691	144.280	100.00	0.000	

default/Integration

Chromleon (c) Dionex 1996-2001
Version 6.50 SP3a Build 986

Figure A2.39 cMC1RL-B43-cyclic; HPLC Trace

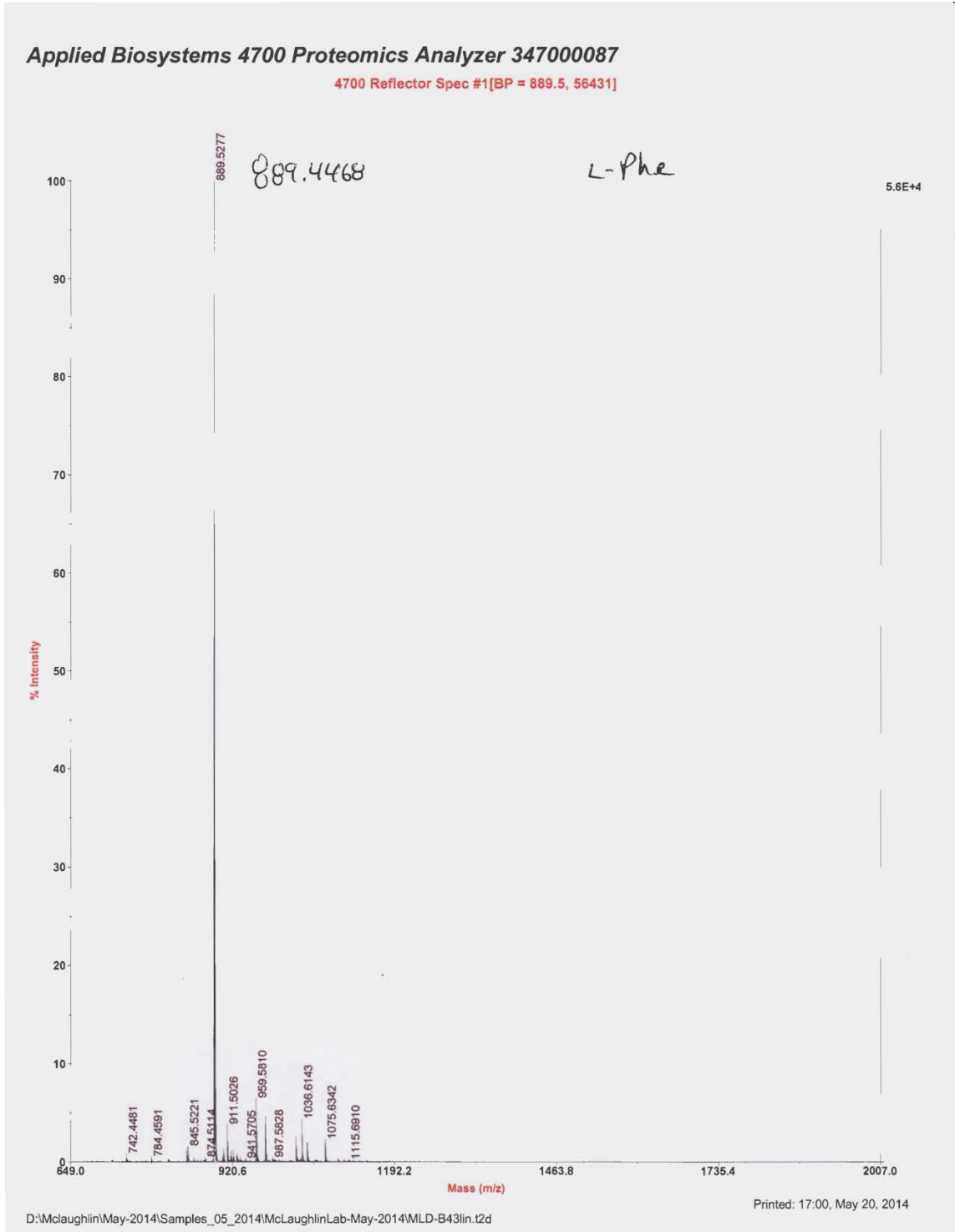
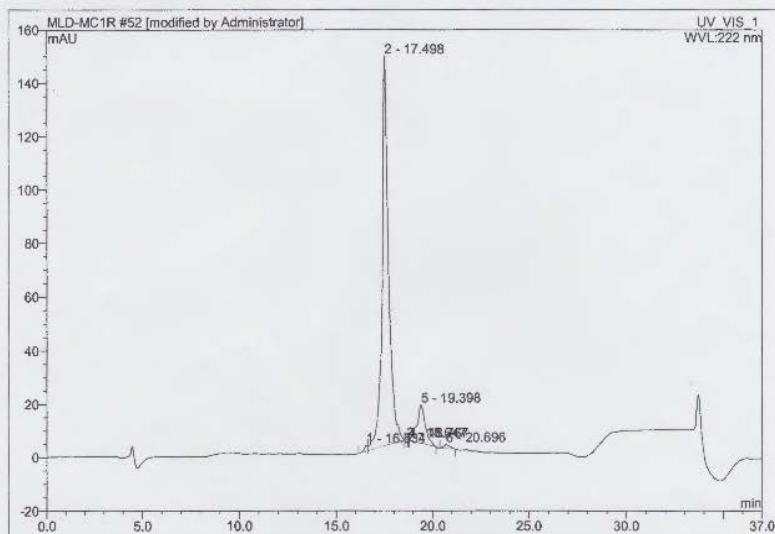


Figure A2.40 cMC1RL-B43-linear; Mass Spectrum

52 MLD-B43lin-MC1RL-L-Phe

Sample Name:	MLD-B43lin-MC1RL-L-Phe	Injection Volume:	75.0
Vial Number:	RA10	Channel:	UV_VIS_1
Sample Type:	unknown	Wavelength:	222
Control Program:	Exploratory gradient_MLD-2-60_20min	Bandwidth:	1
Quantif. Method:	default	Dilution Factor:	1.0000
Recording Time:	5/20/2014 18:21	Sample Weight:	1.0000
Run Time (min):	37.00	Sample Amount:	1.0000



No.	Ret. Time min	Peak Name	Height mAU	Area mAU*min	Rel. Area %	Amount n.a.	Type
1	16.53	n.a.	2.119	0.449	0.69	n.a.	BM
2	17.50	n.a.	145.910	56.902	87.14	n.a.	Mb
3	18.65	n.a.	0.184	0.018	0.03	n.a.	bMb
4	18.77	n.a.	0.080	0.003	0.00	n.a.	bM
5	19.40	n.a.	14.468	7.372	11.29	n.a.	MB
6	20.70	n.a.	1.425	0.558	0.85	n.a.	BMB
Total:			164.185	65.301	100.00	0.000	

default/integration

Chromeleon (c) Dionex 1996-2001
Version 6.50 SP3a Build 986

Figure A2.41 cMC1RL-B43-linear; HPLC Trace

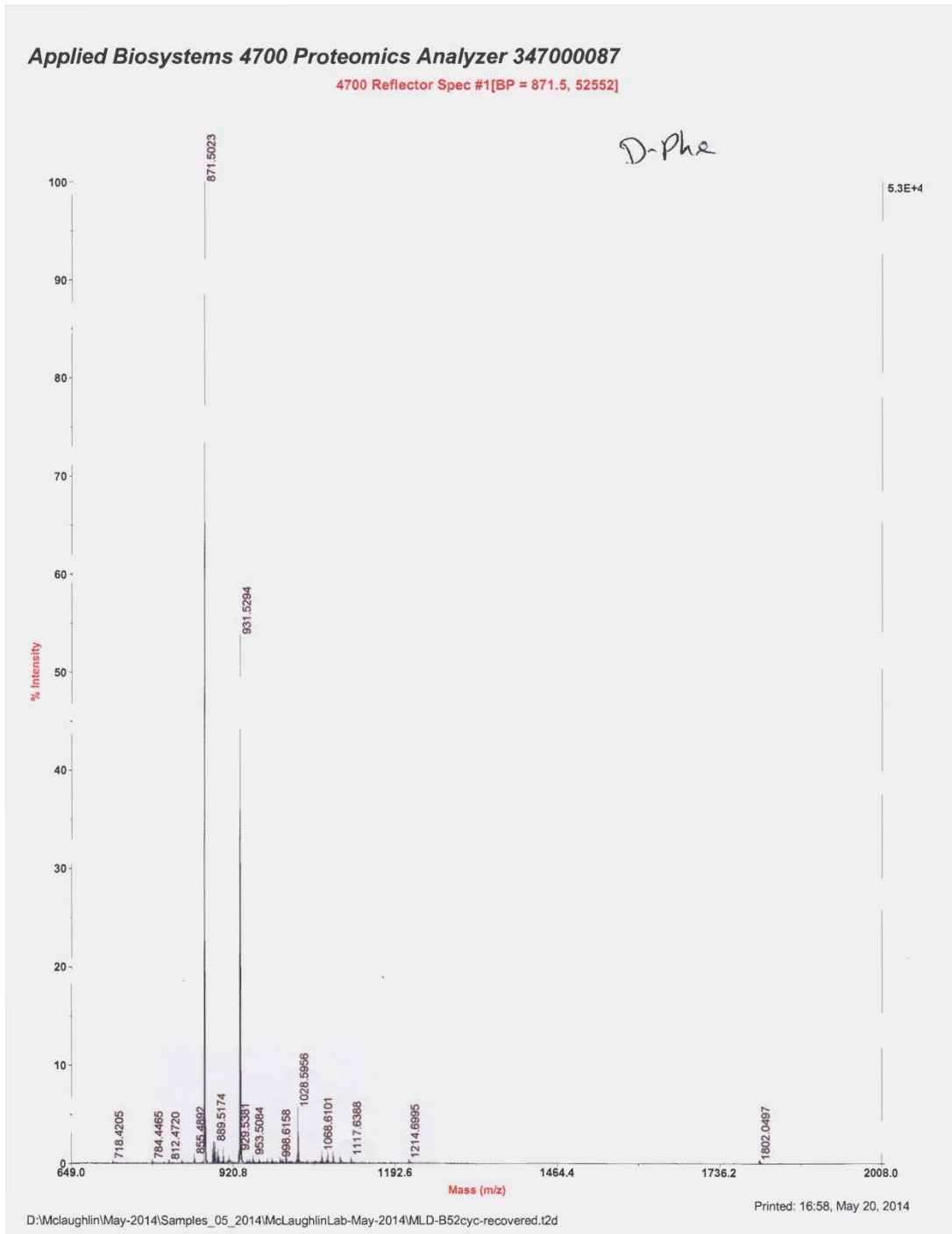
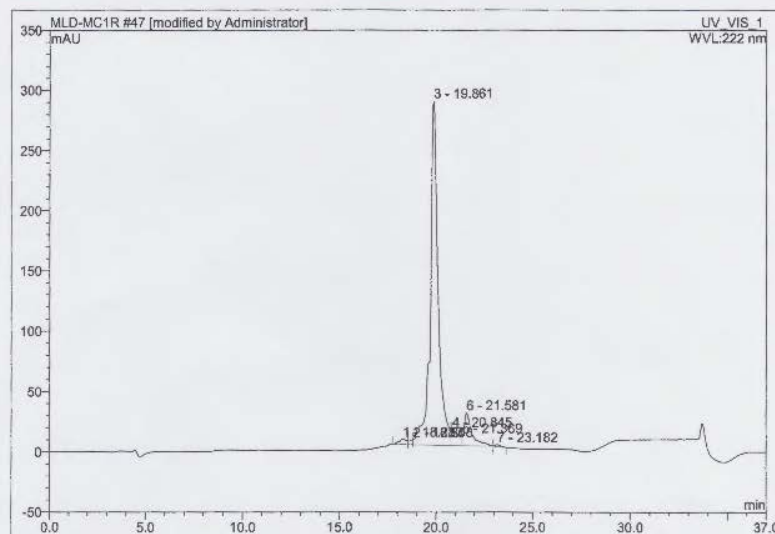


Figure A2.42 cMC1RL-B52-cyclic; Mass Spectrum

47 MLD-B52cyc-cMC1RL-D-Phe

Sample Name:	MLD-B52cyc-cMC1RL-D-Phe	Injection Volume:	75.0
Vial Number:	RA6	Channel:	UV_VIS_1
Sample Type:	unknown	Wavelength:	222
Control Program:	Exploratory gradient_MLD-2-60_20min	Bandwidth:	1
Quantif. Method:	default	Dilution Factor:	1.0000
Recording Time:	5/20/2014 15:04	Sample Weight:	1.0000
Run Time (min):	37.00	Sample Amount:	1.0000



No.	Ret.Time min	Peak Name	Height mAU	Area mAU*min	Rel.Area %	Amount n.a.	Type
1	18.28	n.a.	4.240	2.074	1.31	n.a.	BM
2	18.81	n.a.	4.119	0.876	0.56	n.a.	M
3	19.86	n.a.	285.735	135.298	85.69	n.a.	M
4	20.84	n.a.	13.384	6.207	3.93	n.a.	M
5	21.37	n.a.	0.009	0.000	0.00	n.a.	Rd
6	21.58	n.a.	27.652	12.904	8.17	n.a.	Mb
7	23.18	n.a.	1.795	0.533	0.34	n.a.	bMB
Total:			336.934	157.891	100.00	0.000	

default/Integration

Chromleon (c) Dionex 1996-2001
Version 6.50 SP3a Build 986

Figure A2.43 cMC1RL-B52-cyclic; HPLC Trace

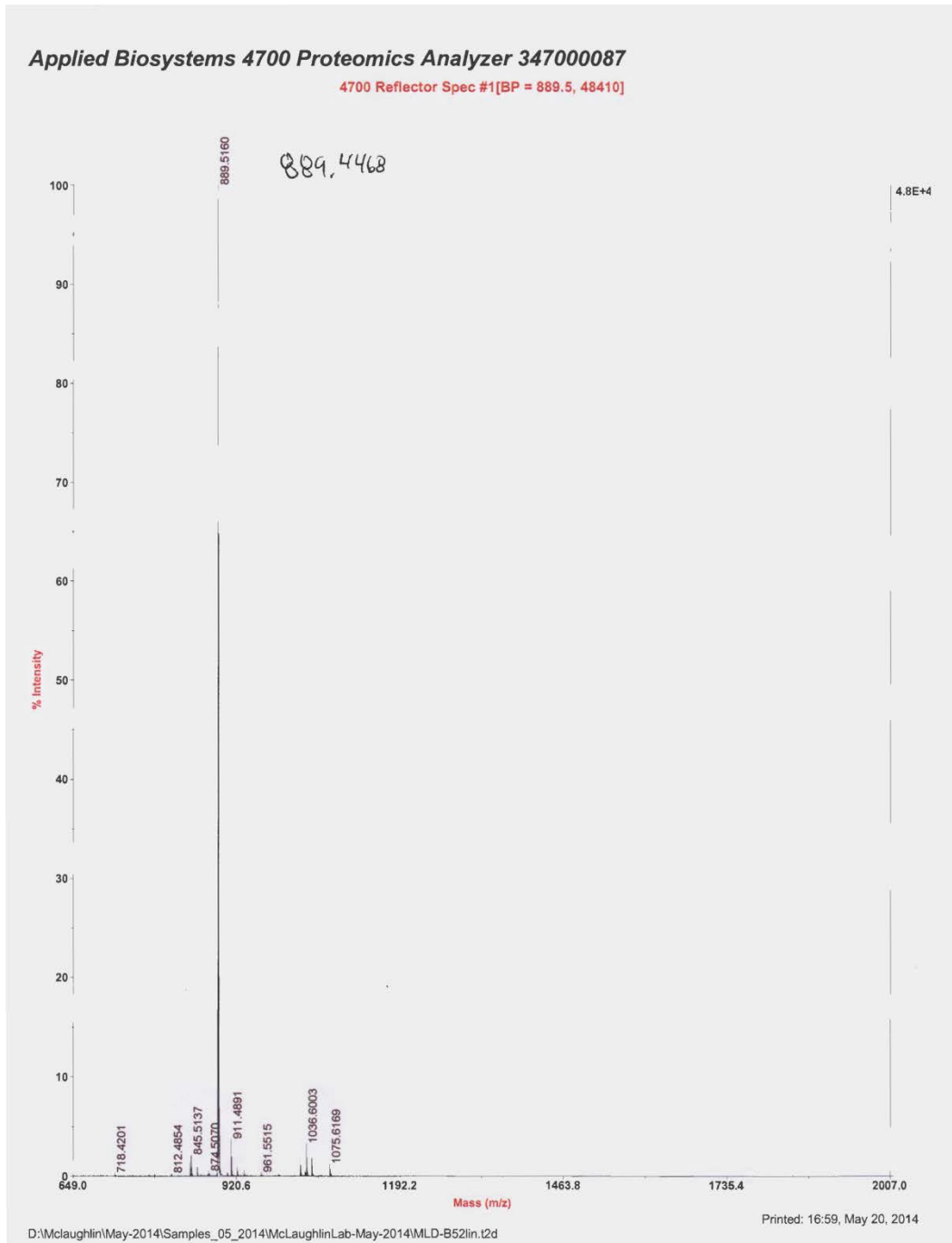
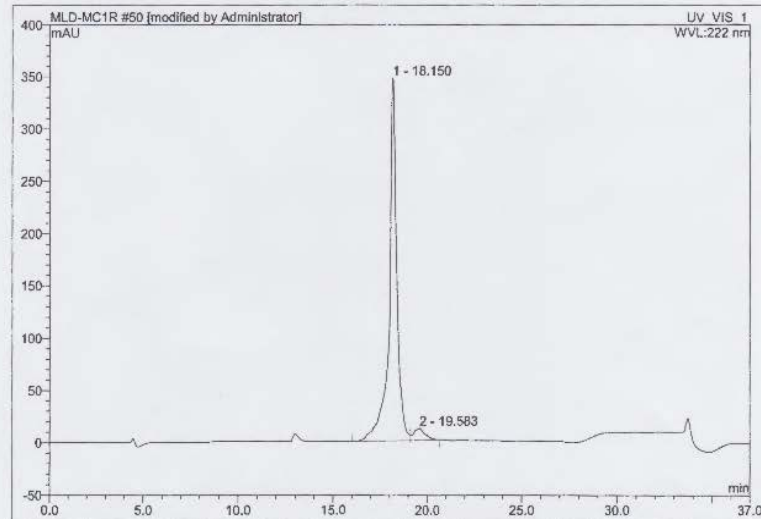


Figure A2.44 cMC1RL-B52-linear; Mass Spectrum

50 MLD-B52lin-MC1RL-D-Phe

Sample Name:	MLD-B52lin-MC1RL-D-Phe	Injection Volume:	75.0
Vial Number:	RA8	Channel:	UV_VIS_1
Sample Type:	unknown	Wavelength:	222
Control Program:	Exploratory gradient_MLD-2-60_20min	Bandwidth:	1
Quantif. Method:	default	Dilution Factor:	1.0000
Recording Time:	5/20/2014 17:02	Sample Weight:	1.0000
Run Time (min):	37.00	Sample Amount:	1.0000



No.	Ret.Time min	Peak Name	Height mAU	Area mAU*min	Rel.Area %	Amount n.a.	Type
1	18.15	n.a.	347.144	164.686	95.47	n.a.	BM
2	19.58	n.a.	11.366	7.816	4.53	n.a.	MB
Total:			358.511	172.502	100.00	0.000	

default/Integration

Chromeleon (c) Dionex 1996-2001
Version 6.50 SP3a Build 986

Figure A2.45 cMC1RL-B52-linear; HPLC Trace

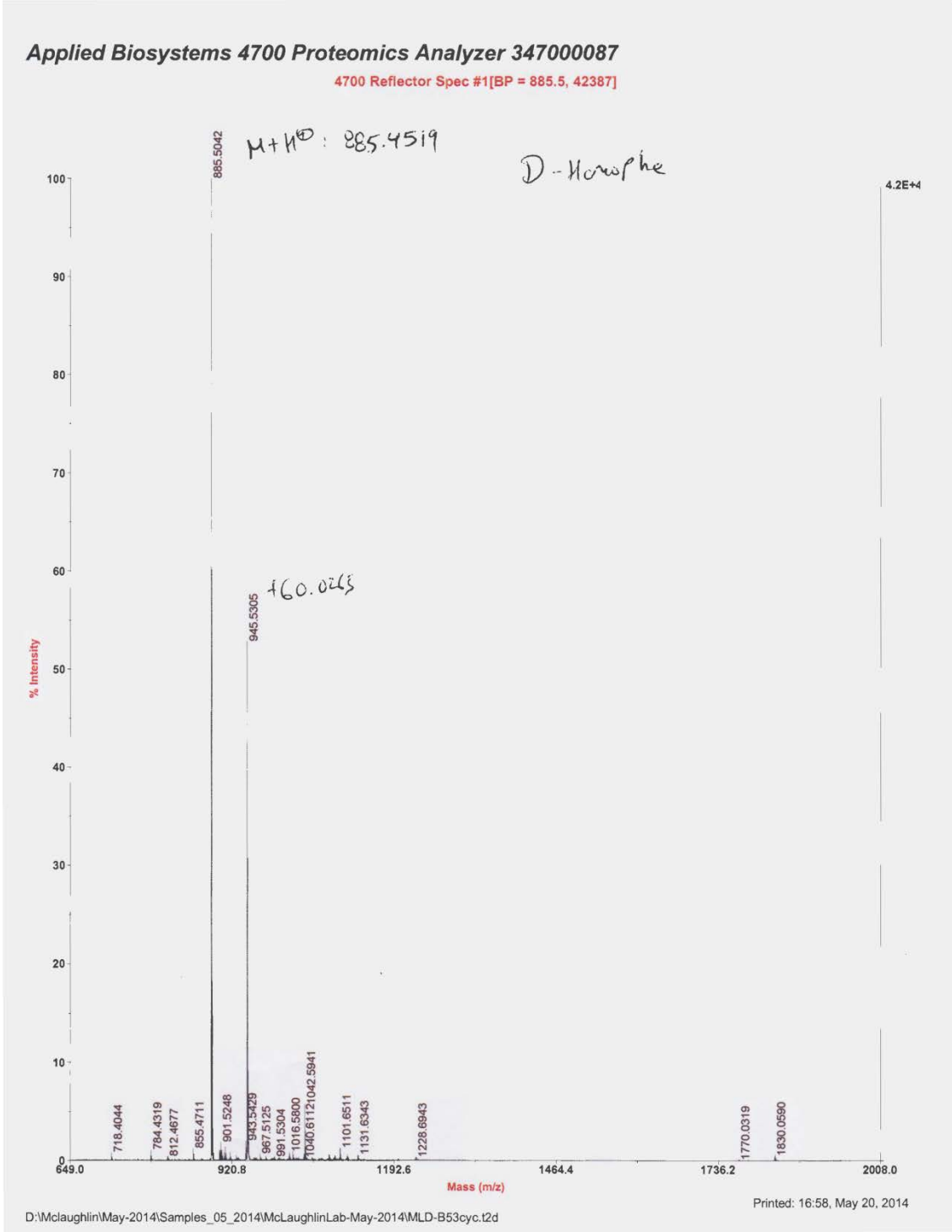
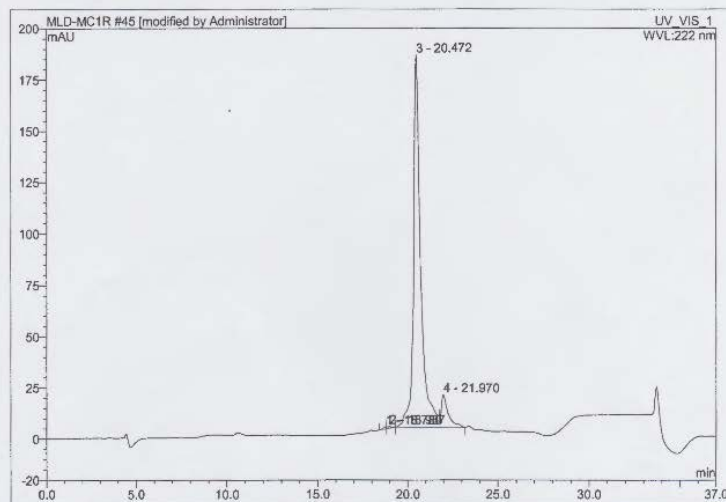


Figure A2.46 cMC1RL-B53-cyclic; Mass Spectrum

45 MLD-B53cyc-cMC1RL-D-HoPhe

Sample Name:	MLD-B53cyc-cMC1RL-D-HoPhe	Injection Volume:	75.0
Vial Number:	RA4	Channel:	UV_VIS_1
Sample Type:	unknown	Wavelength:	222
Control Program:	Exploratory gradient_MLD-2-60_20min	Bandwidth:	1
Quantif. Method:	default	Dilution Factor:	1.0000
Recording Time:	5/20/2014 13:45	Sample Weight:	1.0000
Run Time (min):	37.00	Sample Amount:	1.0000



No.	Ret.Time min	Peak Name	Height mAU	Area mAU*min	Rel.Area %	Amount n.a.	Type
1	18.78	n.a.	1.001	0.228	0.25	n.a.	BM
2	18.99	n.a.	0.882	0.258	0.28	n.a.	Mb*
3	20.47	n.a.	181.448	84.374	91.44	n.a.	bM
4	21.97	n.a.	15.962	7.412	8.03	n.a.	MB
Total:			199.293	92.272	100.00	0.000	

default/integration

Chromeleon (c) Dionex 1996-2001
Version 6.50 SP3a Build 986

Figure A2.47 cMC1RL-B53-cyclic; HPLC Trace

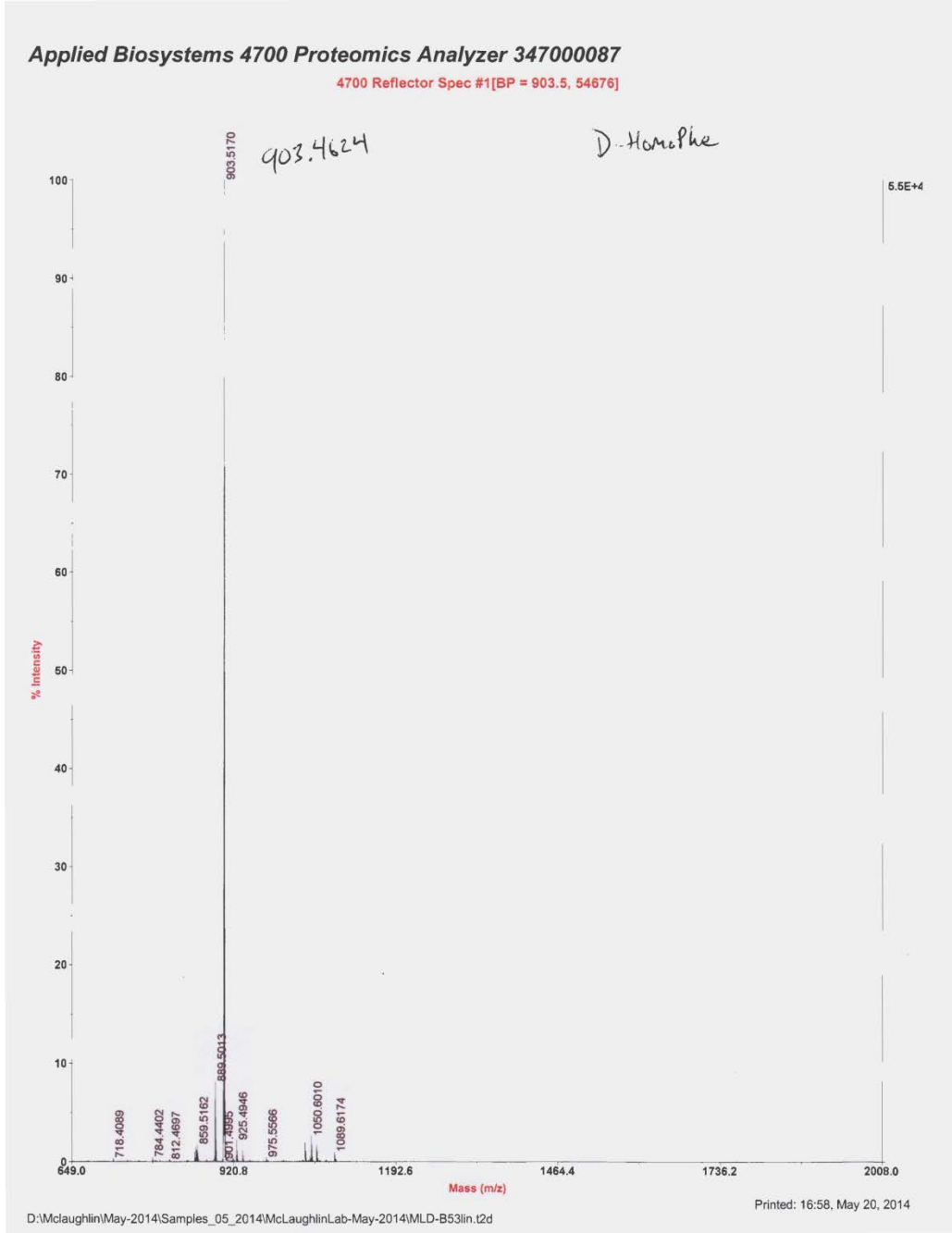
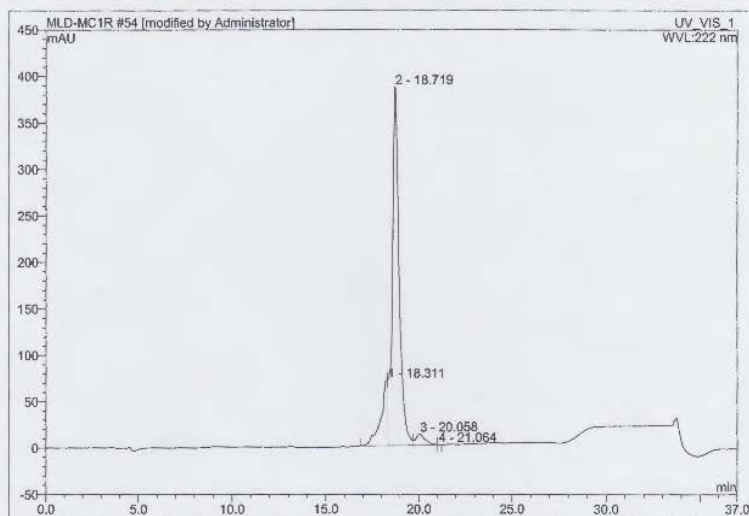


Figure A2.48 cMC1RL-B53-linear; Mass Spectrum

54 MLD-B53lin-MC1RL-D-HoPhe

Sample Name:	MLD-B53lin-MC1RL-D-HoPhe	Injection Volume:	75.0
Vial Number:	RA5	Channel:	UV_VIS_1
Sample Type:	unknown	Wavelength:	222
Control Program:	Exploratory gradient_MLD-2-60_20min	Bandwidth:	1
Quantif. Method:	default	Dilution Factor:	1.0000
Recording Time:	5/20/2014 20:22	Sample Weight:	1.0000
Run Time (min):	37.00	Sample Amount:	1.0000



No.	Ret.Time min	Peak Name	Height mAU	Area mAU*min	Rel.Area %	Amount n.a.	Type
1	18.31	n.a.	70.858	28.263	13.95	n.a.	BM *
2	18.72	n.a.	385.984	167.165	82.53	n.a.	M *
3	20.06	n.a.	11.999	7.089	3.50	n.a.	M *
4	21.06	n.a.	0.306	0.042	0.02	n.a.	MB*
Total:			469.148	202.559	100.00	0.000	

default/Integration

Chromleon (c) Dionex 1996-2001
Version 6.50 SP3a Build 986

Figure A2.49 cMC1RL-B53-linear; HPLC Trace

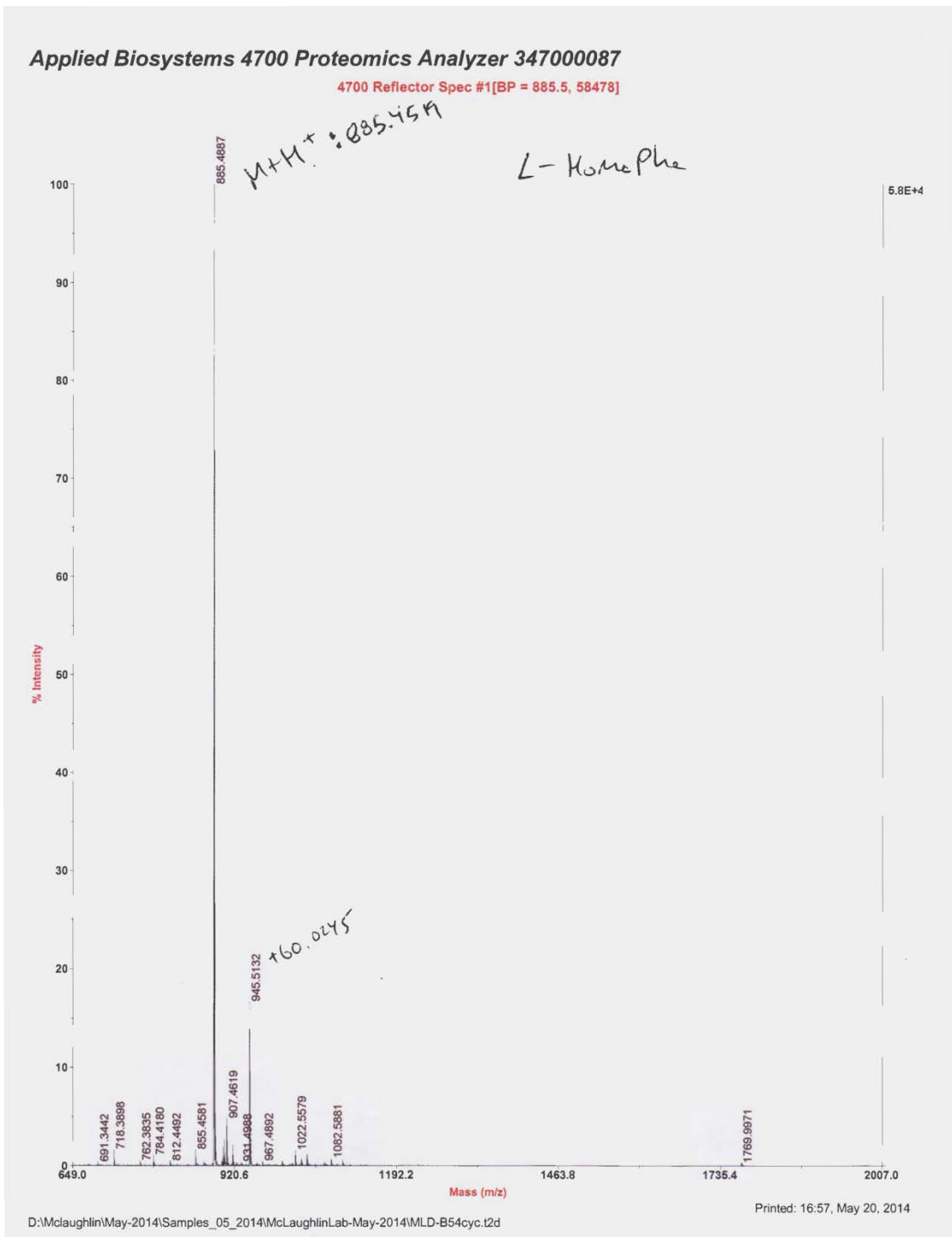
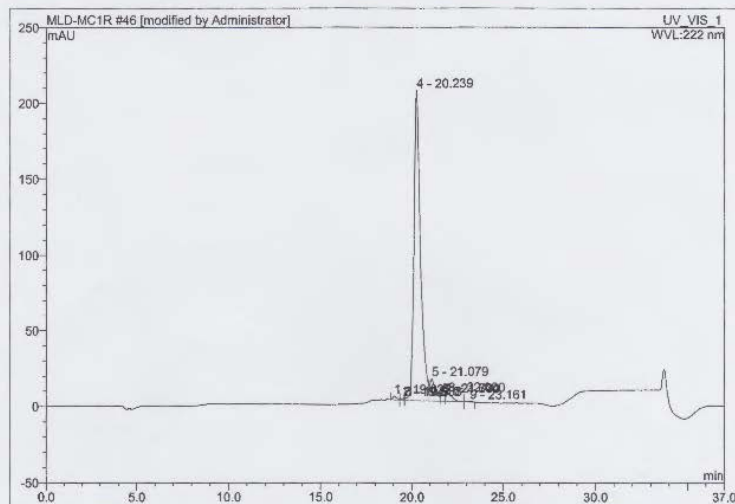


Figure A2.50 cMC1RL-B53-cyclic; Mass Spectrum

46 MLD-B54cyc-cMC1RL-L-HoPhe

Sample Name:	MLD-B54cyc-cMC1RL-L-HoPhe	Injection Volume:	75.0
Vial Number:	RA2	Channel:	UV_VIS_1
Sample Type:	unknown	Wavelength:	222
Control Program:	Exploratory gradient_MLD-2-60_20min	Bandwidth:	1
Quantif. Method:	default	Dilution Factor:	1.0000
Recording Time:	5/20/2014 14:24	Sample Weight:	1.0000
Run Time (min):	37.00	Sample Amount:	1.0000



No.	Ret.Time min	Peak Name	Height mAU	Area mAU*min	Rel.Area %	Amount n.a.	Type
1	19.02	n.a.	2.355	0.611	0.66	n.a.	BM *
2	19.51	n.a.	1.140	0.217	0.23	n.a.	M *
3	19.64	n.a.	1.143	0.071	0.08	n.a.	M *
4	20.24	n.a.	204.525	84.107	90.28	n.a.	M *
5	21.08	n.a.	14.643	5.139	5.52	n.a.	M *
6	21.67	n.a.	3.792	0.937	1.01	n.a.	M *
7	21.70	n.a.	0.088	0.014	0.02	n.a.	Rd
8	22.00	n.a.	4.689	1.916	2.06	n.a.	Mb*
9	23.16	n.a.	0.498	0.155	0.17	n.a.	bMB
Total:			232.873	93.167	100.00	0.000	

default/integration

Chromleon (c) Dionex 1996-2001
Version 6.50 SP3a Build 986

Figure A2.51 cMC1RL-B53-cyclic; HPLC Trace

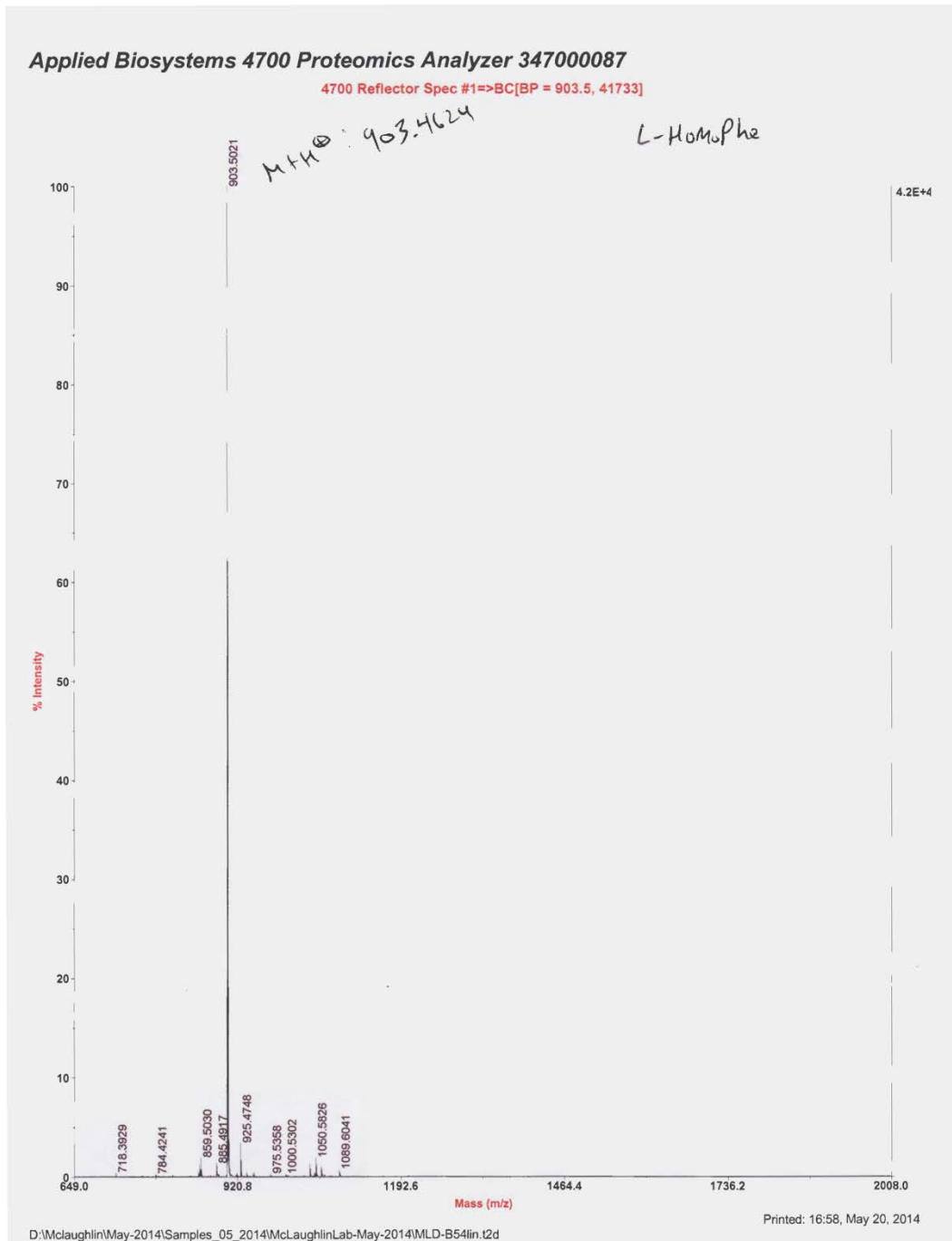
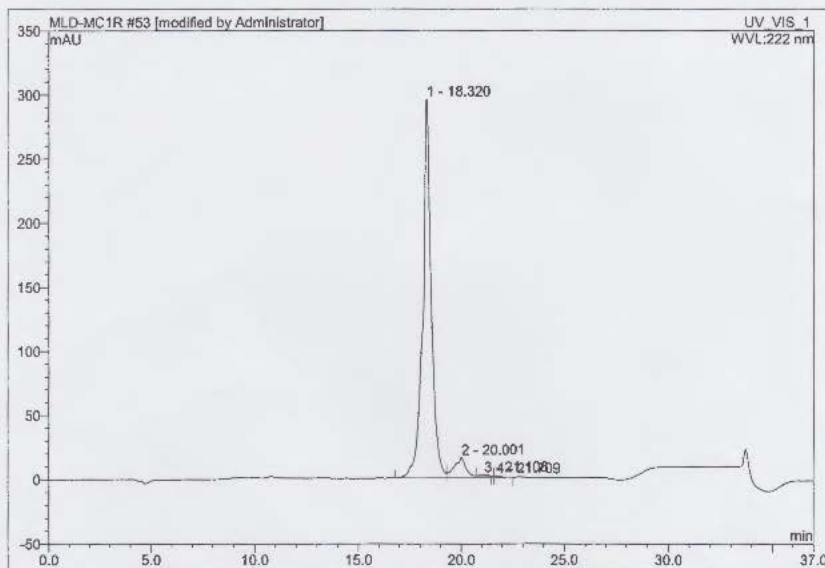


Figure A2.52 cMC1RL-B54-linear; Mass Spectrum

53 MLD-B54lin-MC1RL-L-HoPhe

Sample Name:	MLD-B54lin-MC1RL-L-HoPhe	Injection Volume:	75.0
Vial Number:	RA3	Channel:	UV_VIS_1
Sample Type:	unknown	Wavelength:	222
Control Program:	Exploratory gradient_MLD-2-60_20min	Bandwidth:	1
Quantif. Method:	default	Dilution Factor:	1.0000
Recording Time:	5/20/2014 19:43	Sample Weight:	1.0000
Run Time (min):	37.00	Sample Amount:	1.0000



No.	Ret. Time min	Peak Name	Height mAU	Area mAU*min	Rel. Area %	Amount n.a.	Type
1	18.32	n.a.	295.243	142.254	92.19	n.a.	BM *
2	20.00	n.a.	15.419	11.180	7.25	n.a.	M *
3	21.11	n.a.	0.958	0.417	0.27	n.a.	Rd
4	21.71	n.a.	1.006	0.451	0.29	n.a.	MB*
Total:			312.626	154.302	100.00	0.000	

default/integration

Chromleon (c) Dionex 1996-2001
Version 6.50 SP3a Build 986

Figure A2.53 cMC1RL-B54-linear; HPLC Trace

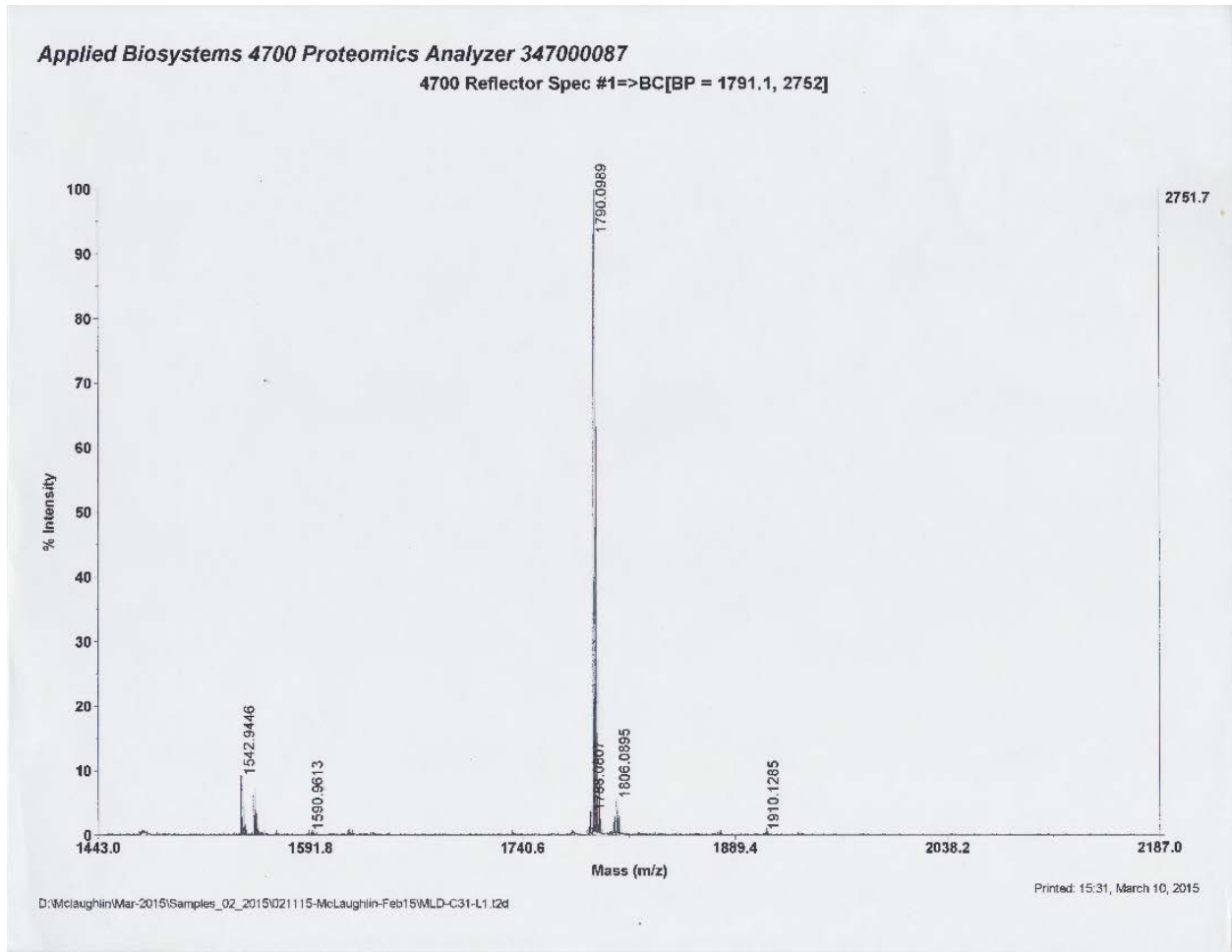


Figure A3.1.TLR2L-780; Mass Spectrum

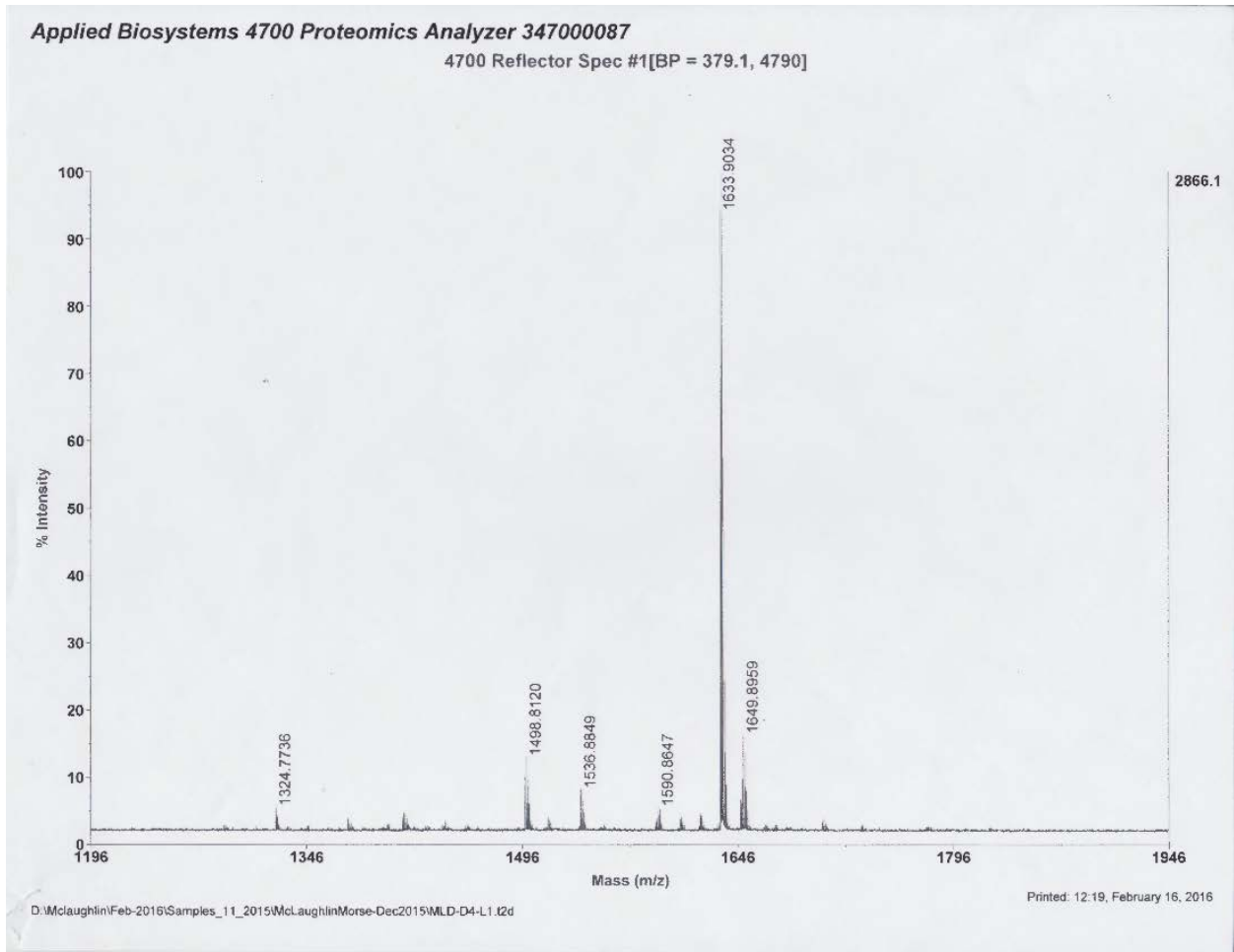
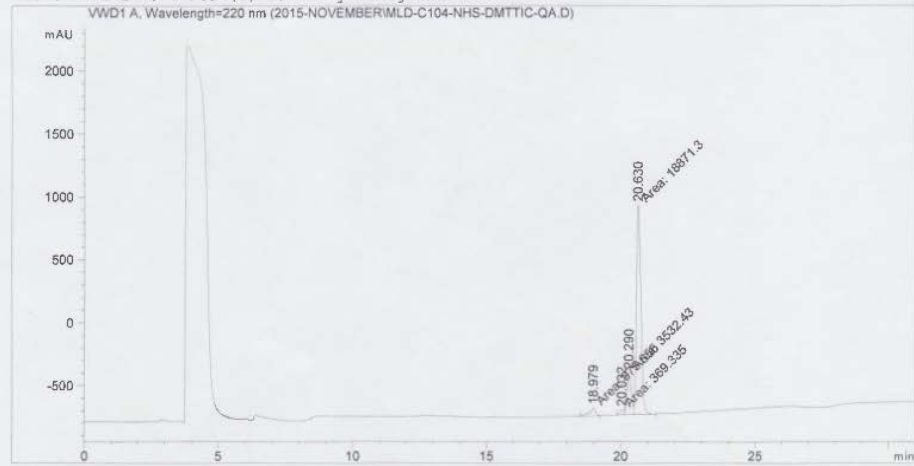


Figure A4.1 Peptide 4.2; Mass Spectrum

Data File C:\CHEM32\1\DATA\2015-NOVEMBER\MLD-C104-NHS-DMTTIC-QA.D
 Sample Name: MLD-C104-NHS-DmtTic-QA

```

=====
Acq. Operator   : SYSTEM
Acq. Instrument : 1260 HPLC
Injection Date  : 12/9/2015 11:14:55 AM
Location       : -
Inj Volume     : No inj
Acq. Method    : C:\CHEM32\1\METHODS\MLD-2-2-100_20MIN_1ML.M
Last changed   : 12/8/2015 3:33:22 PM by SYSTEM
Analysis Method : C:\CHEM32\1\METHODS\DEF_LC.M
Last changed   : 12/3/2015 11:55:05 AM by SYSTEM
Additional Info : Peak(s) manually integrated
  
```



=====
 Area Percent Report
 =====

```

Sorted By      : Signal
Multiplier:    : 1.0000
Dilution:      : 1.0000
Use Multiplier & Dilution Factor with ISTDs
  
```

Signal 1: VWD1 A, Wavelength=220 nm

Peak #	RetTime [min]	Type	Width [min]	Area [mAU*s]	Height [mAU]	Area %
1	18.979	MM	0.2553	975.85468	63.70021	4.1091
2	20.032	MF	0.1515	369.33514	40.64137	1.5552
3	20.290	FM	0.1748	3532.42822	336.77798	14.8741
4	20.630	FM	0.1885	1.88713e4	1668.81067	79.4617

Totals : 2.37489e4 2109.93024

Figure A4.2 Peptide 4.2; HPLC Trace

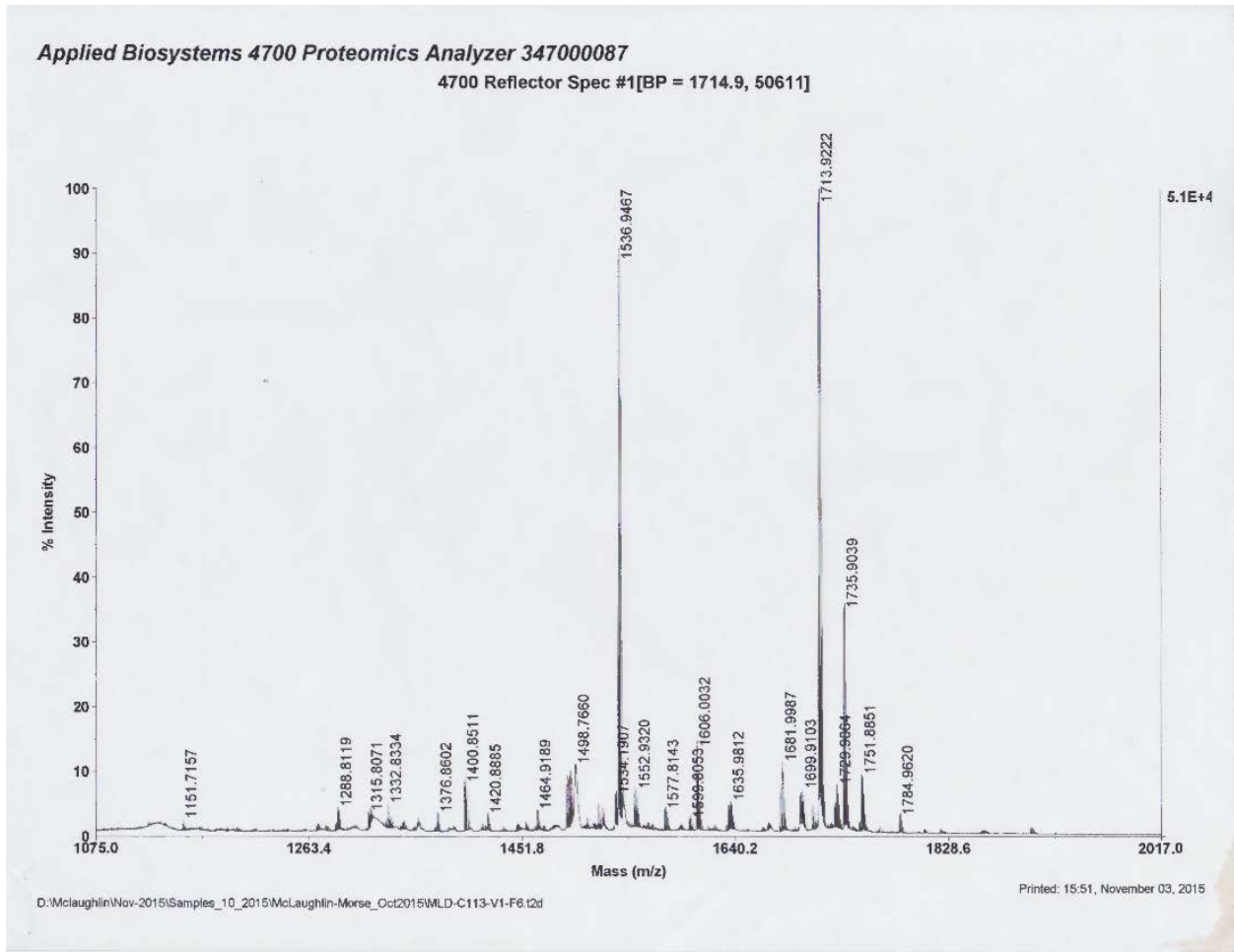


Figure A4.3 Peptide 4.3; Mass Spectrum

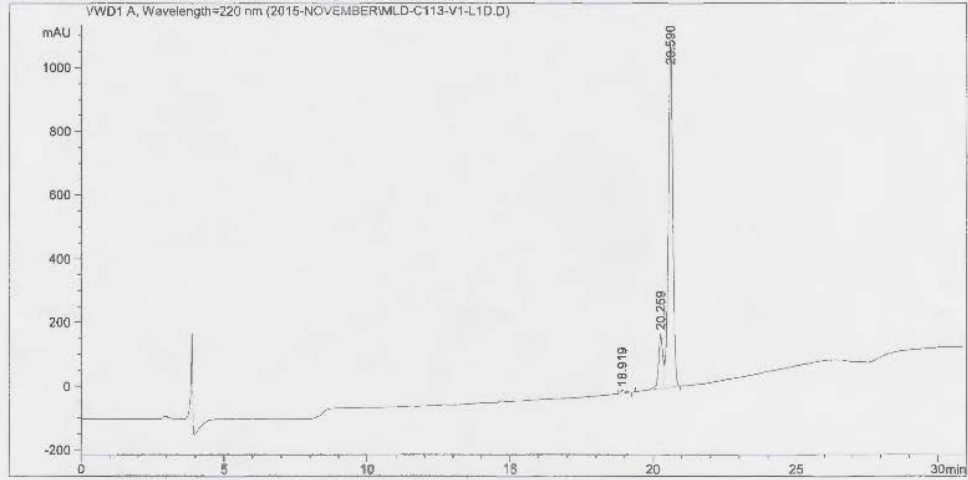
Data File C:\CHEM32\1\DATA\2015-NOVEMBER\MLD-C113-V1-L1.D
 Sample Name: MLD-C113-V1-L1.D

```

=====
Acq. Operator   : SYSTEM
Acq. Instrument : 1260 HPLC
Injection Date  : 11/3/2015 4:53:00 PM
Location       :
Inj Volume     : No inj

Acq. Method    : C:\CHEM32\1\METHODS\MLD-2-2-100_20MIN_LML.M
Last changed   : 11/3/2015 4:06:25 PM by SYSTEM
                (modified after loading)
Analysis Method: C:\CHEM32\1\METHODS\DEF_LC.M
Last changed   : 11/2/2015 10:20:22 AM by SYSTEM
Sample Info    : MLD-C113-V1-L1
  
```

Additional Info : Peak(s) manually integrated



Area Percent Report

```

=====
Sorted By      :      Signal
Multiplier:    :      1.0000
Dilution:      :      1.0000
Sample Amount: :      10.00000 (ng/ul) (not used in calc.)
Use Multiplier & Dilution Factor with ISTDs
  
```

Signal 1: VWD1 A, Wavelength=220 nm

Peak #	RetTime [min]	Type	Width [min]	Area [mAU*s]	Height [mAU]	Area %
1	18.919	BH	0.1720	117.73248	9.28161	0.8724
2	20.259	BV	0.1550	1822.03113	172.78735	13.5012
3	20.590	VB	0.1582	1.15555e4	1076.70251	85.6264

Totals : 1.34953e4 1258.77148

1260 HPLC 11/3/2015 6:14:44 PM SYSTEM

Page 1 of 2

Figure A4.4 Peptide 4.3; HPLC Trace

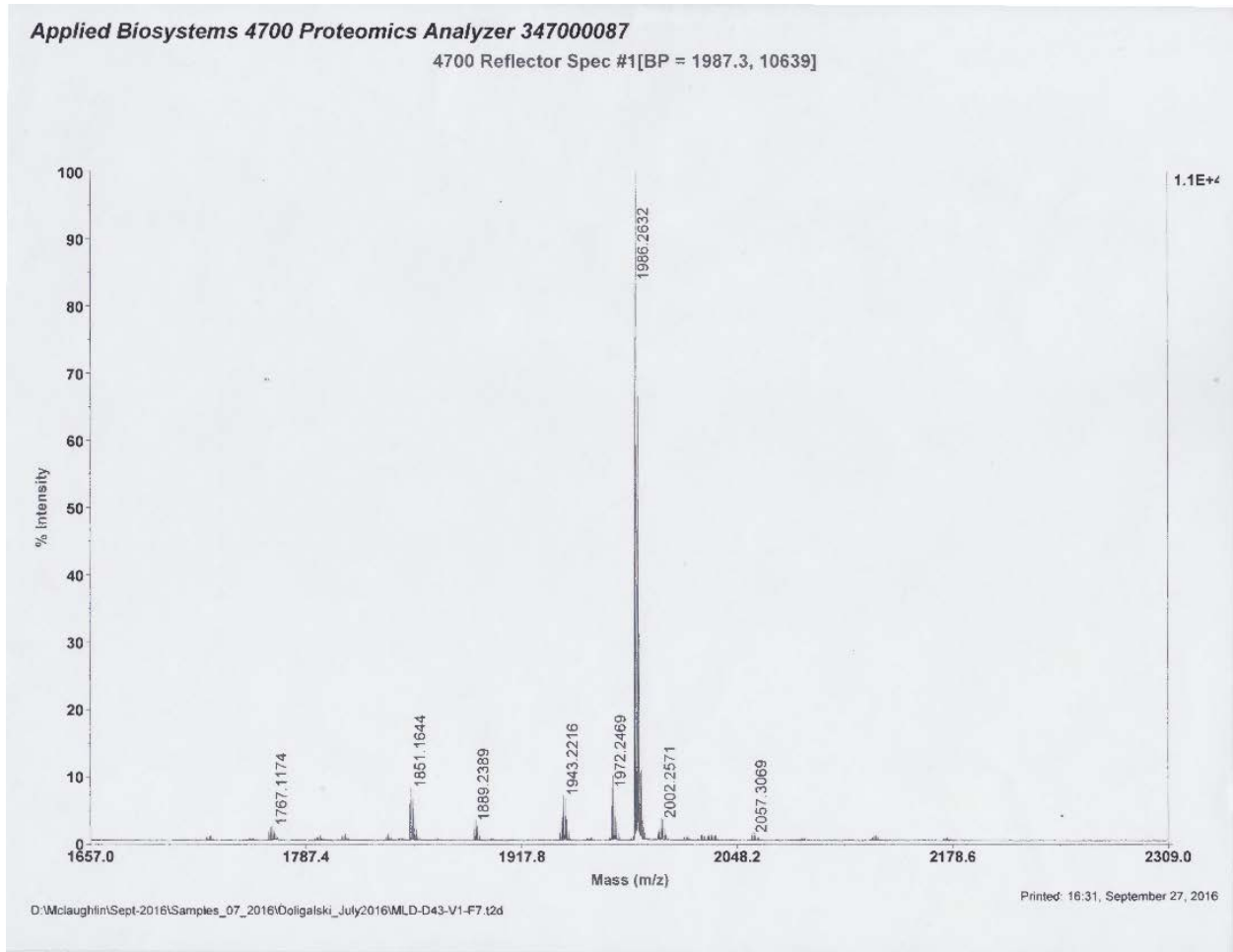


Figure A4.5 Peptide 4.4; Mass Spectrum

Data File C:\CHEM32\1\DATA\MLD\MLD 2016-09-27 15-41-17\MLD-D43-NHS-V1-F7B.D
Sample Name: MLD-D43-NHS-V1-F7

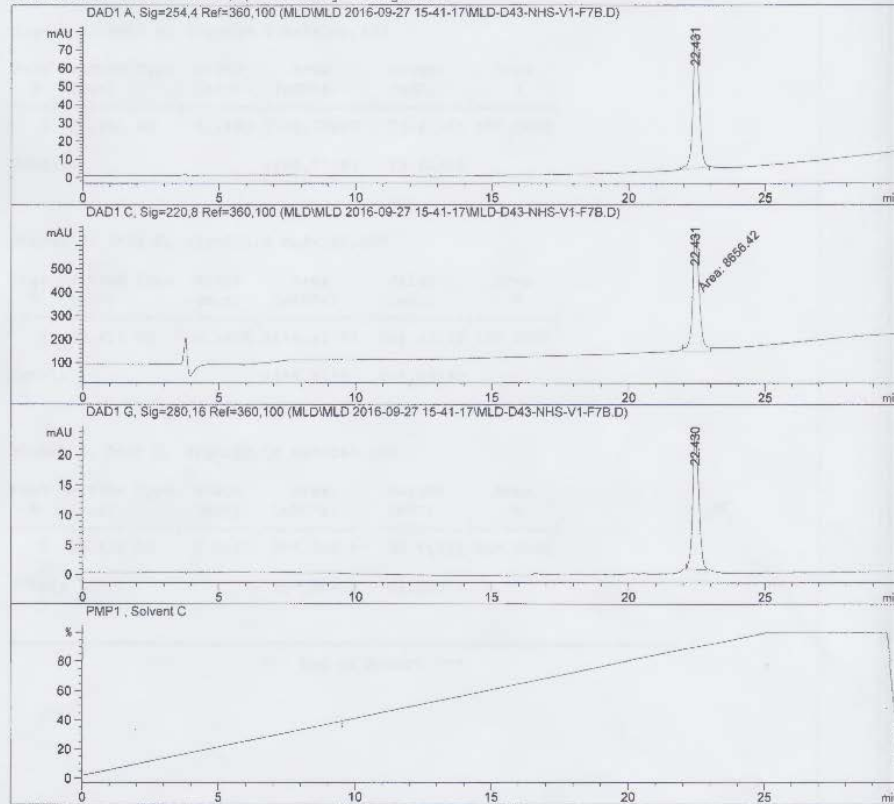
=====

Acq. Operator :		Seq. Line :	3
Acq. Instrument :	Instrument 1	Location :	Vial 41
Injection Date :	9/27/2016 4:57:38 PM	Inj :	1
		Inj Volume :	10.0 µl

Different Inj Volume from Sequence ! Actual Inj Volume : 25.0 µl

Acq. Method :	C:\CHEM32\1\DATA\MLD\MLD 2016-09-27 15-41-17\MLD-2-100_25MIN_1.M
Last changed :	6/21/2016 11:54:00 AM
Analysis Method :	C:\CHEM32\1\METHODS\MLD-10-40-85_20MIN_1.M
Last changed :	2/1/2016 3:16:23 PM

Additional Info : Peak(s) manually integrated



=====

Fraction Information

=====

Fraction collection off

=====

Instrument 1 9/28/2016 10:12:47 AM

Page 1 of 2

Figure A4.6 Peptide 4.4; HPLC Trace

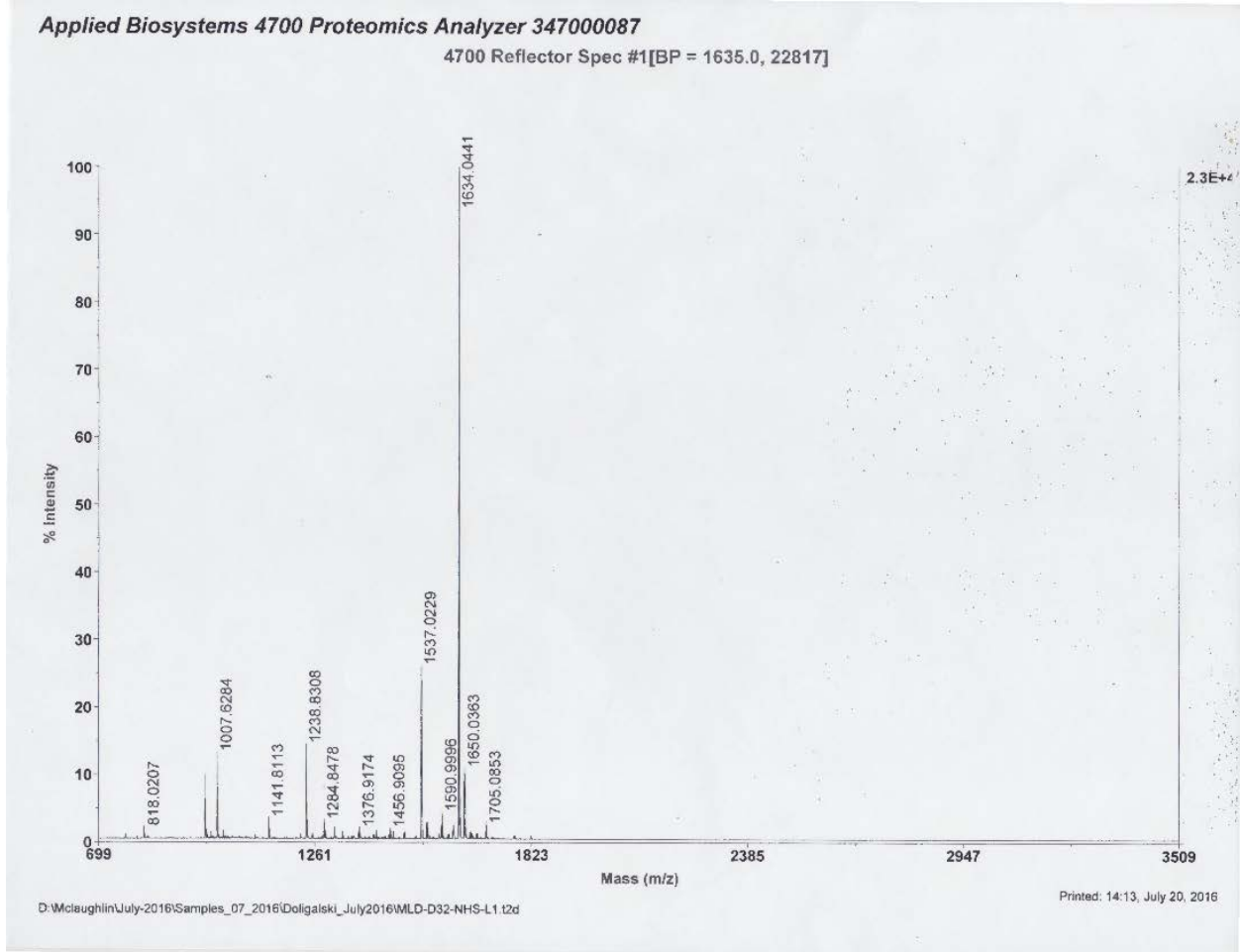
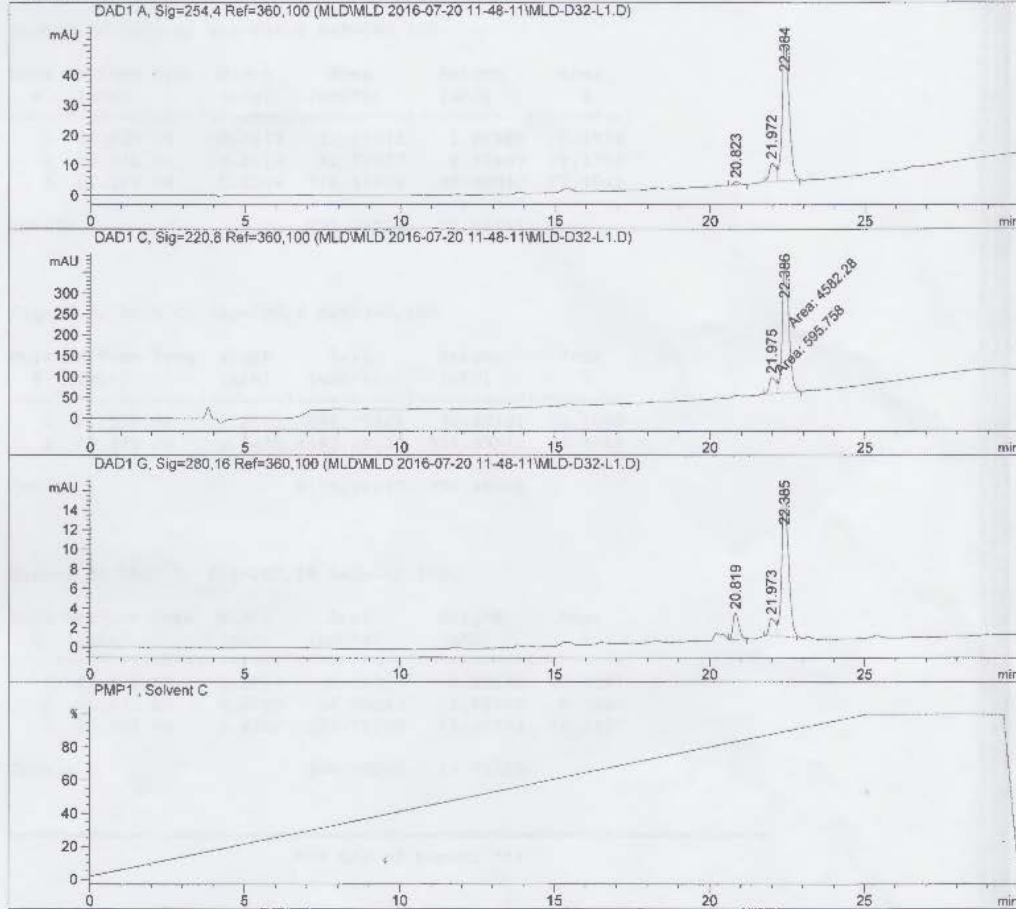


Figure A4.7 Peptide 4.5; Mass Spectrum

Data File C:\CHEM32\1\DATA\MLD\MLD 2016-07-20 11-48-11\MLD-D32-L1.D
Sample Name: MLD-D32-L1

=====

Acq. Operator :	Seq. Line : 1
	Location : Vial 61
Injection Date : 7/20/2016 11:48:28 AM	Inj : 1
	Inj Volume : 10.0 µl
Acq. Method : MLD-2-100_25MIN_1.M	
Analysis Method : C:\CHEM32\1\METHODS\MLD-10-40-85_20MIN_1.M	
Last changed : 2/1/2016 3:16:23 PM	
Additional Info : Peak(s) manually integrated	



Instrument 1 7/20/2016 12:22:15 PM

Page 1 of 2

Figure A4.8 Peptide 4.5; HPLC Trace

APPENDIX B:

SELECTED ^1H AND ^{13}C NMR SPECTRA

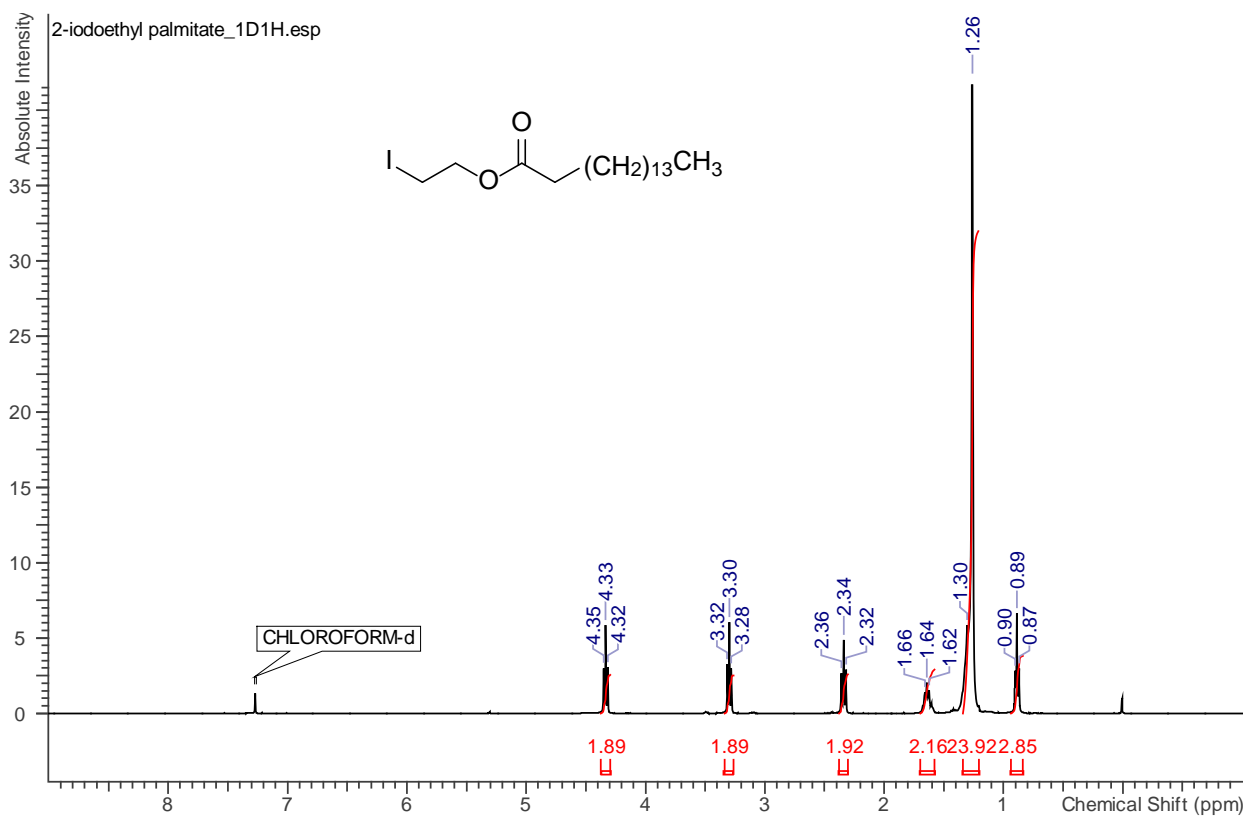


Figure B3.1 ^1H NMR (400 MHz, CDCl_3) spectrum of 3.1.

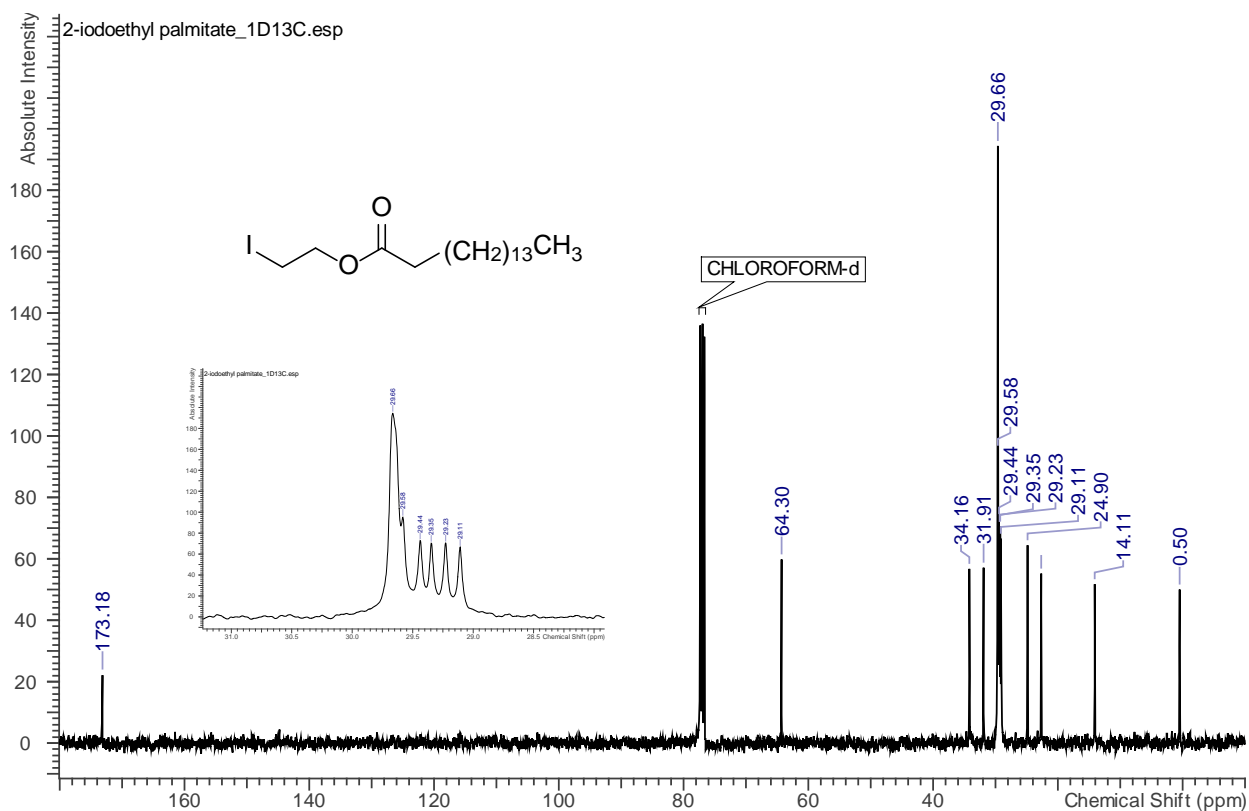


Figure B3.2 ^{13}C $\{^1\text{H}\}$ NMR (400 MHz, CDCl_3) spectrum of 3.1

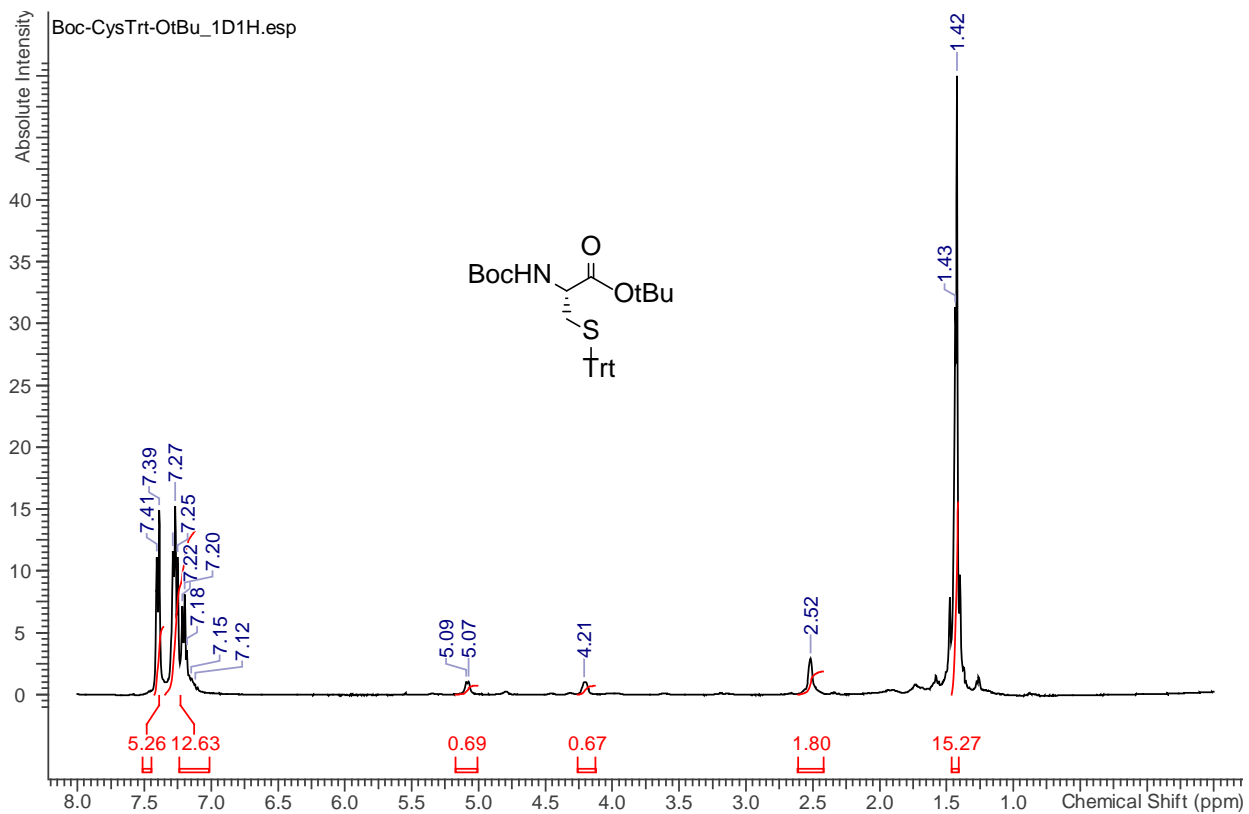


Figure B3.3 ^1H NMR (400 MHz, CDCl_3) spectrum of 3.2

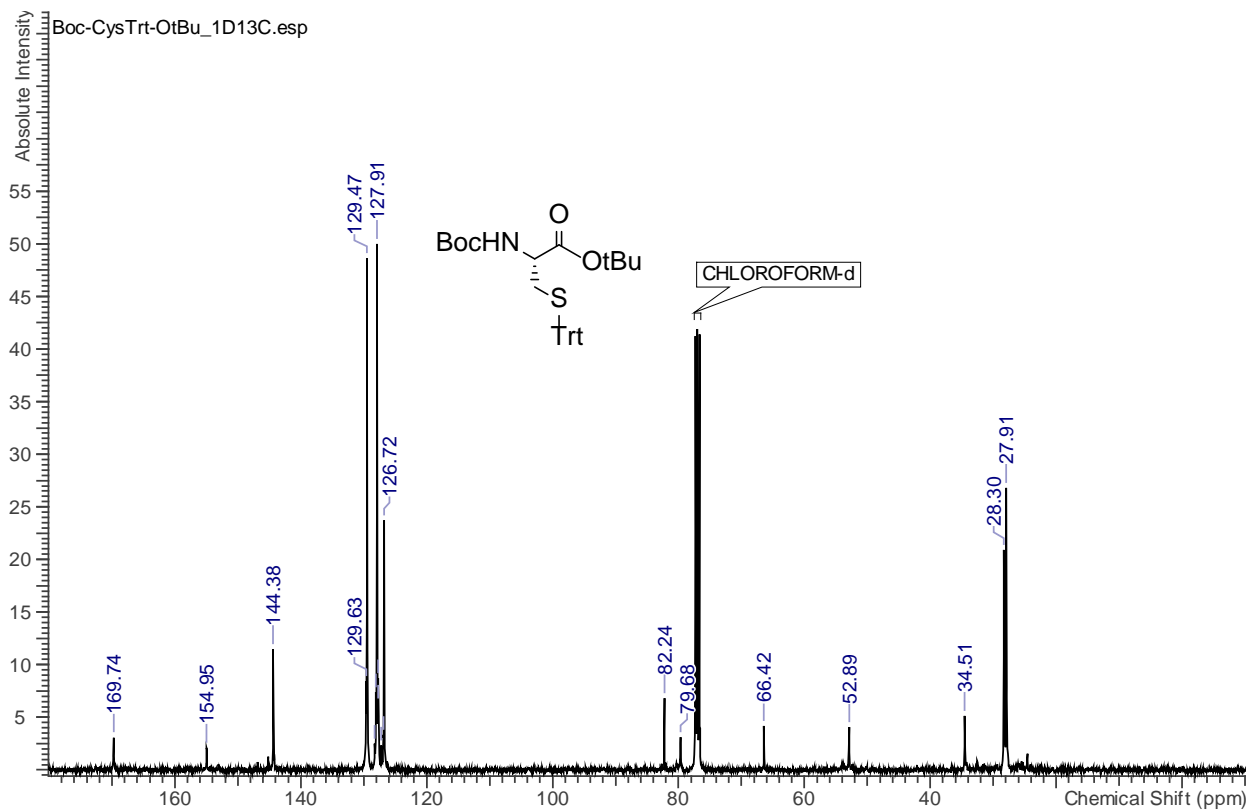
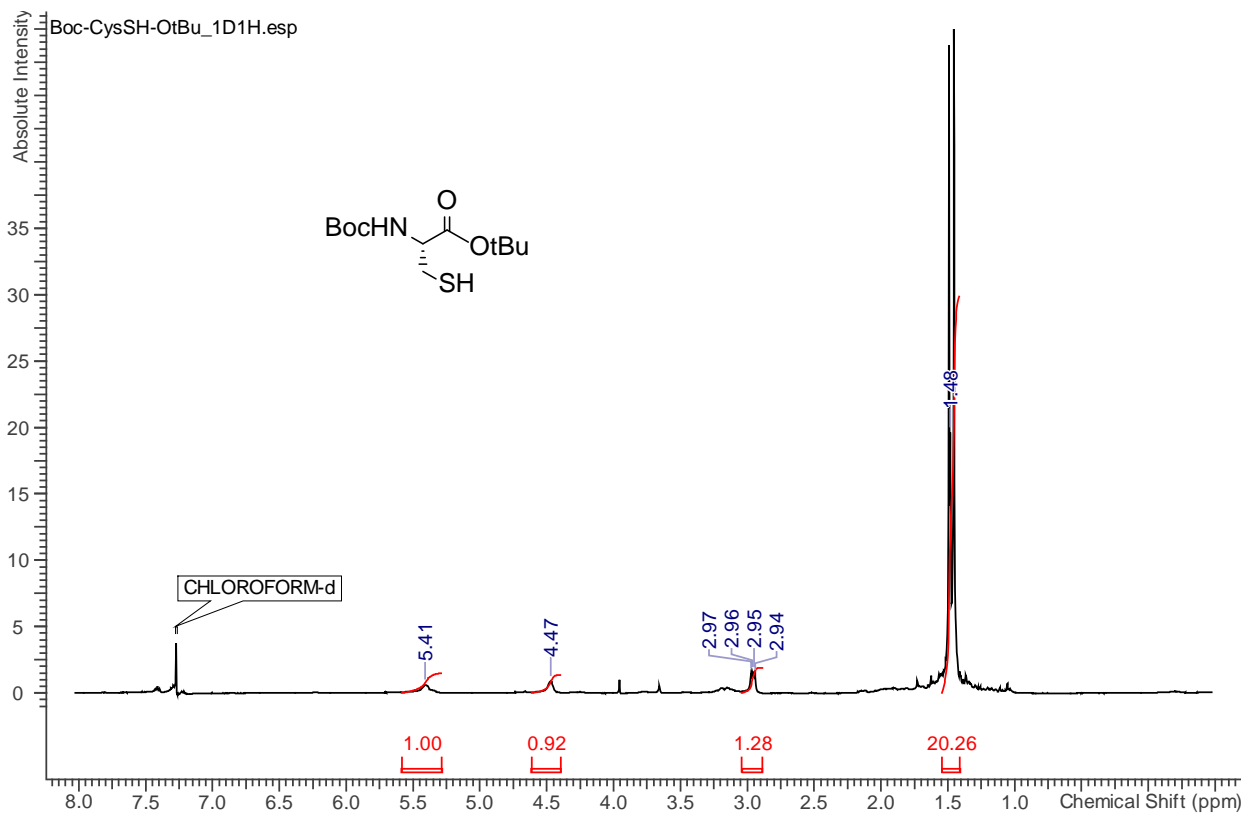


Figure B3.4 ^{13}C $\{^1\text{H}\}$ NMR (101 MHz, CDCl_3) spectrum of 3.2



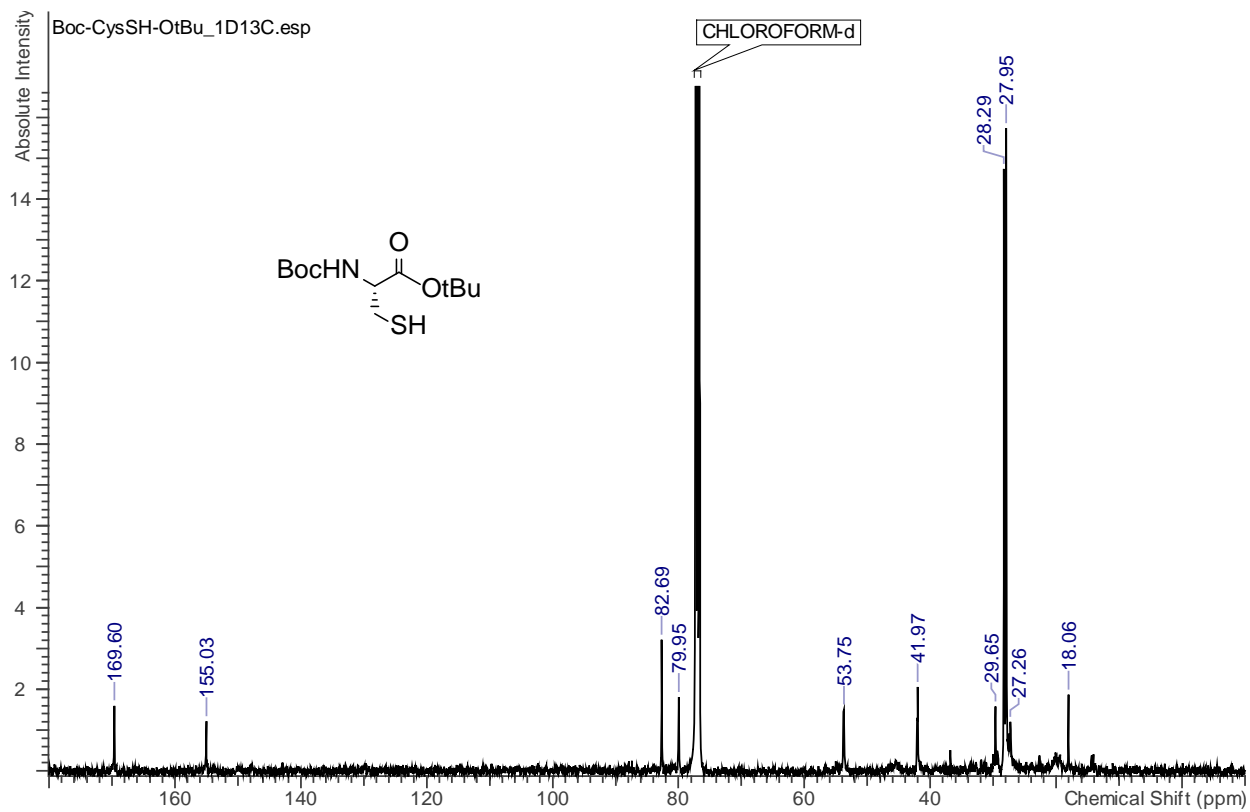


Figure B3.6 ^{13}C $\{^1\text{H}\}$ NMR (101 MHz, CDCl_3) spectrum of 3.3

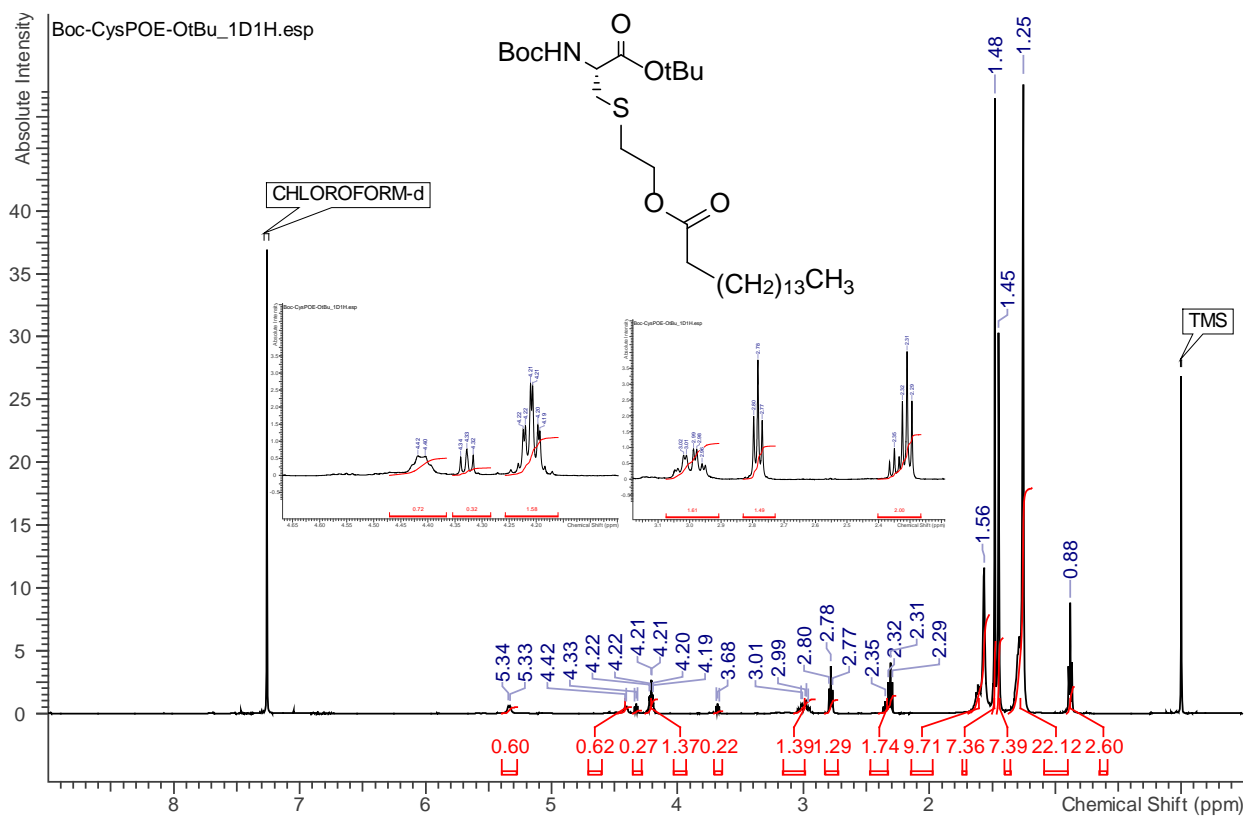


Figure B3.7 ^1H NMR (500 MHz, CDCl_3) spectrum of 3.4

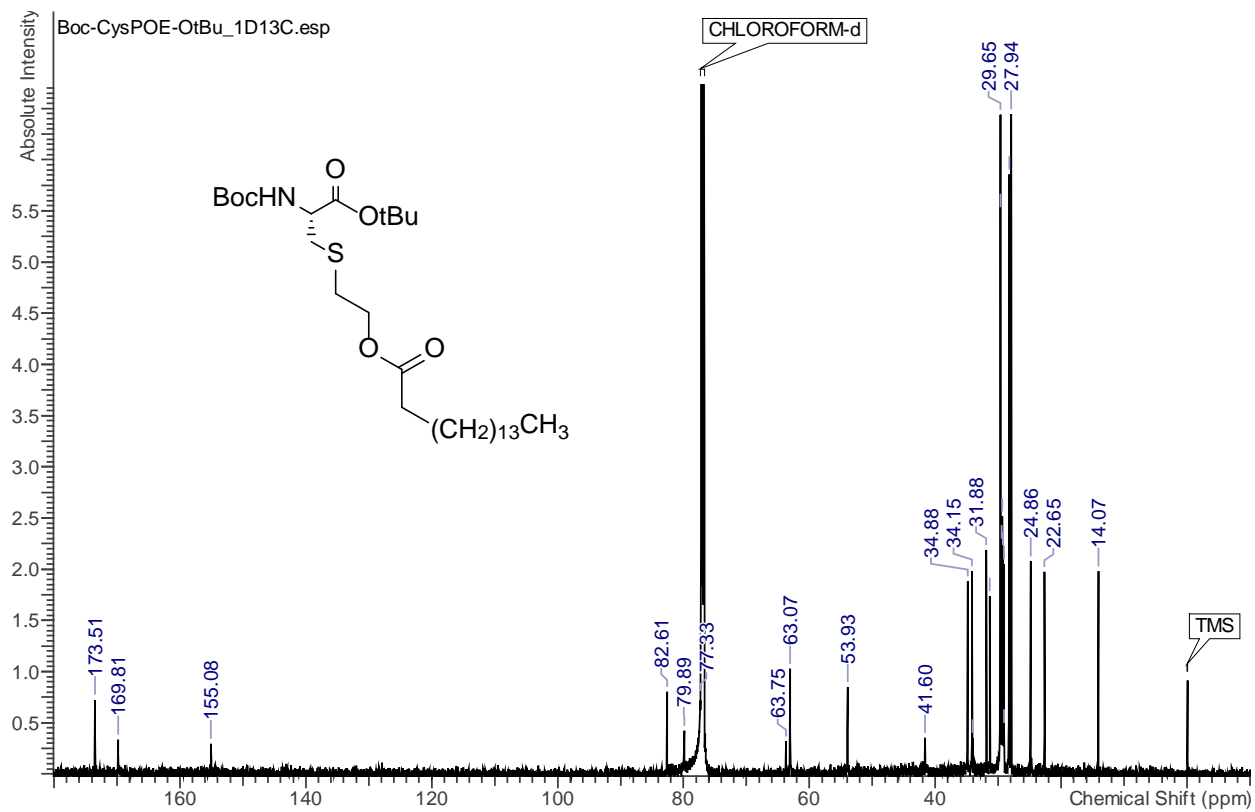


Figure B3.8 ^{13}C $\{^1\text{H}\}$ NMR (151 MHz, CDCl_3) spectrum of 3.4

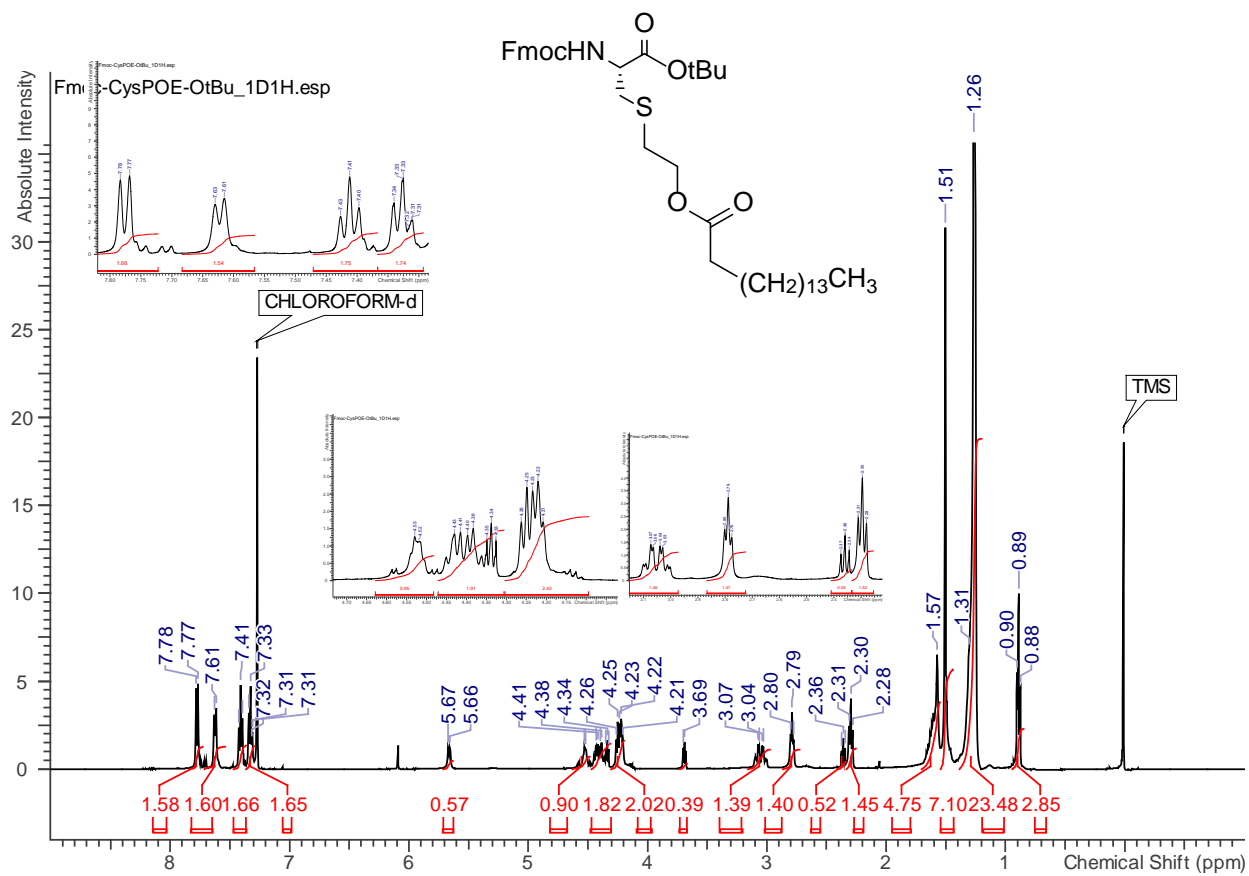


Figure B3.9 ^1H NMR (500 MHz, CDCl_3) spectrum of 3.5

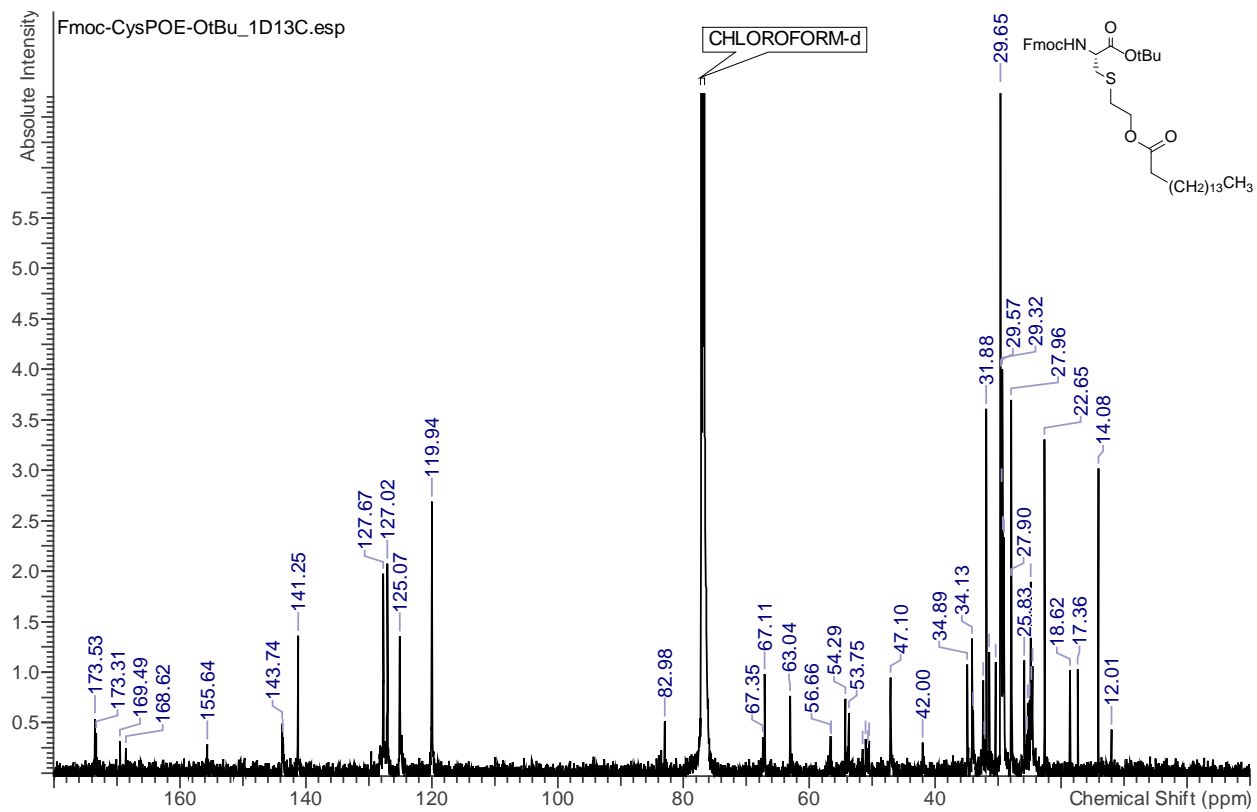


Figure B3.10 ^{13}C $\{^1\text{H}\}$ NMR (151 MHz, CDCl_3) spectrum of 3.5

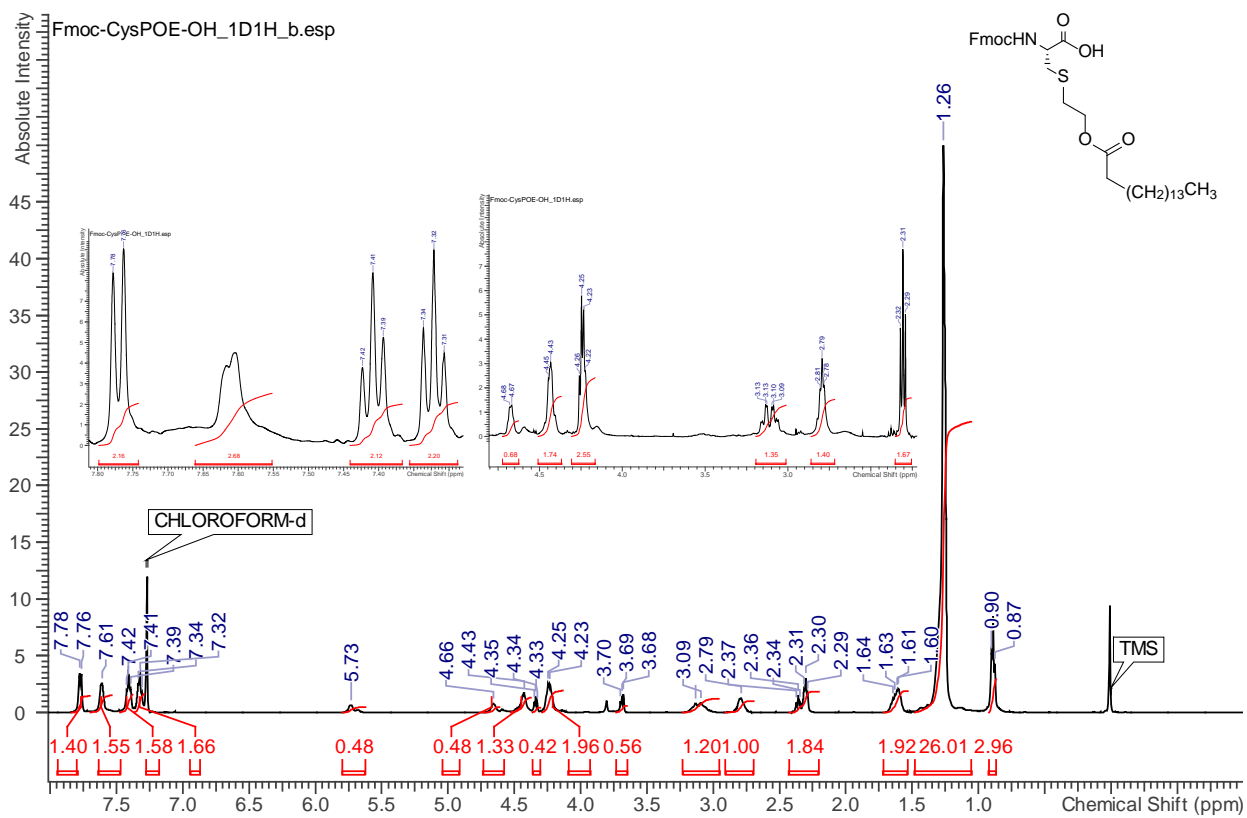


Figure B3.11. ^1H NMR (500 MHz, CDCl_3) spectrum of 3.6

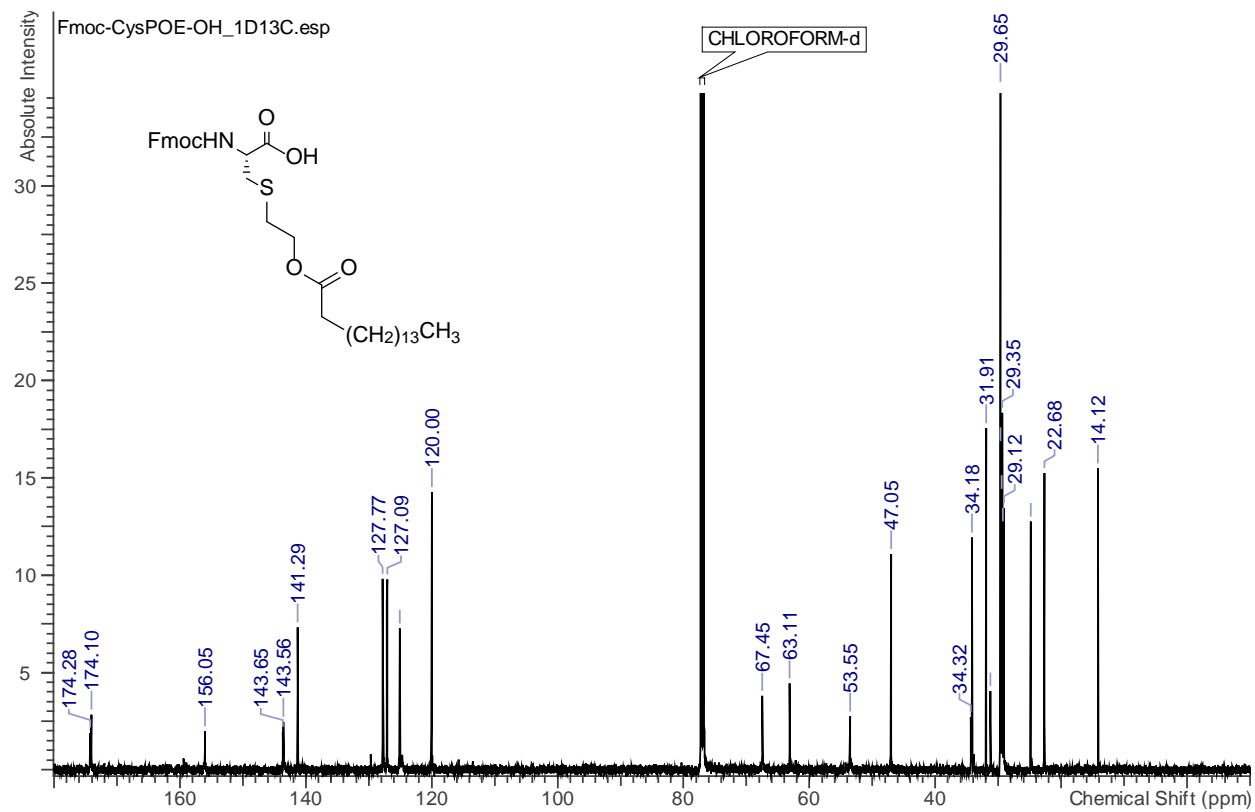


Figure B3.12 ^{13}C $\{^1\text{H}\}$ NMR (126 MHz, CDCl_3) spectrum of 3.6

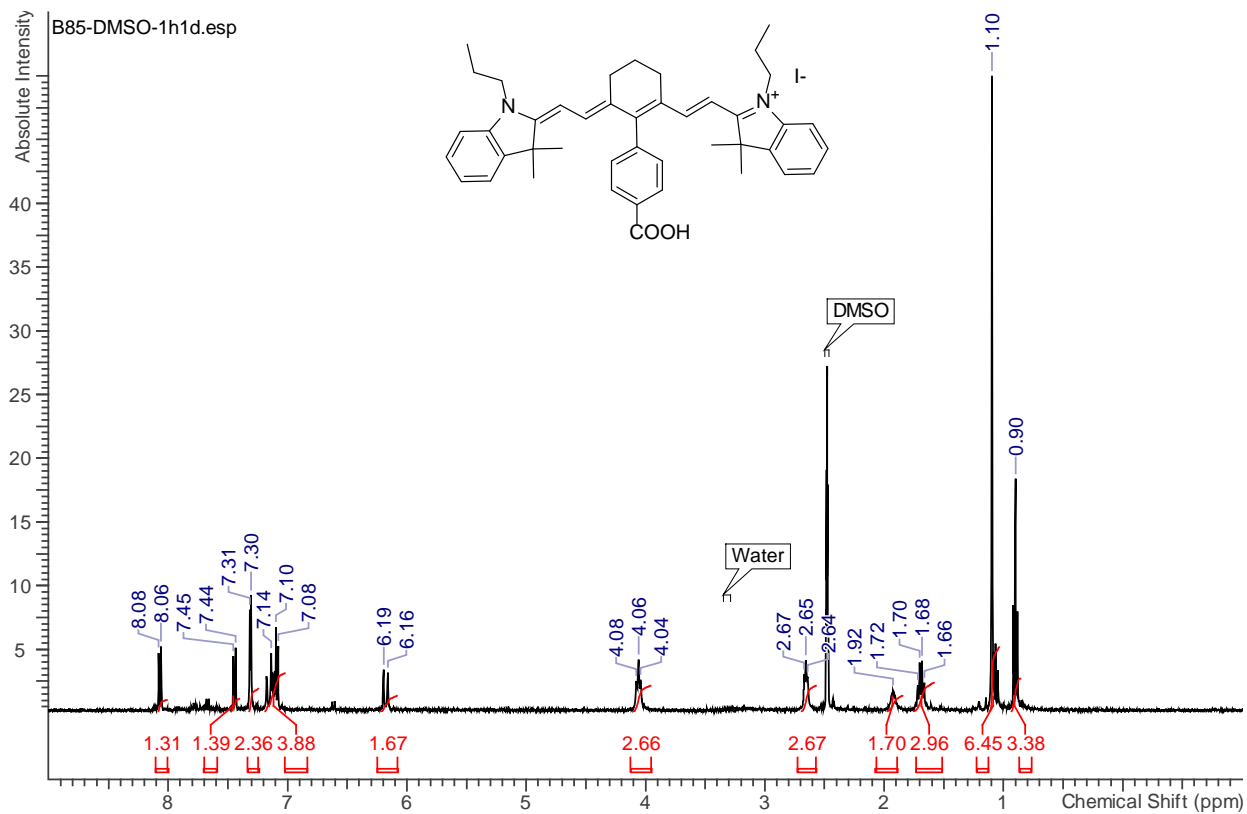


Figure B3.13 ^1H NMR (600 MHz, DMSO) spectrum of 3.7

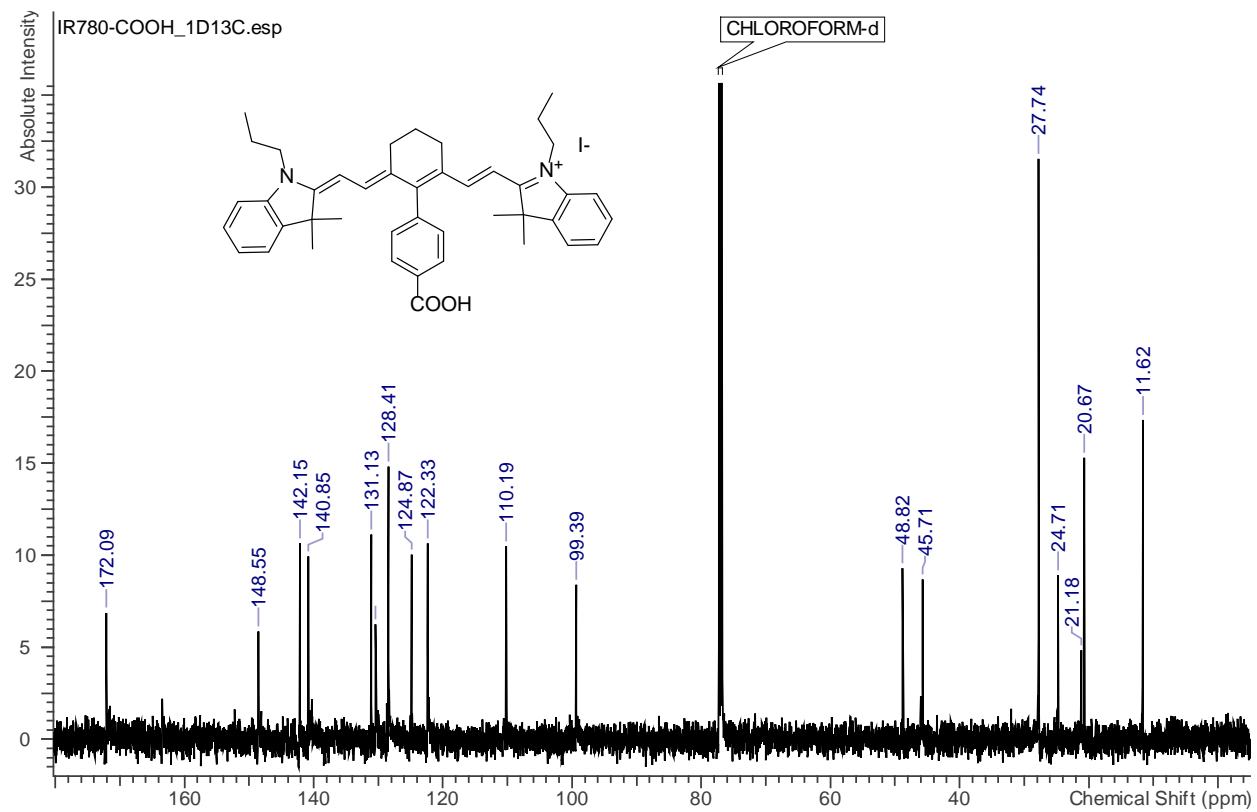


Figure B3.14 ^{13}C $\{^1\text{H}\}$ NMR (151 MHz, CDCl_3) spectrum of 3.7

APPENDIX C:

SELECTED ANTIBODY AND IMMUNOCONJUGATE CHARACTERIZATION

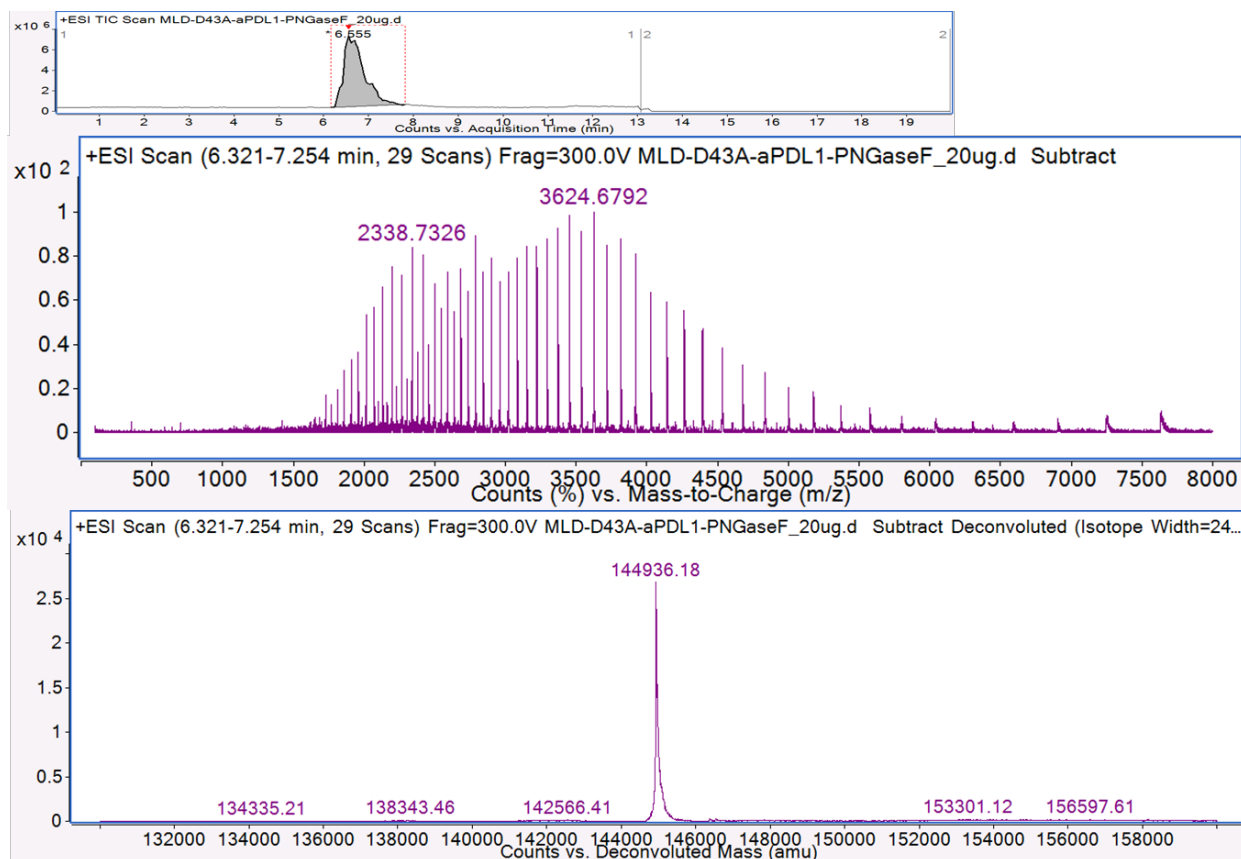


Figure C4.1 α -PD-L1 antibody; Mass Spectra

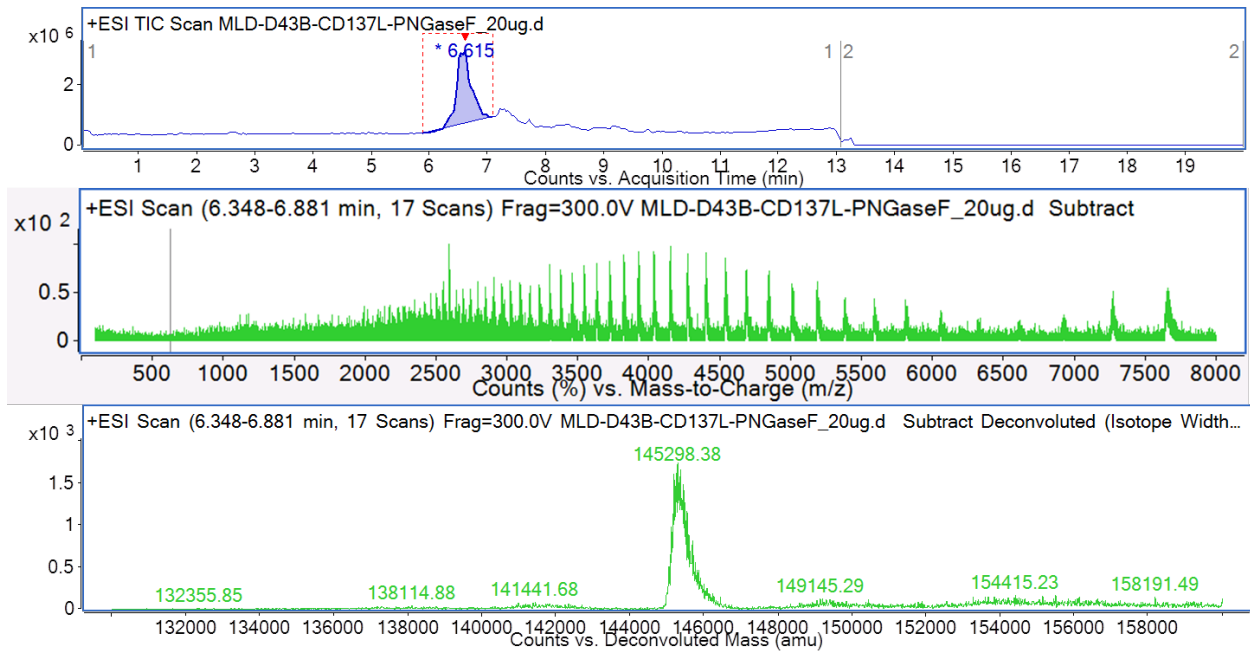


Figure C4.2 α -CD137L antibody; Mass Spectra

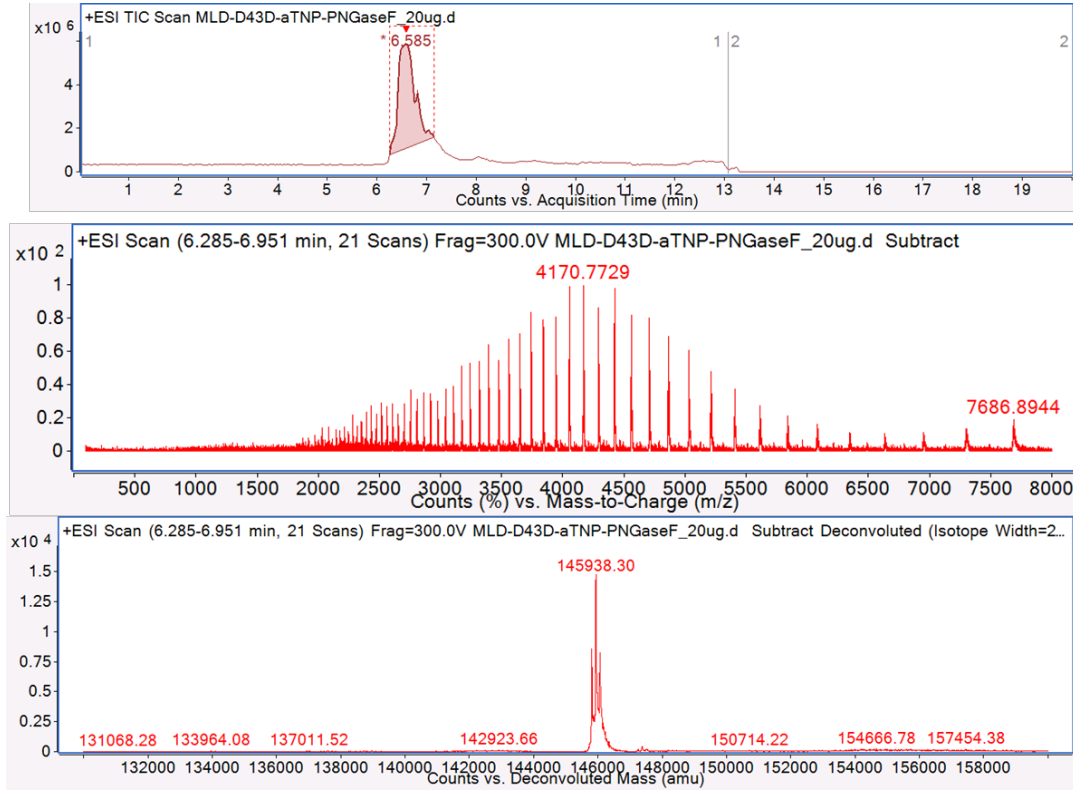


Figure C4.3 α -trinitrophenol antibody; Mass Spectra

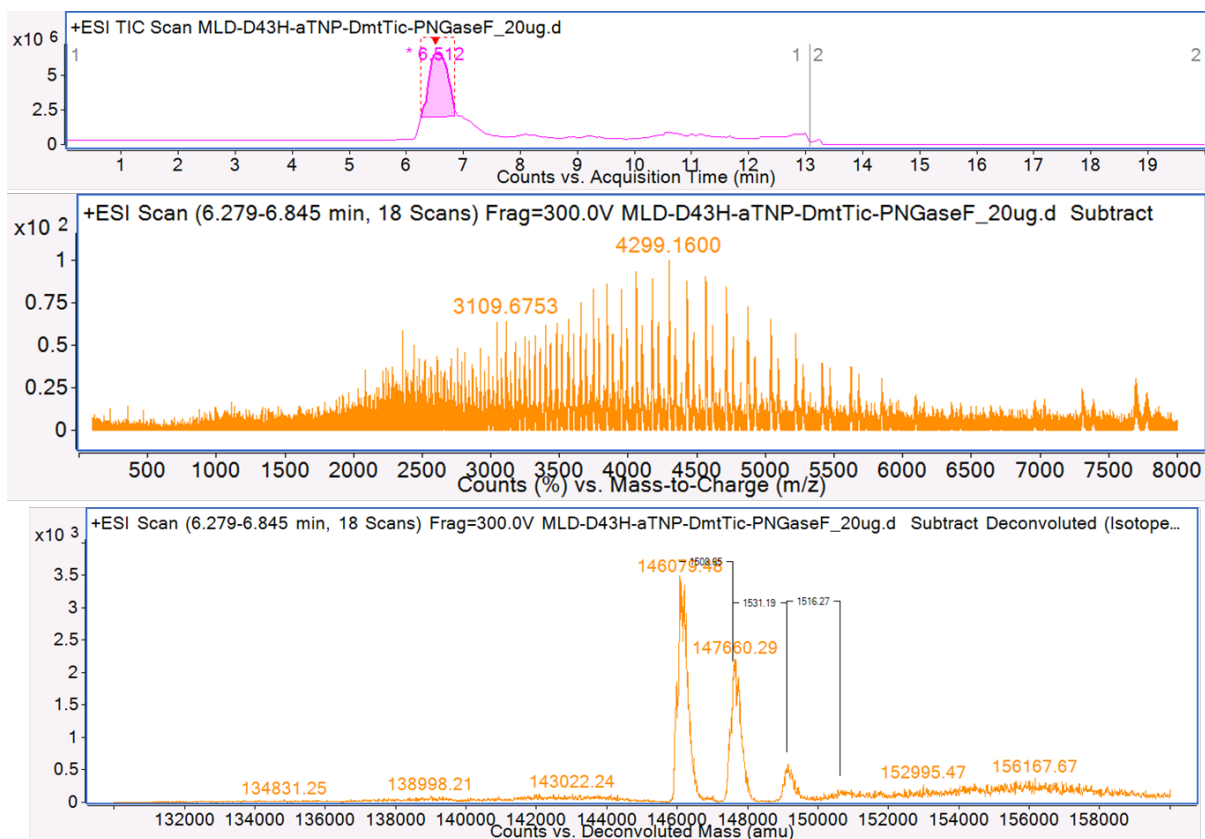


Figure C4.4 Immunoconjugate α -trinitrophenol + DmtTic (4.2), D41; Mass Spectra

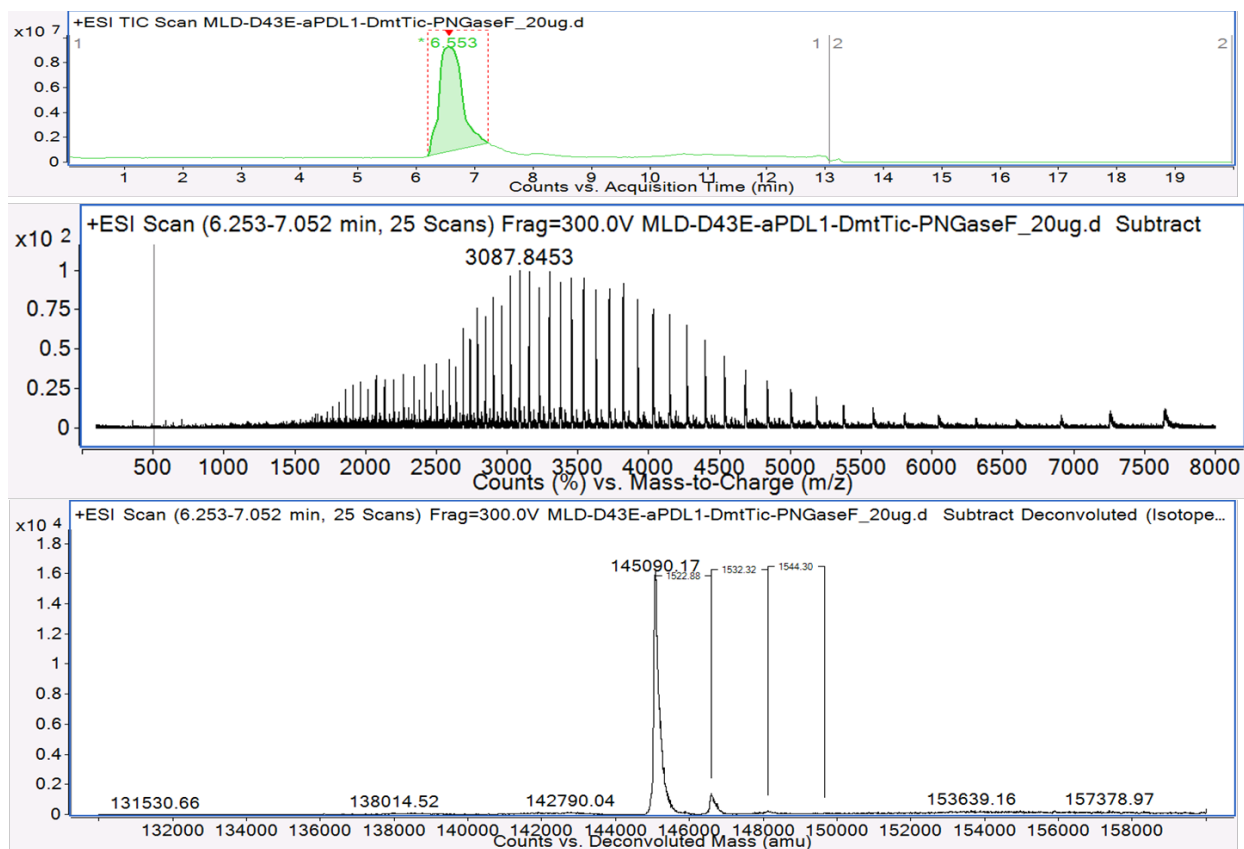
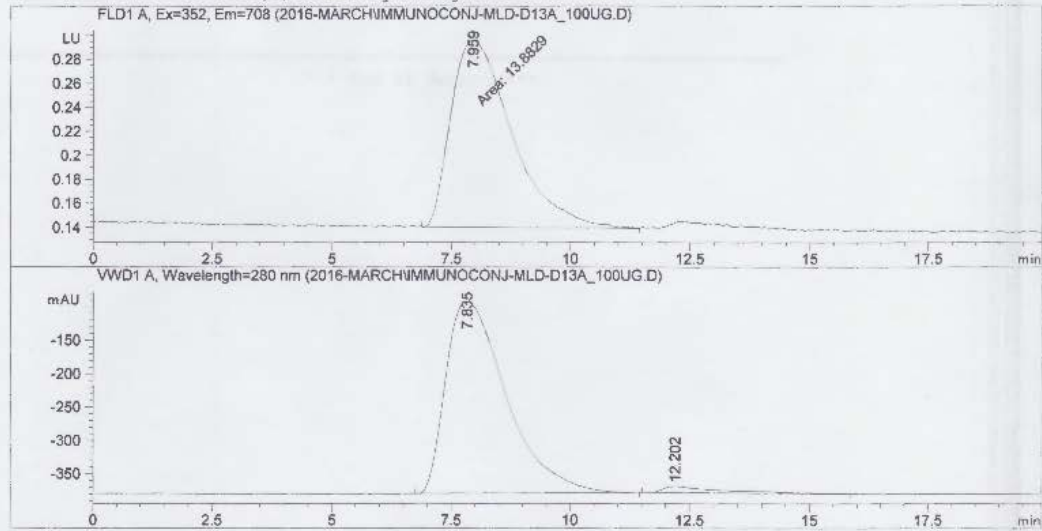


Figure C4.5 Immunoconjugate α -PDL-1 + DmtTic (4.2), D38; Mass Spectra

Data File C:\CHEM32\1\DATA\2016-MARCH\IMMUNOCONJ-MLD-D13A_100UG.D
 Sample Name: IMMUNOCONJ-MLD-D13A_100UG

=====
 Acq. Operator : SYSTEM
 Acq. Instrument : 1260 HPLC Location : -
 Injection Date : 3/22/2016 5:00:53 PM Inj Volume : No inj
 Acq. Method : C:\CHEM32\1\METHODS\MLD-50BISO_60MIN_3000LMIN-FLD.M
 Last changed : 11/17/2015 12:28:59 PM by SYSTEM
 Analysis Method : C:\CHEM32\1\METHODS\DEF_IC.M
 Last changed : 6/17/2016 12:07:51 PM by SYSTEM
 Additional Info : Peak(s) manually integrated



=====
 Area Percent Report
 =====

Sorted By : Signal
 Multiplier: : 1.0000
 Dilution: : 1.0000
 Use Multiplier & Dilution Factor with ISTDs

Signal 1: FLD1 A, Ex=352, Em=708

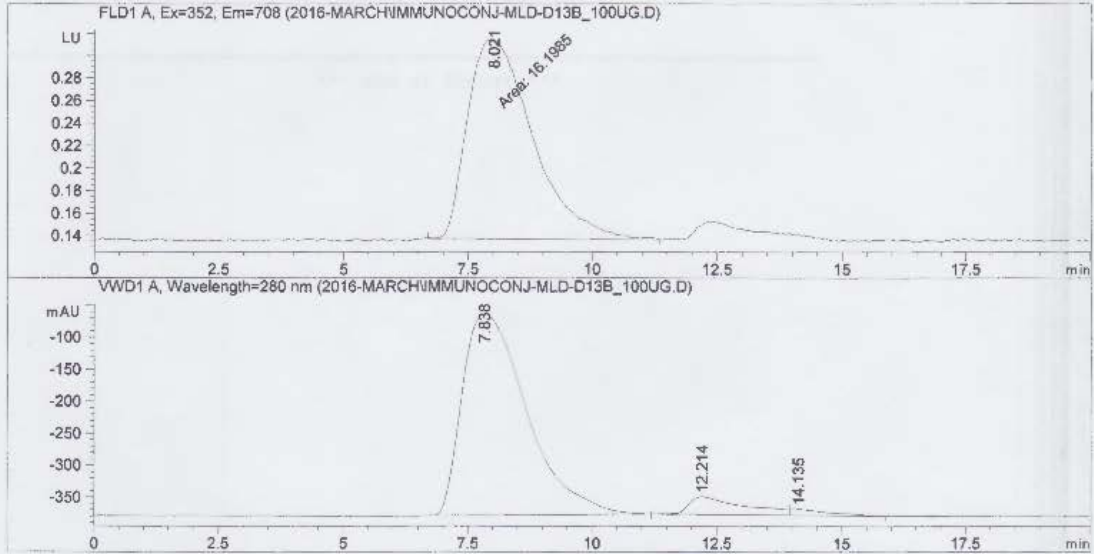
Peak #	RetTime [min]	Type	Width [min]	Area [LU*s]	Height [LU]	Area %
1	7.959	MM	1.4847	13.88294	1.55843e-1	100.0000

Totals : 13.88294 1.55843e-1

Figure C4.6 Immunoconjugate α -PD-1 + DmtTic (4.2), D13A; SEC Chromatograph

Data File C:\CHEM32\1\DATA\2016-MARCH\IMMUNOCONJ-MLD-D13B_100UG.D
 Sample Name: IMMUNOCONJ-MLD-D13B_100UG

=====
 Acq. Operator : SYSTEM
 Acq. Instrument : 1260 HPLC Location : -
 Injection Date : 3/22/2016 5:24:00 PM Inj Volume : No inj
 Acq. Method : C:\CHEM32\1\METHODS\MLD-50BISO_60MIN_300ULMIN-FLD.M
 Last changed : 3/22/2016 5:22:41 PM by SYSTEM
 (modified after loading)
 Analysis Method : C:\CHEM32\1\METHODS\DEF_LC.M
 Last changed : 6/17/2016 12:07:51 PM by SYSTEM
 Additional Info : Peak(s) manually integrated



=====
 Area Percent Report
 =====

Sorted By : Signal
 Multiplier: : 1.0000
 Dilution: : 1.0000
 Use Multiplier & Dilution Factor with ISTDs

Signal 1: FLD1 A, Ex=352, Em=708

Peak #	RetTime [min]	Type	Width [min]	Area [LU*s]	Height [LU]	Area %
1	8.021	MM	1.5260	16.19855	1.76918e-1	100.0000

Totals : 16.19855 1.76918e-1

Figure C4.7 Immunoconjugate α -PD-1 + DmtTic (4.2), D13B; SEC Chromatograph

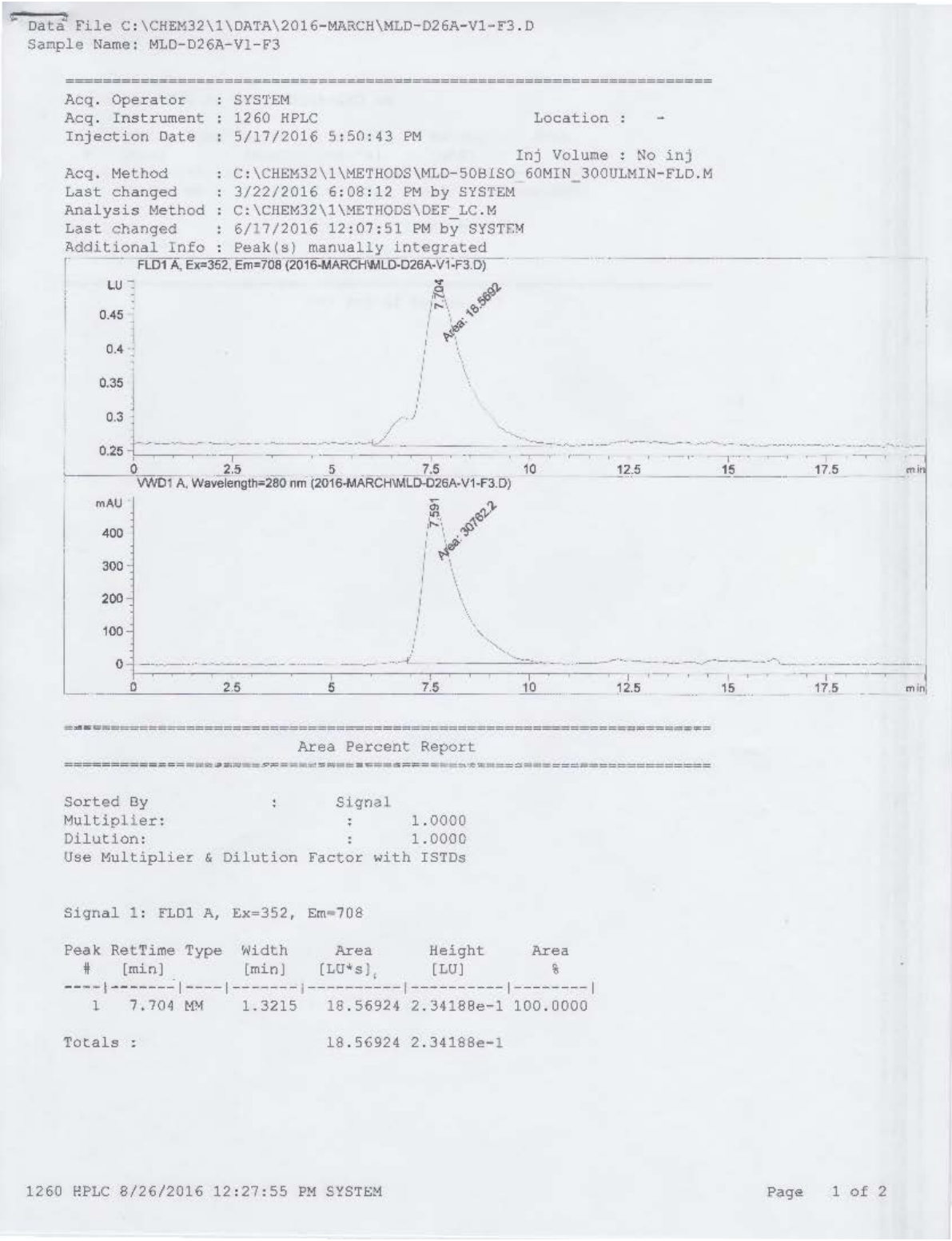
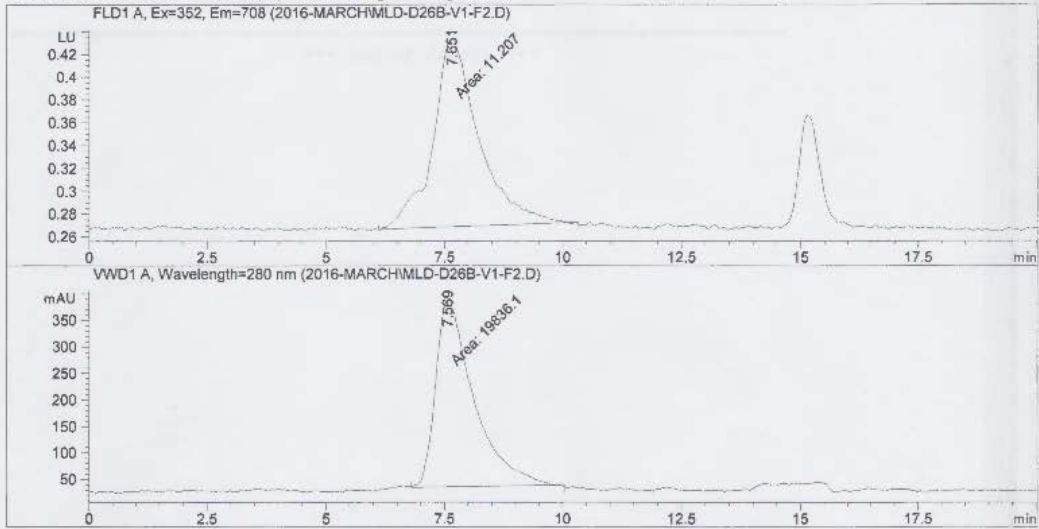


Figure C4.8 Immunoconjugate α -PD-1 + DmtTic (4.2), D26A; SEC Chromatograph

Data File C:\CHEM32\1\DATA\2016-MARCH\MLD-D26B-V1-F2.D
 Sample Name: MLD-D26B-V1-F2

=====
 Acq. Operator : SYSTEM
 Acq. Instrument : 1260 HPLC Location : -
 Injection Date : 5/18/2016 1:28:52 PM Inj Volume : No inj
 Acq. Method : C:\CHEM32\1\METHODS\MLD-50BISO_60MIN_300ULMIN-FLD.M
 Last changed : 3/22/2016 6:08:12 PM by SYSTEM
 Analysis Method : C:\CHEM32\1\METHODS\DEF_LC.M
 Last changed : 6/17/2016 12:07:51 PM by SYSTEM
 Additional Info : Peak(s) manually integrated



=====
 Area Percent Report
 =====

Sorted By : Signal
 Multiplier: : 1.0000
 Dilution: : 1.0000
 Use Multiplier & Dilution Factor with ISTDs

Signal 1: FLD1 A, Ex=352, Em=708

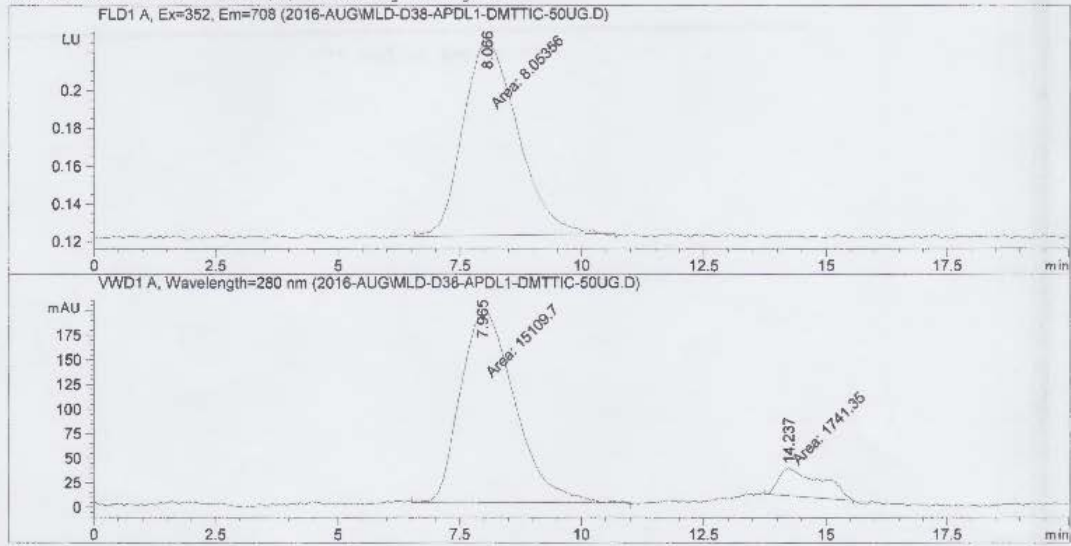
Peak #	RetTime [min]	Type	Width [min]	Area [LU*s]	Height [LU]	Area %
1	7.651	MM	1.1329	11.20699	1.64873e-1	100.0000

Totals : 11.20699 1.64873e-1

Figure C4.9 Immunoconjugate α -PD-1 + DmtTic (4.2), D26B; SEC Chromatograph

Data File C:\CHEM32\1\DATA\2016-AUG\MLD-D38-APDL1-DMTTIC-50UG.D
 Sample Name: MLD-D38-APDKL1-DMTTIC-50UG.D

=====
 Acq. Operator : SYSTEM
 Acq. Instrument : 1260 HPLC Location : -
 Injection Date : 8/15/2016 11:55:05 AM Inj Volume : No inj
 Acq. Method : C:\CHEM32\1\METHODS\MLD-50BISO_60MIN_300ULMIN-FLD.M
 Last changed : 8/15/2016 10:27:20 AM by SYSTEM
 (modified after loading)
 Analysis Method : C:\CHEM32\1\METHODS\DEF_LC.M
 Last changed : 6/17/2016 12:07:51 PM by SYSTEM
 Additional Info : Peak(s) manually integrated



=====
 Area Percent Report
 =====

Sorted By : Signal
 Multiplier: : 1.0000
 Dilution: : 1.0000
 Use Multiplier & Dilution Factor with ISTDs

Signal 1: FLD1 A, Ex=352, Em=708

Peak #	RetTime [min]	Type	Width [min]	Area [LU*s]	Height [LU]	Area %
1	8.066	MM	1.3057	8.05356	1.02799e-1	100.0000

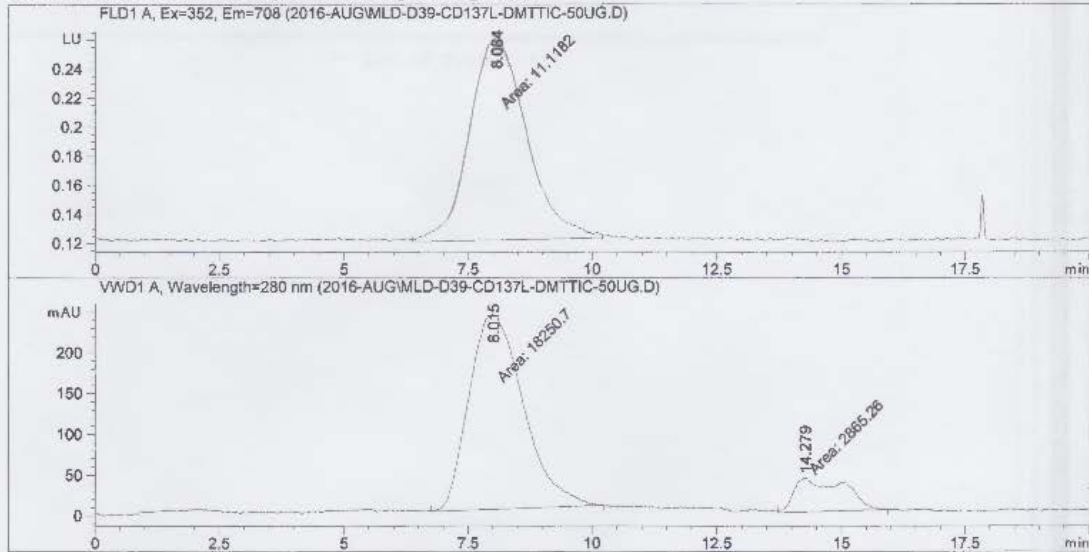
Totals : 8.05356 1.02799e-1

Figure C4.10 Immunoconjugate α -PDL-1 + DmtTic (4.2), D38; SEC Chromatograph

Data File C:\CHEM32\1\DATA\2016-AUG\MLD-D39-CD137L-DMTTIC-50UG.D
 Sample Name: MLD-D39-CD137L-DMTTIC-50UG.D

```

=====
Acq. Operator   : SYSTEM
Acq. Instrument : 1260 HPLC
Injection Date  : 8/15/2016 12:21:33 PM
Location       : -
Inj Volume     : No inj
Acq. Method    : C:\CHEM32\1\METHODS\MLD-50BISO_60MIN_300ULMIN-FLD.M
Last changed   : 8/15/2016 10:27:20 AM by SYSTEM
                (modified after loading)
Analysis Method: C:\CHEM32\1\METHODS\DEF_LC.M
Last changed   : 6/17/2016 12:07:51 PM by SYSTEM
Additional Info: Peak(s) manually integrated
  
```



Area Percent Report

```

Sorted By      : Signal
Multiplier:    : 1.0000
Dilution:      : 1.0000
Use Multiplier & Dilution Factor with ISTDs
  
```

Signal 1: FLD1 A, Ex=352, Em=708

Peak #	RetTime [min]	Type	Width [min]	Area [LU*s]	Height [LU]	Area %
1	8.084	MM	1.3450	11.11818	1.37774e-1	100.0000

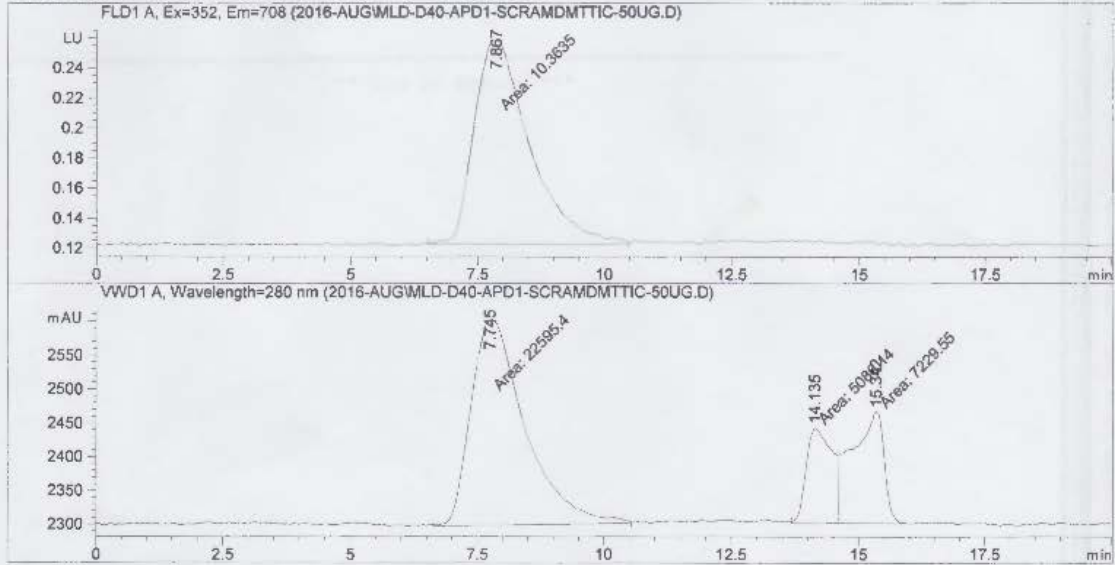
Totals : 11.11818 1.37774e-1

Figure C4.11 Immunoconjugate α -CD137L + DmtTic (4.2), D39; SEC Chromatograph

Data File C:\CHEM32\1\DATA\2016-AUG\MLD-D40-APD1-SCRAMDMTTIC-50UG.D
 Sample Name: MLD-D40-aPD1-scrandmtTic-50ug

```

=====
Acq. Operator   : SYSTEM
Acq. Instrument : 1260 HPLC
Injection Date  : 8/15/2016 11:30:14 AM
Location       : -
Inj Volume     : No inj
Acq. Method    : C:\CHEM32\1\METHODS\MLD-50BISO_60MIN_300ULMIN-FLD.M
Last changed   : 8/15/2016 10:27:20 AM by SYSTEM
                (modified after loading)
Analysis Method: C:\CHEM32\1\METHODS\DEF_LC.M
Last changed   : 6/17/2016 12:07:51 PM by SYSTEM
Additional Info : Peak(s) manually integrated
  
```



Area Percent Report

```

=====
Sorted By      : Signal
Multiplier:    : 1.0000
Dilution:      : 1.0000
Use Multiplier & Dilution Factor with ISTDs
  
```

Signal 1: FLD1 A, Ex=352, Em=708

Peak #	RetTime [min]	Type	Width [min]	Area [LU*s]	Height [LU]	Area %
1	7.867	MM	1.2691	10.36346	1.36101e-1	100.0000
Totals :				10.36346	1.36101e-1	

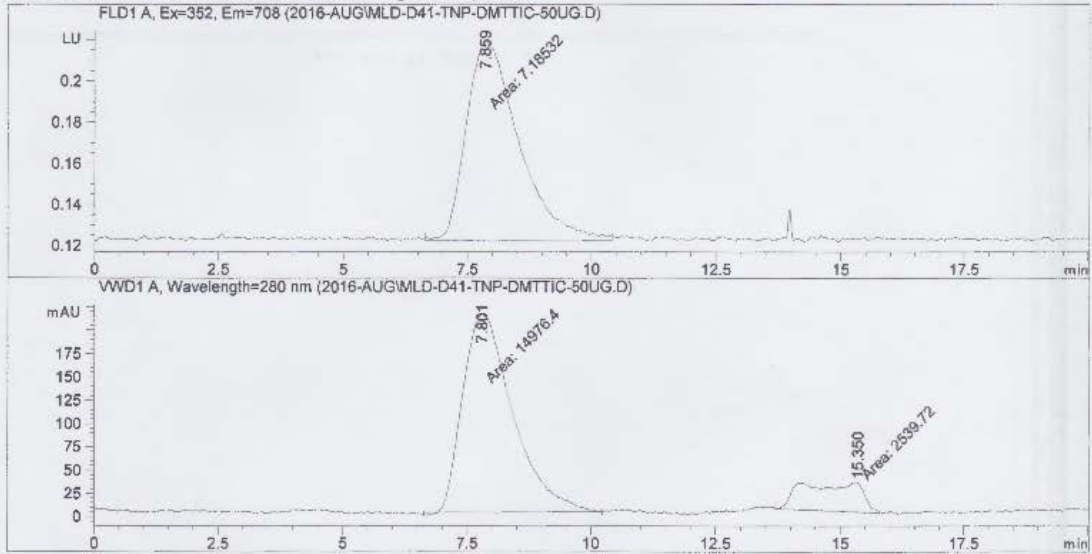
Figure C4.12 Immunoconjugate α -PD-1 + scrambled-DmtTic (4.5), D40; SEC Chromatograph

Data File C:\CHEM32\1\DATA\2016-AUG\MLD-D41-TNP-DMTTIC-50UG.D
 Sample Name: MLD-D41-TNP-DMTTIC-50UG.D

```

=====
Acq. Operator   : SYSTEM
Acq. Instrument : 1260 HPLC
Injection Date  : 8/15/2016 12:47:57 PM
Location       : -
Inj Volume     : No inj

Acq. Method    : C:\CHEM32\1\METHODS\MLD-50BISO_60MIN_300ULMIN-FLD.M
Last changed   : 8/15/2016 10:27:20 AM by SYSTEM
                (modified after loading)
Analysis Method : C:\CHEM32\1\METHODS\DEF_LC.M
Last changed   : 6/17/2016 12:07:51 PM by SYSTEM
Additional Info : Peak(s) manually integrated
  
```



Area Percent Report

```

Sorted By      : Signal
Multiplier:    : 1.0000
Dilution:      : 1.0000
Use Multiplier & Dilution Factor with ISTDs
  
```

Signal 1: FLD1 A, Ex=352, Em=708

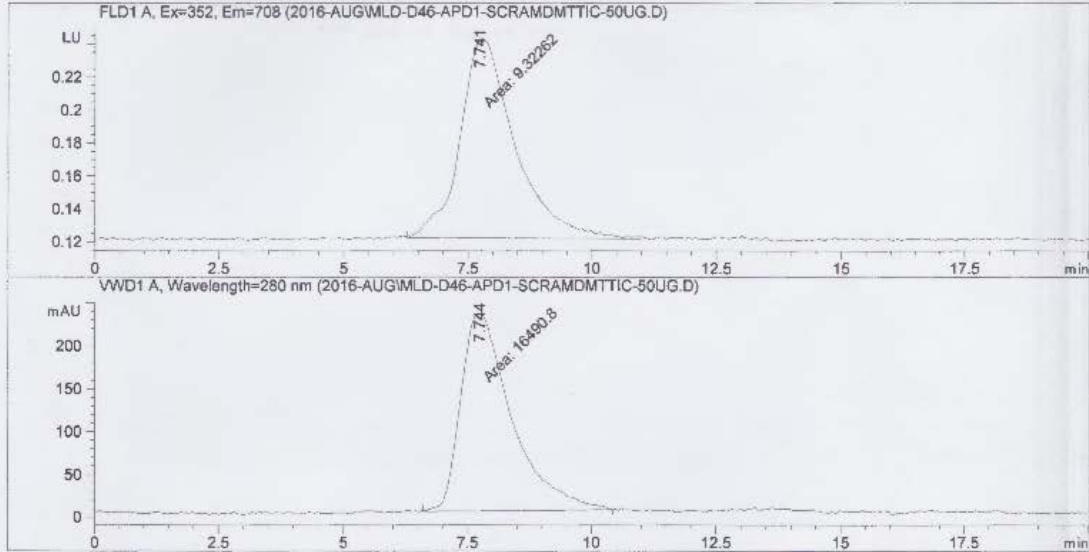
Peak #	RetTime [min]	Type	Width [min]	Area [LU*s]	Height [LU]	Area %
1	7.859	MM	1.2291	7.18532	9.74331e-2	100.0000

Totals : 7.18532 9.74331e-2

Figure C4.13 Immunoconjugate α -trinitrophenol + DmtTic (4.2), D41; SEC Chromatograph

Data File C:\CHEM32\1\DATA\2016-AUG\MLD-D46-APD1-SCRAMDMTTIC-50UG.D
 Sample Name: MLD-D46-aPD1-ScramDmtTic-50ug

=====
 Acq. Operator : SYSTEM
 Acq. Instrument : 1260 HPLC Location : -
 Injection Date : 8/31/2016 4:25:11 PM Inj Volume : No inj
 Acq. Method : C:\CHEM32\1\METHODS\MLD-50BISO_60MIN_300ULMIN-FLD.M
 Last changed : 8/31/2016 2:32:27 PM by SYSTEM
 (modified after loading)
 Analysis Method : C:\CHEM32\1\METHODS\DEF_IC.M
 Last changed : 6/17/2016 12:07:51 PM by SYSTEM
 Additional Info : Peak(s) manually integrated



=====
 Area Percent Report
 =====

Sorted By : Signal
 Multiplier: : 1.0000
 Dilution: : 1.0000
 Use Multiplier & Dilution Factor with ISTDs

Signal 1: FLD1 A, Ex=352, Em=708

Peak #	RetTime [min]	Type	Width [min]	Area: [LU*s]	Height [LU]	Area %
1	7.741	MM	1.2899	9.32262	1.20460e-1	100.0000

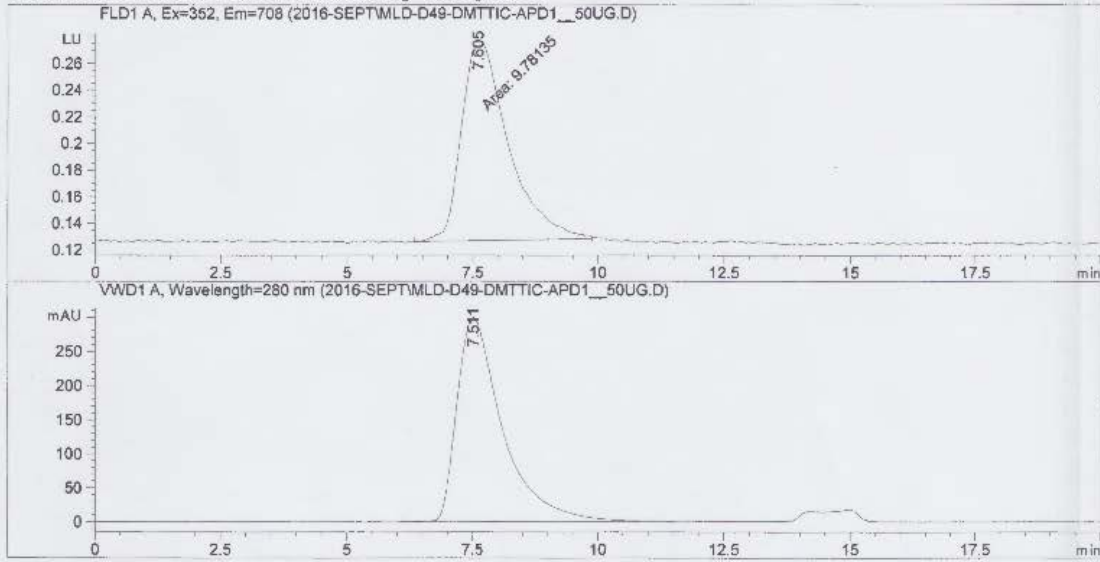
Totals : 9.32262 1.20460e-1

Figure C4.14 Immunoconjugate α -PD-1 + scrambled-DmtTic (4.5), D46; SEC Chromatograph

Data File C:\CHEM32\1\DATA\2016-SEPT\MLD-D49-DMTTIC-APD1_50UG.D
 Sample Name: MLD-D49-DmtTic-aPD1_50ug

```

=====
Acq. Operator   : SYSTEM
Acq. Instrument : 1260 HPLC
Injection Date  : 9/30/2016 5:15:52 PM
Location        : Vial 1
Inj Volume     : No inj
Acq. Method    : C:\CHEM32\1\METHODS\MLD-50BISO_60MIN_300ULMIN-FLD.M
Last changed   : 3/22/2016 6:08:12 PM by SYSTEM
Analysis Method: C:\CHEM32\1\METHODS\DEF_LC.M
Last changed   : 9/13/2016 12:50:25 PM by SYSTEM
Additional Info : Peak(s) manually integrated
  
```



=====
 Area Percent Report
 =====

```

Sorted By      :      Signal
Multiplier:    :      1.0000
Dilution:      :      1.0000
Use Multiplier & Dilution Factor with ISTDs
  
```

Signal 1: FLD1 A, Ex=352, Em=708

Peak #	RetTime [min]	Type	Width [min]	Area [LU*s]	Height [LU]	Area %
1	7.605	MM	1.0871	9.78135	1.49961e-1	100.0000

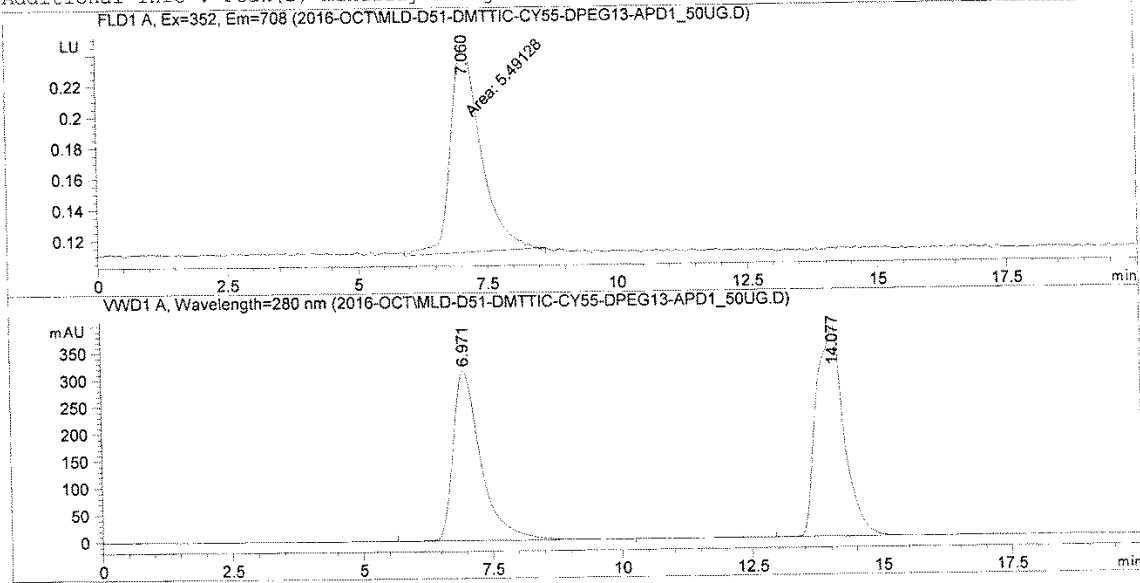
Totals : 9.78135 1.49961e-1

Figure C4.15 Immunoconjugate α -PD-1 + DmtTic (4.2), D49; SEC Chromatograph

Data File C:\CHEM32\1\DATA\2016-OCT\MLD-D51-DMTTIC-CY55-DPEG13-APD1_50UG.D
 Sample Name: MLD-D51-DmtTic-CY55-DPEG13-aPD1_50UG.D

```

=====
Acq. Operator   : SYSTEM
Acq. Instrument : 1260 HPLC
Injection Date  : 10/12/2016 4:41:42 PM
Location       : Vial 1
Inj Volume     : No inj
Acq. Method    : C:\CHEM32\1\METHODS\MLD-50BISO_60MIN_300ULMIN-FLD.M
Last changed   : 3/22/2016 6:08:12 PM by SYSTEM
Analysis Method : C:\CHEM32\1\METHODS\DEF_LC.M
Last changed   : 10/12/2016 4:39:20 PM by SYSTEM
Additional Info : Peak(s) manually integrated
  
```



=====
 Area Percent Report
 =====

```

Sorted By      :      Signal
Multiplier:    :      1.0000
Dilution:      :      1.0000
Use Multiplier & Dilution Factor with ISTDs
  
```

Signal 1: FLD1 A, Ex=352, Em=708

Peak #	RetTime [min]	Type	Width [min]	Area [LU*s]	Height [LU]	Area %
1	7.060	MM	0.6819	5.49128	1.34215e-1	100.0000
Totals :				5.49128	1.34215e-1	

Figure C4.16 Immunoconjugate α -PD-1 + DmtTic (4.4), D51; SEC Chromatograph

APPENDIX D:
IACUC APPROVALS


Page 1 of 2



RESEARCH INTEGRITY AND COMPLIANCE
INSTITUTIONAL ANIMAL CARE & USE COMMITTEE

MEMORANDUM

TO: David Morse,

FROM: 
Farah Moulvi, MSPH, IACUC Coordinator
Institutional Animal Care & Use Committee
Research Integrity & Compliance

DATE: 1/5/2015

PROJECT TITLE: Targeted radiopharmaceuticals for uveal and metastatic melanoma

FUNDING SOURCE: National Cancer Institute; H Lee Moffitt Cancer Center

IACUC PROTOCOL #: R IS00000805

PROTOCOL STATUS: **APPROVED**

The Institutional Animal Care and Use Committee (IACUC) reviewed your application requesting the use of animals in research for the above-entitled study. The IACUC **APPROVED** your request to use the following animals in your **protocol for a one-year period beginning 1/5/2015**:

Mouse: SCID (6-8 weeks, 15-20 g, F and M) 468
Mouse: C57BL/6 (6-8 weeks/15-20 gr/ F and M) 480

Please take note of the following:

- **IACUC approval is granted for a one-year period at the end of which, an annual renewal form must be submitted for years two (2) and three (3) of the protocol through the eIACUC system.** After three years all continuing studies must be completely re-described in a new electronic application and submitted to IACUC for review.
- **All modifications to the IACUC-Approved Protocol must be approved by the IACUC prior to initiating the modification.** Modifications can be submitted to the IACUC for review and approval as an Amendment or Procedural Change through the eIACUC system. These changes must be within the scope of the original research hypothesis, involve the original species and justified in writing. Any change in the IACUC-approved protocol that does not meet the latter definition is considered a major protocol change and requires the submission of a new application.
- **All costs invoiced to a grant account must be allocable to the purpose of the grant.** Costs allocable to one protocol may not be shifted to another in order to meet deficiencies caused by overruns, or for other reasons convenience. Rotation of charges among protocols by month without establishing that the rotation schedule credibly reflects the relative benefit to each protocol is

unacceptable.

RESEARCH & INNOVATION • RESEARCH INTEGRITY AND COMPLIANCE
INSTITUTIONAL ANIMAL CARE AND USE COMMITTEE
PHS No. A4100-01, AAALAC No. 58-15, USDA No. 58-15
University of South Florida • 12901 Bruce B. Downs Blvd., MDC35 • Tampa, FL 33612-4799
(813) 974-7106 • FAX (813) 974-7091


Figure D1 MC1RL IACUC Approval



RESEARCH INTEGRITY AND COMPLIANCE
INSTITUTIONAL ANIMAL CARE & USE COMMITTEE

MEMORANDUM

TO: David Morse,

FROM: 
Farah Moulvi, MSPH, IACUC Coordinator
Institutional Animal Care & Use Committee
Research Integrity & Compliance

DATE: 1/30/2015

PROJECT TITLE: Fluorescence Imaging of Pancreatic Cancer Targeted Agents

FUNDING SOURCE: H Lee Moffitt Cancer Center

IACUC PROTOCOL #: R IS00000946

PROTOCOL STATUS: **APPROVED**

The Institutional Animal Care and Use Committee (IACUC) reviewed your application requesting the use of animals in research for the above-entitled study. The IACUC **APPROVED** your request to use the following animals in your **protocol for a one-year period beginning 1/30/2015:**

Mouse: nu/nu (nude) (6-8 weeks/ M/F/20g)	1008
Mouse: NOD/SCID (6-8 weeks/M/25g)	56
Rat: SD-Tg(GFP) Bal/2Rrrc (>79 days or >299g/M)	14

Please take note of the following:

- **IACUC approval is granted for a one-year period at the end of which, an annual renewal form must be submitted for years two (2) and three (3) of the protocol through the eIACUC system.** After three years all continuing studies must be completely re-described in a new electronic application and submitted to IACUC for review.
- **All modifications to the IACUC-Approved Protocol must be approved by the IACUC prior to initiating the modification.** Modifications can be submitted to the IACUC for review and approval as an Amendment or Procedural Change through the eIACUC system. These changes must be within the scope of the original research hypothesis, involve the original species and justified in writing. Any change in the IACUC-approved protocol that does not meet the latter definition is considered a major protocol change and requires the submission of a new application.
- **All costs invoiced to a grant account must be allocable to the purpose of the grant.** Costs allocable to one protocol may not be shifted to another in order to meet deficiencies caused by overruns, or for other reasons convenience. Rotation of charges among protocols by month without establishing that the rotation schedule credibly reflects the relative benefit to each protocol is unacceptable.

RESEARCH & INNOVATION • RESEARCH INTEGRITY AND COMPLIANCE
INSTITUTIONAL ANIMAL CARE AND USE COMMITTEE
PHS No. A4100-01, AAALAC No.58-15, USDA No. 58-15
University of South Florida • 12901 Bruce B. Downs Blvd., MDC35 • Tampa, FL 33612-4799
(813) 974-7106 • FAX (813) 974-7091

<https://arc.research.usf.edu/Prod/Doc/0/6EGT50TMT0E4H93ECFCLROVH5D/fromStri...> 10/13/2016


Figure D2 TLR2L IACUC Approval



RESEARCH INTEGRITY AND COMPLIANCE
INSTITUTIONAL ANIMAL CARE & USE COMMITTEE

MEMORANDUM

TO: David Morse,

FROM: 
Farah Moulvi, MSPH, IACUC Coordinator
Institutional Animal Care & Use Committee
Research Integrity & Compliance

DATE: 11/5/2014

PROJECT TITLE: Molecular Imaging Probes for Lung Cancer Intraoperative Guidance

FUNDING SOURCE: H. Lee Moffitt Cancer Center

IACUC PROTOCOL #: R IS00000807

PROTOCOL STATUS: **APPROVED**

The Institutional Animal Care and Use Committee (IACUC) reviewed your application requesting the use of animals in research for the above-entitled study. The IACUC **APPROVED** your request to use the following animals in your **protocol for a one-year period beginning 11/5/2014**:

Mouse: nu/nu (6-8 weeks/15-20 grams/Male/Female)	806
Mouse: SCID/beige (6-8 weeks/15-20 grams/Male/Female)	270
Mouse: SCID Hairless Outbred (SHO) (6-8 weeks/15-20 grams/Male/Female)	150
Rat: Sprague-Dawley (>79 days/>299 grams/Male)	102
Rat: SD-Tg(GFP)Bal/2Rrrc (>79 days/>299 grams/Male)	15
Mouse: NOD/SCID (6-8 weeks/25 g/Male)	60

Please take note of the following:

- IACUC approval is granted for a one-year period at the end of which, an annual renewal form must be submitted for years two (2) and three (3) of the protocol through the eIACUC system. After three years all continuing studies must be completely re-described in a new electronic application and submitted to IACUC for review.
- All modifications to the IACUC-Approved Protocol must be approved by the IACUC prior to initiating the modification. Modifications can be submitted to the IACUC for review and approval as

an Amendment or Procedural Change through the eIACUC system. These changes must be within the scope of the original research hypothesis, involve the original species and justified in writing. Any change in the IACUC-approved protocol that does not meet the latter definition is considered a major protocol change and requires the submission of a new application.

• **All costs invoiced to a grant account must be allocable to the purpose of the grant.** Costs allocable to one protocol may not be shifted to another in order to meet deficiencies caused by overruns, or for other reasons convenience. Rotation of charges among protocols by month without establishing that the rotation schedule credibly reflects the relative benefit to each protocol is unacceptable.

RESEARCH & INNOVATION • RESEARCH INTEGRITY AND COMPLIANCE
INSTITUTIONAL ANIMAL CARE AND USE COMMITTEE
PHS No. A4100-01, AAALAC No.58-15, USDA No. 58-15
University of South Florida • 12901 Bruce B. Downs Blvd., MDC35 • Tampa, FL 33612-4799
(813) 974-7106 • FAX (813) 974-7091

Figure D3 DORL IACUC Approval



RESEARCH INTEGRITY AND COMPLIANCE
INSTITUTIONAL ANIMAL CARE & USE COMMITTEE

MEMORANDUM

TO: David Morse,

FROM: 
Farah Moulvi, MSPH, IACUC Coordinator
Institutional Animal Care & Use Committee
Research Integrity & Compliance

DATE: 8/10/2015

PROJECT TITLE: Molecular Imaging Probes for Lung Cancer Intraoperative Guidance

FUNDING SOURCE: Non-Profit (Private Foundations, H. Lee Moffitt Cancer Center, etc.), For Profit (Industry Sponsored) or Other
H Lee Moffitt Cancer Center

IACUC PROTOCOL #: R IS00000807

PROTOCOL STATUS: APPROVED

Your request for continuation of this study was received and will be reported to the Institutional Animal Care and Use Committee (IACUC). The IACUC acknowledges that this study is currently on going as previously approved. Please be advised that **continuation of this study is in effect for a one-year period beginning 11/4/2015:**

Please take note of the following:

- IACUC approval is granted for a one-year period at the end of which, an annual renewal form must be submitted for years two (2) and three (3) of the protocol through the eIACUC system. After three years all continuing studies must be completely re-described in a new electronic application and submitted to IACUC for review.
- All modifications to the IACUC-Approved Protocol must be approved by the IACUC prior to initiating the modification. Modifications can be submitted to the IACUC for review and approval as an Amendment or Procedural Change through the eIACUC system. These changes must be within the scope of the original research hypothesis, involve the original species and justified in writing. Any change in the IACUC-approved protocol that does not meet the latter definition is considered a major protocol change and requires the submission of a new application.

RESEARCH & INNOVATION • RESEARCH INTEGRITY AND COMPLIANCE
INSTITUTIONAL ANIMAL CARE AND USE COMMITTEE
PHS No. A4100-01, AAALAC No. 000434, USDA No. 58-R-0015
University of South Florida • 12901 Bruce B. Downs Blvd., MDC35 • Tampa, FL 33612-4799
(813) 974-7106 • FAX (813) 974-7091

Figure D4 DORL IACUC Approval Renewal

ABOUT THE AUTHOR

Michael Doligalski earned his Bachelor of Science degree in chemistry from the University of North Carolina at Chapel Hill in 2007. Following time as a research associate at Affinergy, a startup biotech company in the Research Triangle Park, Michael joined Dr. Mark McLaughlin's research lab at the University of South Florida in 2011. He was fortunate to have served as a teaching assistant in both the chemistry department's Mass Spectrometry and Nuclear Magnetic Resonance core facilities. The end of his graduate studies afforded him the opportunity to more closely collaborate with Dr. David Morse's research group at the H. Lee Moffitt Cancer Center.

Michael met his wife Christina while they were both attending UNC in 2005. They were married in 2009 after Christina graduated from UNC's School of Pharmacy. They were both thrilled to welcome their son William in June of 2016. The family lives in Tampa with their loyal dog Aliena. Michael will graduate with his doctoral degree in December 2016.